Epidemiological Modelling of the Spread and Transmission of Infectious Diseases

by

Moritz Maximilian SCHÄFER

Baumbacher Straße 9
56410 Montabaur, Germany

*Accepted Dissertation thesis for the partial fulfilment of the requirements
for the degree of* DOCTOR RERUM NATURALIUM

in the

University of Koblenz

Department 3: Mathematics / Applied Sciences
Institute of Mathematics
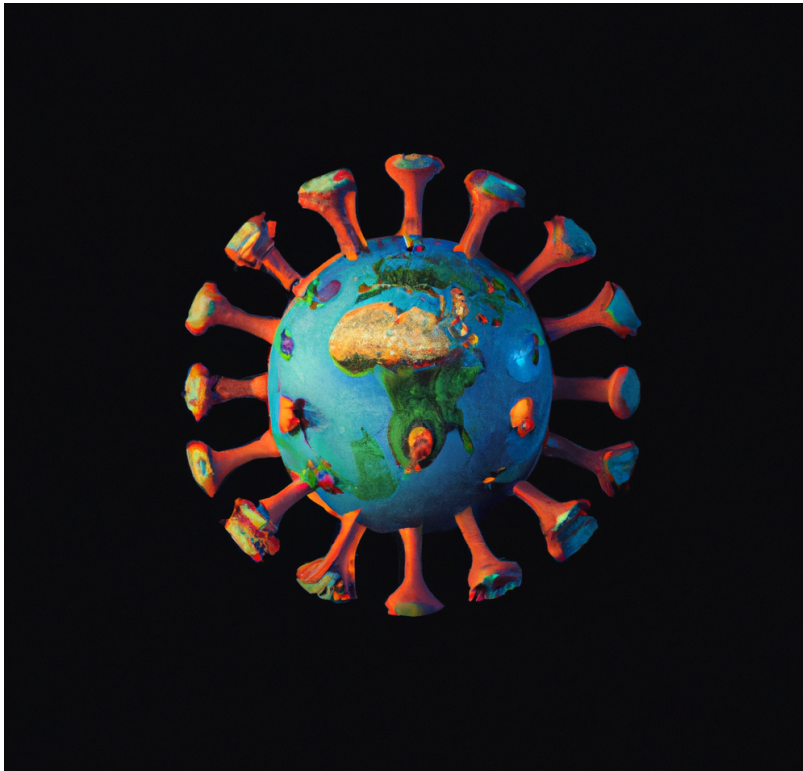
"Mathematics may not teach us how to add love or subtract hate, but it gives us every reason to hope that every problem has a solution."

– unknown

Abstract

In the last years, the public interest in epidemiology and mathematical modeling of disease spread has increased – mainly caused by the COVID-19 pandemic, which has emphasized the urgent need for accurate and timely modelling of disease transmission. However, even prior to that, mathematical modelling has been used for describing the dynamics and spread of infectious diseases, which is vital for developing effective interventions and controls, e.g., for vaccination campaigns and social restrictions like lockdowns. The forecasts and evaluations provided by these models influence political actions and shape the measures implemented to contain the virus.

This research contributes to the understanding and control of disease spread, specifically for Dengue fever and COVID-19, making use of mathematical models and various data analysis techniques. The mathematical foundations of epidemiological modelling, as well as several concepts for spatio-temporal diffusion like ordinary differential equation (ODE) models, are presented, as well as an originally human-vector model for Dengue fever, and the standard (*SEIR*)-model (with the potential inclusion of an equation for deceased persons), which are suited for the description of COVID-19. Additionally, multi-compartment models, fractional diffusion models, partial differential equations (PDE) models, and integro-differential models are used to describe spatial propagation of the diseases.

We will make use of different optimization techniques to adapt the models to medical data and estimate the relevant parameters or finding optimal control techniques for containing diseases using both Metropolis and Lagrangian methods. Reasonable estimates for the unknown parameters are found, especially in initial stages of pandemics, when little to no information is available and the majority of the population has not got in contact with the disease. The longer a disease is present, the more complex the modelling gets and more things (vaccination, different types, etc.) appear and reduce the estimation and prediction quality of the mathematical models.

While it is possible to create highly complex models with numerous equations and parameters, such an approach presents several challenges, including difficulties in comparing and evaluating data, increased risk of overfitting, and reduced generalizability. Therefore, we will also consider criteria for model selection based on fit and complexity as well as the sensitivity of the model with respect to specific parameters. This also gives valuable information on which political interventions should be more emphasized for possible variations of parameter values.

Furthermore, the presented models, particularly the optimization using the Metropolis algorithm for parameter estimation, are compared with other established methods. The quality of model calculation, as well as computational effort and applicability, play a role in this comparison. Additionally, the spatial integro-differential model is compared with an established agent-based model. Since the macroscopic results align very well, the computationally faster integro-differential model can now be used as a proxy for the slower and non-traditionally optimizable agent-based model, e.g., in order to find an apt control strategy.

Abstract (in German)

In den vergangenen Jahren ist das öffentliche Interesse an der Epidemiologie und mathematischen Modellierung der Ausbreitung von Krankheiten gestiegen. Dies wurde hauptsächlich durch die COVID-19-Pandemie verursacht, die die Notwendigkeit einer genauen und zeitnahen Modellierung der Krankheitsübertragung deutlich gemacht hat. Jedoch wurde bereits zuvor mathematische Modellierung genutzt, um die Dynamik und Ausbreitung von Infektionskrankheiten zu beschreiben. Diese Modelle sind entscheidend für die Entwicklung wirksamer Interventionen und Steuerungsmaßnahmen wie Impfkampagnen und etwaiger sozialer Einschränkungen (z.B. Lockdowns). Die Prognosen und Analysen, die aus diesen Modellen resultieren, haben politische Entscheidungen beeinflusst und die Maßnahmen geprägt, die ergriffen wurden, um das Virus einzudämmen.

Diese Forschungsarbeit möchte zum Verständnis und zur Kontrolle der Ausbreitung von Krankheiten, insbesondere von Dengue-Fieber und COVID-19, beitragen. Dabei werden verschiedene mathematische Modelle und Datenanalysetechniken verwendet. Die mathematischen Grundlagen der epidemiologischen Modellierung sowie verschiedene Konzepte für die räumlich-zeitliche Diffusion, wie beispielsweise Mensch-Vektor-Modelle, Modelle gewöhnlicher Differentialgleichungen (ODE), Multi-Compartment-Modelle, Modelle für fraktionale Diffusion, partielle Differentialgleichungsmodelle und integro-differentielle Modelle, werden in dieser Arbeit vorgestellt.

Es werden zudem verschiedene Optimierungstechniken verwendet, um die Modelle an medizinische Daten anzupassen und die relevanten Parameter abzuschätzen. Außerdem werden optimale Steuerungstechniken zur Eindämmung von Krankheiten mittels Metropolis- und Lagrange-Methoden benutzt. Dies ermöglicht sinnvolle Schätzungen für unbekannte Parameter, insbesondere in den Anfangsphasen von Pandemien, wenn nur wenig oder gar keine Daten verfügbar sind und die Mehrheit der Bevölkerung noch keinen Kontakt mit der Krankheit hatte. Je länger eine Krankheit besteht, desto komplexer wird deren Modellierung und es treten mehr Faktoren (wie Impfungen und verschiedene Mutationen) auf, die die Qualität der mathematischen Modelle beeinträchtigen.

Obwohl es möglich ist, hochkomplexe Modelle mit vielen Gleichungen und Parametern zu erstellen, birgt ein solcher Ansatz mehrere Herausforderungen. Dazu gehören Schwierigkeiten bei der Vergleichbarkeit und Bewertung von Daten, ein erhöhtes Risiko von Überanpassung und eine verringerte Verallgemeinerbarkeit. Daher werden auch Kriterien für die Auswahl von Modellen, basierend auf Anpassung und Komplexität sowie die Sensitivität des Modells in Bezug auf bestimmte Parameter berücksichtigt. Dies liefert auch weiterführende Informationen darüber, welche politischen Interventionen bei möglichen Variationen der Parameterwerte vorrangig angegangen werden sollten.

Weiterhin werden die vorgestellten Modelle, insbesondere die Optimierung mithilfe des Metropolis-Algorithmus, die zur Parameterschätzung herangezogen wird, mit anderen etablierten Methoden verglichen. Hierbei spielen die Qualität der Modellberechnung, aber auch Rechenaufwand und Einsetzbarkeit eine Rolle. Ebenfalls wird das räumliche integro-differentielle Modell mit einem etablierten agentenbasierten Modell verglichen. Da die makroskopischen Ergebnisse sehr gut übereinstimmen, kann man nun das – auf den Aufwand bezogen – schnellere integro-differentielles Modell als Proxy für das langsamere und nicht herkömmlich optimierbare agentenbasierte Modell verwenden, um z.B. eine angemessene Kontrollstrategie zu finden.

Notes of Thanks

I would like to thank my doctoral advisor Thomas Götz for giving me the opportunity for a PhD student and for giving me a lot of valuable advice in the last five years, which helped me a great deal in order to be able to finish this thesis. I would also like to thank my coauthors of the research papers, especially Karunia Putra Wijaya, Peter Heidrich and Robert Rockenfeller for their ideas, corrections and advice regarding my work and good collegiality.

I would like to express my heartfelt gratitude to my parents Karina and Bernhard who have been there for me throughout my entire, not only educational, journey, providing me with support and resources for my entire life. Their unwavering encouragement and belief in me are invaluable. I also want to extend my thanks to my friends, especially Sophia for her friendship and support since a long time.

I would also like to thank the following persons or groups (in alphabetical order): Bernd, Birgit, Dago, Dietmar, Else, Fabie, *fue*, Irene, Kai, Michael, Waltraud, Wolfgang and Yannik, as well as anyone else I have **not** forgotten.

Contents

List of Figures

List of Tables

List of Abbreviations

AC	**A**ssociation **C**ommunities
AIC	**A**kaike **I**nformation **C**riterion
Alg.	**Alg**orithm
App.	**App**endix
BFGS	**B**royden-**F**letcher-**G**oldfarb-**S**hanno
BIC	**B**ayesian **I**nformation **C**riterion
CDC	**C**enters for **D**isease **C**ontrol and Prevention
cf.	**c**on**f**er (compare)
CSSE	**C**enter for **S**ystems **S**cience and **E**ngineering
COVID	**CO**rona**VI**rus **D**isease
DDE	**D**elay **D**ifferential **E**quation
Def.	**Def**inition
DENV	**D**engue **V**irus
DFE	**D**isease **F**ree **E**quilibrium
DHF	**D**engue **H**aemorrhagic **F**ever
DIVI	**D**eutsches **I**nstitut für **V**erletztenversorgung und **I**ntensivmedizin
DKG	**D**eutsche **K**rankenhaus **G**esellschaft
DWD	**D**eutscher **W**etter-**D**ienst (German Meteorological Service, Offenbach, Germany)
EE	**E**ndemic **E**quilibrium
e.g.	**e**xempli **g**ratia (for example)
eqn.	**eq**uatio**n**
etc.	**e**t **c**etera (and so on)
Ex.	**Ex**ample
FEM	**F**inite **E**lement **M**ethod
Fig.	**Fig**ure
HIV	**H**uman **I**mmunodeficiency **V**irus
ICU	**I**ntensive **C**are **U**nit
ICM	**I**nterdisciplinary **C**entre for Mathematical and Computational **M**odelling (Warsaw, Poland)
i.e.	**i**d **e**st (that is/means)
i.i.d.	**i**ndependent and **i**dentically **d**istributed
IVP	**I**nitial **V**alue **P**roblem
JHU	**J**ohns **H**opkins **U**niversity (Baltimore, MD, USA)
Lem.	**Lem**ma
MCMC	**M**arkov **C**hain **M**onte **C**arlo
ODE	**O**rdinary **D**ifferential **E**quation
p(p).	**p**age(s)
PACI	**P**ointwise **A**symptotic **C**onfidence **I**nterval
PDE	**P**artial **D**ifferential **E**quation
PSRF	**P**otential **S**cale **R**eduction **F**actor
resp.	**resp**ectively
RK	**R**unge-Kutta

RKI	**R**obert-**K**och-**I**nstitute (Berlin, Germany)
SACI	**S**imultaneous **A**symptotic **C**onfidence **I**nterval
SARS-CoV	**S**evere **A**cute **R**espiratory **S**yndrom **Co**rona**V**irus
S(E)IR(D)	**S**usceptible (- **E**xposed) -**I**nfected - **R**ecovered (- **D**eceased)
Sim.	**Sim**ulation
Tab.	**Tab**le
WHO	**W**orld **H**ealth **O**rganization
wlog	**w**ithout **l**oss **o**f **g**enerality
wrt	**w**ith **r**espect **t**o

Part I

Introduction and Theory

Chapter 1

Introduction

1.1 Motivation

In January 2020, media reported on the appearance of a new pneumonia of unknown origin. This disease, caused by the novel coronavirus *SARS-CoV-2*, later referred to as *COVID-19* or *Corona* (mainly in Germany), would go on to influence economics, politics and the entire community down to its very core. It has spread rapidly across the globe, leading to widespread illness and death. While this was not the first and most likely will not be the last time that epidemics have had a significant impact on global health and society, the unprecedented scale and speed of the pandemic has highlighted the need for accurate and timely modelling of disease spread. Understanding the spread and dynamics of these diseases is crucial for developing effective prevention and control measures. Therefore, mathematical models can provide insights into the transmission dynamics of the virus, as well as inform the design and evaluation of interventions such as vaccination, mask wearing and distancing measures.

Epidemiologists make use of those models to *describe* the current or former behaviour of the disease, *validate* them with medical data, *identify* important parameters and *predict* the futural outcome under certain assumptions, which can later be utilised in order to drive or justify political decisions. The modelling of disease dynamics has been an important topic in applied mathematics for over 100 years, so that many of the models used today are not entirely new; for example, models used to describe other epidemics and pandemics such as Dengue fever behaviour can also be adapted and expanded for modelling of the COVID-19 dynamics.

The objective of this thesis is to utilize mathematical models to enhance our comprehension of the epidemiology of Dengue and COVID-19. The emphasis will be on the creation and assessment of models that can be used to increase our knowledge of the transmission process and potentially even advise political decisions. This research will be grounded in the utilization of data that is relevant to the study, and will encompass various techniques for data analysis and model evaluation. Various numerical methods for the evaluation of those models will be presented and applied. Additionally, the research will strive to identify important parameters via parameter estimation, in order to provide a more accurate understanding of the disease(s); the impact of various parameters with respect to the disease dynamics is also analyzed. Considering the potential high costs associated with implementing control measures such as lockdowns or specific interventions, including political, social, and financial implications, it also becomes essential to develop optimal control strategies which balance the reduction of infected with the costs of such measures.

With this in mind, the next section will provide a brief historical outline of epidemics and epidemiology, setting the stage for a deeper exploration of the role of mathematical modelling in this field.

1.2 A short historical outline

In this section, it is firstly differentiated between three types of disease outbreaks. Thereon, a focus is taken on the two diseases that are considered in this thesis (Dengue fever and COVID-19), and specific properties and the history of both diseases are considered.

1.2.1 Endemics, Epidemics and Pandemics

An infectious disease that occurs recurrently or persistently within a specific region, resulting in a similar number of infections each year, is defined as an *endemic* [1]. A notable example of an endemic disease is Malaria, a disease transmitted by mosquitoes that is endemic in around 100 countries worldwide. Other examples include yellow fever and Ebola.

When an infectious disease appears in a specific region and the number of cases rapidly increases within a short period of time, it is referred to as an *epidemic* [2]. The rate of growth and time frame are crucial factors in this distinction. Fast-growing epidemics, such as Typhus and Cholera, often decrease quickly over time, while slower-developing, yet more persistent, epidemics – such as HIV – may persist for a longer period. Epidemics are often related to the seasonality of certain infectious agents. For example, influenza and the common cold occur predominantly in the winter; vector-borne infections, particularly those spread by mosquitoes, typically occur during the breeding cycle, which is connected to rain or monsoon periods in tropical regions, cf. World Health Organization (WHO) [3]. Epidemics may be caused by an increase in virulence or the 'import' of a disease to a new geographical area with different conditions, according to the Centers for Disease Control and Prevention (CDC) [4].

When an epidemic spreads quickly across regions and occurs worldwide, it is called a *pandemic* [2]. This often applies to new or newly-mutated viruses. As more and more people become infected with the disease or are vaccinated (in case of existence of a vaccine), they typically gain a certain level of *immunity* to the disease, resulting in the pandemic eventually becoming an endemic.

It is important to note that the distinction between endemic, epidemic, and pandemic is based on the time period and number of cases, and not on the severity or fatality of the disease. The social, economic, and physical costs can be high, especially in terms of deaths and long-term impacts on those infected or recovered. Adopting a strategy that relies on the expectation that a pandemic will eventually transition to an endemic state is often an inadequate approach.

An infectious disease is only able to spread by the presence of a *pathogen*. These pathogens, which be found in humans, animals, or the environment, can take various forms, including bacteria (e.g., tuberculosis), viruses (HIV, Dengue or COVID-19), fungi, parasites, or prions. Transmission can happen through different means, including person-to-person contact (HIV, COVID-19), through the air (influenza), through vectors such as mosquitoes (e.g. Dengue or Malaria), through food (Cholera) or vertically from mother to fetus (HIV).

Dengue Fever

The first records of a disease that is similar to Dengue are found in Chinese medical encyclopedia from the Jin Dynasty (3rd–5th centuries), describing a "water poison" associated with flying insects. In the 18th and 19th centuries, growing international

trading and urbanization have prepared ideal conditions for mosquitoes of the type *aedes agypti*, and thus the spread of Dengue to new regions and countries. However, only a few epidemics per century were registered, primarily because of long shipping routes which hindered the transmission of the vector. This drastically changed in times of globalisation in the later half of the 20th century and resulted in increased infection numbers in many tropical and subtropical countries [5].

The Dengue virus is not transmitted directly from human to human but via vectors, which makes the fever a so-called *vector-borne disease*. The majority of the vectors are mosquitoes of the species *aedes albopictus* and especially *aedes aegypti* [3]. These mosquitoes prefer high temperatures and high humidity throughout the entire year. There are four main serotypes of Dengue, called *DENV-1* to *DENV-4*. After a bite of an infectious mosquito and a 'successful' transmission of the disease, the incubation of time of Dengue is typically one week. Infectious persons are also the primary carrier to infect healthy mosquitoes in case of a bite. After recovery, the formerly infective person is immune against all strains for about 12 weeks. Thereon, the patient remains immune against the specific serotype he was infected with for a long time, but is susceptible to all other types and can get reinfected with any other strain [3].
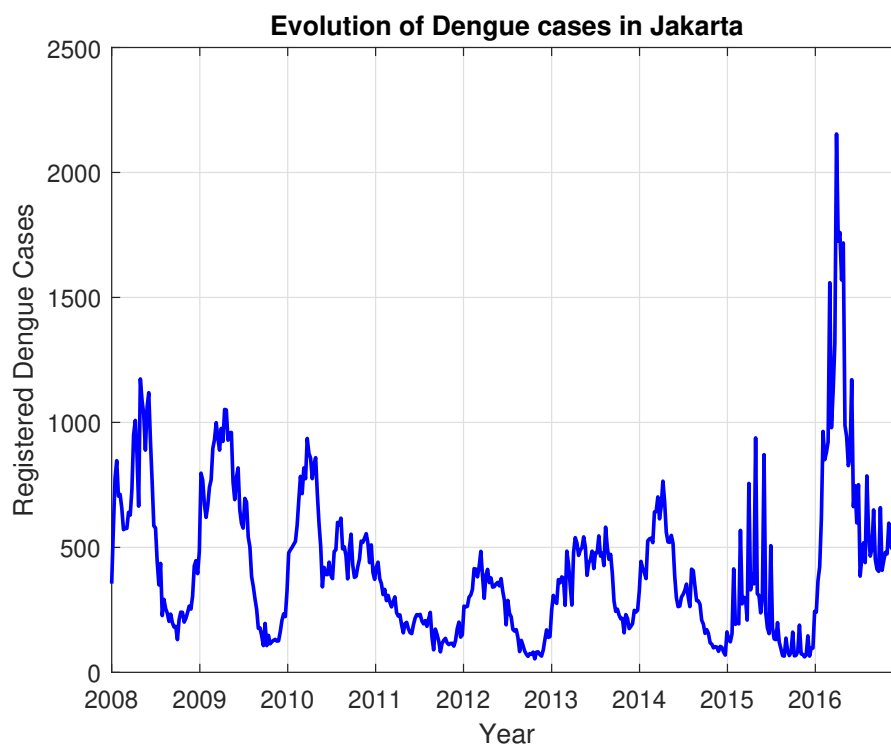
FIGURE 1.1: Reported Dengue cases in Jakarta, 2008–2016 [6].

As of today, Dengue fever is not only one of the most impactful diseases in Southern Asia, but also affects millions of people worldwide. Its symptoms can range from mild to severe, including fever, headache, muscle or joint pain, nausea, vomiting, and skin rash. In some cases, more severe symptoms such as abdominal pain, persistent vomiting, and nose or gum bleeding can occur. An occasionally life-threatening form of Dengue is called Dengue haemorrhagic fever (DHF) that especially occurs during reinfections [7]. There are between 100–400 million annual

infections with Dengue (roughly 1% of which is DHF) and 20,000–25,000 deaths worldwide [3, 7] .

Since 2016, first vaccines to be used for persons who have been infected with Dengue are available [8]; however, no vaccines that can be used in order to *avoid* getting infected are available of today [9, 10]. Despite ongoing efforts to control Dengue transmission (especially toward a reduction of the vector population), the disease continues to spread to new areas and cause outbreaks, e.g. in France [11]. The growing infection rates and worldwide spread highlight the need for accurate and reliable mathematical models of Dengue transmission, especially including the seasonality and the life-cycle of the vectors.

As an example, which will be of interest in chapter 3, Jakarta, the capital of Indonesia, presents ideal conditions for mosquitoes to thrive, with daily mean temperatures of 26–27 °C throughout the year and minimal seasonal variation. The city experiences a significant rainy period from December to March, with each month receiving an average rainfall of over 200 litres per square meter, alongside high humidity. In contrast, during the period of July to September, the average rainfall drops below 100 litres per month, while the humidity remains relatively unchanged. The seasonal dependence of Dengue cases in Jakarta has been investigated in several works such as Olinky et al. [12] or Augerand-Véron and Sari [13]. Dengue cases in Jakarta from 2008–2016, showing strong seasonal dependence, are presented in Fig. 1.1.

COVID–19

The COVID-19 pandemic is one of the most significant global events of the 21st century. It has affected millions of people worldwide, caused significant loss of life, and had a severe impact on economies and societies. The origins of the disease can be traced back to late 2019, when an outbreak of a new respiratory illness was reported in the city of Wuhan, China. The disease soon spread across the globe, and the World Health Organization declared it to be a pandemic in March 2020, after the virus had spread to over 100 countries.

In response to the pandemic, scientists and researchers around the world worked together to develop COVID-19 vaccines, with the first vaccine receiving emergency use authorization in December 2020. In 2021, the focus shifted towards vaccine distribution and administration. Despite progress in vaccination efforts, new variants of the virus emerged, posing new challenges to the control of the pandemic, so that the pandemic situation was still ongoing.

However, as more people have come into contact with the virus until 2022 (through vaccination and/or infection), as well as less severe variants of COVID-19 have become dominant, the fatality rate declined. On 25 May, 2022, the WHO declared the end of the COVID-19 pandemic, while local epidemics could still pose a threat to the population. One year later, on 5 May, 2023, WHO chief Tedros Ghebreyesus declared the end to COVID-19 as a global health emergency [14].

Situation in Germany   The first case of COVID-19 in Germany was reported on 27 January, 2020 in Bavaria [15]. Initially, the majority of cases were imported by travelers from China, Iran or Italy, as well as tourists returning from ski holidays in Austria and Italy. By the start of March, more than 100 cases had been reported in Germany, and a (quasi-)exponential rise in the number of cases was visible. The first death cases were reported on 9 March [16]. A rapid increase in cases and hospitalizations was thereon followed by a decline in cases and hospitalizations during the summer of 2020. This time period is commonly referred to as the "first wave" of the pandemic in

Germany. Fig. 1.2 shows the temporal evolution of COVID-19 cases in Germany from 26 January until 30 September, as reported by the Johns-Hopkins-University (JHU). The weekly fluctuations derive from specific delays in registration on weekends.
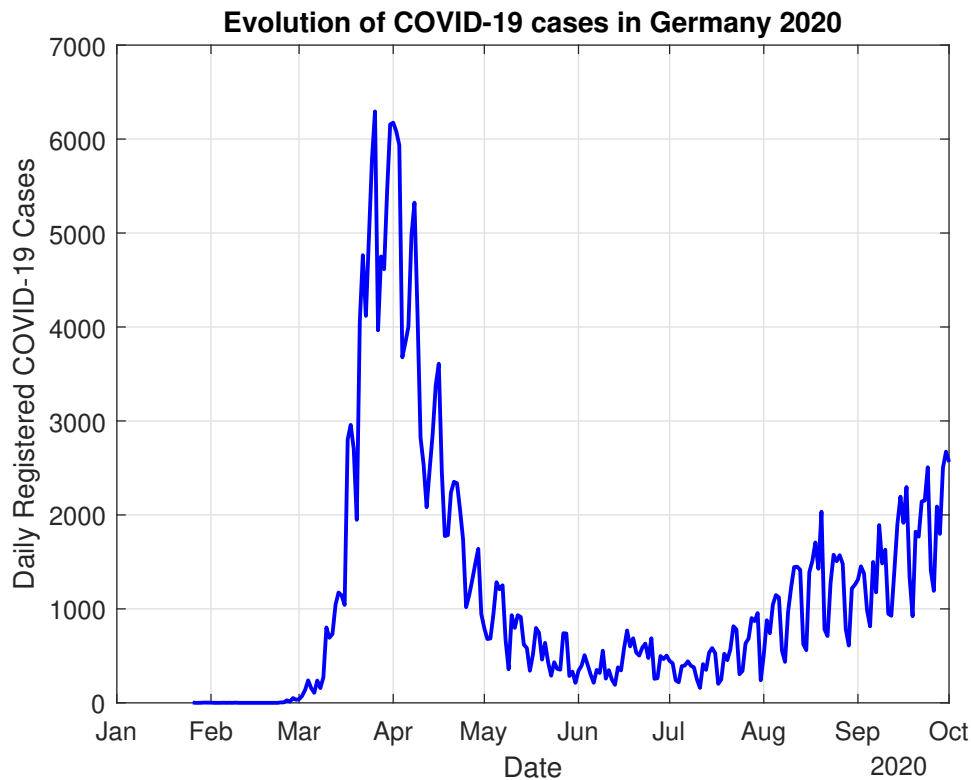
FIGURE 1.2: Confirmed daily COVID-19 cases in Germany during the first wave [17].

Since then, Germany has implemented a series of measures to slow the spread of the virus, including lockdowns, distancing measures, and the mandatory of wearing masks. The country has also rolled out a mass vaccination campaign, at first with a focus on the most vulnerable populations. Despite these efforts, the country has encountered several further waves of infections, with numbers rising and falling depending on the transmission rate of the current variant, the severity of the restrictions and the success of the vaccination campaign. In response to the growing outbreak in the first wave, the German federal government introduced measures to reduce the spread of the disease on 16 March. Schools, kindergartens and universities were closed, and on 22 March, these measures were tightened with a national curfew and contact ban being implemented. People were advised to stay at home, leaving only for work-related activities, necessary shopping, medical treatment or sports [18].

By the mid of April, these mitigation measures, but also the cautiousness of the population, had shown some success, with the number of new infections declining from its peak of 6,933 on 28 March to less than 1,000 from 2 May onwards. In May, a relaxation of the imposed restrictions to social and economic life was announced. On 10 June, only 16 new infection cases were detected [17]. In the mid of June, travel-related restrictions were relaxed within Europe [19]. However, the pandemic still progressed worldwide. By the end of August, new maxima for the daily cases worldwide set another record for that time [20]. Towards the end of the summer holidays in the first German states in mid to end of August, a second rise of case

numbers was detected, with over 1,000 new infection cases per day [17]. The specific impact of travellers on the disease dynamics was analyzed in the paper in chapter 5.

This second wave of the pandemic developed in the fall of 2020 and a resurgence of cases and hospitalizations was seen, leading to a nationwide lockdown from December 2020 to spring 2021. The number of cases and hospitalizations peaked in December, and then slowly decreased in early 2021. The third wave of the pandemic began in the spring of 2021, and saw a spike in cases and hospitalizations due to the emergence of new variants of the virus. This wave was characterized by a higher number of cases among younger age groups. By the summer of 2021, Germany had made significant progress in controlling the spread of the virus and vaccinating its population. The country began to ease restrictions, allowing businesses and cultural events to reopen and allowing travel within Europe. Nevertheless, a fourth wave of the pandemic started in the end of 2021, which was characterized by a further increase in cases and hospitalizations, as well as the emergence of new variants of the virus, particularly the B.1.1.7 variant first identified in the United Kingdom. In 2022, less severe variants of the virus dominated and several measures were easened. The mandatory of wearing masks was stepwise disestablished until 2023.

Overall, the pandemic in Germany has been characterized by fluctuations in the number of cases and hospitalizations, with several peaks and declines over the course of the past two years. These fluctuations have been influenced by a variety of factors, including the emergence of new variants of the virus, changes in social and economic activity, and the implementation of various public health measures. Comparing different waves of a disease outbreak poses challenges due to various factors such as differences in the method of infection registration, variations in the implementation of lockdown and testing strategies, and genetical evolution of the virus. For example, accommodating changes in strategies of containing the disease or measuring the amount of infected can be achieved by incorporating several piecewise constant transmission rates or detection rates, which we will see in chapters 4 and 5. However, estimating parameters in a federal and non-homogeneous structure with numerous time-restricted measurements becomes increasingly difficult due to cross-correlation and the small sensitivity values associated with the process. This is also a reason why the cumulative data presented in Figs. 1.3 and 1.4 for the time span of 2020–2022 have to be taken with caution.

1.2.2   Medical data of Dengue fever and COVID-19

The thesis will restrict its analysis of Dengue fever dynamics to epidemics in Indonesia. An important source of medical data in this country are the local health departments. These departments collect data on Dengue cases within their respective regions. They also work closely with the healthcare facilities within their regions to provide treatment and care to those affected by Dengue and are responsible for providing regular updates to the Ministry of Health [21] which collects and reports data on Dengue cases from various healthcare facilities, including hospitals and clinics. This information is used to develop national and regional level surveillance reports. The infection data we will use in chapter 3 to fit the parameters, is originating from private communications with Dipo Aldila [6].
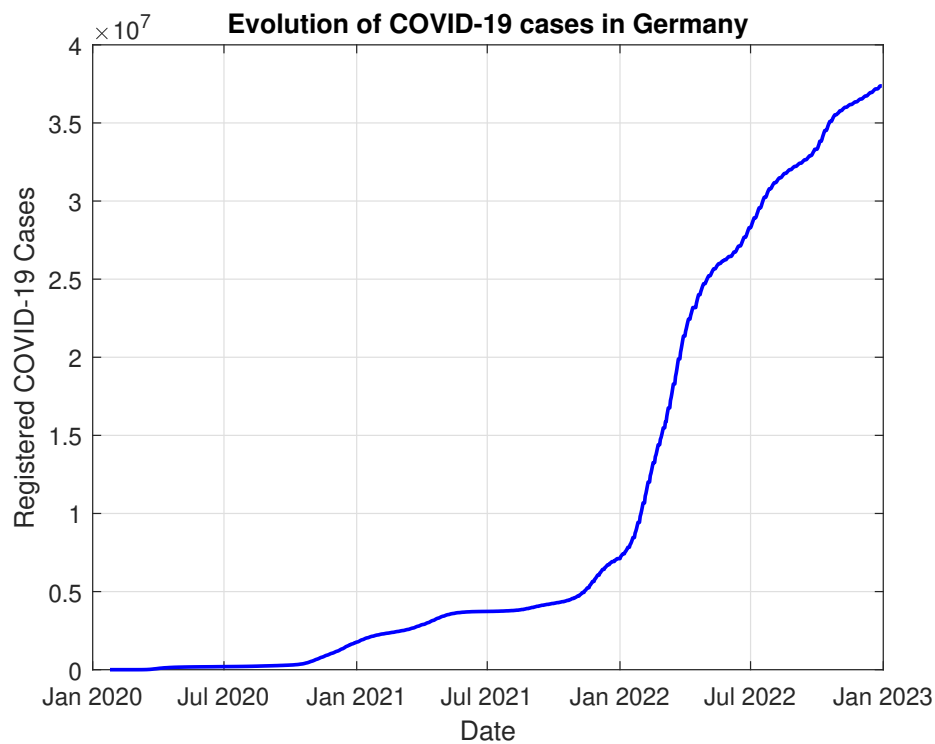
FIGURE 1.3: Evolution of the cumulative COVID-19 infections in Germany from 2020–2022 [17], linearly scaled.
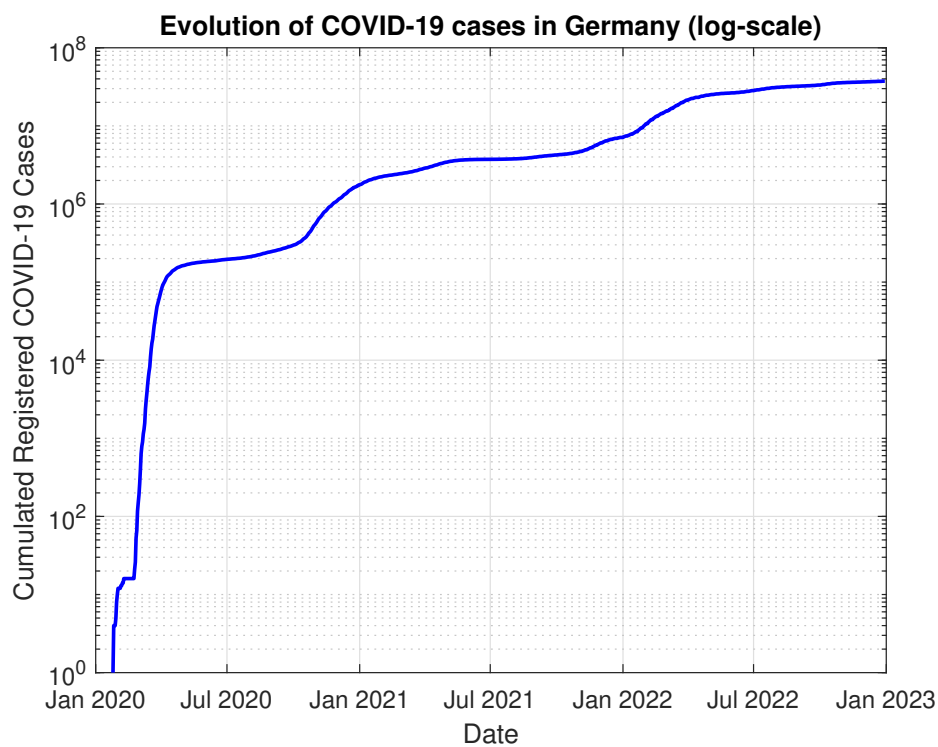
FIGURE 1.4: Evolution of the cumulative COVID-19 infections in Germany from 2020–2022 [17], semi-logarithmically scaled.

For the COVID-19 data in Germany, confirmed cases and deaths were collected by the Robert Koch Institute (RKI) [16], the country's national public health institute. The RKI received data from the country's 16 states on a daily basis, and published this information on its website (see Fig. 1.2). Additionally, the RKI also conducted surveillance of COVID-19 cases through sentinel testing of general practitioners, which helps to provide an estimate of the number of people with symptoms of the disease in the population. This data was used to inform the decisions made by German authorities regarding measures such as lockdowns and social distancing guidelines. Furthermore, data on hospitalizations and intensive care unit (ICU) admissions were collected by the German Interdisciplinary Association for Intensive Care and Emergency Medicine (DIVI) and the German Hospital Federation (DKG). Additionally, data on vaccination coverage was also collected and published by the RKI.

To obtain the most accurate and up-to-date information on the spread of COVID-19 in Germany, it is important to consult multiple sources of data. This will allow for a more complete understanding of the pandemic and help inform decisions about how to respond. In addition to data from the RKI, other organizations also tracked COVID-19 cases in Germany and worldwide. From 21 January onwards, WHO's daily situation reports [20] or Johns Hopkins University [17] (JHU) contain the latest figures on confirmed cases and deaths for almost all countries. The Johns Hopkins University (JHU) Center for Systems Science and Engineering (CSSE) also provides detailed data on confirmed cases, deaths, and recoveries at the national and regional level. The JHU data is widely used by researchers and media outlets, and is updated on a daily basis. In chapters 4 and 5, we relied on the data published by the JHU due to their rapid updates and easy accessibility.

1.3   Epidemiology

Epidemiology is the study of the *patterns*, *causes*, and *effects* of health and disease conditions in defined populations. It is the cornerstone of public health and informs policy decisions and evidence-based practice by identifying risk factors for disease and targets for preventive healthcare. The origins of epidemiology can be traced back to ancient civilizations, where observations on the spread of disease were recorded. In the the 18th and 19th centuries, epidemiology began to develop as a scientific discipline. John Snow, a British physician, is considered to be the father of modern epidemiology for his work in identifying the source of a cholera outbreak in London in 1854. He used a map to plot the locations of cholera cases and identified a contaminated water pump as the source of the outbreak [22]. In the late 19th and early 20th centuries, advances in microbiology and public health led to further development of epidemiological methods. The introduction of vaccination and improvements in sanitation also contributed to a decline in infectious disease deaths.

In 1902, British physician Sir Ronald Ross was awarded the Nobel Prize in Medicine for his work on malaria, particularly for his discovery that *anopheles* mosquitoes are carriers of the disease. Despite his groundbreaking contribution, Ross faced criticism for his belief that malaria could be eradicated by reducing the number of mosquitoes. Therefore, he used mathematical models to underpin his statement. One of his models, which takes on similar assumptions as an *SI-model*, is a mathematical representation of the transmission dynamics of malaria. It starts with several definitions and takes into account various factors that impact the spread of

malaria [23, 24]. For the mathematical background of the used *differential equations*, which is anticipated here, refer to sections 2.1 and 2.3.

- Population N: The total number of individuals, assumed to be constant in time.

- Infected $I(t)$: The individuals which are infected with the disease and infectious (and thus *infectious* for mosquitoes) at time t.

- Vector population M: The total number of vectors, in this case anopheles mosquitoes, also assumed to be constant in time.

- Infected vectors $V(t)$: The amount of infected mosquitoes (and thus *infectious* for humans) at time t. Contact with a susceptible individual can therefore lead to transmission of the disease.

- Frequency f of bites: The amount of times a single vector bites humans in a certain time unit.

- Transmission probability p: Given a bite of an infected mosquito on a non-infected person – or a bite of a non-infected mosquito on an infected person –, this denotes the probability that a previously uninfected gets infected with the disease.

- Recovery rate r: The rate at which humans recover from the disease.

- Death rate m: The fraction of mosquitoes which die in a certain time interval.

During a time interval dt, any infected mosquito thus bites $f\,dt$ humans, of which the fraction $(N - I(t))/N$ is not yet infected, and a transmission occurs with the probability p. This way, he computed the amount of newly infected humans in a certain time interval by

$$I'(t) = fp\,V(t) \cdot \frac{N - I(t)}{N} - rI(t). \tag{1.1}$$

Any non-infected mosquito thus bites $f\,dt$ humans, of which the fraction $I(t)/N$ is infected, and a transmission occurs with the probability p. This way, he computed the amount of newly infected mosquitoes in a certain time interval by

$$V'(t) = fp\,(M - V(t)) \cdot \frac{I(t)}{N} - mV(t). \tag{1.2}$$

As Malaria is permanently existent in the observed African countries, he restricted his observations on the *stationary points* of the system, where the amount of infected humans and mosquitoes are constant in time, i.e., $I'(t) = V'(t) = 0$. A trivial solution is $I^* = V^* = 0$, equivalent to the absence of Malaria. It is easy to show that another stationary equilibrium exists at

$$I^* = N \cdot \frac{1 - rmN/(f^2p^2M)}{1 + rN/(fpM)}, \tag{1.3}$$

$$V^* = M \cdot \frac{1 - rmN/(f^2p^2M)}{1 + m/(fp)}. \tag{1.4}$$

If the amount of mosquitoes lies above a certain threshold $M > rmN/(f^2p^2)$, the stationary solutions satisfy $I^* > 0$ and $V^* > 0$, supporting Ross' assumption *qualitatively*. The model allows for a better understanding of the interactions between

the disease and its environment, and helps to identify potential control measures for malaria. However, despite searching for realistic parameter values, Ross could not find meaningful *quantitative* results as any numerical results were very sensitive towards small changes of the values. Nevertheless, this model remains an important tool for epidemiologists and public health professionals to understand and control the spread of malaria, and Ross' work was a significant contribution to the field of epidemiology and demonstrated the importance of using mathematical models to understand complex health problems.

During the 20th century, the role of epidemiology in understanding the causes of chronic diseases such as cancer and heart disease grew significantly. An example is the Framingham Heart Study, which is one of the longest-running epidemiological studies (since 1948) which has provided important insights into risk factors for heart disease [25]. Epidemiology continues to evolve as new technologies and data sources become available. The field of molecular epidemiology, which uses genetic and molecular markers to study the spread of disease, is one area of growth. As of today, epidemiology plays a crucial role in the identification, monitoring and control of emerging infectious diseases, not only since COVID-19 and its worldwide impact.

1.4 Structure of the thesis

Part I continues with a comprehensive theoretical overview in chapter 2, serving as the foundation for understanding the contributions presented in Part II. It encompasses the fundamental definitions, theorems, and examples of ordinary, partial, fractional and integral differential equations, along with the corresponding solution theory, including commonly used numerical methods. Also, the most important concepts in epidemiology are listed and explained. Further on, optimization techniques like the Markov-chain Monte-Carlo method and the Forward-Backward method using Lagrangian multipliers are presented.

Part II showcases six research papers, four of which have already been published, highlighting the findings of our studies. Chapter 3 discusses the temporal modelling of Dengue in Jakarta using a *SIRUV*-model, including model reduction through time-scale separation and a transition from the human-vector based *SIRUV*-model to an *SIR*-model with a time-dependent transmission rate. Also, it is made usage of periodic transmission rates and a mobility matrix to include spatial spread. In chapter 4, we model the epidemics of the initial phase of COVID-19 in Germany, and make use of parameter estimation to identify important values using the Metropolis algorithm. Chapter 5 considers the impact of travellers and the effect of the policies in summer 2020 in Germany, and makes a comparison of the outcomes of the Metropolis algorithm and an adjoint based approach. A more theoretical study of fractional diffusion is presented in chapter 6, which includes several numerical methods to deal with various boundary conditions in fractional diffusion equations, yet also introduces a simple epidemiological model with fractional diffusion. In chapter 7, we consider an epidemiological model with diffusion and model the spatio-temporal spread of COVID-19 using the example of a German district. Lastly, chapter 8 introduces an integro-differential model and use Lagrange multipliers to optimize the control (i.e., political measures) in order to regulate the disease dynamics under specific conditions, taking both the amount of infected and the political and economical costs of a lockdown into account, with a comparison to the results of an agent-based model.

In Part III, the research contributions are summarized and discussed and an outlook on potential future research is provided.

References

[1] Kalra, S. et al. "Endemic or epidemic? Measuring the endemicity index of diabetes". In: *Indian J Endocrinol Metab.* 19.1 (2015), pp. 5–7. DOI: `10.4103/2230-8210.144633`.

[2] Columbia Mainland School of Public Health. *Epidemic, Endemic, Pandemic: What are the Differences?* `https://www.publichealth.columbia.edu/news/epidemic-endemic-pandemic-what-are-differences`. last visited: 18 December, 2023.

[3] World Health Organization. *Dengue and severe dengue.* `https://www.who.int/news-room/fact-sheets/detail/dengue-and-severe-dengue`. last visited: 18 December, 2023.

[4] Centers for Disease Control and Prevention. *Principles of Epidemiology.* `https://www.cdc.gov/csels/dsepd/ss1978/SS1978.pdf`. last visited: 18 December, 2023.

[5] Gubler, D.J. "Dengue and Dengue Hemorrhagic Fever". In: *Clinical Microbiology Reviews* 11.3 (1998), pp. 480–496. DOI: `10.1128/cmr.11.3.480`.

[6] *Privat communication with Dipo Aldila, Department of Mathematics, University of Indonesia, Depok.*

[7] Centers for Disease Control and Prevention. *Dengue and Dengue Hemorrhagic Fever.* `https://www.cdc.gov/dengue/resources/denguedhf-information-for-health-care-practitioners_2009.pdf`, last visited: 18 December, 2023.

[8] Centers for Disease Control and Prevention. *Dengue vaccine.* `https://www.cdc.gov/dengue/vaccine/index.html`, last visited: 18 December, 2023.

[9] Huremović, D. *Psychiatry of Pandemics.* Springer Nature Switzerland, 2019, Chapter 2: Brief History of Pandemics (Pandemics Throughout History).

[10] Gubler, D.J. "Dengue/dengue haemorrhagic fever: history and current status". In: *Novartis Found Symp.* 277 (2006), pp. 3–16. DOI: `10.1002/0470058005.ch2`.

[11] Cochet, A. et al. "Autochthonous dengue in mainland France, 2022: geographical extension and incidence increase". In: *Euro. Surveill.* 27.44 (2022). DOI: `10.2807/1560-7917.ES.2022.27.44.2200818`.

[12] Olinky, R., Huppert, A., and Stone, L. "Seasonal dynamics and thresholds governing recurrent epidemics". In: *J. Math. Biol.* 56 (2008), pp. 827–839.

[13] Augeraud-Véron, E. and Sari, N. "Seasonal dynamics in an SIR epidemic system". In: *J. Math. Biol.* 68 (2014), pp. 701–725.

[14] United Nations News. *WHO chief declares end to COVID-19 as a global health emergency.* `https://news.un.org/en/story/2023/05/1136367`. last visited: 18 December, 2023.

[15] Böhmer, M.M. et al. "Investigation of a COVID-19 outbreak in Germany resulting from a single travel-associated primary case: a case series". In: *The Lancet* 20.8 (2020), pp. 920–928. DOI: `10.1016/S1473-3099(20)30314-5`.

[16] Robert-Koch-Institute. *Daily situation reports.* `www.rki.de/DE/Content/InfAZ/N/Neuartiges_Coronavirus/Situationsberichte/Gesamt.html`.

[17] Johns Hopkins University. *Time series of confirmed COVID-19 cases globally.* `github.com/CSSEGISandData/COVID-19/blob/master/csse_COVID_19_data/csse_COVID_19_time_series/time_series_COVID19_confirmed_global.csv`. last visited: 18 December, 2023.

[18] Federal Government of Germany. *Guidelines for reducing social contacts*. `https:`
       `//www.bundesregierung.de/breg-de/themen/coronavirus/besprechung-`
       `der-bundeskanzlerin-mit-den-regierungschefinnen-und-regierungsch`
       `efs-der-laender-vom-22-03-2020-1733248`. last visited: 18 December, 2023.

[19] Federal Foreign Office of Germany. *Coronavirus / Covid-19: Reisewarnung für
       Staaten außerhalb der EU/Schengen-Gebiet*. `https://www.auswaertiges-amt.`
       `de/de/ReiseUndSicherheit/covid-19/2296762`. last visited: 18 December,
       2023.

[20] World Health Organization. *Coronavirus disease (COVID-19) Weekly Epidemio-
       logical Update and Weekly Operational Update*. `https://www.who.int/emergen`
       `cies/diseases/novel-coronavirus-2019/situation-reports`. last visited:
       18 December, 2023.

[21] Ministry of Health Republic of Indonesia. `https://www.kemkes.go.id/`. last
       visited: 18 December, 2023.

[22] Hempel, S. *The Medical Detective: John Snow and the Mystery of Cholera*. London:
       Granta, 2006.

[23] Ross, R. *The Prevention of Malaria*. John Murray, London, 1911.

[24] Bacaër, N. and Binder, C. *Eine kurze Geschichte der mathematischen Populations-
       dynamik*. Cassini, 2008.

[25] Mahmood, S.S. et al. "The Framingham Heart Study and the Epidemiology of
       Cardiovascular Diseases: A Historical Perspective". In: *Lancet* 383.9921 (2014),
       pp. 999–1008. DOI: `10.1016/S0140-6736(13)61752-3`.

Chapter 2

Mathematical and Epidemiological Tools

For readers of this thesis, pre-knowledge in linear algebra, calculus, integral theory, stochastics and statistics is required. However, some of the most important definitions, theorems and concepts that are required for understanding the upcoming mathematical theory and the research papers in Part II are introduced here.

2.1 Ordinary differential equations

2.1.1 Definitions

Before dealing with relevant models for disease dynamics, the most important mathematical tool in modelling the temporal evolution of quantities is introduced: the fundamental research findings related to ordinary differential equations. This will encompass a comprehensive overview of the theoretical foundations for finding solutions, as well as the numerical techniques used.

Definition 2.1 (Ordinary Differential Equations)**.** Let $\Omega \subset \mathbb{R} \times (\mathbb{R}^m)^n$ be an open set and let $f : \Omega \to \mathbb{R}^m$ be continuous. An *ordinary differential equation* (ODE) of order n is an equation of the form

$$u^{(n)}(t) = f\left(t, u(t), u'(t), u''(t), \ldots, u^{(n-1)}(t)\right). \tag{2.1}$$

Let the function $u : I \subset \mathbb{R} \to \mathbb{R}^m$ be n-times continuously differentiable, i.e., $u \in \mathcal{C}^n$, it is called a solution of the ordinary differential equation if it satisfies eqn. (2.1) and

$$\left(t, u(t), u'(t), u''(t), \ldots, u^{(n-1)}(t)\right) \in \Omega. \tag{2.2}$$

Definition 2.2 (Types of ODEs)**.** There are several types of ordinary differential equations, including:

- *First-Order ODEs*: Equations involving the first derivative of a dependent variable with respect to an independent variable, which are of the form

$$u'(t) = f(t, u).$$

- *Second-Order ODEs*: Equations involving the second derivative of a dependent variable with respect to an independent variable, which are of the form

$$u''(t) = f(t, u, u').$$

- *Linear ODEs*: Equations of the form

$$\sum_{k=0}^{n-1} a_k(t) u^{(k)}(t) = b(t).$$

- *Homogeneous ODEs*: Equations in which $b(t)$ is equal to zero, e.g.,

$$u'(t) + u(t) = 0.$$

- *Nonhomogeneous ODEs*: Equations in which $b(t)$ is not equal to zero, e.g.,

$$u'(t) + u(t) = t + 1.$$

- *Nonlinear ODEs*: Equations in which the coefficients of the derivatives and dependent variable are nonlinear, e.g.,

$$u'(t) = t^2 e^{u(t)}.$$

- *Autonomous ODEs*: Equations in which the right-hand side does not depend explicitly on the independent variable, e.g.,

$$u'(t) = u^2(t).$$

In the following, we will mainly restrict on *autonomous* and generally *nonlinear* ODEs.

Definition 2.3 (Initial Value Problem). Let $I \subset \mathbb{R}$ be an interval and $D \subset I \times \mathbb{R}^{n \times k}$ be the domain of definition of u with $k \in N$. Finding a continuously differential function $u : D \to R$ satisfying the (ordinary) differential equation (ODE)

$$\begin{aligned}
u'(t) &= f(t, u(t)) & \text{for all } t \in \mathbb{R}, \\
u(t_0) &= u_0 & \text{for } t_0 \in I
\end{aligned} \tag{2.3}$$

is called an *initial value problem* (IVP).

The theory of ODEs makes use of some results from functional analysis, which will be presented in the following.

2.1.2 Some results from functional analysis

Definition 2.4 (Banach Space). Let X be a vector space over the scalar field $\mathbb{K}$ (typically, $\mathbb{K} = \mathbb{R}$ or $\mathbb{K} = \mathbb{C}$), and let $\|\cdot\|$ be a norm. Let the metric $d(x, y) := \|x - y\|$ be induced over the norm. Any normed space $(X, \|\cdot\|)$ is called a *Banach space* if every Cauchy sequence with elements out of X converges with respect to the metric d.

This especially holds true for the space of continuous functions $V = \mathcal{C}(I, \mathbb{R}^m)$ and the infinity norm $\|\cdot\|_\infty$.

Definition 2.5 (Operator, Functional). A mapping $T : D \to W$ for a subset $D \subset V$ in two real and normed vector spaces $(V, \|\cdot\|_V)$ and $(W, \|\cdot\|_W)$ is referred to as an *operator*. It is called a *functional* if $W = \mathbb{R}$ or $W = \mathbb{C}$. Further on, T is called

- *linear* if $T[\alpha u + \beta v] = \alpha T[u] + \beta T[v]$ for all $\alpha, \beta \in \mathbb{R}$ and for all $u, v \in D$.

- *continuous* if for all sequences u_n satisfying $\lim\limits_{n \to \infty} u_n = u_0$, it holds true that $\lim\limits_{n \to \infty} T[u_n] = T[u_0]$.

- *Lipschitz (continuous)* if $\|T[u] - T[v]\|_W \leq q \|u - v\|_V$ for a constant $q > 0$ and for all $u, v \in D$.

- a *contraction* if T is Lipschitz with $q \in [0, 1)$.

- *bounded* if $\|T[u]\|_W \leq C \|u\|_V$ for a $C > 0$ and for all $u \in D$.

Theorem 2.6 (Banach's fixed point theorem). We consider a complete metric space (X, d), typically a Banach space with the distance metric $d(x, y) = \|x - y\|$. Let $M \subset X$ be a non-empty and closed set and let $\phi : M \to M$ be a contraction, i.e., $d(\phi(x), \phi(y)) \leq k \cdot d(x, y)$ for a $k \in [0, 1)$ and all $x, y \in M$. Further, let $x_{n+1} := \phi(x_n)$ be an iterative sequence with $x_0 \in M$. Then there exists a unique $\tilde{x} \in M$ satisfying $\phi(\tilde{x}) = \tilde{x}$ and $\lim\limits_{n \to \infty} x_n = \tilde{x}$.

Proof. For this proof, cf. e.g. Walter [1]. $\qquad \square$

2.1.3 Existence and uniqueness of solutions

With those results, we can now investigate the existence and uniqueness of solutions of IVPs.

Theorem 2.7 (Picard-Lindelöf theorem). Consider an IVP of the type as in Def. 2.3, let the function f be continuous wrt t and Lipschitz wrt u on D. Then the IVP (2.3) admits a unique solution on I.

Proof. A proof of the theorem can be found in Arnold [2]. $\qquad \square$

Another important theorem, in case the function is not Lipschitz, gives the existence (not uniqueness) of solutions if the function f is at least continuous.

Theorem 2.8 (Peano's theorem). Given a compact interval $I \subset \mathbb{R}$ and $m \in \mathbb{N}$, a closed and (simply) connected subset $G \subset \mathbb{R}^m$, another set $\Omega := I \times G$, a bounded function $f \in \mathcal{C}(\Omega)$, and $\xi, \eta \in \Omega$. Then, the IVP $u'(t) = f(x, u)$ with $u(\xi) = \eta$ has at least one solution in $\tilde{I} := I \cap \{|x - \xi| < \delta / \|f\|_\infty\}$, where δ is defined as the distance of η and ∂G.

Proof. A detailed proof of this theorem, built on the fixed point theorems of both *Arzelà-Ascoli* and *Schauder*, can e.g. be found in Walter [1]. $\qquad \square$

2.1.4 Analytical solution methods

In several cases, the solution of IVPs can be explicitly calculated by various techniques, e.g., by separation of variables (cf. Aulbach [3]):

Example 2.9. Let $u'(t) = \alpha \cdot u$, with some initial condition $u(0) = u_0$. To solve this ODE, the separation of variables involves isolating the variable u on one side of the equation and the variable t on the other side. Solving the ODE by separation of variables, we get the exponential growth function

$$\ln |u| = \alpha t + c,$$
$$u(t) = c e^{\alpha t} = u_0 e^{\alpha t}, \tag{2.4}$$

where c is a constant of integration and is calculated by the initial condition $u(0) = u_0$. The solution along the *directional field* can be seen in Fig. 2.1 for parameter choices of $\alpha = 1/3$ and $u_0 = 1$. An example of this exponential growth in epidemiology can be found in the early stages of a disease outbreak.
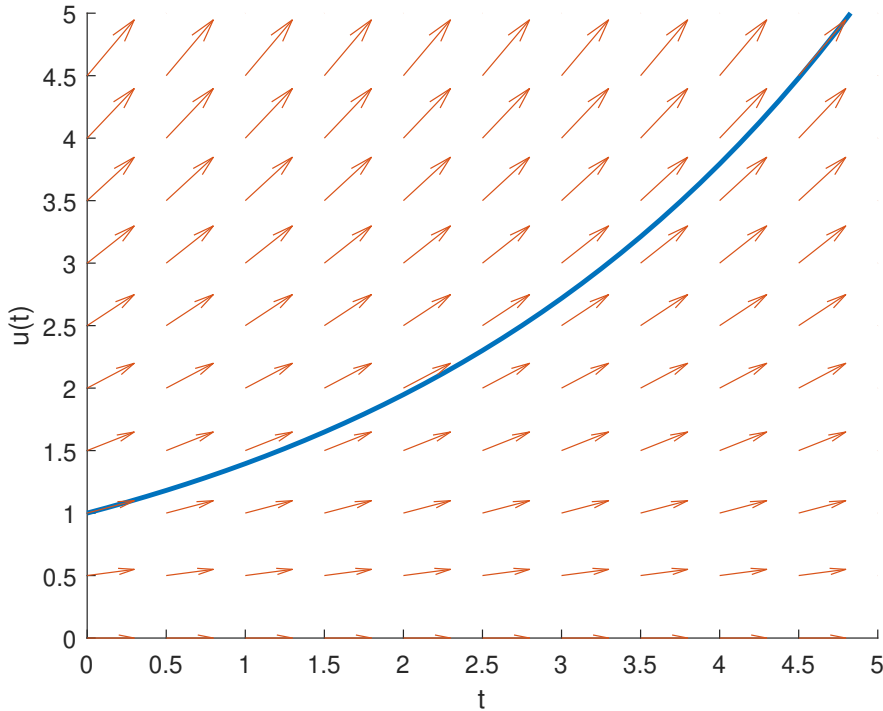
FIGURE 2.1: Directional fields and solution of the ODE in Ex. 2.9.

Example 2.10. Let $u : \mathbb{R} \to \mathbb{R}^2$, $u(t) = (x(t), y(t))^T$ and $\alpha > 0$. Also let $x + y = 1$. Consider the following equations:

$$x'(t) = -\alpha xy, \qquad\qquad\qquad x(0) = x_0, \qquad\qquad (2.5a)$$
$$y'(t) = \alpha xy, \qquad\qquad\qquad y(0) = y_0. \qquad\qquad (2.5b)$$

To solve the system, we can substitute $y = 1 - x$ into the second equation to obtain a single first-order ordinary differential equation:

$$\frac{dx}{dt} = -\alpha x(1 - x) \qquad\qquad (2.6)$$

First, the variables are seperated by moving terms involving x to one side and terms involving t to the other side, so that the integrated equation looks as follows:

$$\int \frac{dx}{x(1 - x)} = -\int \alpha \, dt \qquad\qquad (2.7)$$

After some mathematical manipulations, we find

$$x(t) = \frac{1}{ce^{\alpha t} + 1}. \qquad\qquad (2.8)$$

To determine the constant c, we use the initial condition $x(0) = x_0$ and find

$$c = \frac{1 - x_0}{x_0} = \frac{y_0}{x_0}. \tag{2.9}$$

This gives an analytic solution to a simple *SI*-model which is one of the basic tools in this work. More complicated models, where an analytical solution can not be found that easily, are presented in chapter 2.3 and several papers in part II.

2.1.5 Numerical solution methods

In many of the upcoming problems, however, we can only solve the problems *numerically* as no analytical solution methods for the (complex) problems are available. Therefore, we make use of numerical methods. One of the most simple ones is the

Definition 2.11 (Euler method). Given the IVP as of Def. 2.3, we discretize the derivative $u'(t)$ using the forward difference

$$u'(t) \approx \frac{u(t + h) - u(t)}{h}, \tag{2.10}$$

such that

$$u(t + h) \approx u(t) + h \cdot f\left(t, u(t), u'(t), \dots, u^{(k)}(t)\right). \tag{2.11}$$

We discretize of the previously continuous time interval $[t_0, T]$ into $t_i = t_0 + (i - 1)h$ for all $i = 1, \dots, n$ and $h = (T - t_0)/n$, such that $u_i := y(t = t_i)$ is defined over

$$u_{i+1} = u_i + h \cdot f(t_i, x_i). \tag{2.12}$$

In this notation, $\psi(t_i, u_i) = f(t_i, u_i)$ is called *increment function* of the method. We can also discretize the right-hand side such that we receive an *implicit* Euler method, which in general leads to a non-linear equation we have to solve in each step:

$$u_{i+1} = u_i + h \cdot f(t_{i+1}, u_{i+1}) \tag{2.13}$$

Definition 2.12 (Consistency). For an IVP of the form (2.3), let ψ be the increment function. Then the *consistency error* e_h is defined as

$$e_h(t, u) = \frac{u(t + h) - u(t)}{h} - \psi(t, u, h). \tag{2.14}$$

For the explicit Euler method, this reads as $\psi(t, u, h) = f(t, u)$. The method is *consistent* if for $h \to 0$, it holds $|e_h| \to 0$ for all $t_0 < t < T$. If $e_h(t, u) = \mathcal{O}(h^p)$, then the system is *consistent of order p*.

Both Euler methods are first-order consistent, such that the error is linearly dependent on the step size. A classical example for higher-order schemes is the so-called

Definition 2.13 (Runge-Kutta scheme). Given an IVP as of Def. 2.3, the (fourth-order) *Runge-Kutta scheme* reads as follows:

$$k_1 = f(t_i, x_i), \tag{2.15a}$$

$$k_2 = f\left(t_i + \frac{h}{2}, x_i + \frac{h}{2}k_1\right), \tag{2.15b}$$

$$k_3 = f\left(t_i + \frac{h}{2}, x_i + \frac{h}{2}k_2\right), \tag{2.15c}$$

$$k_4 = f\left(t_i + h, x_i + hk_3\right), \tag{2.15d}$$

$$u_{i+1} = u_i + \frac{h}{6}\left(k_1 + 2k_2 + 2k_3 + k_4\right). \tag{2.15e}$$

Higher-order schemes are possible by using more grid points for each calculation and/or adaptive step sizes h_i. For this we introduce the notation via the

Definition 2.14 (Butcher tableau). Let $\psi(t, u, h) : [t_0, T] \times \mathbb{R} \times \mathbb{R}_+ \to \mathbb{R}$ be the increment of a numerical one-step or multi-step method, defined over the step functions $k_i, i = 1, \ldots, n$:

$$k_i(t, x, h) = f\left(t_i + c_i h, x + h \sum_{i=1}^{n} a_{ij} k_j\right), \tag{2.16}$$

$$\psi(t, x, h) = \sum_{i=1}^{n} b_i k_i. \tag{2.17}$$

Then the coefficients b_i, c_i and a_{ij} are collected in the Butcher tableau as follows:

$$\begin{array}{c|c} c & A \\ \hline & b^T \end{array} \tag{2.18}$$

For the Runge-Kutta scheme as of eqns. (2.15), the Butcher tableau has the following form:

$$\begin{array}{c|cccc} 0 & 0 \\ \frac{1}{2} & \frac{1}{2} & 0 \\ \frac{1}{2} & 0 & \frac{1}{2} & 0 \\ 1 & 0 & 0 & 1 & 0 \\ \hline & \frac{1}{6} & \frac{1}{3} & \frac{1}{3} & \frac{1}{6} \end{array}$$

The standard solvers in MATLAB and PYTHON use a Runge-Kutta scheme *RK4(5)* according to Fehlberg, which is of order $\mathcal{O}(h^5)$. It is a type of adaptive step size control method, which means that the step size h is adjusted during the computation to ensure a desired level of accuracy. For more information, refer e.g. to Deuflhard [4], p. 209.

The *RK4(5)* method uses four stages, as in the standard Runge-Kutta method, yet additionally includes a fifth stage to estimate the error in the solution. This is done by combining a fourth-order and a fifth-order method to approximate the solution at each step, and then comparing the results. If the error exceeds a certain tolerance, the step size is decreased, and if the error is below the tolerance, the step size is increased.

For the Butcher tableau representation, we require two different vectors b_1 and b_2:

$$
\begin{array}{c|cccccc}
\frac{1}{4} & \frac{1}{4} \\
\frac{3}{8} & \frac{3}{32} & \frac{9}{32} \\
\frac{12}{13} & \frac{1932}{2197} & -\frac{7200}{2197} & \frac{7296}{2197} \\
1 & \frac{439}{216} & -8 & \frac{3680}{513} & -\frac{845}{4104} \\
\frac{1}{2} & -\frac{8}{27} & 2 & -\frac{3544}{2565} & \frac{1859}{4104} & -\frac{11}{40} \\
\hline
& \frac{25}{216} & 0 & \frac{1408}{2565} & \frac{2197}{4104} & -\frac{1}{5} & 0 \\
& \frac{16}{135} & 0 & \frac{6656}{12825} & \frac{28561}{56430} & -\frac{9}{50} & \frac{2}{55}
\end{array}
$$

Using the increment ψ_1 leads to a Runge-Kutta method of order $p = 5$, while ψ_2 leads to a Runge-Kutta method of order $p = 4$. We calculate the update of the step size by

$$
h_{new} = \min\left(h_{\max}, qh, h\,^{p+1}\!\sqrt{\frac{\rho\tau}{\epsilon}} \right), \tag{2.19}
$$

with $h_{\max}$ as a maximum bound on the step size h, τ as the difference of the numerical solutions, and ρ, q being two arbitrary parameters. Typically, it is set $q \approx 5$ and $\rho \in [0.5, 0.75]$. The error between those two methods is as usual denoted by

$$
\text{TE} = |\psi_1 - \psi_2|. \tag{2.20}
$$

If $\text{TE} > \varepsilon$, the current step is repeated with h_{new}, otherwise we move on to the next step. For order schemes, e.g. the eigth-order scheme of Dormand-Prince, refer e.g. to Deuflhard [4], p. 209.

2.1.6 Equilibria and stability

Definition 2.15 (Equilibrium)**.** Let $f : \mathbb{R}^n \to \mathbb{R}^n$ be a continuously differentiable function, and let the resulting autonomous ODE $u'(t) = f(u(t))$. Then, a stationary solution $u^* : \mathbb{R} \to \mathbb{R}^n$ with $f(u^*) = 0$ is called an *equilibrium* of the ODE. It has to be noted that the equilibria are independent of the respective initial condition.

Example 2.16. Reconsider Ex. 2.10. The equilibria for eqn. (2.6) are $x_1^* \equiv 0$ and $x_2^* \equiv 1$.

At any of the equilibria, we aim to observe on how the systems behave given small disturbances. Therefore, we will make use of the *stability theory*.

Definition 2.17 (Stability)**.** For an $\alpha > 0$, let f be a continuous function on the space

$$
S_\alpha := \{(t, y) : 0 \le t < \infty, \|y - u(t)\| < \alpha\}. \tag{2.21}
$$

A solution $u(t)$ of $u' = f(t, u)$ on the interval $[0, \infty)$ is called *stable*, if for any $\varepsilon > 0$ and $t \in \mathbb{R}_+$, there exists a $\delta = \delta(\varepsilon) > 0$ such that for all solutions λ with initial values $\lambda_0 \in \mathbb{R}^n$ with $\|\lambda_0 - u(0)\| < \delta$, the solutions $\lambda(t)$ exist for all $t \ge 0$ and satisfy $\|\lambda(t) - u(t)\| < \varepsilon$. It is called *asymptotically stable*, if it is stable and additionally it holds

$$
\lim_{t \to \infty} \|\lambda(t) - u(t)\| = 0. \tag{2.22}
$$

It is called *unstable* if it is not stable. Summing things up, this means that if $u(t) \to u^*$ in a neighbourhood of u^* for $t \to \infty$, then the equilibrium is stable, otherwise instable.

To prove the stability or instability of an equilibrium of linear autonomous systems, we introduce the

Definition 2.18 (Jacobian, Hessian)**.** Let $f : \mathbb{R}^n \to \mathbb{R}^n$ be a function whose first-order partial derivatives exist on $\mathbb{R}^n$. Then, the *Jacobian* of this function reads as

$$J_f = \begin{pmatrix} \frac{\partial f_1}{\partial x_1} & \cdots & \frac{\partial f_1}{\partial x_n} \\ \vdots & \ddots & \vdots \\ \frac{\partial f_n}{\partial x_1} & \cdots & \frac{\partial f_n}{\partial x_n} \end{pmatrix} \tag{2.23}$$

The *Hessian* of this function reads as

$$H_f = \begin{pmatrix} \frac{\partial^2 f_1}{\partial x_1^2} & \cdots & \frac{\partial^2 f_1}{\partial x_1 \partial x_n} \\ \vdots & \ddots & \vdots \\ \frac{\partial^2 f_n}{\partial x_m \partial x_1} & \cdots & \frac{\partial^2 f_n}{\partial x_n^2} \end{pmatrix} \tag{2.24}$$

Definition 2.19. Given a continuously differentiable function $f : \mathbb{R}^n \to \mathbb{R}^n$ and a stationary point u^* of the linear and non-autonomous ODE $u' = A(t)u + b(t)$, where $A(t) : \mathbb{R}^+ \to \mathbb{R}^{n \times n}$ and $b(t) : \mathbb{R}^+ \to \mathbb{R}^n$ are continuous functions. Let $D_f(u^*)$ be the Jacobian of f evaluated at u^*. Then u^* is called

- *stable* if the real part $\Re(\lambda) \leq 0$ for all $\lambda \in \sigma\left(D_f(u^*)\right)$.

- *asymptotically stable* if $\Re(\lambda) < 0$ for all $\lambda \in \sigma\left(D_f(u^*)\right)$.

- *unstable* if $\Re(\lambda) > 0$ for at least one $\lambda \in \sigma\left(D_f(u^*)\right)$.

For non-linear ODEs, which we will mainly consider in the upcoming epidemiological models, we have to make use of *linearization*, which can be done applying the *Taylor expansion* around the stability point, i.e.,

$$f(u) = f(u^*) + f'(u^*)(u - u^*) + \mathcal{O}(|u - u^*|^2). \tag{2.25}$$

This leads us to the following

Definition 2.20 (Asymptotic Stability)**.** Given a continuously differentiable function $f : \mathbb{R}^n \to \mathbb{R}^n$ and a stationary point u^* of the non-linear, but autonomous ODE $u'(t) = f(u(t))$, let $D_f(u^*)$ be the Jacobian of f evaluated at u^*. Then the stationary solution u^* is *asymptotically stable* if for all $\lambda \in \sigma(D_f(u^*)$ it holds $\Re(\lambda) < 0$. It is *unstable* if there exists at least one $\tilde{\lambda} \in \sigma(D_f(u^*)$ satisfying $\Re(\tilde{\lambda}) < 0$.

This means, that the asymptotic stability or non-stability of the linearization leads to asymptotic stability or non-stability of the nonlinear problem. However, if the linearized problem is 'only' stable, no direct statement about the nonlinear problem is possible. Another technique to show stability are *Lyapunov functions* (cf. e.g. Aulbach [3], Walter [1] or Deuflhard and Bornemann [4]).

An aspect we will also consider in the contributions is the dependence of the solution u with respect to certain parameters, e.g., the parameter α in Ex. 2.10.

Definition 2.21 (Sensitivity)**.** Let $f : \mathbb{R}^n \to \mathbb{R}^n$ be a continuously differentiable function and $\lambda = \left(\lambda_1, \ldots, \lambda_p\right)^T \in \mathbb{R}^p$. Consider the following IVP:

$$u'(t) = f(t, u, \lambda), \qquad\qquad u(t_0) = u_0(\lambda). \tag{2.26}$$

Then

$$\sigma_i(t) := \frac{\partial}{\partial \lambda_i} u(t, \lambda) \tag{2.27}$$

is called the *sensitivity* of u wrt the parameter λ_i. For all $i = 1, \ldots, p$, the sensitivity can be computed by (cf. [5])

$$\sigma_i' = \frac{\partial f}{\partial u} \cdot \sigma_i + \frac{\partial f}{\partial \lambda_i} \qquad \text{for all } t \in \mathbb{R},$$

$$\sigma_i(t_0) = \frac{\partial u_0}{\partial \lambda_i}. \tag{2.28}$$

Example 2.22. Again we consider a problem similar to Ex. 2.10. Let $\lambda = (\alpha, \beta)^T$ and let the IVP be defined as follows:

$$x'(t) = -\alpha x(1 - x) =: f(t, x, \alpha), \qquad x(0) = x_0(\beta) := \beta, \tag{2.29}$$

with the solution

$$x(t, \alpha, \beta) = \frac{c}{e^{\alpha t} + c} = \frac{\beta}{(1 - \beta) e^{\alpha t} + \beta}. \tag{2.30}$$

Then the sensitivities of this IVP are computed by

$$\sigma_\alpha(t) = \frac{\partial}{\partial \alpha} x(t, \lambda) = -\frac{(1 - \beta)\beta \, t \, e^{\alpha t}}{((1 - \beta) e^{\alpha t} + \beta)^2}, \tag{2.31a}$$

$$\sigma_\beta(t) = \frac{\partial}{\partial \beta} x(t, \lambda) = \frac{e^{\alpha t}}{((1 - \beta) e^{\alpha t} + \beta)^2}, \tag{2.31b}$$

and satisfy the IVPs

$$\sigma_\alpha' := \frac{\partial f}{\partial x} \cdot \sigma_\alpha + \frac{\partial f}{\partial \alpha} = -\alpha(1 - 2x) \cdot \sigma_\alpha - x(1 - x), \qquad \sigma_\alpha(0) = \frac{\partial u_0}{\partial \alpha} = 0, \tag{2.32a}$$

$$\sigma_\beta' := \frac{\partial f}{\partial x} \cdot \sigma_\beta + \frac{\partial f}{\partial \beta} = -\alpha(1 - 2x) \cdot \sigma_\beta, \qquad \sigma_\beta(0) = \frac{\partial u_0}{\partial \beta} = 1. \tag{2.32b}$$

For Ex. 2.22, solving the IVPs in eqns. (2.32) will lead back to the solution of eqn. (2.30).

2.2 Partial differential equations

Before presenting the central term of this section, the definition of partial differential equations, we will first introduce the following notation for the

Definition 2.23 (Multi-Index, Multivariate Partial Derivative)**.** We denote

$$D^\alpha(u) := \frac{\partial^{|\alpha|} u}{\partial_{x_1}^{\alpha_1} \ldots \partial_{x_n}^{\alpha_n}} = \partial_{x_1}^{\alpha_1} \ldots \partial_{x_n}^{\alpha_n} u \tag{2.33}$$

as the *multivariate partial derivative* of u wrt the *multi-index* $\alpha = (\alpha_1, \ldots, \alpha_n)$, where $|\alpha| := \sum_{i=1}^{n} \alpha_i$.

Using this notation, differential equations with functions depending on more than one parameter can be defined as follows:

Definition 2.24 (Partial Differential Equation). Let $\Omega \subset \mathbb{R}^n$ be an (open) domain, $u : \Omega \to \mathbb{R}$ and $f : \Omega \times \mathbb{R} \times \mathbb{R}^n \times \cdots \times \mathbb{R}^{n \times k}, k \in N$.

$$f\left(x, u(x), Du(x), D^2u(x), \ldots, D^k u(x)\right) = 0 \tag{2.34}$$

is called an kth *order partial differential equation* (PDE) of u. If $u : \Omega \to \mathbb{R}$ solves the PDE (2.34) for all $x \in \Omega$, we call u a *classical solution* of the PDE.

Definition 2.25 (Types of second-order PDEs). Given functions $a, b, c, d, e, f : \mathbb{R}^2 \to \mathbb{R}$, let a second-order PDE be notated as

$$a \frac{\partial^2 u}{\partial x_1{}^2} + b \frac{\partial^2 u}{\partial x_1 \partial x_2} + c \frac{\partial^2 u}{\partial x_2{}^2} + d \frac{\partial u}{\partial x_1} + e \frac{\partial u}{\partial x_2} + fu = g. \tag{2.35}$$

Then the corresponding PDE is called

- *hyperbolic* if $b^2 - 4ac > 0$. The solutions are classically describing wave propagation.

- *parabolic* if $b^2 - 4ac = 0$. Those are used e.g. in the heat conduction equation.

- *elliptic* if $b^2 - 4ac < 0$. The most simple example is the Laplace equation, i.e., $\Delta u(x) = u_{xx} + u_{yy} = 0$, which is equivalent to the steady-state heat equation.

Specific properties of each of the three types make it possible to determine appropriate solution methods for each of those types, and the smoothness of a solution given the geometry and initial/boundary conditions can be determined by its type. For example, the wave propagation in hyperbolic PDEs indicates that 'jumps' in the initial condition will propagate onwards.

Definition 2.26 (Boundary conditions for PDEs). Given functions $f, a, b : \mathbb{R}^2 \to \mathbb{R}$ and a PDE as of eqn. (2.34), boundary conditions can be of the following types:

- *Dirichlet* type if $u(x, y) = f(x, y)$ on the boundary $\partial \Omega$.

- *Neumann* type if $\partial_n u(x, y) = f(x, y)$ on the boundary $\partial \Omega$, where $\partial_n u$ denotes the *outer normal derivative* of the function u at the boundary $\partial \Omega$.

- *Robin* type if $au(x, y) + b \partial_n u(x, y) = f(x, y)$ on the boundary $\partial \Omega$.

Example 2.27. As an example of an analytical solution to a PDE, we consider the linear advection equation $u_t + u_x = 0$ with the initial condition $u(0, x) = \cos(x)$ which can be solved using the *method of characteristics*. Its characteristic equations are given by:

$$\frac{dt}{ds} = 1, \qquad\qquad t(0) = 0 \tag{2.36a}$$

$$\frac{dx}{ds} = 1, \qquad\qquad x(0) = x_0 \tag{2.36b}$$

$$\frac{du}{ds} = 0, \qquad\qquad u(0, x_0) = \cos(x_0). \tag{2.36c}$$

Solving the first two equations gives $t = s$ and $x = s + x_0$. Using the initial condition $u(0, x) = \cos(x_0)$, we have $u(s, x_0) = \cos(x_0)$ along the characteristic curve $x = t + x_0$.

Solving for x_0 yields $x_0 = x - t$, and substituting this into the expression for $u(t, x)$ gives the solution:

$$u(t, x) = \cos(x - t) \tag{2.37}$$

A practical example of a numerical solution technique for PDEs can be found in section 2.3.6.

2.3 Epidemiological models

We will first introduce the three most common epidemic models which are the basis for the upcoming modelling papers. Also, vector populations can be included in those

2.3.1 SIS-/SIR-/SEIR-models

A standard tool in epidemiological modelling is the *SIR*-model introduced by Kermack and McKendrick [6], the *SEIR*–model, as well as their variations. Analogously to e.g. [7], consider functions $S, E, I, R, N \in \mathcal{C}(V, \mathbb{R})^{2,1}$ (which means they are twice continuously differentiable wrt space and once continuously differentable wrt time) as follows:
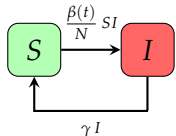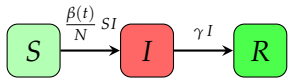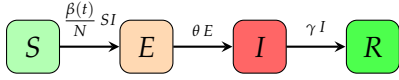
- Susceptibles S: Depending on the transmission route, these individuals can become infected with the disease when contact occurs.

- Exposed E: The corresponding indiviuals have already ingested the pathogen, but are not yet infectious because they are still in the latency period.

- Infected I: These individuals are infected with the disease and infectious. A contact with a susceptible individual can therefore lead to transmission of the disease.

- Recovered R: After facing out an infection, individuals are considered recovered. These individuals can no longer transmit the disease or get infected. Sometimes, an additional subdivision of deceased persons D is introduced in order to describe the amount of persons which have died as a result of the disease.

For instance, $I(t)$ indicates the number of infected individuals at time $t \geq 0$. The total number of individuals is typically the sum of the subdivision, i.e., $N = S + E + I + R$, and is typically assumed to be constant. The systems of three commonly used models, presented in the form of ODEs, are outlined in Tab. 2.1.

At the core of every epidemiological model is the incidence term $\frac{\beta(t)}{N} SI$, which shows how many people are newly infected with the disease at time t. The incidence term relies on a transmission rate $\beta : [0, t_{end}] \rightarrow (0, \infty)$ that can vary over time, potentially due to changes in population restrictions. The exact value of β is usually unknown and must be determined using data. The *SIR*- and *SEIR*-models also include the recovery rate γ, which is the inverse of the average time it takes for an individual to recover from the disease. For example, if recovery takes 10 days on average, then $\gamma = 0.1$. The *SEIR*-model makes use of the parameter θ, which is the inverse of the latency period, or the time between contracting the pathogen and becoming infectious. For example, if the latency period is 3 days, then $\theta = 1/3$. It is important to say that the latency period does not have to be the same as the incubation period, which is the

time between infection and the onset of symptoms. In regards to COVID-19, research has shown that individuals can be infectious before displaying symptoms [8].

TABLE 2.1: Basic examples of epidemiological ODE models with flow chart and equation system.

Model	Structure	ODE System
SIS		$S' = -\dfrac{\beta(t)}{N}SI + \gamma I, \quad S(t=0) = S_0,$ $I' = \dfrac{\beta(t)}{N}SI - \gamma I, \qquad I(t=0) = I_0,$ $N = S + I.$
SIR		$S' = -\dfrac{\beta(t)}{N}SI, \qquad S(t=0) = S_0,$ $I' = \dfrac{\beta(t)}{N}SI - \gamma I, \quad I(t=0) = I_0,$ $R' = \gamma I, \qquad\qquad R(t=0) = R_0,$ $N = S + I + R.$
SEIR		$S' = -\dfrac{\beta(t)}{N}SI, \qquad S(t=0) = S_0,$ $E' = \dfrac{\beta(t)}{N}SI - \theta E, \quad E(t=0) = E_0,$ $I' = \theta E - \gamma I, \qquad I(t=0) = I_0,$ $R' = \gamma I, \qquad\qquad R(t=0) = R_0,$ $N = S + E + I + R.$

Many models also integrate birth rates, denoted by μ, which contribute to the amount of susceptible persons. Typically, it is assumed that the population remains constant, with birth and immigration rates equal death and emigration rates; thus, μ^{-1} can be interpreted the average life expectancy. This is likely not accurate in reality. As an example, Jakarta and its districts, which we will examine in chapter 3, like most large cities, feature a growing population. However, this will not have a significant impact on a small time scale we are considering for the overall population numbers. For models that cover a longer time frame, it may be necessary to incorporate varying birth and death rates. For more information about that, also refer to e.g. Martcheva [9].

2.3.2 SIRUV-model

We can include the dynamics of *vector populations* in our disease models for a more realistic approach. In practice, we add both the susceptible vector population U and the infected vector population V to the classical epidemiological model, referred to as the *SIRUV* model, which includes the human populations of S, I, and R. Assuming that the birth and death rate of vector populations, such as mosquitoes in the case of

Dengue, are constant and equal, the total number of vectors M is also constant:

$$M = U + V \tag{2.38}$$

Assuming that all susceptible humans and vectors have the same 'chance' of coming into contact with infected individuals, the probability of disease transmission is then proportional to the product of the respective susceptible and infectious populations. The amount of susceptible humans who become infected is equal to $\frac{\beta}{M} \cdot S \cdot V \, dt$, and the amount of susceptible vectors who become infected is equal to $\frac{\rho}{N} \cdot U \cdot I \, dt$. We assume that both transmission rates β and ρ are constant. The (human) recovery rate is then equivalent to the inverse of the recovery time, i.e., τ^{-1}, and thus the number of individuals who recover in a certain time interval is $\tau \cdot I \, dt$. Recovered individuals can become infected again after a time κ^{-1}, so the number of recovered individuals returning to the susceptible population is $\kappa \cdot R \, dt$. Since vectors do not have an immune system, there is no recovery after being infected and also no subpopulation of recovered vectors. The differential equation system, enhanced by equal birth and death rates μ for humans and ϑ for vectors, reads as follows:

$$S' = \mu \cdot (N - S) - \frac{\beta \cdot S \cdot V}{M} + \kappa \cdot R \tag{2.39a}$$

$$I' = -(\mu + \tau) \cdot I + \frac{\beta \cdot S \cdot V}{M} \tag{2.39b}$$

$$R' = -(\mu + \kappa) \cdot R + \tau \cdot I \tag{2.39c}$$

$$U' = \vartheta \cdot (M - U) - \frac{\rho \cdot U \cdot I}{N} \tag{2.39d}$$

$$V' = -\vartheta \cdot V + \frac{\rho \cdot U \cdot I}{N} \tag{2.39e}$$

One issue for practical computation of the ODE system (2.39) lies in the lack of reliable data on the number of vectors. However, by using the *steady-state approximation*, it is possible to eliminate the vector populations from the model:

Given that the life expectancy of vectors is much shorter than that of humans, i.e. $\vartheta^{-1} \ll \mu^{-1}$, after a relatively short initial period, both vector populations do not change over time and remain constant. This allows for the calculation of their equilibrium values and replacement of the infected vector population in eqns. (2.39) with the equilibrium value. This approximation is only valid if the observed time interval is significantly larger than ϑ^{-1}, which, in the case of mosquitoes, is typically a value of around 2 weeks. For more information on this, cf. [10, 11].

The equilibria of the vector populations are reached if $U' = 0$ and $V' = 0$. Defining $\lambda := \frac{\vartheta}{\rho} \cdot N$, this is equivalent to

$$U^* = \frac{M}{1 + \frac{\rho}{\vartheta \cdot N} I^*} = \frac{\lambda M}{\lambda + I^*} \tag{2.40a}$$

$$V^* = \frac{M \cdot I^*}{\frac{\vartheta N}{\rho} + I^*} = \frac{M \cdot I^*}{\lambda + I^*} \tag{2.40b}$$

We can now substitute the infected vector population V in equations (2.40) with its equilibrium, effectively disregarding the vector populations in the model. Additionally, since we know that $S(t) + I(t) + R(t) = N$ for all $t \geq 0$, one of the three human population equations can be omitted due to redundancy. In this case, we eliminate the equation for susceptibles, as the infectious class is the most critical to consider

and the equation for recovered individuals is simpler to compute. This results in the following system:

$$I' = -(\mu + \tau) \cdot I + \frac{\beta \cdot (N - I - R) \cdot I}{\lambda + I} \tag{2.41a}$$

$$R' = -(\mu + \kappa) \cdot R + \tau \cdot I \tag{2.41b}$$

While μ, τ, κ and N are parameters which we 'know' or are able to estimate by provided medical or statistical data, λ and β still remain variable. For the case of Dengue, with seasonal and other effects which have to be considered, assuming both of them to be constant is also not very useful. To account for these effects, there are several options. Two of the most common approaches are presented in the following. Firstly, we can assume that β is piecewise constant over a period of time $[t_i, t_{i+1}]$. This, for example, applies well for a time-restricted lockdown, effectively reducing the transmission rate $\beta = \beta(t)$.

$$\beta(t) := \begin{cases} \beta_0, & t_0 \leq t < t_1 \\ \quad \dots \\ \beta_n, & t_n \leq t < t_{n+1} \end{cases} \tag{2.42}$$

Another possibility that accounts more for seasonally changing transmission rates – which is, e.g., the case for the Dengue transmission in regions with monsoon seasons – is the following: Suppose that β is a periodic function of time, represented by a finite Fourier series:

$$\beta = \beta(t) = \beta_0 + \sum_{i=1}^{K} c_i \cdot \cos(2\pi\omega_i t + \phi_i) \tag{2.43}$$

With the restriction

$$\beta_0 \geq \sum_{i=1}^{K} c_i, \tag{2.44}$$

it is assured that $\beta(t) \geq 0$ for all t. Because of that, given a transmission, a biologically implausible possibility of an *increasing* number of susceptible persons after transmission, together with a *decreasing* amount of infectious persons, is prevented. In order to find reasonable values of λ and all parameters related to β, we have to perform *parameter estimation* in some way which finds the optimal parameters compared to scientific data sets. This will be discussed in detail in section 2.4.

2.3.3   Equilibria and stability of the SIRUV-model

As already mentioned for the vector population in section 3.1, the equilibria of the model as described in eqns. (2.41) are computed by $(I', R') = (0, 0)$. Here, we only consider the autonomous part of $\beta(t)$ which is β_0, neglecting the non-autonomous, periodic part.

   A *disease-free equilibrium* (DFE) is reached at $(I_1^*, R_1^*) = (0, 0)$; this means that there is an equilibrium if the disease dies out and the whole human population belongs to the susceptible class, i.e., $N = S$. The *endemic equilibrium* is reached if the following

equations hold:

$$I_2^* = \frac{\beta_0 \cdot N - \lambda \cdot (\mu + \tau)}{\mu + \tau + \beta_0 \cdot (1 + \frac{\tau}{\mu + \kappa})}, \tag{2.45a}$$

$$R_2^* = \frac{\tau}{\mu + \kappa} \cdot I_2^*. \tag{2.45b}$$

For stability analysis, we compute the *basic reproductive number* $\mathcal{R}_0$ by the next-generation method according to van den Driessche and Watmough [12]. For that, we only need to consider all infectious subpopulations, which, in this model, is just I. Eqn. (2.41) is divided into two parts: the number of new infections in the infective department F_I, and the number of outgoing individuals W_I:

$$I' = F_I - W_I \tag{2.46}$$

with

$$F_I = \frac{\beta_0 \cdot (N - I - R) \cdot I}{\lambda + I}, \tag{2.47a}$$

$$W_I = (\mu + \tau) \cdot I. \tag{2.47b}$$

The basic reproductive number can be interpreted as the number of secondary infections of a single infected person in an entirely susceptible population. The next step involves calculating the Jacobian matrices of F_I (denoted as J_F) and W_I (denoted as J_W). After derivation of F_I and W_I after I, we set $I = R = 0$, as we are assuming an initially entirely susceptible population and observing the changes that occur when a single infective individual is introduced.

$$J_F = \left. \frac{\partial F_I}{\partial I} \right|_{I=R=0} = \frac{\beta_0 \cdot N}{\lambda}, \tag{2.48a}$$

$$J_W = \left. \frac{\partial W_I}{\partial I} \right|_{I=R=0} = \mu + \tau. \tag{2.48b}$$

For the next-generation matrix, we compute the largest eigenvector of FW^{-1}, i.e.,

$$\mathcal{R}_0 = \rho(FW^{-1}) = \frac{\beta_0 N}{(\mu + \tau) \cdot \lambda}. \tag{2.49}$$

If $\mathcal{R}_0 > 1$, meaning $\beta_0 N > (\mu + \tau) \cdot \lambda$, the expected number of secondary infections exceeds the number of primary infections and thus the disease becomes epidemic. In this case, the DFE (I_1^*, R_1^*) is unstable. This can be shown by linearizing the system around the equilibrium and computing the largest real eigenvalues of the Jacobian, which are negative if $\mathcal{R}_0 > 1$; if $\mathcal{R}_0 < 1$, the number of secondary infections is lower than the number of primary infections and thus the disease dies out eventually. This corresponds to an asymptotically stable disease-free equilibrium, which can also be shown by linearizing the system.

The endemic equilibrium (I_2^*, R_2^*) is asymptotically stable if $\mathcal{R}_0 > 1$, this can also be shown using linearization. In case of $\mathcal{R}_0 < 1$, eqn. (2.45) implies $I_2^* < 0$ as the denominator is always greater than 0 and the nominator gets less than 0; thus, a realistic endemic equilibrium does not exist.

2.3.4   PDE models

In order to be able to model the spatial spread of infections, we use an epidemiological reaction–diffusion model. For this purpose, we consider a corresponding two-dimensional area Ω and a time interval $\mathcal{T}$. We are looking for a function $u : V \to \mathbb{R}^m$ with $V = \Omega \times \mathcal{T}$, which is twice continuously differentiable on Ω and once continuously differentiable on $\mathcal{T}$, briefly $u \in \mathcal{C}(V, \mathbb{R}^m)^{2,1}$. Assuming no flux at the boundary $\partial\Omega$, the following PDE system with homogeneous Neumann boundary conditions has to be fulfilled:

$$\partial_t u = \kappa \Delta_{x,y} u + f(u), \tag{2.50a}$$

$$u = u_0, \qquad\qquad t = 0, \tag{2.50b}$$

$$\partial_\nu u = 0, \qquad\qquad (x,y) \in \partial\Omega. \tag{2.50c}$$

Here, $\partial_t u$ stands for the component-wise derivative of u in the direction of time, i.e.,

$$\partial_t u = \left(\frac{\partial u_1}{\partial t}, \dots, \frac{\partial u_m}{\partial t} \right)^T, \tag{2.51a}$$

$$\Delta_{x,y} = \left(\frac{\partial^2 u_1}{\partial x^2} + \frac{\partial^2 u_1}{\partial y^2}, \dots, \frac{\partial^2 u_m}{\partial x^2} + \frac{\partial^2 u_m}{\partial y^2} \right)^T \tag{2.51b}$$

for the Laplacian in Ω. The parameter κ describes the diffusivity of the system and the function $f(u)$ contains the epidemiological component(s). As an initial condition at time $t_0 = 0$, a function $u_0 : \Omega \to \mathbb{R}^m$ is used with $u(x,y,t=0) = u_0(x,y)$. In addition, Neumann boundary conditions are used, where

$$\frac{\partial u}{\partial \nu} = \left(\frac{\partial u_1}{\partial \nu}, \dots, \frac{\partial u_m}{\partial \nu} \right)^T \tag{2.52}$$

represents the derivative in the direction of the outward pointing unit normal ν and $\partial\Omega$ represents the boundary of Ω. In terms of context, the latter means that there is no movement into or out of the area Ω.

We use the *SEIR*-model as an example to show how the models are prepared for later data fitting. Let $S(x,y,t)$, $E(x,y,t)$, $I(x,y,t)$, and $R(x,y,t)$ indicate the number of susceptible, exposed, infected and recovered individuals in the spatial coordinate $(x,y) \in \Omega$ at time $t \in \mathcal{T}$. Based on these presented groups, different epidemiological models can be derived. We will present the PDE systems of three commonly used models.

Example 2.28 (Types of disease models with PDEs)**.** Analogously to Tab. 2.1, we define the following infection models with PDEs:

- *SIS*-PDE model

$$\partial_t S = \kappa \Delta_{x,y} S - \frac{\beta(t)}{N} SI + \gamma I, \qquad S(t=0) = S_0, \tag{2.53a}$$

$$\partial_t I = \kappa \Delta_{x,y} I + \frac{\beta(t)}{N} SI - \gamma I, \qquad I(t=0) = I_0, \tag{2.53b}$$

$$\partial_\nu S = \partial_\nu I = 0, \qquad\qquad (x,y) \in \partial\Omega, \tag{2.53c}$$

$$N = S + I. \tag{2.53d}$$

- *SIR*-PDE model

$$\partial_t S = \kappa \Delta_{x,y} S - \frac{\beta(t)}{N} SI, \qquad\qquad S(t=0) = S_0, \qquad\qquad (2.54a)$$

$$\partial_t I = \kappa \Delta_{x,y} I + \frac{\beta(t)}{N} SI - \gamma I, \qquad\qquad I(t=0) = I_0, \qquad\qquad (2.54b)$$

$$\partial_t R = \kappa \Delta_{x,y} R + \gamma I, \qquad\qquad R(t=0) = R_0, \qquad\qquad (2.54c)$$

$$\partial_\nu S = \partial_\nu I = \partial_\nu R = 0, \qquad\qquad (x,y) \in \partial\Omega, \qquad\qquad (2.54d)$$

$$N = S + I + R. \qquad\qquad (2.54e)$$

- *SEIR*-PDE model

$$\partial_t S = \kappa \Delta_{x,y} S - \frac{\beta(t)}{N} SI, \qquad\qquad S(t=0) = S_0, \qquad\qquad (2.55a)$$

$$\partial_t E = \kappa \Delta_{x,y} E + \frac{\beta(t)}{N} SI - \theta E, \qquad\qquad E(t=0) = E_0, \qquad\qquad (2.55b)$$

$$\partial_t I = \kappa \Delta_{x,y} I + \theta E - \gamma I, \qquad\qquad I(t=0) = I_0, \qquad\qquad (2.55c)$$

$$\partial_t R = \kappa \Delta_{x,y} R + \gamma I, \qquad\qquad R(t=0) = R_0, \qquad\qquad (2.55d)$$

$$\partial_\nu S = \partial_\nu E = \partial_\nu I = \partial_\nu R = 0, \qquad\qquad (x,y) \in \partial\Omega, \qquad\qquad (2.55e)$$

$$N = S + E + I + R. \qquad\qquad (2.55f)$$

Considering the *SEIR*-model (2.55), it should be noted that also for N, a PDE has to be solved:

$$\partial_t N = \kappa \Delta_{x,y} N, \qquad\qquad\qquad (2.56a)$$

$$N = S_0 + E_0 + I_0 + R_0, \qquad\qquad t = 0, \qquad\qquad (2.56b)$$

$$\partial_\nu N = 0, \qquad\qquad (x,y) \in \partial\Omega. \qquad\qquad (2.56c)$$

In the first step, we substitute $R = N - S - E - I$ and thus reduce the system to an *SEI* model. We define $u : \mathbb{R}^{2\times 1} \to R^3$, $u(x,y,t) = (u_1, u_2, u_3)^T := \frac{1}{N}(S, E, I)^T$ and obtain a function $f : \mathcal{C}(V, \mathbb{R}^3)^{2,1} \to \mathbb{R}^3$,

$$f(u) = (-\beta(t)u_1 u_3, \beta(t)u_1 u_3 - \theta u_2, \theta u_2 - \gamma u_3). \qquad\qquad (2.57)$$

The results for the *SIS*-model (2.53) and the *SIR*-model (2.54) can be derived analogously. Tab. 2.2 summarizes the reduced systems for the respective system.

TABLE 2.2: Summary of $f(u)$ for the reduced models (2.53–2.55).

Reduced System	$f(u)$
$SIS \to I$	$\beta(t)(1-u)u - \gamma u$
$SIR \to SI$	$(-\beta(t)u_1 u_2, \beta(t)u_1 u_2 - \gamma u_2)$
$SEIR \to SEI$	$(-\beta(t)u_1 u_3, \beta(t)u_1 u_3 - \theta u_2, \theta u_2 - \gamma u_3)$

In order to meaningfully incorporate the biological context, we require $\beta, \gamma, \theta > 0$ and $\kappa \geq 0$. Restricting on the reduced *SEI* model, we as well require initial conditions $u_0 := (u_{1,0}, u_{2,0}, u_{3,0})^T \geq 0$ in the region Ω, it must also hold that $\int_\Omega u_{3,0} \, d\omega > 0$,

using the notation $u_j(x, y, 0) := u_{j,0}$. We define

$$\mathcal{N}(t) := \int_\Omega N(x, y, t) \, d\omega \tag{2.58}$$

as the total population in the area Ω at time t and $\mathcal{N}_0 := N(t_0)$ as the total number of individuals at time $t = 0$ in Ω. It is required that $\mathcal{N}_0 > 0$. Using Gauss's theorem and the Neumann boundary conditions, we find

$$\partial_t \mathcal{N} = \int_\Omega \partial_t N \, d\omega = \int_\Omega \kappa \, \Delta_{x,y} N \, d\omega = \int_{\partial\Omega} \kappa \, \partial_\nu N \, ds = 0 \tag{2.59}$$

and thus $\mathcal{N} = \mathcal{N}_0$ for any $t > 0$. As a result, the total population in the domain Ω is constant with respect to time. The PDE systems (2.53)–(2.55) with the presented $f(u)$ in Tab. 2.2 in conjunction with the mentioned preconditions, have a unique solution.

Since the total population is being modeled with diffusion, an equilibrium will only be established when the population density is equal throughout the district. Thus, the temporal equilibrium will be similar to the equilibrium of the system without diffusion.

Another possibility to model spatial dependency in the spread of diseases is the inclusion of a so-called *mobility matrix*, which is explained in detail in chapter 3.

2.3.5   Hilbert and Lebesgue spaces

Definition 2.29 (Hilbert Space). Let $\mathcal{H}$ be a real or complex vector space. If it is equipped with an inner product $\langle \cdot, \cdot \rangle : \mathcal{H} \times \mathcal{H} \to \mathbb{R}$ or $\mathbb{C}$, and this inner product induces a norm on $\mathcal{H}$, making it a complete space with respect to the norm (i.e., every Cauchy sequence in $\mathcal{H}$ converges), then $\mathcal{H}$ is called a *Hilbert space*.

Definition 2.30 (Lebesgue Space). Let $p \geq 1$ and $\Omega \in \mathbb{R}^n$. Then, the space of p-integrable functions

$$\mathcal{L}^p(\Omega) := \left\{ f : \Omega \to \mathbb{R}, \int_\Omega |f(x)|^p \, dx < \infty \right\} \tag{2.60}$$

is called the *Lebesgue space*.

The space $\mathcal{L}^p$ is a Banach space, i.e., every Cauchy sequence in $\mathcal{L}^p$ is convergent with respect to the p-norm defined by

$$\|f\|_p := \left(\int_\Omega |f(x)|^p \, dx \right)^{\frac{1}{p}}. \tag{2.61}$$

Also, $\mathcal{L}^2$ is a Hilbert space with the inner product

$$\langle f, g \rangle = \int_\Omega f(x) g(x) \, dx. \tag{2.62}$$

Definition 2.31 (Sobolev space). Let $\Omega \subseteq \mathbb{R}^n$ be an open set. Then, the space $\mathcal{H}^1$, defined over the subset of functions $f \in \mathcal{L}^2$, where all partial dervatives of f are also in $\mathcal{L}^2$, i.e.,

$$\mathcal{H}^1(\Omega) := \left\{ f \in \mathcal{L}^2(\Omega), \partial_i f \in \mathcal{L}^2(\Omega) \text{ for } i = 1, \dots, n \right\}, \tag{2.63}$$

is called *Sobolev space* with the associated scalar product

$$\langle f, g \rangle_1 := \langle f, g \rangle + \sum_{i=1}^{n} \langle \partial_i f, \partial_i g \rangle. \tag{2.64}$$

We additionally define the Sobolev space with zero boundary conditions, i.e.,

$$\mathcal{H}_0^1(\Omega) := \left\{ f \in H^1(\Omega), f \equiv 0 \text{ at } \partial\Omega \right\}. \tag{2.65}$$

The spaces $\mathcal{H}^1(\Omega)$ and $\mathcal{H}_0^1(\Omega)$ are Hilbert spaces with the scalar product

$$\langle f, g \rangle_{\mathcal{H}^1} := \int_\Omega f(x)g(x) + \nabla f(x)\nabla g(x)\,dx. \tag{2.66}$$

The general concept we will use in hindsight to computing *weak solutions* is the following: On $\mathcal{H}_0^1(\Omega)$, we define the alternative scalar product

$$\langle f, g \rangle_{\mathcal{H}^1} := \int_\Omega \nabla f(x)\nabla g(x)\,dx. \tag{2.67}$$

which is possible due to the Poincaré-Friedrichs inequality. Assuming $\mathcal{H}$ is a Hilbert space, $a : \mathcal{H} \times \mathcal{H} \to \mathbb{R}$ is a symmetric, bounded, coercive (i.e., $a(u, u) \geq c \|u\|^2$ for a $c > 0$), and bilinear form, and $b : \mathcal{H} \to \mathbb{R}$ is a linear and continuous functional, the variational problem

$$\min_{u \in \mathcal{H}} \quad \frac{1}{2}a(u, u) - b(u) \tag{2.68}$$

has a unique solution, and the minimization problem is equivalent to finding $u \in \mathcal{H}$ such that $a(u, v) = b(v)$ for all $v \in \mathcal{H}$. We will make use of this concept using *weak solutions* in section 2.3.6.

2.3.6 Finite element method for the diffusion equation

In this section, which partially makes use of the results in chapter 7, a solution method for the parabolic diffusion equation (2.50) for an *SIR*-PDE-model. Therefore, define $u \in \mathbb{R}^4$ and $g(u) : \mathbb{R}^4 \to \mathbb{R}^3$ as follows:

$$u = (u_1, u_2, u_3)^T = \left(\frac{S}{N}, \frac{I}{N}, \frac{R}{N}, N \right)^T, \tag{2.69a}$$

$$g(u) = (-\beta u_1 u_2, \beta u_1 u_2 - \theta u_2, \theta u_2, 0)^T. \tag{2.69b}$$

Applying initial conditions at time $t_0 = 0$ and *Neumann* boundary conditions, the PDE system reads as follows:

$$\partial_t u_1 = \kappa \, \Delta_{x,y} u_1 - \beta(t) u_1 u_3, \qquad u_1(t=0,x,y) = u_1^0(x,y) \quad \text{for } (x,y) \in \Omega;$$
$$\partial_\nu u_1 = 0 \quad \text{for } (x,y) \in \partial\Omega \qquad (2.70\text{a})$$

$$\partial_t u_2 = \kappa \, \Delta_{x,y} u_2 + \beta(t) u_1 u_3 - \theta u_2, \qquad u_2(t=0,x,y) = u_2^0(x,y) \quad \text{for } (x,y) \in \Omega;$$
$$\partial_\nu u_2 = 0 \quad \text{for } (x,y) \in \partial\Omega \qquad (2.70\text{b})$$

$$\partial_t u_3 = \kappa \, \Delta_{x,y} u_3 + \theta u_2 - \gamma u_3, \qquad u_3(t=0,x,y) = u_3^0(x,y) \quad \text{for } (x,y) \in \Omega;$$
$$\partial_\nu u_3 = 0 \quad \text{for } (x,y) \in \partial\Omega \qquad (2.70\text{c})$$

$$\partial_t u_4 = \kappa \, \Delta_{x,y} u_4 \qquad \text{for } (x,y) \in \Omega;$$
$$\partial_\nu u_4 = 0 \quad \text{for } (x,y) \in \partial\Omega \qquad (2.70\text{d})$$

For the finite element method, we seperate eqns. (2.70) in two parts of the form $\partial_t u_i = \kappa \, \Delta_{x,y} u_i$ and $\partial_t u_i = g_i(u)$. These two are handled by two different schemes, we can make use of an *operator splitting* to solve the system [13]. E.g., for one time step Δt, this procedure is as follows:

(I) Solve $\partial_t u_i = \kappa \, \Delta_{x,y} u_i$ for $t = \Delta t / 2$ with the corresponding initial and boundary conditions for $i = 1, 2, 3$.

(II) Solve $\partial_t u_i = f_i(u)$ for $t = \Delta t$ with the corresponding initial and boundary conditions for $i = 1, 2, 3$.

(III) Solve $\partial_t u_i = \kappa \, \Delta_{x,y} u_i$ for $t = \Delta t / 2$ with the corresponding initial and boundary conditions for $i = 1, 2, 3$.

The equation in (II) is a simple ODE equation which can be solved by any standard solver, e.g. the Euler method or the method of Runge-Kutta. To solve the equations in (I) and (III) on the domain Ω with initial and homogeneous Neumann boundary conditions on $\partial\Omega$, we consider its weak form gained by multiplication with a test function $v \in H_0^1(\Omega)$; this means, that v vanishes at the boundary, i.e., $v \equiv 0$ at $\partial\Omega$. The weak form reads as follows: Instead of the 'strong' solution $u \in \mathcal{C}^{2,1}$ for the PDEs as of 2.70, we now aim to find a weak solution $u_i \in H^1(\Omega)$ solving

$$a(u_i, v) := \int_\Omega \partial_t u_i \, v \, d\omega + \int_\Omega \nabla u_i \, \nabla v \, d\omega - \int_{\partial\Omega} u_i \, v \, d\lambda$$
$$= \int_\Omega \partial_t u_i \, v \, d\omega + \int_\Omega \nabla u_i \, \nabla v \, d\omega$$
$$= 0. \qquad (2.71)$$

For the numerical solution of this infinite-dimensional problem, we aim to find a solution $u_{i,h}$ in a finite-dimensional subspace V_h solving

$$a(u_{i,h}, v_h) = a_1(u_{i,h}, v_h) + a_2(u_{i,h}, v_h)$$
$$= \int_\Omega \partial_t u_{i,h} \, v_h \, d\omega + \int_\Omega \nabla u_{i,h} \, \nabla v_h \, d\omega$$
$$= 0. \qquad (2.72)$$

We define the subspace V_h on a rectangular grid and linearly independent basis functions ϕ_j piecewise over subregions $\Omega_k = [x_1, x_2] \times [y_1, y_2] \subset \Omega$, whereby x_1, x_2, y_1, y_2 satisfy $x_2 - x_1 = \Delta x$ and $y_2 - y_1 = \Delta y$, i.e. the corresponding step sizes in x-and

y-direction:

$$V_h = \left\{ u_h = \sum_k \sum_{j=1}^{4} c_j^{(k)} \, \phi_j^{(k)}(x,y) \right\},$$
(2.73)

where

$$\phi_1^{(k)}(x,y) = \frac{(x-x_2)(y-y_2)}{(x_1-x_2)(y_1-y_2)},$$
(2.74a)

$$\phi_2^{(k)}(x,y) = \frac{(x-x_2)(y-y_1)}{(x_1-x_2)(y_2-y_1)},$$
(2.74b)

$$\phi_3^{(k)}(x,y) = \frac{(x-x_1)(y-y_2)}{(x_2-x_1)(y_2-y_2)},$$
(2.74c)

$$\phi_4^{(k)}(x,y) = \frac{(x-x_1)(y-y_1)}{(x_2-x_1)(y_2-y_1)},$$
(2.74d)

for $(x,y) \in \Omega_k$; otherwise, those functions vanish, i.e., $\phi_j^{(k)}(x,y) \equiv 0$ for $(x,y) \notin \Omega_k$, $j = 1,\ldots,4$. Then the weak form $a(u_{i,h}, v_h) = 0$ reads as follows:

$$a(u_{i,h}, v_h) = a\left(\sum_k \sum_{j=1}^{4} c_j^{(k)} \, \phi_j^{(k)}(x,y), \, \phi_{j*}^{(k^*)}(x,y) \right) = 0$$
(2.75)

and, due to the linearity of a,

$$\sum_k \sum_{j=1}^{4} a\left(\phi_j^{(k)}(x,y), \, \phi_{j*}^{(k^*)}(x,y) \right) c_j^{(k)} = 0.$$
(2.76)

The stiffness matrices A and B are defined by

$$A_{nm} = a_1\left(\phi_j^{(k)}(x,y), \, \phi_{j*}^{(k^*)}(x,y) \right)$$
(2.77a)

$$B_{nm} = a_2\left(\phi_j^{(k)}(x,y), \, \phi_{j*}^{(k^*)}(x,y) \right)$$
(2.77b)

where n represents the row corresponding to (j^*, k^*) and m the column corresponding to (j, k), which depends on the chosen order within the matrices. More information about this can e.g. be found in [14]. The linear equation system with a mass matrix

$$A \, \partial_t u_i + B \, u_i = 0$$
(2.78)

can be solved by any scheme; e.g., a 4-step Runge-Kutta scheme, cf. e.g. [15].

Example 2.32. Consider the following elements in Fig. 2.2. In the graphic, we only consider a part of the problem, the right upper case elements for the finite element R1 that has its center at $(0,0)$. The other results for the upper left, lower left, and lower right elements follow from symmetry.
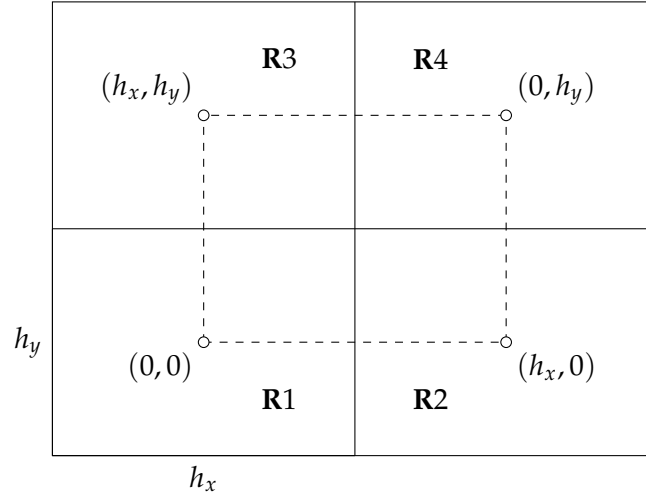
FIGURE 2.2: FEM example.

Then, a_{ij} and b_{ij} can be computed by eqns. 2.72 and 2.74 as follows:

$$a_{11} = 4 \cdot \int_0^{h_x} \int_0^{h_y} \frac{x^2 y^2}{h_x^2 h_y^2} \, dy \, dx = \frac{4}{9} h_x h_y, \tag{2.79a}$$

$$a_{12} = 2 \cdot \int_0^{h_x} \int_0^{h_y} \frac{xy \cdot (h_x - x)y}{h_x^2 h_y^2} \, dy \, dx = \frac{1}{9} h_x h_y, \tag{2.79b}$$

$$a_{13} = 2 \cdot \int_0^{h_x} \int_0^{h_y} \frac{xy \cdot x(h_y - y)}{h_x^2 h_y^2} \, dy \, dx = \frac{1}{9} h_x h_y, \tag{2.79c}$$

$$a_{14} = 1 \cdot \int_0^{h_x} \int_0^{h_y} \frac{xy \cdot (h_x - x)(h_y - y)}{h_x^2 h_y^2} \, dy \, dx = \frac{1}{18} h_x h_y, \tag{2.79d}$$

and

$$b_{11} = 4 \cdot \int_0^{h_x} \int_0^{h_y} \frac{y^2 + x^2}{h_x^2 h_y^2} \, dy \, dx = \frac{4}{h_x h_y} \left(h_x^2 + h_y^2 \right), \tag{2.80a}$$

$$b_{12} = 2 \cdot \int_0^{h_x} \int_0^{h_y} \frac{-y^2 + x(h_x - x)}{h_x^2 h_y^2} \, dy \, dx = \frac{1}{3 h_x h_y} \left(h_x^2 - 2h_y^2 \right), \tag{2.80b}$$

$$b_{13} = 2 \cdot \int_0^{h_x} \int_0^{h_y} \frac{y(h_y - y) - x^2}{h_x^2 h_y^2} \, dy \, dx = \frac{1}{3 h_x h_y} \left(h_y^2 - 2h_x^2 \right), \tag{2.80c}$$

$$b_{14} = 1 \cdot \int_0^{h_x} \int_0^{h_y} \frac{y(y - h_y) + x(x - h_x)}{h_x^2 h_y^2} \, dy \, dx = -\frac{1}{6 h_x h_y} \left(h_x^2 + h_x^2 \right). \tag{2.80d}$$

The system matrix is then well-defined by the values for a_{ij} and b_{ij}.

2.3.7   Space-fractional derivatives

The term *fractional calculus* is defined by calculus using non-integer powers of integration and derivation. Nowadays, it is used in many applications, e.g., network dynamics [16], field theory and gravity [16, 17], price fluctuations in financial markets [18], as well as in diffusion processes in epidemiology [16, 19].

In the following, we will generalize the concept of derivatives from integer to non-integer orders. There are different concepts for this, but we will rely on the definitions introduced by Riemann and Liouville and the according discretization

given by Grünwald and Letnikov [20, 21, 17]). While this research is restricted to space-fractional derivatives, the concept can also be extended to time-fractional derivatives. Parts of this chapter are adapted from [22], cf. chapter 6.

For the start, we introduce fractional integrals of order $\alpha \in \mathbb{R}$.

Definition 2.33 (Fractional Riemann-Liouville integrals). Let $f : [a, b] \to \mathbb{R}$ be a sufficiently smooth function on an interval $[a, b]$ ($a = -\infty$ and $b = \infty$ are allowed as well). Let

$$\Gamma(n) = \int_0^\infty t^{n-1} e^{-t} \, dt = (n-1)! \tag{2.81}$$

denote the gamma function. Then, for $n \in \mathbb{N}$, its right-sided n-fold repeated integral is defined as follows, cf. [23, 24]:

$$I_{a+}^{(n)} f(x) = \int_a^x d\xi_1 \int_a^{\xi_1} d\xi_2 \cdots \int_a^{\xi_{n-1}} f(\xi_n) \, d\xi_n = \frac{1}{\Gamma(n)} \int_a^x f(\xi)(x - \xi)^{n-1} \, d\xi \tag{2.82}$$

We can straightforwardly extend this to non–integer order $\alpha \in \mathbb{R} \setminus \{-1, -2, \ldots\}$ by

$$I_{a+}^{(\alpha)} f(x) = \frac{1}{\Gamma(\alpha)} \int_a^x f(\xi)(x - \xi)^{\alpha-1} \, d\xi \,. \tag{2.83}$$

The above integral is called the *right-sided fractional Riemann–Liouville integral of order α*. Analogously, we can define the *left-sided fractional integral* by

$$I_{b-}^{(\alpha)} f(x) = \frac{1}{\Gamma(\alpha)} \int_x^b f(\xi)(\xi - x)^{\alpha-1} \, d\xi \,. \tag{2.84}$$

It is easy to prove (cf. [21]) that for the fractional Riemann–Liouville integral it holds

$$I_{a+}^{(\alpha)} I_{a+}^{(\beta)} f = I_{a+}^{(\alpha+\beta)} f, \tag{2.85a}$$

$$I_{b-}^{(\alpha)} I_{b-}^{(\beta)} f = I_{b-}^{(\alpha+\beta)} f. \tag{2.85b}$$

According to the fundamental theorem of calculus, we identify the derivative of order α as the inverse operators to the integrals of order α, i.e.,

$$D_{a+}^{(\alpha)} f = \frac{d^n}{dx^n} I_{a+}^{(n-\alpha)} f \,, \tag{2.86a}$$

$$D_{b-}^{(\alpha)} f = \frac{d^n}{dx^n} I_{b-}^{(n-\alpha)} f \,. \tag{2.86b}$$

To define the fractional derivative of order $\alpha > 0$, let $n = \lceil \alpha \rceil = \min_{k \in \mathbb{N}} \{k > \alpha\}$ denote the smallest integer larger than α. Formally, taking the nth-derivative of the fractional Riemann–Liouville integral of order $n - \alpha$, i.e., $\frac{d^n}{dx^n} I^{(n-\alpha)}$, yields the Riemann–Liouville definition of the fractional derivative of order $0 < \alpha < 1$.

Definition 2.34 (Riemann-Liouville derivatives). Given the function $f \in \mathcal{C}^n([a, b])$, we call

$$D_{a+}^\alpha f(x) = \frac{\partial^\alpha}{\partial_{a+} x^\alpha} f(x) := \frac{1}{\Gamma(n-\alpha)} \frac{d^n}{dx^n} \int_a^x f(\xi)(x - \xi)^{n-\alpha-1} d\xi \tag{2.87}$$

the (right-sided) *Riemann–Liouville derivative of fractional order α* with left boundary a and

$$D_{b-}^{\alpha}f(x) = \frac{\partial^{\alpha}}{\partial_{b-}x^{\alpha}}f(x) := \frac{(-1)^{n}}{\Gamma(n-\alpha)}\frac{d^{n}}{dx^{n}}\int_{x}^{b}f(\xi)(\xi-x)^{n-\alpha-1}d\xi \qquad (2.88)$$

the (left-sided) *Riemann–Liouville derivative of fractional order α* with right boundary b [20].

The above fractional derivatives are *linear*, i.e., for all $f, g \in C^{n}([a,b])$, all $\lambda, \mu \in \mathbb{R}$ and any $\alpha > 0$, we have

$$D_{a+}^{\alpha}[\lambda f + \mu g] = \lambda D_{a+}^{\alpha}f + \mu D_{a+}^{\alpha}g, \qquad (2.89a)$$
$$D_{b-}^{\alpha}[\lambda f + \mu g] = \lambda D_{b-}^{\alpha}f + \mu D_{b-}^{\alpha}g. \qquad (2.89b)$$

Example 2.35. As an example, we consider the monomial x^{k} and compute its fractional derivative of order α. In alignment with the formal generalization of the integer order derivative

$$\frac{d^{m}}{dx^{m}}x^{k} = k(k-1)\cdots(k-m+1)x^{k-m} = \frac{k!}{(k-m)!}x^{k-m} = \frac{\Gamma(k+1)}{\Gamma(k-m+1)}x^{k-m}, \qquad (2.90)$$

we obtain

$$D_{a+}^{(\alpha)}x^{k} = \frac{1}{\Gamma(n-\alpha)}\frac{d^{n}}{dx^{n}}\int_{a}^{x}\xi^{k}(x-\xi)^{n-\alpha-1}d\xi \qquad (2.91)$$

$$= \frac{1}{\Gamma(n-\alpha)}\frac{d^{n}}{dx^{n}}\frac{k}{n-\alpha}\int_{a}^{x}\xi^{k-1}(x-\xi)^{n-\alpha}d\xi = \ldots \qquad (2.92)$$

$$= \frac{1}{\Gamma(n-\alpha)}\frac{d^{n}}{dx^{n}}\frac{\Gamma(k+1)\Gamma(n-\alpha)}{\Gamma(n+k-\alpha+1)}(x-a)^{n+k-\alpha} \qquad (2.93)$$

$$= \frac{\Gamma(k+1)}{\Gamma(k-\alpha+1)}(x-a)^{k-\alpha}, \qquad (2.94)$$

and analogously

$$D_{b-}^{(\alpha)}x^{k} = \frac{\Gamma(k+1)}{\Gamma(k-\alpha+1)}(b-x)^{k-\alpha}. \qquad (2.95)$$

For $a = 0$ and $\alpha := n \in \mathbb{N}$, this corresponds to the well-known n^{th} derivatives of the monomials.

Example 2.36. We can also examine the exponential function $f(x) = e^{cx}$ with $c > 0$ and $x \in [0,\infty)$. By utilizing the series representation of the exponential and applying the right-sided fractional derivative to monomials, we can derive the following:

$$D_{0+}^{(\alpha)}e^{cx} = \sum_{k=0}^{\infty}\frac{c^{k}}{k!}D_{0+}^{(\alpha)}x^{k} = \sum_{k=0}^{\infty}\frac{c^{k}}{\Gamma(k+1)}\frac{\Gamma(k+1)}{\Gamma(k-\alpha+1)}x^{k-\alpha}$$

$$= x^{-\alpha}\sum_{k=0}^{\infty}\frac{(cx)^{k}}{\Gamma(k-\alpha+1)} \qquad (2.96)$$

By making some algebraic manipulations and utilizing the incomplete gamma function $\Gamma(-\alpha, cx) = \int_{cx}^{\infty} t^{-\alpha-1} e^{-t}, dt$, we arrive at the following expression:

$$D_{0+}^{(\alpha)} e^{cx} = e^{cx} c^{\alpha} \cdot \left(1 - \frac{\Gamma(-\alpha, cx)}{\Gamma(-\alpha)}\right). \tag{2.97}$$

Again, for the special case of $\alpha = n \in \mathbb{N}$, this result corresponds to the standard n^{th} derivative of the exponential function.

For a detailed view into the methods of fractional calculus, we refer to [18, 21, 23]. Numerical methods for evaluating the accuracy of modeling initial value problems (IVPs) involving fractional derivatives can be established by setting up appropriate schemes,which is explained in detail in chapter 6.

2.3.8 Integro-differential equations

In this section, which makes use of the results in chapter 6, we reconsider the *SIR*-model by Kermack and McKendrick [6] with continuously differentiable functions S, I, R, N. Consider a one-dimensional model with $n = 1$. We normalize the three states S, I, and R by dividing all rows by N, resulting in $s := \frac{S}{N}, z := \frac{I}{N}, r := \frac{R}{N}$ with $s + z + r = 1$. In order to avoid confusion, we use a different lower case letter z instead of i. Again following the model by Kermack and McKendrick, we assume the virus is transmitted from infected persons to susceptible persons at a time-independent rate $\beta > 0$ and a recovery rate of $\gamma > 0$ so that loss of infectivity is gained after γ^{-1} days. Then, replacing $s = (1 - z - r)$, the relative *sir*-model for each time point $t \in [0, T] \subset \mathbb{R}$ and point in space $x \in [0, 1]^n \subset \mathbb{R}^n$ as follows:

$$\frac{d}{dt} z(t, x) = \beta(1 - z - r)z - \gamma z \qquad z(t = 0, x) = z_0(x) \tag{2.98a}$$

$$\frac{d}{dt} r(t, x) = \gamma z \qquad r(t = 0, x) = r_0(x) \tag{2.98b}$$

In a spatial model this means that the disease dynamics in a certain point x would entirely depend on the initial relations z_0 and r_0 and the parameters β and γ. To include interaction between the spatial points, we replace the factor z in the term $\beta(1 - z - r)z$ by an integral kernel, where the interaction term between x and y is modelled by a kernel function $k(t, x - y)$ which depends on the time and the distance between x and y:

$$\frac{d}{dt} z(t, x) = \beta(1 - z - r) \int_0^1 z(t, y) k(t, x - y) \, dy - \gamma z \quad z(t = 0, x) = z_0(x) \tag{2.99a}$$

$$\frac{d}{dt} r(t, x) = \gamma z \qquad r(t = 0, x) = r_0(x) \tag{2.99b}$$

The basic reproductive number, making use of the next-generation ansatz as of [12], can be calculated by $\mathcal{R}_0 = \frac{\beta}{\gamma} \|k\|_2$ according to [25], so that it also depends on the kernel function $k : [0, \mathcal{T}] \times [0, 1] \to \mathbb{R}$. For the purpose of reasonable modelling of scenarios, k should consist of three terms as follows:

- an *space-dependent* part $a(x - y)$ which is monotonously decreasing wrt $|x - y|$, e.g., an exponential function decreasing with the distance, i.e., $a(x - y) = c\, e^{-\delta|x-y|}$. This part can be controlled with

- a *control function $u(t) \in \mathcal{U} = \mathcal{C}([0,1])$* which represents the effectiveness of non-pharmaceutical interventions (lockdown, school closings, obligation of wearing masks etc.). Here, $u(t) \equiv 0$ implies no regulations and $u(t) \equiv 1$ implies total lockdown.

- a *non-adjustable* part k_0 which represents the fraction of transmission or a kind of 'background noise' you cannot control, e.g. household related infections. We also assume that this fraction does not depend on the spatial distance as interactions between distances can be prevented by political or social measures. For a more detailed view on the importance of households, cf. Dönges et al. [26].

These considerations lead to the following formula:

$$k(t, x - y) = (1 - u(t)) \cdot a(x - y) + k_0. \tag{2.100}$$

The following assumptions regarding the interaction kernel k should be met for the stationary case $k = k(x - y)$, i.e., $u \equiv 0$:

1. k is continuous.

2. k is non–negative.

3. $k(0) = k_0 > k > 0$.

4. k is monotonically decreasing wrt $|x - y|$.

5. $k_1 := \|k\|_1 = \int_0^1 k(r)\,dr > 0$

6. $k_1 < K = \max_{x \in [0,1]} \int_0^1 k(x - y)\,dy$

Note, that in the case of a strict monotonically decreasing kernel, we get $K = 2 \int_0^{1/2} k(r)\,dr$. An optimization model which aims to minimize both the relative share of infected z and the control term u, related to costs of political measures like lockdowns etc., could look as follows:

$$\min_{u(t) \in \mathcal{U}} J(u, z) = \max_{u(t) \in \mathcal{U}} -J(u, z) = \max_{u(t) \in \mathcal{U}} - \int_0^T \int_0^1 z(t, x)\,dx\,dt - \frac{\eta}{2} \int_0^T u^2(t)\,dt$$

subject to   system (2.99),

$$z(t, x) \leq z_{\max}. \tag{2.101}$$

A strategy to optimize this kind of *infinite-dimensional* optimization problems can be found in section 2.6.2.

2.4   Basic definitions and tools in optimization

In this chapter we present different optimization techniques, such as *Markov chain* methods and the *Forward-Backward sweep* method which can be used to either identify parameters in models or optimize time and/or space-dependent controls. Before presenting the two techniques, we list a few general definitions in optimization that hold true for all optimization problems. A comparison of the two methods can e.g. be found in [7].

Definition 2.37 (Minimization Problem)**.** Consider an optimization problem with an objective function $J(u)$. The goal is to find the solution that maximizes or minimizes $J(u)$ subject to the constraints $g_i(u) = 0$. We can write this as the following optimization problem: Let $g_i : \mathbb{R}^m \to \mathbb{R}$ for all $i = 1, \ldots, n$. Then the problem

$$\min_{u(t) \in \mathcal{U}} J(u, z)$$
$$U = \{u \in \mathbb{R}^m \mid g_i(u) = 0 \text{ for all } i = 1, \ldots, n\} \tag{2.102}$$

is called the *constrained minimization problem* with respect to the target function J and the constraint function(s) g_i.

Definition 2.38 (Types of Minima)**.** Let an optimization problem of type (2.102) be given. A (feasible) solution $u^* \in U$ is called

- *local minimum* if $J(u^*) \leq J(u)$ for all $u \in B_\epsilon(u^*)$,

- *strict local minimum* if $J(u^*) < J(u)$ for all $u \in B_\epsilon(u^*)$,

- *global minimum* if $J(u^*) \leq J(u)$ for all $u \in U$,

- *strict global* or *unique minimum* if $J(u^*) < J(u)$ for all $u \in U$.

The definitions for the maxima can be defined analogously.

In the following sections 2.5 and 2.6, we will present the two main optimization techniques that are used for parameter estimation and optimization in the research papers.

2.5 The Metropolis algorithm

The first technique we will consider, the *Metropolis algorithm*, derives from Bayesian statistics, Markov chains and Monte Carlo simulations. Several passages in this chapter have been updated and enhanced from chapter 3.

2.5.1 Markov chain theory

Given the observed data D and the set of model parameters θ, the posterior density is denoted by $P(\theta|D)$, the likelihood (defined by the probability model) is denoted by $P(D|\theta)$ and the prior distribution is denoted by $\pi_0(\theta)$. Let a joint distribution be given as follows:

$$P(D) = \pi_0(\theta)P(D|\theta) \tag{2.103}$$

The following formula describes the posterior distribution of θ, given an observation D (cf. Gilks [27]):

$$P(\theta|D) = \frac{\pi_0(\theta) \cdot P(D|\theta)}{\int \pi_0(\theta)P(D|\theta)\,d\theta} \tag{2.104}$$

To calculate the expectation value of the posterior distribution, given a function $f(\theta|D)$, we would need to calculate the integral

$$E[f(\theta|D)] = \frac{\int f(\theta) \cdot \pi_0(\theta) \cdot P(D|\theta)\,d\theta}{\int \pi_0(\theta) \cdot P(D|\theta)\,d\theta}, \tag{2.105}$$

which is hard or even impossible to integrate using analytic tools. For this, *Markov chain theory* proves to be helpful.

The fundamental idea behind MCMC methods is the generation of samples from a probability distribution that approximates the desired posterior distribution $f(\theta|D)$. This is accomplished by constructing a Markov chain with the posterior distribution as its equilibrium distribution. Before delving into the specifics of MCMC algorithms, it is important to first understand the underlying theory of Markov chains and how they can be used to prove that the algorithms in question converge to the desired posterior distribution.

Definition 2.39 (Markov Chain). Let $S = \{X_k\}_{k \in K \subset \mathbb{R}}$ be the state space containing all K possible states. A *Markov chain* is a sequence of random states, starting in any state X_0, and progressing from one state to the next. The sequence is written as $X = (X_0, X_1, ...)$. The outcome of the current state X_i only depends on the previous state X_{i-1}. This means that if the system is in state X_i, it will transition to state X_j with probability p_{ij}, which only depends on the current state and not any other previous states. Formally, we can express this as

$$p_{ij} = p(X_{i+1} = X_j | X_i, X_{i-1}, ..., X_0) = P(X_{i+1} = X_j | X_i). \tag{2.106}$$

The initial probability of starting in a certain state X_i is denoted by p_i^0 for all states. The set of all transition probabilities p_{ij} can be represented by a transition matrix $\Pi = (p_{ij})$, where i and j run through all (finite) possible states.

The probability to move from state i to state j in exactly n time steps is denoted by

$$p_{ij}^{(n)} = P(X_n = X_j | X_0 = X_i). \tag{2.107}$$

An important theorem is the

Theorem 2.40 (Chapman-Kolmogorov equation). *For n time steps and any k with $0 \le k \le n$ and the state space S, it holds*

$$p_{ij}^{(n)} = \sum_{r \in S} p_{ir}^{(k)} \cdot p_{rj}^{(n-k)}. \tag{2.108}$$

Also, the distribution of the chain at the nth step using the initial probability p^0 and the matrix Π is denoted by

$$p^{(n)} = p^0 \cdot \Pi^n. \tag{2.109}$$

Proof. A proof of this can be found in Ross [28]. □

In MCMC methods, the goal is to find an approximative distribution that eventually converges to the posterior distribution in question. The limiting distribution of $p^0 \cdot \Pi^n$ as $n \to \infty$ is important in this process. Although it is not known yet if the chain converges at all, it is assumed that a limit, denoted as π, exists. The limit transition is determined using the following equation:

$$\pi = \lim_{n \to \infty} p^0 \cdot \Pi^n = \lim_{n \to \infty} p^0 \cdot \Pi^{n+1} = \pi \cdot \Pi \tag{2.110}$$

Before utilizing this result later on, a few characteristics of Markov chains are presented in the following

Definition 2.41 (Ergodicity)**.** A state $X_i \in X$ is called *ergodic* if it is *aperiodic*, i.e., no states are visited in regular intervals, and *positively recurrent*, i.e. there is a number $N < \infty$ such that the state X_i can be reached from any other state X_j in less than N steps. If all states in a Markov chain are ergodic, then the Markov chain itself is called ergodic.

Definition 2.42 (Irreducibility)**.** A Markov chain is called *irreducible* if its state space X consists of only one equivalence class, i.e. $i \longleftrightarrow j$ (i.e., state i can be reached from space j) for all $X_i, X_j \in X$.

One can demonstrate that a finite state irreducible Markov chain is ergodic when it possesses at least one aperiodic state. In the case of a fully connected transition matrix, where all transitions have a non-zero probability, this condition is satisfied with $N = 1$.

Lemma 2.43. Let a Markov chain be ergodic and finite (i.e., it has a finite state set). Then, for a certain $N > 0$, it holds that $\Pi^n > 0$ for all $n > N$.

Proof. For a proof, refer e.g. to [29]. $\qquad\square$

Theorem 2.44 (Perron-Frobenius theorem)**.** If a matrix $A \in \mathbb{R}^{n \times n}$ is strictly positive, i.e. $A > 0$, all of its eigenvectors v_j have the same algebraic and geometric multiplicity 1. For matrices $B \in \mathbb{R}^{n \times n}$ with $B^n > 0$ for all $n > N$, the result holds true as well, even if B is not strictly positive.

Proof. Proofs of this theorem can e.g. be found in [30, 31]. $\qquad\square$

Now let $\Pi \geq 0$ be the transition matrix of an ergodic Markov chain. From the irreducibility, it follows that $p_{ij}^n > 0$ for all i and j, and thus $\Pi^n > 0$. By the Perron-Frobenius theorem, Π has the algebraic and geometric multiplicity of 1. This means there is a unique stationary distribution satisfying the formula $\pi = \pi \cdot \Pi$, implying that all ergodic Matrix chains have a unique stationary distribution, which is also independent of the initial distribution.

2.5.2 Algorithm formulation

The *Metropolis algorithm* is based on *Bayes' theorem* and is used to update a hypothesis probability estimate under new data. In Markov chain theory, we aim to find a unique stationary distribution for the given probability matrix. The goal in Markov Chain Monte Carlo (MCMC) methods is somewhat the opposite: We want to draw random samples from a target distribution. To do this, we want to find an ergodic Markov chain that has the (given) distribution as its limit. This Markov chain has to be reversible to this distribution, satisfying the balance condition: Summing this equation up for all i, we find

$$\sum_i \pi_i \cdot p_{ij} = \sum_i \pi_j \cdot p_{ji} = \pi_j \cdot \sum_i p_{ji} = \pi_j \tag{2.111}$$

This is the limit condition for a stationary distribution as in eqn. (2.110). The 'update' of the states is done with random numbers: Starting with an arbitrary parameter set, we draw a sample from a proposal distribution q, i.e., $\theta_{new} \sim q(\theta_{new}|\theta_{i-1})$ in every iteration i. The sample is accepted with a certain probability $\alpha(\theta_{new}|\theta_{i-1})$, then $\theta_i = \theta_{new}$; if it is not accepted, we remain in the previous sample, i.e., $\theta_i = \theta_{i-1}$. This is an adaptation of a random walk method using an accept-or-reject rule to converge to the desired posterior distribution.

The main advantages of MCMC methods are that they are simple to set up efficient algorithms for sampling, even for rather complicated and high-dimensional posterior distributions $P(\theta|D)$, and also enable the analysis of all model parameters in terms of mean and standard deviation. Another useful feature is that for the purpose of sampling, a full analytical description of the normalized product likelihood times prior is actually not needed at all [32].

The work of Metropolis et al. [33] presents a simple method to implement the concept of MCMC methods in practice. It is a direct applications for symmetric proposal distributions q (mostly, a normal distribution is used) with a predefined acceptance probability calculated by

$$\alpha(\theta_{new}|\theta_{i-1}) = \min\left(1, \frac{\pi(\theta_{new}) \cdot q(\theta_{i-1}|\theta_i)}{\pi(\theta_i) \cdot q(\theta_i|\theta_{i-1})}\right) = \min\left(1, \frac{\pi(\theta_{new})}{\pi(\theta_i)}\right). \tag{2.112}$$

Here, $\pi(\theta)$ is the approximating target distribution. When comparing distributions with given data, we use the sum of squares

$$Y = \sum_i \left(D_i - \hat{D}_i(\theta_{new})\right)^2 \tag{2.113}$$

between the real data D_i, i.e. the target distribution, and the estimated data $\hat{D}_i(\theta_{new})$, both at data point i. Let σ be the standard deviation of the prior. The approximating distribution is evaluated by

$$\pi(\theta) = c \cdot e^{-\frac{Y^2}{2\sigma^2}}. \tag{2.114}$$

Determining the proportionality constant c in eqn. (2.114) is redundant since it cancels out in eqn. (2.112). Obviously, the sum of squares Y should optimally be 0, which results in the approximative distribution converging to the target distribution if the Markov chain is set up correctly. If the balance condition

$$\pi(\theta_i) \cdot P(\theta_i|\theta_{new}) = \pi(\theta_{new}) \cdot P(\theta_{new}|\theta_i) \tag{2.115}$$

holds true, the Metropolis sampling is correct and the chain converges to the limiting distribution [32]. For any IVP with dependency on parameters, e.g., the *SEIRD*-model as described in [7], a Metropolis algorithm (cf. [33, 34, 27]) can be set up using the initial history and initial values for the to-be-estimated parameter set u. Using starting conditions u_0, we assign random draws u_{new} from a normally distributed (and thus symmetric) proposal function q, i.e. $u_{new} \sim q(u_{new}|u_{i-1})$, in every iteration i.

Using $J(u)$ as the target distribution, we calculate the approximating distribution by

$$\pi(u) = c \cdot \exp\left(-\frac{J(u)^2}{2\sigma^2}\right), \tag{2.116}$$

whereby c is an arbitrary value in $\mathbb{R}$. For the acceptance probability, it follows

$$\alpha(u_{new}|u_{i-1}) = \min\left\{1, \frac{\pi(u_{new}) \cdot q(u_{i-1}|u_i)}{\pi(u_i) \cdot q(u_i|u_{i-1})}\right\} = \min\left\{1, \frac{\pi(u_{new})}{\pi(u_i)}\right\}. \tag{2.117}$$

In eqn. (2.117), we can see that the value of c is redundant as it cancels out in the division. If the sample is accepted with the probability α, we set $u_i = u_{new}$; with the

probability $1 - \alpha$, the sample is declined, meaning $u = u_{i-1}$ [32, 35].

Algorithm 1 Pseudocode for the Metropolis algorithm.

1: $u, Y, Z \leftarrow$ load initial values for u and data
2: $x, z \leftarrow$ solve IVP for state variable
3: $J \leftarrow$ compute objective function regarding u
4: $s \leftarrow$ set step size (standard deviation) for the algorithm, e.g. $s := \sigma(u)$
5: **repeat**
6:     $u_{old} \leftarrow$ u from previous draw
7:     $\hat{u}_{new} \leftarrow u \sim \mathcal{N}(u_{old}, s)$
8:     $x, z, J(\hat{u}_{new}) \leftarrow$ update depending on u
9:     $\alpha \leftarrow \min\left\{1, \exp\left(J(u_{old})^2 - J(u_{new})^2/2\sigma^2\right)\right\}$
10:     $u_{new} \leftarrow \hat{u}_{new}$ with probability α and $u_{new} := u$ with probability $1 - \alpha$
11: **until** maximum value of draws is reached
12: $u^*, x^*, J^* \leftarrow$ means of all u, x, J

Alg. 1 describes the basic framework for iterative optimization using the Metropolis algorithm. In step 1, the mean values for the distribution are chosen based on the problem and any potential restrictions on the parameters. In step 2, the initial value problem (IVP) is solved using Runge-Kutta methods, such as MATLAB's *ode45* and *dde23* solvers. In step 5, the step size s is chosen as a fraction of the initial guess for the parameter set u, allowing the parameters to move through the search space at different 'speeds'. Steps 6 through 12 are repeated for all draws or until the system 'converges'. We will later address what this means in a probabilistic model.

The update of the parameter set u is done by taking a random value from a normal distribution with mean u and step size s in step 8. The cost functional $J(u)$ is then compared to the previous cost functional using the function α in step 10, and the new parameter set is accepted or rejected according to eqn. (2.117) in step 11. The estimation parameter set can be computed from the mean value of the draws in step 13. In the case of non-convergence, the best fitting u from the set can be used as the initial value in step 1 again, in order to improve the results.

The definition of 'convergence' in a probabilistic model can be problematic. Simple methods for checking convergence include graphical methods such as the trace plot, which shows how well the chain is mixing within the state space, and the running mean plot, which shows the current mean of all iterations up to the current one against the number of the iteration and is assumed to converge to a fixed number. Another graphical method is to plot histograms of the parameter values throughout all the MCMC runs and checking for convergence by comparison with Gaussian curves, as seen in the appendix of chapter 4. If no convergence has taken place, the algorithm should be continued, as discussed in [36].

Gelman and Rubin [37] addressed the problem by constructing two different estimators of the variance.

Definition 2.45 (Variance estimates, potential scale reduction factor)**.** Let $\tilde{u}_{i,\cdot}$ be the mean of the ith chain for $i = 1, \ldots, m$, and $\tilde{u}_{\cdot,\cdot}$ the overall mean. Then we define

(i) the *within-chain variance estimate* as

$$W = \sum_{i=1}^{m} \sum_{i=1}^{n-1} \frac{(u_{ij} - \tilde{u}_{i,\cdot})^2}{m(n-1)}, \tag{2.118}$$

(i) and the *pooled variance estimate* as

$$\hat{V} = \frac{n-1}{n} \cdot W + \sum_{i=1}^{n-1} \frac{(u_{i\cdot} - \tilde{u}_{\cdot\cdot})^2}{m-1}. \tag{2.119}$$

Then the *potential scale reduction factor* (PSRF) is defined by the ratio of those, i.e.,

$$\hat{R} = \frac{\hat{V}}{W} = (n-1)\left(\frac{1}{n} + \frac{m}{m-1} \frac{\sum_{i=1}^{n-1}(u_{i\cdot} - \tilde{u}_{\cdot\cdot})^2}{\sum_{i=1}^{m}\sum_{i=1}^{n-1}(u_{ij} - \tilde{u}_{i\cdot})^2} \right). \tag{2.120}$$

The numerator in eqn. (2.120) overestimates the target variance whereas the denominator underestimates it, so that $\hat{R} > 1$, as the initial distribution of the chain is overdispersed in finite samples. This means we can stop the simulation for $\hat{R} \approx 1$ [37].

While the Metropolis algorithm is a powerful tool in optimization and can be used in a broad bandwidth of optimization problems, especially for complicated target functions, it features disadvantages in case the number of to-be-optimized parameters is too high. In the next section, we will therefore consider the Lagrange formalism as an alternative optimization technique.

2.6 Lagrange formalism

Another method we can use to optimize problems is the so-called *Lagrange formalism*, which is a mathematical method for finding the maximum or minimum of a function subject to constraints. This generally requires the objective function to be (twice) continuously differentiable. The Metropolis algorithm works well with low-dimensional, discrete problems. Here, the addition of *Lagrange formalism* is a simple, yet extremely helpful tool.

2.6.1 Lagrange function

In this method, we construct a Lagrange function, also known as the Lagrangian, which is a combination of the original objective function and a set of constraints. The Lagrangian is then optimized to find the desired solution.

Picking up from Def. 2.37, we first introduce necessary and sufficient optimality conditions for functions $J \in \mathcal{C}^2(\mathbb{R}^m)$. Using the definition of the Hessian as of Def. 2.18, we can now define

Definition 2.46 (Necessary and Sufficient Conditions)**.** Let $J : \mathbb{R}^m \to \mathbb{R}$ be twice continuously differentiable. A point $u^* \in \mathbb{R}^m$ is a local minimum of J if the following *necessary* conditions hold true:

(i) the gradient vanishes at u^*, i.e., $\nabla_u J(u^*) = 0$ *and*

(ii) the Hessian matrix $H_f = \nabla_{uu}^2 J(u^*)$ is positive semi-definite at u^*.

If the Hessian H_f is positive definite at u^*, then there is a strict local minimum at u^* with respect to J. This condition is then called *sufficient*.

However, using this most simple definition of optimality, the constraints on the parameter set 'prevent' a simple computation of optima. For constrained optimal problems as of as of Def. 2.37, optimality conditions can be specified as well given $u, g \in \mathcal{C}^2$:

Definition 2.47 (Sufficient optimality conditions for constrained minimization, strict local minimum). Consider a constrained minimization problem with Lagrange function L as of eqn. (2.102). If there exist $(u^*, \lambda^*) \in \mathbb{R}^m \times \mathbb{R}^l$ such that all $\nabla g_i(u^*)$, $i = 1, \ldots, l$ are linearly independent, and the *sufficient optimality conditions*

i) $\nabla L(u^*, \lambda^*) = 0$,

ii) $s^T \nabla^2_{uu} L(u^*, \lambda^*) s > 0$

are satisfied for all $s \in \mathbb{R}^m$, satisfying $\nabla g_i(u^*)^T s = 0$ for all $i = 1, \ldots, l$ and $s \neq 0$, then $u^* \in U$ is a *strict local minimum* for J in eqn. (2.102).

In order to solve the optimal control problem, we introduce a set Lagrange multipliers λ_i associated with each constraint $g_i(x)$:

Definition 2.48 (Lagrange function). Consider the minimization problem as of eqn. (2.102). Let $\lambda \in \mathbb{R}^n$. Then the function

$$\mathcal{L}(u, \lambda) = J(u) + \sum_{i=1}^{n} \lambda_i g_i(u) \tag{2.121}$$

is called the *Lagrange function*, whereby all λ_i are called *Lagrange multipliers*. Note that for $u \in \mathcal{U}$, it holds $g_i = 0$ by definition, such that $\mathcal{L}(u, \lambda) = J(u)$ inside $\mathcal{U}$.

This newly attained function $\mathcal{L}$ can now be treated as the new target function, i.e. we replace the system (2.102) by

$$\min_{u \in U, \lambda \in \mathbb{R}^n} \mathcal{L}(u, \lambda). \tag{2.122}$$

In order to find the critical points of the Lagrangian $\mathcal{L}$, which correspond to the optimal solutions of the original optimization problem, we compute the stationary points of $\mathcal{L}(x, \lambda)$, satisfying the optimality conditions. This will be part of the forward-backward sweep method presented in section 2.6.2.

2.6.2 Forward-backward sweep method

The forward-backward sweep method provides an iterative approach for solving optimal control problems by combining forward and backward integrations. It allows for the computation of optimal control and state trajectories as well as the gradients of the cost function. This method is widely used in the field of optimal control and offers a powerful tool for solving a variety of dynamic optimization problems.

We will introduce the forward-backward method alongside an example of a comparatively simple *SI*-model:

Example 2.49 (Optimization of an *SI*-model using Lagrange Multipliers). In order to illustrate the optimization technique using Lagrange multipliers, consider a simple *SI*-model with a control on the transmission rate as follows:

$$S'(t) = -\frac{\beta}{N} \cdot (1 - u(t)) \, S(t) I(t) \tag{2.123a}$$

$$I'(t) = \frac{\beta}{N} \cdot (1 - u(t)) \, S(t) I(t) - \tau I(t) \tag{2.123b}$$

We aim to optimize the system with regard to both the total cases and also the impact control. In a first formulation of the optimal control problem, we aim to minimize

the total amount of infected, along keeping the costs, i.e. the control $u(t)$, as low as possible. In order to maintain convexity of the problem and avoid bang-bang controls due to linearity in u, the cost function term is squared:

$$\max_{u(t)\in[0,1]} -J(u,I) = \max_{u(t)\in[0,1]} -\frac{1}{2}\int_0^T I(t)^2 + u(t)^2\, dt \qquad (2.124)$$

A critical point, represented by (u^*, I^*), must meet the necessary optimality condition

$$\nabla \mathcal{L}(u^*, I^*) = 0, \qquad (2.125)$$

where the Lagrangian $\mathcal{L}$ is defined as

$$\mathcal{L}(z,u,r) = \int_0^T \lambda(t)\left[I'(t) - \frac{\beta}{N}\cdot(1-u(t))\,S(t)I(t) - \tau I(t)\right]dt - J(u, I(t)). \quad (2.126)$$

We now want to find the stationary points of the partial derivatives of $\mathcal{L}$ with respect to u and I:

$$\frac{\partial \mathcal{L}}{\partial u} = \int_0^T \left[-\lambda'(t) + \frac{\beta}{N}\cdot \lambda(t)S(t)I(t) - u(t)\right]dt \qquad \overset{!}{=} 0 \qquad (2.127a)$$

$$\frac{\partial \mathcal{L}}{\partial I} = \int_0^T \left[\frac{\beta}{N}\cdot \lambda(t)\,(1-u(t))\,S(t) - \tau - I(t)\right]dt \qquad \overset{!}{=} 0 \qquad (2.127b)$$

This leads us to the following system:

$$S' = -\frac{\beta}{N}\cdot(1-u(t))\,SI \qquad\qquad S(0) = S_0 \qquad (2.128a)$$

$$I' = \frac{\beta}{N}\cdot(1-u(t))\,SI - \tau I \qquad\qquad I(0) = I_0 \qquad (2.128b)$$

$$\lambda' = \frac{\beta}{N}\cdot \lambda SI - u(t) \qquad\qquad \lambda(T) = 0 \qquad (2.128c)$$

$$u(t) = 1 - \frac{N(\tau + I(t))}{\lambda \beta S(t)} \qquad\qquad (2.128d)$$

Starting with an initial guess of the control u over the whole interval, we solve the forward problem according to the differential equations for first solution of $I(t)$ on the whole time interval. The transversality conditions $\lambda(t = T) = 0$ and the values for u and I are used to solve the backward problem for λ. Using the results for λ and I, we calculate an update $\hat{u}$ on the time-dependent control function. The update of $u(t)$ is done by moving only a fraction σ of the previous u_{old} towards $\hat{u}(t)$:

$$u_{\text{new}}(t) = (1 - \sigma)\, u_{\text{old}}(t) + \sigma\, \hat{u}(t) \qquad \text{for all } t \in [0, T] \qquad (2.129)$$

This procedure will be repeated until the norm of two subsequent controls is 'close enough', i.e., $\|u_{\text{new}} - u_{\text{old}}\| < \text{TOL}$. The procedure of the forward-backward algorithm. is shown in Alg. 2.

Algorithm 2 Pseudocode for the Forward-Backward Sweep Method

1: $u \leftarrow$ load initial 'guess' for u
2: **repeat**
3:     $z, r \leftarrow$ solve forward problem
4:     $J \leftarrow$ compute Lagrange multipliers λ_i out of u, z and r and $\lambda_i(T) = 0$
5:     $\hat{u} \leftarrow$ compute update of u out of λ_i
6:     $u \leftarrow (1 - \sigma)u + \sigma\hat{u}$
7: **until** $\|\hat{u} - u\| <$ TOL or maximum value of draws is reached

---

More information about this so-called Forward-Backward sweep method can be found in Lenhart et al. [38]. For convergence and stability results, also refer to Hackbusch [39]. The formalism provides a convenient and flexible approach for solving optimization problems with constraints. By combining the objective function and constraints into a single function, the optimal solution is gained by finding the critical points of the Lagrangian and verifying that the constraints are satisfied. An advantage of the Lagrange formalism compared to the Metropolis algorithm is that it is able to optimize continuously and does not require discretization. On the other hand, we have to make several requirements on the optimal function (e.g., differentiability), so that it is necessary to use adapted Lagrange methods or other methods like the Metropolis algorithm.

References

[1] Walter, W. *Ordinary Differential Equations*. Springer, 1998.

[2] Arnold, V. I. *Ordinary Differential Equations*. Cambridge, MA: M.I.T. Press, 1973.

[3] Aulbach, B. *Gewöhnliche Differentialgleichungen*. Spektrum, 2004.

[4] Deuflhard, P. and Bornemann, F. *Scientific Computing with Ordinary Differential Equations*. Springer, 2002.

[5] Vukobratović, R. T. M. *General Sensitivity Theory*. New York, NY, USA: Elsevier, 1962.

[6] Kermack, W.O. and McKendrick, A.G. "Contributions to the mathematical theory of epidemics-I. 1927." In: *Bull. Math. Biol.* 53 (1991), pp. 33–55. DOI: 10.1098/rspa.1927.0118.

[7] Heidrich, P. et al. "The COVID-19 outbreak in Germany – Models and Parameter Estimation". In: *Commun. Biomath. Sci.* 3 (2020), pp. 37–59. DOI: 10.5614/cbms.2020.3.1.5.

[8] Tindale, L. et al. "Evidence for transmission of COVID-19 prior to symptom onset". In: *eLife* 9.3 (2020). DOI: 10.7554/eLife.57149.

[9] Martcheva, M. *An introduction to mathematical epidemiology*. Springer, 2015.

[10] Souza, M. O. "Multiscale analysis for a vector-borne epidemic model". In: *J. Math. Biol.* 68 (2014), pp. 1269–1293.

[11] Rocha, F. et al. "Time-scale separation and centre manifold analysis describing vector-borne disease dynamics". In: *Int. J. Comput. Math.* 90 (2013), pp. 2105–2125.

[12] Driessche, P. van den and Watmough, J. "Reproduction numbers and sub-threshold endemic equilibria for compartmental models of disease transmission". In: *Math. Biosci.* 180 (2002), pp. 29–48. DOI: 10.1016/s0025-5564(02)00108-6.

[13] MacNamara, S. and Strang, G. "Operator Splitting". In: *Splitting Methods in Communication, Imaging, Science, and Engineering*. Ed. by Glowinski, R., Osher, S., and Yin, W. Springer, Cham, 2016, pp. 95–114.

[14] Evans, G., Blackledge, J., and Yardley, P. *Numerical Methods for Partial Differential Equations*. London: Springer, 1999.

[15] Dormand, J.R.. and Prince, P.J. "A family of embedded Runge-Kutta formulae". In: *Journal of Computational and Applied Mathematics* 6.1 (1980), pp. 19–26.

[16] Baleanu, D. and Kumar (eds.), D. *Fractional Calculus and its Applications in Physics*. Frontiers Media, Lausanne, 2019.

[17] Calcagni, G. "Towards Multifractional Calculus". In: *Frontiers in Physics* 6.58 (2018).

[18] Baleanu, D. et al. *Fractional Calculus - Models and Numerical Methods, CNC Series on Complexity, Nonlinearity and Chaos, Vol. 5 (2nd edition)*. World Scientific, New Jersey, 2016.

[19] Oldham, K. and Spanier, J. *The Fractional Calculus (1st Edition)*. Academic Press, New York, 1974.

[20] Soczkiewicz, E. "Application of Fractional Calculus in the Theory of Viscoelasticity". In: *Mol. Quant. Acoust.* 23 (2002), pp. 397–404.

[21] Meerschaert, M.M. and Tadjeran, C. "Finite difference approximations for fractional advection-dispersion flow equations". In: *Journal of Computational and Applied Mathematics* 172 (2004), pp. 65–77.

[22] Schäfer, M. and Götz, T. "A numerical method for space-fractional diffusion models with mass-conserving boundary conditions". In: *Mathematical Methods in the Applied Sciences* (2023). DOI: 10.1002/mma.9310.

[23] Tadjeran, C., Meerschaert, M.M., and Scheffler, H.-P. "A second-order accurate numerical approximation for the fractional diffusion equation". In: *Journal of Computational Physics* 213 (2006), pp. 205–213.

[24] Tadjeran, C. and Meerschaert, M.M. "A second-order accurate numerical method for the two-dimensional fractional diffusion equation". In: *Journal of Computational Physics* 220 (2007), pp. 813–823.

[25] Bollobás, B., Janson, S., and Riordan, O. "The phase transition in inhomogeneous random graphs". In: *Random Structures and Algorithms* 31 (2007), pp. 3–122. DOI: 10.1002/rsa.20168.

[26] Dönges, P. and Götz, T. and Krüger, T. and Niedzielewski, K. and Priesemann, V. and Schäfer, M. *SIR-Model for Households (preprint)*. arXiv https://arxiv.org/pdf/10.48550/arXiv.2301.04355. 2023.

[27] Gilks, W.R., Richardson, S., and Spiegelhalter, D.J. *Markov chain Monte Carlo in Practice*. London: Chapman and Hall/CRC, 1996.

[28] Ross, S. *Introduction to Probability Models*. Elsevier India, 2014.

[29] Andrieu, C. et al. "An Introduction to MCMC for Machine Learning". In: *Mach. Learn.* 50 (2003), pp. 5–43.

[30] Perron, O. "Zur Theorie der Matrices". In: *O. Math. Ann.* 64 (1907), pp. 248–263.

[31] Frobenius, G. "Ueber Matrizen aus nicht negativen Elementen". In: *Sitzungsberichte der Koeniglich Preussischen Akademie der Wissenschaften. Jahrgang 1912. Erster Halbband. Januar bis Juni* (1912), pp. 456–477.

[32] Rusatsi, D.N. "Bayesian analysis of SEIR epidemic models". last visited: 18 December, 2023. PhD thesis. Lappeenranta University of Technology, 2015.

[33] Metropolis, N. et al. "Equation of State Calculations by Fast Computing Machines". In: *J.Chem. Phys.* 21 (1953), pp. 1087–1092. DOI: 10.1063/1.1699114.

[34] Gelman, A. et al. *Bayesian Data Analysis, 2nd Edition*. London: Chapman and Hall, 1996.

[35] Schäfer, M. and Götz, T. "Modelling Dengue Fever Epidemics in Jakarta". In: *Int. J. Appl. Comput. Math* 6 (2020). DOI: 10.1007/s40819-020-00834-1.

[36] Roy, V. "Comparative Sensitivity Analysis of Muscle Activation Dynamics". In: *Annual Review of Statistics and Its Application* 7 (2020), pp. 387–412. DOI: 10.1146/annurev-statistics-031219-041300.

[37] Gelman, A. and Rubin, D. B. "Inference from iterative simulation using multiple sequences". In: *Statistical Science* 7 (1992), pp. 457–472. DOI: 10.1214/ss/1177011136.

[38] Lenhart, S. and Workman, J.T. *Optimal control applied to biological models*. CRC Press, 2007.

[39]   Hackbusch, W. "A numerical method for solving parabolic equations with opposite orientations". In: *Computing* 20.3 (1978), pp. 229–240. DOI: 10.1007/bf02251947.

Part II

Contributions

Chapter 3

Modelling Dengue Fever Epidemics in Jakarta

This article by Moritz Schäfer and Thomas Götz has been released in the JOURNAL OF MATHEMATICAL BIOLOGY in 2020, and is based on the first author's master thesis at the University of Koblenz-Landau, referred to as [1]. The theory, formulation and numerical calculations were done by Moritz Schäfer. Thomas Götz provided advice and some linguistic revisions. The format is changed to meet the thesis standard.

Abstract

This article thematizes the qualitative estimation of transmission dynamics of Dengue fever. At first, a single-compartment vector-host model for the total infective cases in one homogeneous area has been set up and simplified using a steady-state approximation. Seasonality has been considered in the transmission parameter which is modelled by a Fourier sum. The equilibria of the model and their stability as well as the computation of the basic reproductive number are presented. As a modification, models considering a segmenting of the area in separate districts and their inter-district mobility have been set up, both with and without dependence of the disease transmission parameters on the district. Those have also been analyzed in terms of equilibria and stability. Parameter estimation on available Dengue data from Jakarta in the time interval of 2008–2016 using the Metropolis algorithm has been done. $\mathcal{L}_1$ and $\mathcal{L}_2$ comparisons show that using the multi-patch model with district-dependent parameters a decent approximation to the infection data is possible.

3.1   Introduction

Dengue fever is a fast-spreading viral disease and according to the World Health Organization (WHO), people in more than 100 countries, equalling 40% of the total world population, are exposed to the virus. About 50 to 100 million people (as of 2012) are infected annually. Estimates of the death rate of the disease range between 1% to 2.5%, mainly caused by untreated diseases and diseases with a very severe outcome (according to WHO [2]). This work deals investigates the dynamics of Dengue using mathematical models. Population models like the SIR model or its extensions have been widely used in the past decades.

The Dengue virus is not transmitted directly from human to human but via vectors, which makes the fever a so-called *vector-borne disease*. The majority of the vectors are mosquitoes of the species *aedes albopictus* and especially *aedes aegypti*. These mosquitoes prefer all-year around high temperatures and high humidity. For more information about epidemiological models including vector populations, read

e.g. [3]. Until now, there are only slight efforts in terms of vaccination (according to [2]).

In these regards, Jakarta is an optimal resting place for the mosquitoes. Jakarta features quite constant daily mean temperatures of 26 – 27 °C throughout the whole year, with little seasonal variation. It also shares a significant rain period from December to March (each month has an average of more than 200 litres of rainfall), coming across with high humidity; during the period of July to September, the average amount of rain is below 100 litres per month, yet with only slightly lower humidity (according to the Deutscher Wetterdienst / DWD). Seasonal dependence has also been investigated in several works; e.g. in [4] and [5].

There are four main serotypes of Dengue, called *DENV-1* to *DENV-4*. After a bite of an infectious mosquito and given transmission of the disease, the incubation of time of Dengue fever is typically one week. Infectious persons are also the primary carrier to infect healthy mosquitoes in case of a bite. After recovery, the formerly infected person is immune for about 12 weeks. Thereon, the patient remains immune against the specific type he was infected with, but is susceptible to all other types and can get infected with those again. Jakarta, for instance, has experienced a few severe disease waves in the past few years showing a certain seasonality. This will be investigated first before constructing the models.

This article is structured as follows: Section 3.2 introduces several tools used for parameter estimation, including the theoretical background of the Metropolis algorithm later used to optimize the parameters. In section 3.3, a dynamic disease model for whole Jakarta is set up and implemented and the results are presented. In section 3.4, a model which considers the five main districts of Jakarta with district-independent parameter values, and another one including district-dependent parameter values are considered, which are also implemented and presented. In section 3.5, the three models are compared and the results are discussed.

3.2   Metropolis algorithm

As to be seen in sections 3.3 and 3.4 we will optimize a large number of parameters with respect to all the data points. Because of this large parameter space, it will not be useful to use standard optimization tools, e.g. least-squares methods, to estimate the unknown parameters. A solution to this problem is found in the *Metropolis algorithm* based on *Bayes' theorem* which is used to update a hypothesis probability estimate under new data, and which returns not just a single value for the parameter estimates, but the mean with standard deviation of a chain of parameters.

3.2.1   Markov chain theory

Let D be the observed data and θ be the set of model parameters. Then, we denote the posterior density by $P(\theta|D)$, the likelihood (defined by the probability model) by $P(D|\theta)$ and the prior distribution by $\pi_0(\theta)$. Let a joint distribution be given as follows:

$$P(D) = \pi_0(\theta)P(D|\theta) \tag{3.1}$$

Then, the posterior distribution $P(\theta|D)$ is given by (cf. Gilks [6]):

$$P(\theta|D) = \frac{\pi_0(\theta) \cdot P(D|\theta)}{\int \pi_0(\theta)P(D|\theta)\,d\theta} \tag{3.2}$$

For the explicit calculation of the expectation value of a posterior distribution, say given a function $f(\theta|D)$ for a parameter set θ and given data D, we would need to calculate the integral

$$E[f(\theta|D)] = \frac{\int f(\theta) \cdot \pi_0(\theta) \cdot P(D|\theta)\, d\theta}{\int \pi_0(\theta) \cdot P(D|\theta)\, d\theta}, \tag{3.3}$$

where $P(D|\theta)$ is the likelihood function which is defined by the probability model, $\pi_0(\theta)$ is the prior distribution and $P(D)$ is a normalizing constant. The integral in eqn. (3.3) is hard or even impossible to integrate using analytic tools, especially for large parameter sets [6].

In order to solve this problem, we make use of *Markov chain theory*, whose basic idea lies in drawing samples of a probability distribution which approximates the posterior distribution $f(\theta|D)$. This is done by calculating a *Markov chain* that has the posterior distribution as its equilibrium distribution. In Markov chain theory, the probability p_{ij} of moving from the current state X_i to X_j with a probability only depends on the previous state and no other. The initial probability, meaning the probability that the initial state is e.g. X_i, is denoted by p_i^0 for all states. We can create a transition matrix $\Pi = (p_{ij})$ out of all transition possibilities where i and j run through all possible states.

The probability to move from state i to state j in exactly n time steps is denoted by p_{ij}. An important theorem is the *Chapman-Kolmogorov equation* [7]:

Lemma 3.1. For n time steps and any k with $0 \leq k \leq n$ and the state space S, it holds

$$p^{(n)} = \sum_{r \in S} p_{ir}^{(k)} \cdot p_{rj}^{(n-k)}. \tag{3.4}$$

The distribution of the chain at the nth step using the initial probability p^0 and the matrix Π is denoted by

$$p^{(n)} = p^0 \cdot \Pi^n. \tag{3.5}$$

In MCMC methods, our goal is to find an approximative distribution that eventually converges to the posterior distribution in question. This is why the limiting distribution of $p^0 \cdot \Pi^n$ for $n \to \infty$ is important. We do not know yet if the chain converges at all, but for now, we just assume that a limit, call it π, exists. We use the limit transition to determine it:

$$\pi = \lim_{n \to \infty} p^0 \cdot \Pi^n = \lim_{n \to \infty} p^0 \cdot \Pi^{n+1} = \pi \cdot \Pi \tag{3.6}$$

We now make use of the following result (as of Andrieu et al. [8]):

Lemma 3.2. For ergodic and finite Markov chains and a certain $N > 0$, it holds $\Pi^n > 0$ for all $n > N$.

Let $\Pi \geq 0$ be the transition matrix of an irreducible and aperiodic, thus ergodic, Markov chain. From the irreducibility, $p_{ij}^n > 0$ for all i and j and thus $\Pi^n > 0$. Next, use is made of the Perron-Frobenius theorem [9, 10]:

Lemma 3.3. If a matrix A is a strictly positive matrix, i.e., $A > 0$, the spectral radius $\rho(A)$ has the same algebraic and geometric multiplicities of 1. For matrices B with $B^n > 0$ for all $n > N$, the result holds true as well, even if B is not strictly positive.

By applying this theorem, we know the spectral radius $\rho(\Pi)$ has the algebraic and geometric multiplicity of 1. Thus, there exists a unique stationary distribution satisfying the formula $\pi = \pi \cdot \Pi$, implying that all ergodic Matrix chains have a unique stationary distribution which is also independent of the initial distribution.

3.2.2 Markov Chain Monte Carlo methods

Regarding Markov chains, the goal is to find a unique stationary distribution for the given probability matrix. The goal in MCMC methods is somewhat the opposite: We want to draw random samples from a target distribution [11]. To do this, we want to find an ergodic Markov chain that has the (given) distribution as its limit. This Markov chain has to be reversible to this distribution, satisfying the balance condition (summed up for all i):

$$\sum_i \pi_i \cdot p_{ij} = \sum_i \pi_j \cdot p_{ji} = \pi_j \cdot \sum_i p_{ji} = \pi_j \tag{3.7}$$

This is the limit condition for a stationary distribution as of eqn. (3.6) [12].

The 'update' of the states is done with random numbers: Starting with an arbitrary parameter set, we draw a sample from a proposal distribution q, i.e., $\theta_{new} \sim q(\theta_{new}|\theta_{i-1})$ in every iteration i. The sample is accepted with a certain probability $\alpha(\theta_{new}|\theta_{i-1})$, such that $\theta_i = \theta_{new}$; if it is not accepted, we set $\theta_i = \theta_{i-1}$. This is an adaptation of a random walk method using an accept-or-reject rule to converge to the desired posterior distribution.

The main advantages of MCMC methods are that they are simple to set up efficient algorithms for sampling, even for rather complicated and high-dimensional posterior distributions $P(\theta|D)$, and also enable the analysis of all model parameters in terms of mean and standard deviation. Another useful feature is that for the purpose of sampling, a full analytical description of the normalized product likelihood times prior is actually not needed at all [12].

The work of Metropolis et al. [13] presents a simple method to implement the concept in practice. It is a direct application of the MCMC method for symmetric proposal distributions q (typically a normal distribution) with a predefined acceptance probability, calculated by

$$\alpha(\theta_{new}|\theta_{i-1}) = \min\left(1, \frac{\pi(\theta_{new}) \cdot q(\theta_{i-1}|\theta_i)}{\pi(\theta_i) \cdot q(\theta_i|\theta_{i-1})}\right) = \min\left(1, \frac{\pi(\theta_{new})}{\pi(\theta_i)}\right), \tag{3.8}$$

where $\pi(\theta)$ is the approximative target distribution (cf. Gilks [6]). By comparison distributions with given data, we use the sum of squares of the difference between the real data D_i i.e., the target distribution, and the estimated data $\hat{D}_i(\theta_{new})$, both at data point i:

$$Y = \sum_i \left(D_i - \hat{D}_i(\theta_{new})\right)^2 \tag{3.9}$$

The approximative distribution is then evaluated by

$$\pi(\theta) = c \cdot e^{-\frac{Y^2}{2\sigma^2}}. \tag{3.10}$$

Determining the proportionality constant c in eqn. (3.10) is redundant, since it cancels out in equation (3.8). Obviously, Y should optimally be 0. This is why the approximative distribution converges to the target distribution if the Markov chain is

set up correctly. If the balance condition

$$\pi(\theta_i) \cdot P(\theta_i|\theta_{new}) = \pi(\theta_{new}) \cdot P(\theta_{new}|\theta_i) \tag{3.11}$$

holds true, the Metropolis sampling is correct and the chain converges to the limiting distribution [12].

3.3 Single-compartment SIRUV models

We will now describe the basic epidemiological model for a single compartment, i.e., the disease dynamics for a single district Ω. As an application of the method, we use Dengue data for the city of Jakarta in the time interval of 2008 – 2016 and apply the parameter estimation using the Metropolis algorithm, minimizing the difference between the model and the data.

3.3.1 Dengue cases in Jakarta

Before dealing with the model, we will first consider the demographical and epidemiological situation in Jakarta.

The data that will be used to fit the parameters is originating from private communications with Dipo Aldila, Department of Mathematics, University of Indonesia, Depok [14]. Over the given time interval from 2008 – 2016, it features weekly infection data in a total time interval of 468 weeks. The data is shown in Fig. 3.1.
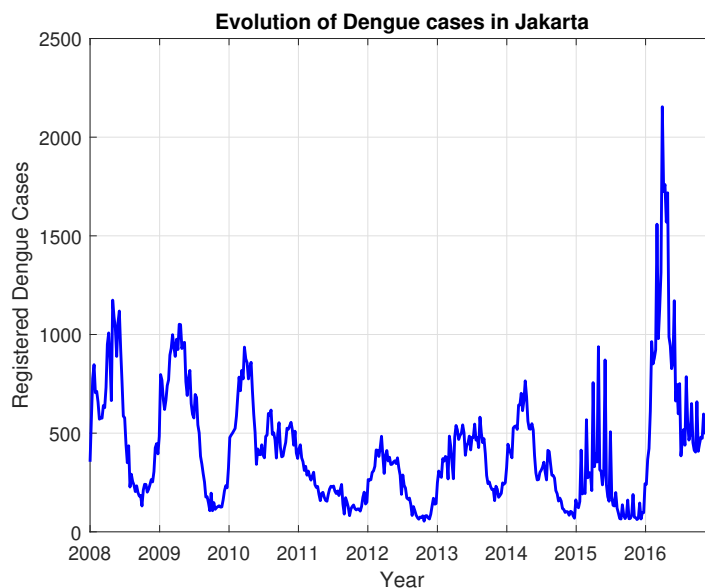
FIGURE 3.1: Reported Dengue cases in Jakarta, 2008–2016.

It is important to know that this data only shows the registered cases of Dengue (i.e., those being cured in hospital). But it is obvious that a high number of cases is not treated in hospitals and thus does not get registered, which will be considered in the single-compartment *SIRUV*-model introduced in the following section.

3.3.2   Introduction and model equations

Over the past decades, there have been many descriptions of classical epidemiological models. A comprehensive representation can be found in [15, pp. 315-394]. In general, the population whose disease dynamics we want to describe is assumed to be homogeneously mixed in certain subpopulations, i.e., there are no spatial differences in the population shares and the spread of the epidemic. In a classical epidemiological model, the *SIR-model*, there are three distinctive classes: The susceptibles S are the part of the population which is healthy but can get infected with the disease; the infectives (or infected) I have been infected with the disease and carry it out; finally, the recovered R have had the disease but are currently (yet only temporarily) immune against the disease. The total population N is the sum of all three subpopulations:

$$N = S + I + R \tag{3.12}$$

We assume there is a constant birth (plus immigration) rate and a constant death (plus emigration) rate. All newborns and newly immigrated persons are assumed to be susceptible. To simplify things slightly, we assume that the total population is constant, so that birth or immigration rate and death or emigration rate are the same (called μ from now on). This will most likely not be correct in reality; Jakarta, in particular, features – as most large towns – a growing population. But it will not cause significant changes in the observed time interval of 9 years, at least not in the epidemiological data (yet of course in the total population numbers). For models covering a significantly larger time intervals, the birth and death rates might have to differ in order to stay realistic.

As Dengue fever is a vector-borne disease, vector dynamics are also included in the model. Two more populations, the susceptible vectors U and the infected vectors V, are added to the three human populations S, I and R (making it a *SIRUV*-model). We assume that the birth and death rate of vectors are constant and equal as well, named ϑ from now on. Thus, the total amount of vectors M also is constant:

$$M = U + V \tag{3.13}$$

The transmission of the disease is modelled as follows, assuming the disease is transmitted directly between the infected and susceptible subpopulations: Consider that all susceptible humans have the same 'chance' to get in contact with any infected vector, as well as all susceptible vectors have the same 'chance' to get in contact with any infected human. The probability of disease transmission is then proportional to the product of the respective susceptibles and infectious populations, i.e., the amount of susceptible humans who get infected is equal to $\frac{\beta \cdot S \cdot V}{M}$, and the amount of susceptible vectors who get infected is equal to $\frac{\varrho \cdot U \cdot I}{N}$. As a first step, we assume that β and ρ are constant. The recovery time of the disease for humans is τ^{-1}, and thus the amount of persons who recover in a certain time interval is $\tau \cdot I$. The recovered persons can get infected again after a time κ^{-1}; because of that, the number of recovered persons returning to the suceptible department equals $\kappa \cdot R$. Since vectors do not have an immune system, there is no recovery after being infected, and no subpopulation of recovered vectors. The differential equation system for this model reads as follows:

$$S' = \mu \cdot (N - S) - \frac{\beta \cdot S \cdot V}{M} + \kappa \cdot R, \tag{3.14a}$$

$$I' = -(\mu + \tau) \cdot I + \frac{\beta \cdot S \cdot V}{M}, \tag{3.14b}$$

$$R' = -(\mu + \kappa) \cdot R + \tau \cdot I, \tag{3.14c}$$

$$U' = \vartheta \cdot (M - U) - \frac{\rho \cdot U \cdot I}{N}, \tag{3.14d}$$

$$V' = -\vartheta \cdot V + \frac{\rho \cdot U \cdot I}{N}. \tag{3.14e}$$

The ODE system (3.14) consists of five equations that, in the later algorithms, have to be computed in each draw. One problem arises in that there is no reliable data on the amount of vectors. However, by the so-called *steady-state approximation*, it is possible to eliminate the vector populations from the above model. Several of the parameter are identified by the 2010 census and epidemiological data from the WHO, cf. Tab. 3.1.

TABLE 3.1: Fixed parameter values.

N	μ	τ	κ
$9.6 \cdot 10^6$	$(69 \cdot 52 \, \text{w})^{-1}$	$(2 \, \text{w})^{-1}$	$(12 \, \text{w})^{-1}$

It obviously holds $\vartheta^{-1} \ll \mu^{-1}$. This means that after a comparatively short initial time period, both vector populations do not change with time any more and remain constant. This approximation only holds true if the observed time interval is significantly larger than $\vartheta^{-1} = 2$ weeks. For an interval of 9 years, this is a valid simplification. For further information about this, see e.g. [3] or [16].

The equilibria of the vector populations are reached if $U' = 0$ and $V' = 0$. This is equivalent to

$$U^* = \frac{M}{1 + \frac{\rho}{\vartheta \cdot N} I^*} := \frac{M}{1 + \frac{I^*}{\lambda}}, \tag{3.15a}$$

$$V^* = \frac{M \cdot I^*}{\frac{\vartheta}{\rho} \cdot N + I^*} = \frac{M \cdot I^*}{\lambda + I^*}. \tag{3.15b}$$

with $\lambda = \frac{\vartheta}{\rho} \cdot N$. As discussed above, we can now replace V in eqns. (3.14) with its equilibrium and 'ignore' the vector populations in the model.

Furthermore, since we know $S + I + R = N$ at all times t, we can leave out one of the three human population equations as it is redundant. In our case, the susceptibles are left-out, as the infectious class is the most important to handle and the recovered equation is more simple in its computation. This results in the following system:

$$I' = -(\mu + \tau) \cdot I + \frac{\beta \cdot (N - I - R) \cdot I}{\lambda + I}, \tag{3.16a}$$

$$R' = -(\mu + \kappa) \cdot R + \tau \cdot I. \tag{3.16b}$$

While μ, τ, κ and N are parameters which we know or are able to estimate decently, λ and β still remain variable. Assuming both of them to be constant is also not very useful, as obviously, seasonal and other effects have to be considered. In this regard,

we claim (without loss of generality) that β is a periodic function of time, represented by a (finite) Fourier series:

$$\beta(t) = \beta_0 + \sum_{i=1}^{N} c_i \cdot \cos(2\pi \cdot \omega_i \cdot t + \phi_i) \tag{3.17}$$

With the restriction

$$\beta_0 \geq \sum_{i=1}^{N} c_i, \tag{3.18}$$

it is assured that $\beta(t) \geq 0$ for all t. Because of that, given a transmission, a biologically implausible possibility of an *increasing* number of susceptibles after transmission, together with a *decreasing* amount of infected, is prevented.

Testing has shown that to keep the model 'as simple as possible, but no simpler', an apt number of summands is $N = 3$. The aspect of seasonality has to be considered; therefore, the first frequency parameter is fixed to $\omega_1 = (52\,w)^{-1}$.

Another not yet considered problem is that our model does not yet take care of the fact that the amount of registered infections is not the amount of actual infections. As there is no evidence on the relation of those two numbers, we assume that the ratio of registered and total infections is a fixed value η. As of 2016, however, Dengue treatment in Jakarta's hospitals became free (according to Badan Pusat Statistik (2010), which most likely has changed the ratio η. So, we assume two different ratios η_1 and η_2 in the respective time intervals Jan 2008 – Dec 2015 and Jan 2016 – Dec 2016.

The parameter set $\theta = (\beta_0, c_1, c_2, c_3, \omega_2, \omega_3, \phi_1, \phi_2, \phi_3, \lambda, \eta_1, \eta_2)$ is unknown, and it needs to be estimated by simulation of the disease dynamics and optimization of those parameters under the given data, as to be seen in subsection 3.5. Before, the equilibrium points of the system and their stability are analyzed.

3.3.3   Equilibria of the model and stability

As already mentioned for the vector population in subsection 3.1, the equilibria of the model as described in eqns. (3.16) are computed by $(\dot{I}, \dot{R}) = (0,0)$. Here, we only consider the autonomous part of $\beta(t)$ which is β_0, neglecting the non-autonomous and periodic part.

A disease-free equilibrium (DFE) is reached at $(I_1^*, R_1^*) = (0,0)$; this means that there is an equilibrium if the disease dies out and the whole human population belongs to the susceptible class, i.e., $N = S$. The endemic equilibrium is reached if the following equations hold:

$$I_2^* = \frac{\beta_a \cdot N - \lambda \cdot (\mu + \tau)}{\mu + \tau + \beta_a \cdot (1 + \frac{\tau}{\mu + \kappa})}, \tag{3.19a}$$

$$R_2^* = \frac{\tau}{\mu + \kappa} \cdot I_2^* = \frac{\tau \cdot (\beta_a \cdot N - \lambda \cdot (\mu + \tau))}{(\mu + \kappa) \cdot (\mu + \tau + \beta_a \cdot (1 + \frac{\tau}{\mu + \kappa}))}. \tag{3.19b}$$

For stability analysis, we compute the *basic reproductive number* $\mathcal{R}_0$ by the next-generation method according to Badan Pusat Statistik (2010). For that, we only need to consider all infectious subpopulations, which is only I in this model. Eqn. (3.16a) is divided into two parts, the number of new infections in the infective department F_I

and the number of outgoing individuals W_I:

$$I' = F_I - W_I \tag{3.20}$$

with

$$F_I = \frac{\beta_a \cdot (N - I - R) \cdot I}{\lambda + I}, \tag{3.21a}$$

$$W_I = (\mu + \tau) \cdot I. \tag{3.21b}$$

The basic reproductive number $\mathcal{R}$, can be interpreted as the number of secondary infections originating from a single infected person in an entirely susceptible population. The Jacobian matrices of F_I, noted as J_F, and W_I, noted as J_W, are computed by

$$J_F = \frac{\partial F_I}{\partial I} = \frac{\beta_a \cdot N \cdot \lambda}{(\lambda + I)^2} = \frac{\beta_a \cdot N}{\lambda}, \tag{3.22a}$$

$$J_W = \frac{\partial W_I}{\partial I} = \mu + \tau. \tag{3.22b}$$

Here, $N - I - R$ is replaced by N and I is equal to 0, because we assume an at first entirely susceptible population and then observe the changes given a single infected individual. The next-generation matrix is computed by the largest eigenvector of FW^{-1}, i.e.,

$$\mathcal{R}_0 = \rho(FW^{-1}) = \frac{\beta_a \cdot N}{(\mu + \tau) \cdot \lambda}. \tag{3.23}$$

If $\mathcal{R}_0 > 1$, meaning $\beta_a \cdot N > \lambda \cdot (\mu + \tau)$, the expected number of secondary infections exceeds the number of primary infections and thus the disease becomes epidemic. In this case, the DFE (I_1^*, R_1^*) is unstable. This can be shown by linearization of the system around the equilibrium and computing the largest real eigenvalues of the Jacobian, which is negative if $\mathcal{R}_0 > 1$. If $\mathcal{R}_0 < 1$, the number of secondary infections is lower than the number of primary infections and thus the disease dies out eventually, resulting in an asymptotically stable disease-free equilibrium, which also can be shown by linearization.

The endemic equilibrium (I_2^*, R_2^*) is asymptotically stable if $\mathcal{R}_0 > 1$, which can also be shown using linearization. In case of $\mathcal{R}_0 < 1$, eqn. (2.45) implies $I_2^* < 0$ as the denominator is always > 0 and the nominator gets < 0; thus, a realistic endemic equilibrium does not exist.

3.4 Multi-compartment SIRUV model

In the previous section, a model based on one single geographical segment is discussed – consisting of the whole city of Jakarta. This might not reflect the actual disease values aptly, as in Jakarta's districts, the infection rates can be significantly different, due to different environments, population size, demography or wealth. We will first have a look on the real data before setting up a model considering several compartments instead of a single patch.

3.4.1 Population and infection data

As in section 3.3.1, we will first consider the data situation in Jakarta. The size of the population in all districts is shown in table 3.2, according to [17].

TABLE 3.2: Population in the districts of Jakarta [17].

District	Central	North	West	South	East
Population [10^6]	0.9	1.6	2.3	2.1	2.7

As a first step, we have a look at the relevant infection data for the districts. Compared to the respective amount in Jakarta, multiplied with the share of population in the district, we can see that some districts follow the infection dynamics well, while others show significantly different behaviour. As an example, we plot the data of infected for East Jakarta in Fig. 3.2 and the data of infected for West Jakarta in Fig. 3.3; the data is originating from private communication with Dipo Aldila [14]. The data values have been averaged over a period of 11 weeks, five weeks before and five after the respective week, in order to smoothen the data and eliminate potential outliers. The blue line shows the total amount of registered infections in the various districts. The green line shows the total amount of infections in Jakarta, which has been 'normalized' over the population share of the respective district.
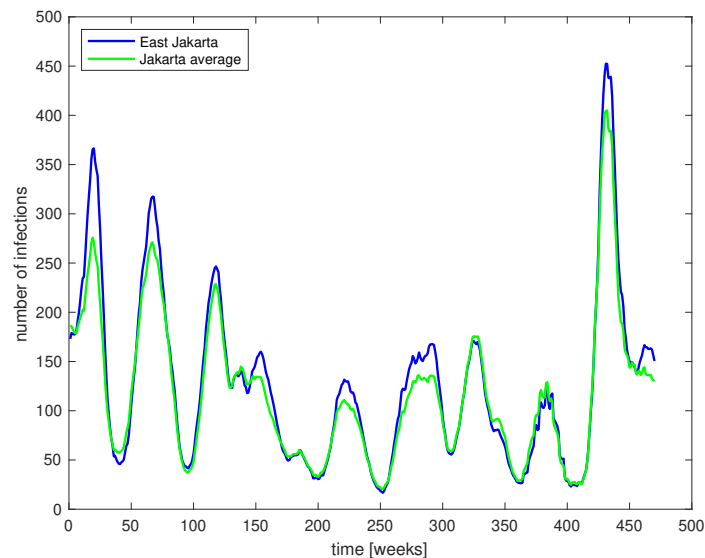
FIGURE 3.2: Reported Dengue cases in East Jakarta, 2008–2016.
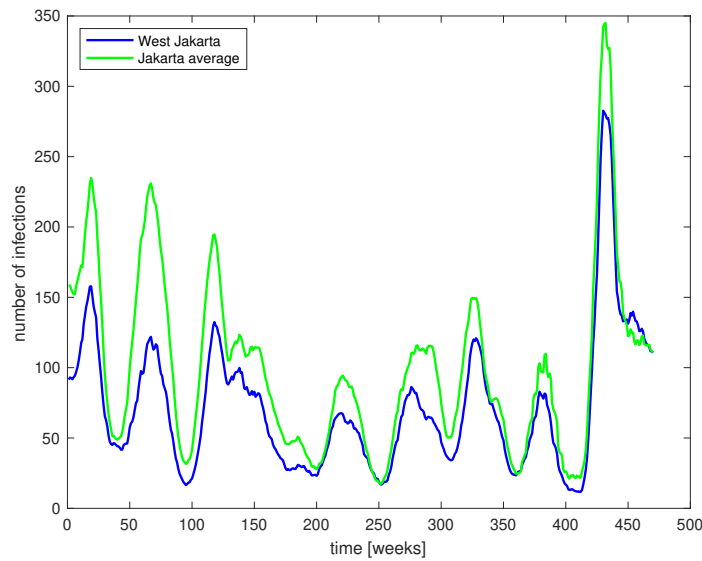
FIGURE 3.3: Reported Dengue cases in West Jakarta, 2008–2016.

Some districts that seem to have a significantly lower or higher infection rate than the Jakarta average, even if only in certain years. In Central Jakarta and North Jakarta, the infection rates are mostly slightly above average. In West Jakarta, the infection rate is generally lower, while in South and East Jakarta, the rates are roughly in line with the city average.

TABLE 3.3: Correlation between the Dengue cases in the districts of Jakarta and the total Dengue cases.

District	Central	North	West	South	East
Correlation	0.9402	0.9059	0.9167	0.9445	0.9734

The correlations between the respective district and the average are computed and shown in Tab. 3.3. It shows that all districts correlate highly with the data of the whole city, as all (main) districts have correlations over 0.9. North and West Jakarta appear to be the least well correlating districts, while East Jakarta correlates extremely well with the data of whole Jakarta. In the figures, it can also be seen that any model applied only on the total amount of infected in Jakarta cannot appropriately describe the dynamic of the disease in all districts. This is why in the following subsection, a model is set up that handles all districts and the local infections individually. For this, we will also allow mobility between districts, so that the infection can not only spread vertically in one district, but also between the districts.

A *mobility matrix* $G = \{g_{ij}\}$ of Jakarta is introduced (also originating from private communication with Dipo Aldila, University of Indonesia), which we will use in the following models. It is important that this mobility matrix is only an evaluation of the commuters from the year 2011 and is just a rough approximation for the whole time interval. The districts Central Jakarta, North Jakarta, West Jakarta, South Jakarta and East Jakarta are ordered as $i = 1, ..., 5$ in this order. The mobility matrix G is given in Tab. 3.4; the values (in percent) represent the fraction of the amount of resident humans in district i which move from i to district j (represented by row and column, respectively). Additionally, all entries on the diagonal are set to $m_{ii} := 1$,

which represent the total resident population within a district and which will also be helpful in the later model descriptions. Using this, we can set up a model including equations for the separate districts and also the mobility matrix G.

TABLE 3.4: Inter-district mobility matrix for Jakarta in 2011.

from \ to	Central	North	West	South	East
Central	100	7.79	11.05	11.82	5.56
North	11.54	100	6.61	3.14	4.19
West	11.76	10.61	100	6.73	1.15
South	13.03	2.71	5.19	100	6.41
East	10.06	7.21	3.50	11.52	100

3.4.2 Model equations

The main idea of the model lies in 'dividing' the total population N into n (in case of Jakarta $n = 5$) districts with a resident population N_i, each of which is assumed to be constant with equal birth and death rates. Analogously to before, there are three sub-compartments per district S_i, I_i and R_i, which are the susceptible, infected, and recovered persons in district i. The parameters μ, τ and κ are assumed to be equal for all districts and take on the same values as in the previous sections, while the parameters describing the transmission of the disease, i.e., β_i and λ_i, can alter in the various districts. Furthermore, mobility between the five districts has to be considered – otherwise, we would gain five independent single-department models. Humans from district i commute or travel to district j at a rate m_{ij} (which represents percentage of commuters resident in district i, compared to the total population N_i), but are assumed to return to their resident district after some time; there is no parameter that deals with the mobility of people who move from one district to the other. Vectorial mobility is hardly observable and thus also neglected.

We first consider some theory regarding multi-district epidemiological models. The multi-patch model is based upon the single-department model represented in eqns. (3.14), where effects of mobility have to be included in the transmission parts. This is why our first goal is to find an adequate formulation for the transmission parameters. Thus, there are three possible ways of disease transmission in district i:

1. Transmission from infected vectors in district i to susceptible humans resident in district i, i.e., $\beta_i \cdot S_i \cdot \frac{V_i}{M_i}$.

2. Transmission from infected vectors in all other districts j to susceptible humans commuting from district i into district j, i.e., $\sum\limits_{j \neq i} \beta_j \cdot g_{ij} S_i \cdot \frac{V_j}{M_j}$.

3. Transmission from infected humans commuting from district j into district i to susceptible vectors in district i, i.e., $\sum\limits_{j} \rho_i \cdot U_i \cdot g_{ji} \cdot \frac{I_j}{N_i}$.

As $m_{ii} = 1$, the first two equations can be combined into a single sum, but without the condition $j \neq i$. The multi-compartment model thus reads as follows:

$$S_i' = \mu \cdot (N_i - S_i) - \sum_j \beta_j g_{ij} S_i \cdot \frac{V_j}{M_j} + \kappa \cdot R_i, \tag{3.24a}$$

$$I_i' = -(\mu + \tau) \cdot I_i + \sum_j \beta_j g_{ij} S_i \cdot \frac{V_j}{M_j}, \tag{3.24b}$$

$$R_i' = -(\mu + \kappa) \cdot R_i + \tau I_i, \tag{3.24c}$$

$$U_i' = \theta \cdot (M_i - U_i) - \sum_j \rho_i U_i m_{ji} \cdot \frac{I_j}{N_i}, \tag{3.24d}$$

$$V_i' = -\theta V_i + \sum_j \rho_i U_i m_{ji} \cdot \frac{I_j}{N_i}. \tag{3.24e}$$

As in section 3, the equilibria of the vector population are calculated, then the susceptible class is omitted to reduce the dimensionality of the system. With some simple algebra, we find

$$I_i' = -(\mu + \tau) \cdot I_i + \sum_j \frac{\beta_j g_{ij} \cdot (N_i - I_i - R_i) \cdot \sum_k g_{kj} \cdot I_k}{\lambda_j + \sum_k g_{kj} \cdot I_k}, \tag{3.25a}$$

$$R_i' = -(\mu + \kappa) \cdot R_i + \tau \cdot I_i. \tag{3.25b}$$

3.4.3 Equilibria and stability

Analogously to section 2.3.3, we analyze the equilibria and their stability of the multi-compartment model with eqns. (3.25). Therefore, it must hold $(\dot{I}_i, \dot{R}_i) = (0,0)$ for every compartment i. This results in the equation system

$$I_i^* = \sum_j \frac{\beta_j g_{ij} \cdot (N_i - (1 + \frac{\tau}{\mu+\kappa}) \cdot I_i^*)) \cdot \sum_k g_{kj} I_k^*}{(\mu + \tau) \cdot (\lambda_j + \sum_k g_{kj} I_k^*)}, \tag{3.26a}$$

$$R_i^* = \frac{\tau}{\mu + \kappa} \cdot I_i^*. \tag{3.26b}$$

Obviously, there exists a disease-free equilibrium (DFE) if $(I_i^*, R_i^*) = (0,0)$ for all i. Unfortunately, eqn. (3.26) is an expression that cannot be explicitly solved for I_i^*, so we cannot explicitly compute the endemic equilibrium or equilibria (as there can be more than one).

However, the basic reproductive number can be calculated using eqns. (3.26). We find that F and W are 5×1 vectors with

$$F_i = \sum_j \frac{\beta_j g_{ij} \cdot (N_i - I_i - R_i) \cdot \sum_k g_{kj} I_k}{\lambda_j + \sum_k g_{kj} I_k}, \tag{3.27a}$$

$$W_i = (\mu + \tau) \cdot I_i. \tag{3.27b}$$

for $i = 1 \ldots 5$. The partial derivatives of F_i and W_i with respect to the infected of any district q (including i) are

$$(J_F)_{iq} = \frac{\partial F_i}{\partial I_q} = \sum_j \frac{\beta_j g_{ij} g_{qj} N_i}{\lambda_j}, \tag{3.28a}$$

$$(J_W)_{iq} = \frac{\partial W_i}{\partial I_q} = \begin{cases} \mu + \tau & q = i \\ 0 & q \neq i \end{cases}. \tag{3.28b}$$

Eqn. (3.28a) holds because it is assumed there are no infected in the respective compartment at the start, and thus the derivatives are evaluated at $I_j = 0$ for all districts j. The basic reproductive number is then calculated by the determinant of $J_F J_W^{-1}$. After some simplifications, it follows

$$\mathcal{R}_0 = (\mu + \tau)^{-\frac{1}{2}} \cdot \det(G)^{\frac{1}{n}} \cdot \left(\prod_{i=1}^n \frac{\beta_i \cdot N_i}{\lambda_i} \right)^{\frac{1}{2n}}. \tag{3.29}$$

This result will become important later when the basic reproductive number can be computed out of the means of the parameters of the Metropolis chains.

Another interesting aspect of the equilibria of multi-district models is the behaviour of the whole system in case of one district being at its DFE or its EE. Therefore, regarding eqns. (3.26), if the system is at an equilibrium, then $(I_i', R_i') = (0,0)$ for all districts i. If one district i^* is in the DFE, then it additionally holds $I_{i^*} = R_{i^*} = 0$. For this district i^*, it follows from equation (3.26)

$$\sum_j \frac{\beta_j g_{i^*j} N_{i^*} \cdot \sum_k g_{kj} I_k}{\lambda_j + \sum_k g_{kj} I_k} = 0. \tag{3.30}$$

As all summands are non-negative, any summand in this formula must be equal to 0. It also holds true that the denominator is larger than 0, as for all j, it holds $\lambda_j > 0$ and thus

$$\beta_j g_{i^*j} N_{i^*} \cdot \sum_k g_{kj} I_k = 0 \tag{3.31}$$

for all j. Further simplification yields

$$g_{i^*j} \cdot \sum_k g_{kj} I_k = 0 \tag{3.32}$$

for all j. There are only three possibilities to satisfy eqn. (3.32). The first is that $I_k = 0$ for all k. The other two are that either for those k where $I_k \neq 0$, it must hold $g_{kj} = 0$ or $g_{i^*j} = 0$ for all j, so that there is either no mobility from district k to district j, or there are no commuters from district i^*. The latter two conditions might be valid in case the observed areas are much larger (e.g., a whole country), but for non-isolated areas, this is unreasonable. So, in case of an equilibrium, if one district is in the DFE, then all other non-isolated districts are in the DFE as well.

If the system is at an equilibrium and one district i^* is in the EE, so that $I_{i^*} > 0$, it is easy to see that disease in all other districts that can be reached from district i is in the EE as well. If one of the other districts, say i', would be in the DFE, then by the previous result all other districts would be in the DFE as well, which contradicts the statement that district i^* is in the EE.

3.5 Results

Applying the theoretical results of the previous sections, we can now make use of the Metropolis algorithm (see section 3.2.2) to the three described models, the single-compartment model and the multi-compartment models with district-dependent and district-independent parameters. It is not trivial to see the number of draws is 'high enough' to receive a decent parameter estimation, so that density plots of the parameters after $r = 2 \cdot 10^4$ draws are discussed later.

3.5.1 Single-compartment model

Using the data and the theoretical results from section 3.3, we now implement the algorithm on the single-compartment model as of eqns. (3.16).

For values of the fixed parameters μ, τ, κ see Tab. 3.1. Starting values for the infective and recovered populations are not modelled, but taken out of the data. It is presumed that the initial value for the recovered is $R_0 = 0$ as for any biologically realistic value of $R_0 \in [0, N]$ the estimated infection data is not affected significantly in the long run. The starting value for the number of registered infected persons I_0 is computed out of the starting value of the (flattened) epidemiological data, divided by η_1, which changes in each run of the algorithm.

After several test runs, correlations of all 12 parameters were computed. In these tests, it appeared ω_2 and ϕ_2 are highly correlated ($\rho > 0.95$), because of this we fixed ϕ_2 to the estimated value $\phi_2 = 47.8$ as identification of both parameters is not possible due to high correlation. Thus, the mutable parameter vector is reduced to $\theta = (\beta_0, c_1, c_2, c_3, \omega_2, \omega_3, \phi_1, \phi_3, \lambda, \eta_1, \eta_2)$. All other parameter combinations had correlations < 0.8.

The standard deviation of the estimated infected σ_I in the infection dynamics we find for the initial parameter set is used to find an reasonable value for the standard deviation of the target distribution. The proposal distribution draws samples from the parameter set with this standard deviation (which can be called the 'step size' of the algorithm) and a resulting normal distribution $q \sim \mathcal{N}(\theta_{i-1}, \sigma_I)$. To implement the accept/reject choice, a random number $\alpha^* \sim \mathcal{U}(0, 1)$ is drawn; if $\alpha > \alpha^*$ with α as of eqn. (3.8), the new state is accepted, otherwise rejected. We cannot be certain to have achieved convergence of the algorithm after r draws with respect to the parameter set θ according to [15, 11]. However, there are several tools for determining convergence [12]. This will be part of the discussion in section 3.6.

Parameter statistics of the algorithm are shown in Tab. 3.5 for the single-patch model are provided. For a better understanding of the parameter values, all ω_i are normalized so that they have the unit $[y^{-1}]$.

TABLE 3.5: Parameter statistics, single-compartment model.

	Parameter Mean	Standard Deviation
β_0	$2.4589 \cdot 10^{-4}$	$0.0219 \cdot 10^{-4}$
c_1	$6.4788 \cdot 10^{-5}$	$0.1614 \cdot 10^{-5}$
c_2	$3.0351 \cdot 10^{-5}$	$0.2575 \cdot 10^{-5}$
c_3	$1.0255 \cdot 10^{-4}$	$0.0231 \cdot 10^{-4}$
ω_2	4.2438	0.0940
ω_3	$2.4353 \cdot 10^{1}$	$0.0216 \cdot 10^{1}$
ϕ_1	$2.3290 \cdot 10^{1}$	$0.0150 \cdot 10^{1}$
ϕ_2	$4.7796 \cdot 10^{1}$	parameter fixed
ϕ_3	$7.0732 \cdot 10^{1}$	$0.0061 \cdot 10^{1}$
λ	$3.8029 \cdot 10^{2}$	$0.0378 \cdot 10^{2}$
η_1	3.2197	0.0188
η_2	1.3151	0.0245

3.5.2 Model with compartment-independent parameters

Next, we will consider the multi-compartment model as of eqns. (3.25). It is assumed that all β_i are independent of the compartment i, thus the autonomous part β_0 is the same in all compartments, as well as λ_i, η_1 and η_2. Thus, no local differences except of the total population of the compartments, starting values for the infective and mobility between classes are considered. Optimization is done with respect to the sum of squares function as of eqn. (3.9), for the data of all five districts.

The fixed parameters μ, τ, κ remain the same as before (see Tab. 3.1). $I_{i,0}$ is the starting value of infective persons in each district, divided by the parameter η_1 which changes in each draw, while $R_{i,0} = 0$ for all districts. The mutable parameter set still consists of the 11 parameters as in subsection 3.5.1. The parameter means and standard deviations are shown in Tab. 3.6.

TABLE 3.6: Parameter statistics, multi-district, district-independent transmission and hospitalization parameters.

parameter	unit	mean value	standard deviation
β_0	$[10^{-4}]$	2.2860	0.0189
c_1	$[10^{-5}]$	7.2466	0.0289
c_2	$[10^{-5}]$	3.9310	0.1540
c_3	$[10^{-5}]$	8.1134	0.2428
ω_2	$[10^{0}]$	4.4319	0.0464
ω_3	$[10^{1}]$	1.8682	0.1314
ϕ_1	$[10^{1}]$	2.3266	0.0037
ϕ_2	$[10^{1}]$	5.4305	parameter fixed
ϕ_3	$[10^{1}]$	7.0131	0.0114
λ	$[10^{1}]$	9.6255	0.1852
η_1	$[10^{0}]$	5.1401	0.0115
η_2	$[10^{0}]$	1.7321	0.0763

3.5.3 Model with compartment-dependent parameters

Similar to subsection 3.5.2 (see there for more information about the 'setup'), we will use the algorithm on eqns. (3.25), including local differences in transmission and registration rates. This means that the transmission and hospitalization parameters β_i, λ_i and $\eta_{1,2}$ are assumed to be variable as well. The means and standard deviations of the parameter set are shown in Tab. 3.7.

TABLE 3.7: Parameter means and standard deviations.

parameter	unit	C mean	C std	N mean	N std	W mean	W std	S mean	S std	E mean	E std
β_0	$[10^{-4}]$	2.3031	0.0049	2.3448	0.0683	2.2668	0.0310	2.2634	0.0087	2.2264	0.0014
c_1	$[10^{-5}]$	6.7742	0.0671	6.9125	0.1596	6.9869	0.0801	6.7701	0.0618	7.7733	0.2692
c_2	$[10^{-5}]$	3.8024	0.0378	4.2536	0.0721	3.5507	0.0798	4.7544	0.1266	4.3061	0.1122
c_3	$[10^{-5}]$	8.6899	0.1122	7.8066	0.0660	8.5680	0.0247	8.4691	0.0382	7.9756	0.0079
ω_2	$[10^{0}]$	4.3519	0.0449	4.9020	0.0398	3.1474	0.0381	4.8015	0.0357	4.4661	0.0464
ω_3	$[10^{1}]$	1.815	0.0596	2.2035	0.1469	2.5976	0.0106	1.6225	0.0256	1.8054	0.0631
ϕ_1	$[10^{1}]$	2.3353	0.0037	2.3211	0.0199	2.3214	0.0021	2.3357	0.0017	2.3246	0.0011
ϕ_2	$[10^{1}]$	5.3931	fixed	5.4407	fixed	5.4465	fixed	5.4678	fixed	5.4287	fixed
ϕ_3	$[10^{1}]$	6.9882	0.0062	7.0502	0.0138	7.0709	0.0032	6.9819	0.0049	7.0029	0.0054
λ	$[10^{1}]$	9.5301	0.0941	9.9895	0.0433	9.8583	0.0519	9.5031	0.0442	8.4255	0.0614
η_1	$[10^{0}]$	4.9173	0.0408	4.4751	0.1446	6.3710	0.0723	5.3111	0.0454	4.4445	0.0371
η_2	$[10^{0}]$	1.8235	0.0594	1.6728	0.0333	2.4642	0.0711	1.7108	0.0251	1.4502	0.0250

3.6 Discussion of the Models

In this section, the results of the models in sections 3.5.1 – 3.5.3 are compared in terms of the basic reproductive number as well as their $\mathcal{L}_1$ and $\mathcal{L}_2$ errors. The solutions of the disease dynamics with the mean of the estimated parameters are also presented. In this section, 'model 1' refers to the single-compartment model, 'model 2' to the multi-compartment model with district-independent parameters, and 'model 3' to the multi-district model with district-dependent parameters.

Tab. 3.8 lists the computed (mean) basic reproductive numbers $\mathcal{R}_0$ for the three analyzed models computed out of eqn. (3.23) and (3.29) as well as the minimum and maximum values taken out of the standard deviation ranges from all parameters.

TABLE 3.8: Mean, minimal and maximal values for $\mathcal{R}_0$ for the different models.

	model 1	model 2	model 3
$\mathcal{R}_0$	6.21	8.22	8.63
$\mathcal{R}_{0,\,\min}$	6.09	8.00	8.54
$\mathcal{R}_{0,\,\max}$	6.32	8.45	8.73

All models feature basic reproductive numbers considerably larger than 1 and thus the disease is assumed to be endemic. In the model with district-dependent parameters, $\mathcal{R}_0$ is significantly higher than in the single-district model.

In Fig. 3.4, the results for the multi-district model of all three models are plotted. In Fig. 3.5 and Fig. 3.6, examplary plots of the estimated and real numbers of infections in East and West Jakarta are shown for all three models.
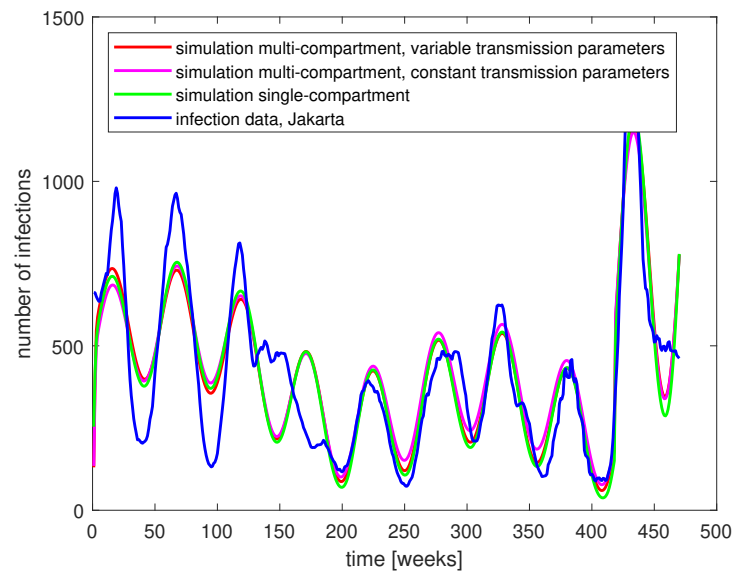
FIGURE 3.4: Real and estimated Dengue cases in Jakarta.
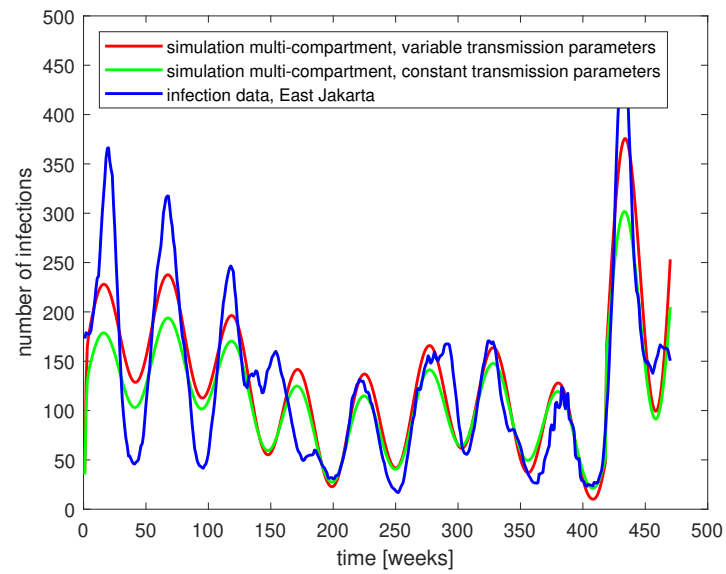
FIGURE 3.5: Real and estimated Dengue cases in East Jakarta.
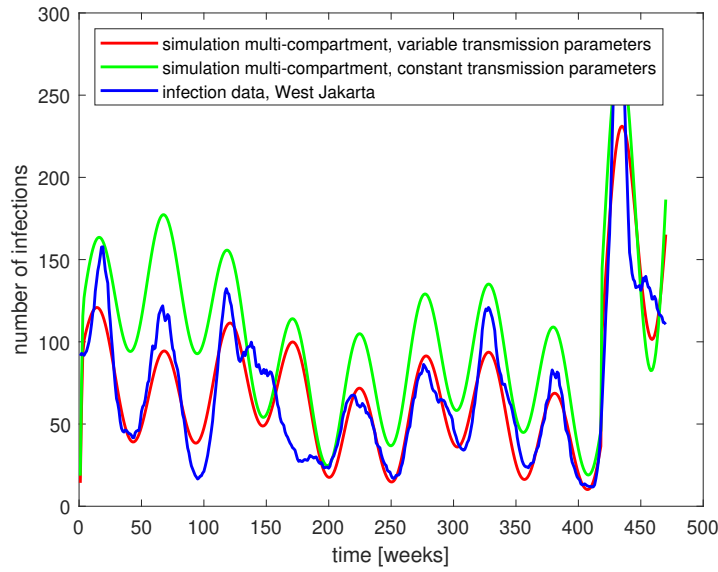
FIGURE 3.6: Real and estimated Dengue cases in West Jakarta.

For the quantitative comparison of all models with the data sets, we use both $\mathcal{L}^1$ and $\mathcal{L}^2$ errors for Jakarta and each of its districts. In the case of the single-compartment model, the estimation of the various districts, which were not required in the model, is done by multiplying the total estimated infections with the relative amount of persons in the respective district according to Tab. 3.2, e.g., by $\frac{0.9}{9.6}$ in Central Jakarta. Tab. 3.9 shows the errors of the models for Jakarta and all districts.

TABLE 3.9: Comparison of the models with real data using $\mathcal{L}_1$ and $\mathcal{L}_2$ norms.

district	model 1, $\mathcal{L}^1$	model 2, $\mathcal{L}^1$	model 3, $\mathcal{L}^1$	model 1, $\mathcal{L}^2$	model 2, $\mathcal{L}^2$	model 3, $\mathcal{L}^2$
Jakarta	0.2319	0.2338	0.2294	0.2513	0.2340	0.2504
Central Jakarta	0.2934	0.2910	0.2866	0.3620	0.3323	0.3138
North Jakarta	0.2590	0.2624	0.2348	0.2811	0.2881	0.2549
West Jakarta	0.4555	0.4607	0.2128	0.4618	0.4644	0.2500
South Jakarta	0.2683	0.2689	0.2563	0.2874	0.2831	0.2772
East Jakarta	0.2612	0.2807	0.2593	0.2984	0.3257	0.2820

In Fig. 3.4 and Tab. 3.9, it is visible that all three models are approximating the total amount of infected in Jakarta decently and both $\mathcal{L}_1$ and $\mathcal{L}_2$ norms are quite similar in all three models. As to be expected, the single-district model is significantly 'worse' when comparing the results for Jakarta's districts. The multi-district model with district-independent parameters improves the results for the districts, while the model with district-dependent parameters generally yields the best results for the districts.

As also to be seen in Fig. 3.5, both multi-district models are decent approximates for East Jakarta. In Fig. 3.6, the model including the district-dependent parameters for all districts is not a decent approximation, while the one with variable transmission parameters is much more accurate. In all figures, some peaks are underestimated even in the 'best' model; however, from week 200 onwards, the dynamics are approximated quite well.

For diagnostics of convergence, see also Appendix A where the density plots of the parameter set after $r = 2 \cdot 10^5$ draws are shown. Most of the parameter plots

show a normally or almost normally distributed behaviour. It is visible, however, that several parameters appear to not be normally distributed (e.g., θ_3 in Fig. 3.9), although the bandwidth is comparatively small. This can be a hint of hidden correlations with other parameters or a small impact of the parameter in the equations, which can be caused by the model itself. Methods like burn-in or thinning as of e.g. [11] do not lead to better mixing parameters.

3.7   Conclusion

The multi-district model with district-dependent parameters yields satisfying results to real data and appears to model spatial heterogeneity and mobility visibly better compared to the single-patch model and the multi-patch model with district-independent parameters. Theoretical findings make it possible to calculate, e.g., the basic reproductive numbers $\mathcal{R}_0$ for the model. Problems like seasonality in the data, jumps because of a different counting strategy of infections or a change in the health policy are addressed. Handling of mobility and the quality of the model is strongly dependent on reliable data. The mobility matrix G we have used in the models is a rough estimate in a single year of the time period while the data obviously cannot cover all infected – only the registered – persons. This, together with the time dependency of transmission rates and jumps in the infection data, make it difficult to the find decent estimates of the real infected data. The methods we have implemented to solve these problems can be used in other infection scenarios as well, if only partially in case, e.g., mobility data is not present. More pre-knowledge about the parameters (e.g., the vector population and disease-related information) can be a valuable aid in their identification and reduce the diagnostic problems.

Declarations

Competing interests

The authors declare that there exist no competing interests.

Acknowledgements

The authors want to thank the (unknown) reviewers for having pointed out mistakes and providing helpful suggestions.

Authors' contributions

All authors contributed a significant part and reviewed the manuscript.

A Density plots of parameters

A.1 Single-district model
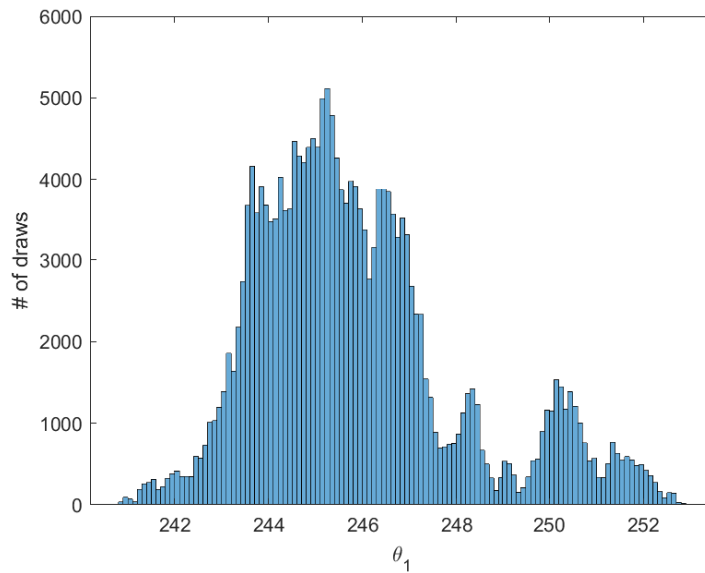
FIGURE 3.7: Density plot of β_0 for model 1.
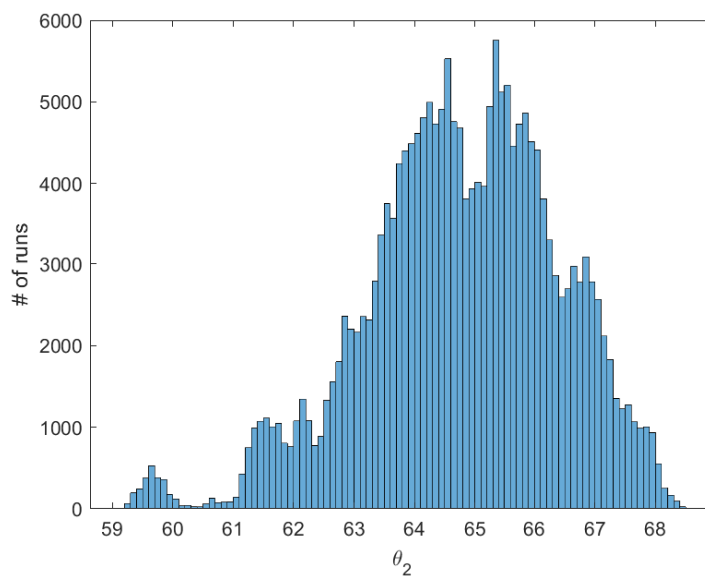
FIGURE 3.8: Density plot of c_1 for model 1.
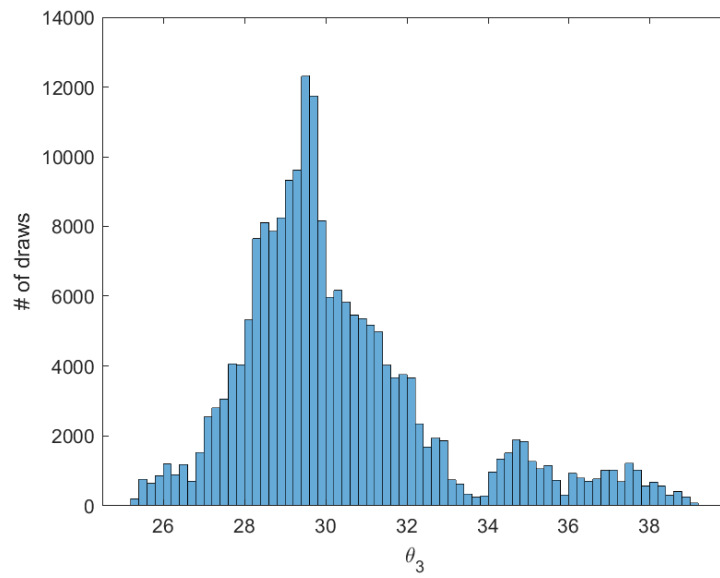
FIGURE 3.9: Density plot of c_2 for model 1.
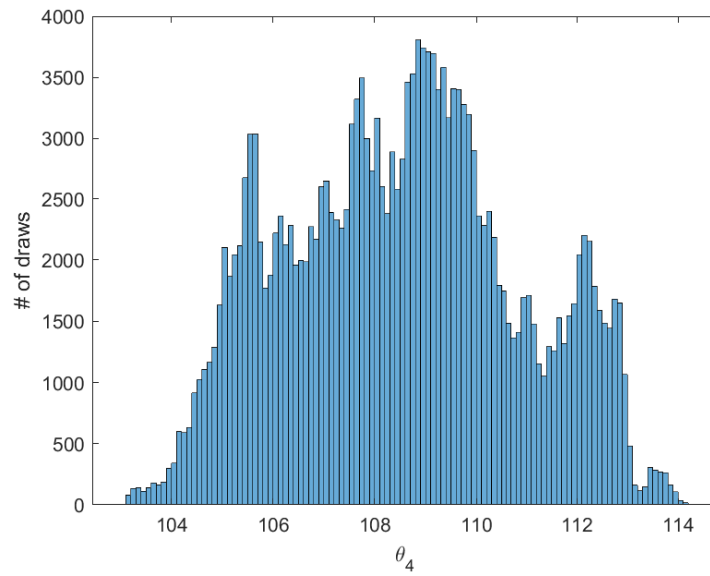
FIGURE 3.10: Density plot of c_3 for model 1.
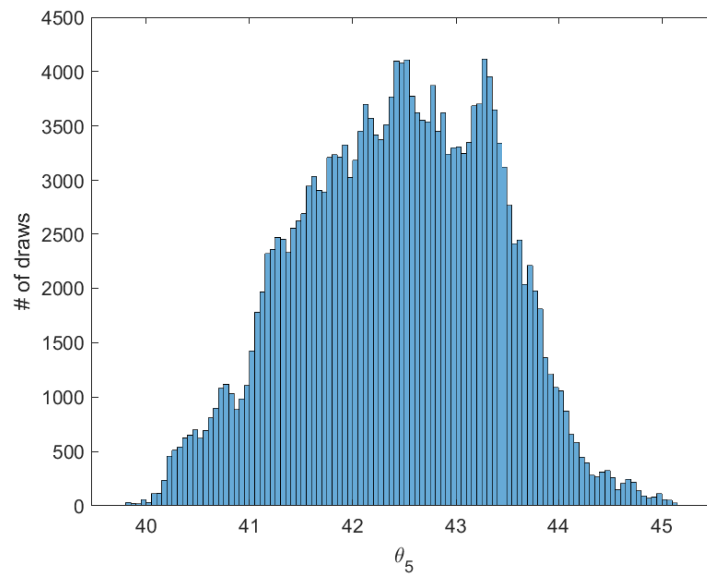
FIGURE 3.11: Density plot of ω_2 for model 1.
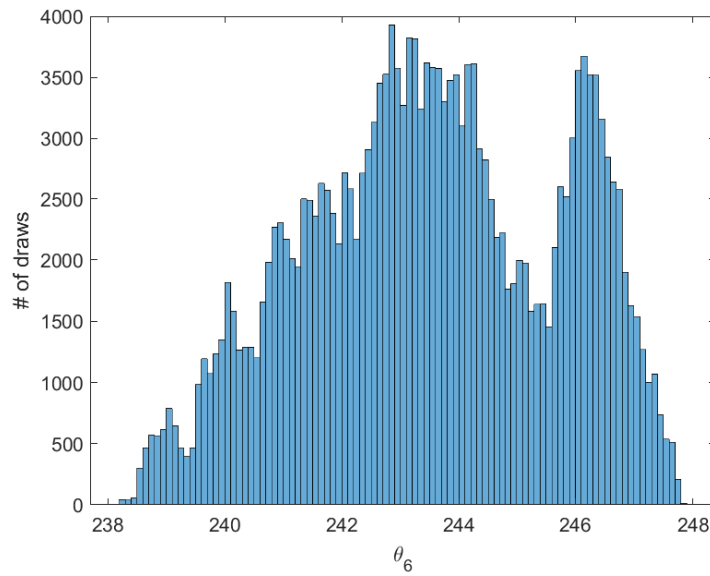
FIGURE 3.12: Density plot of ω_3 for model 1.
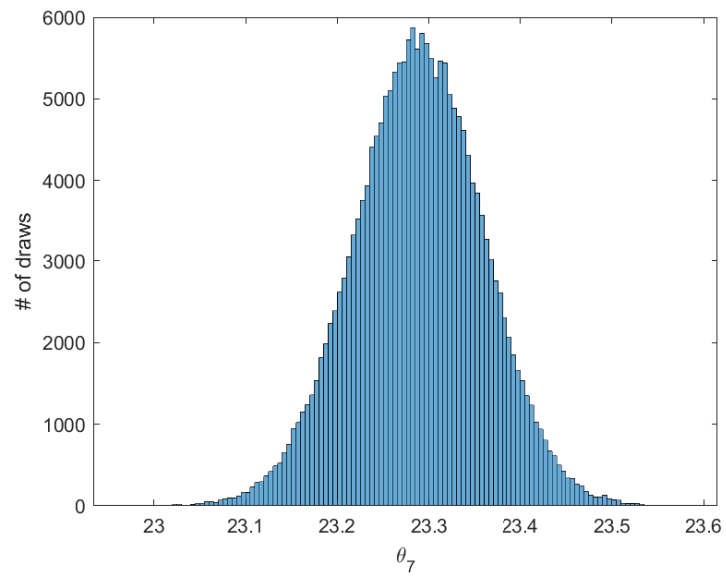
FIGURE 3.13: Density plot of ϕ_1 for model 1.
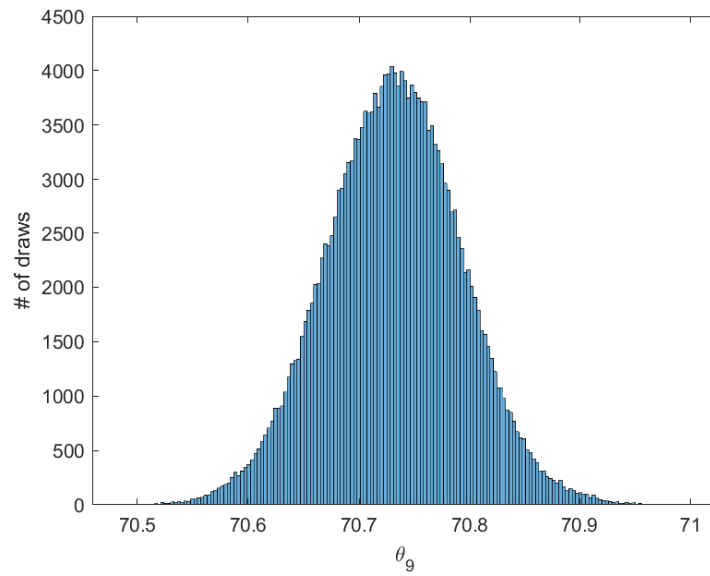
FIGURE 3.14: Density plot of ϕ_2 for model 1.
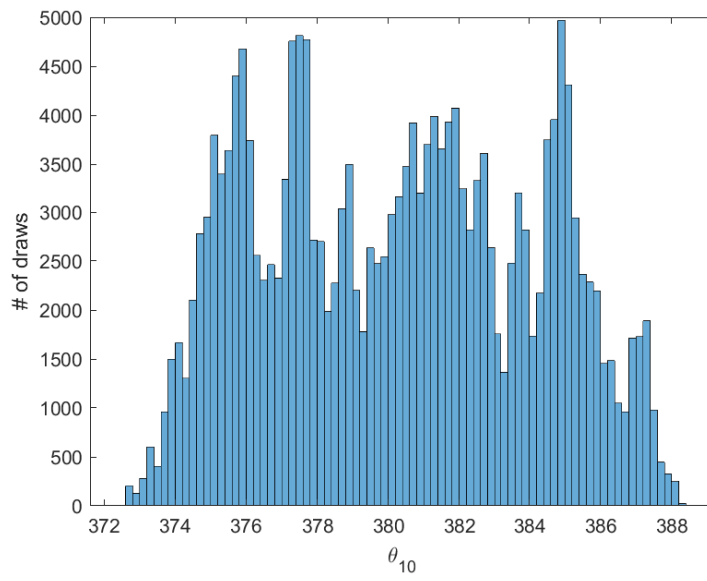
FIGURE 3.15: Density plot of ϕ_3 for model 1.
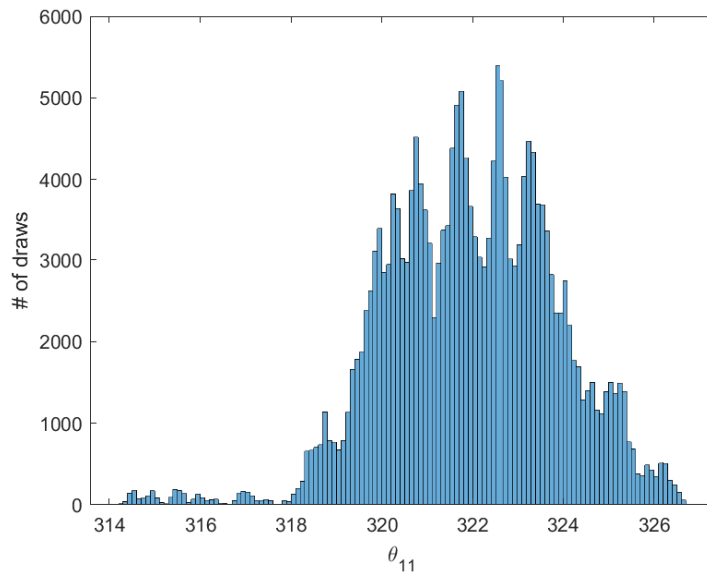
FIGURE 3.16: Density plot of η_1 for model 1.
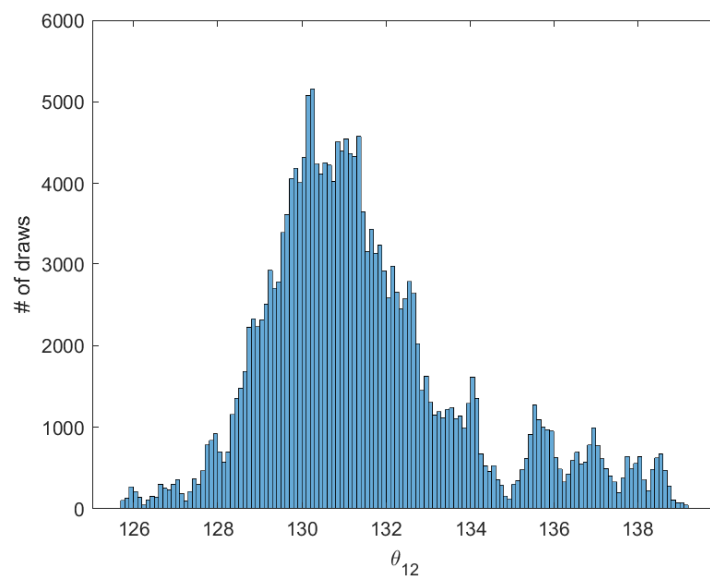
FIGURE 3.17: Density plot of η_2 for model 1.

A.2 Multi-district model with district-independent parameters
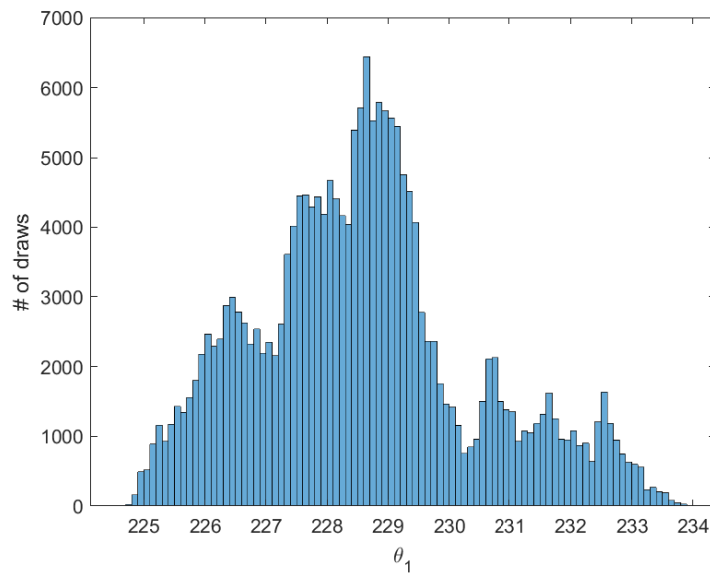
FIGURE 3.18: Density plot of β_0 for model 2.
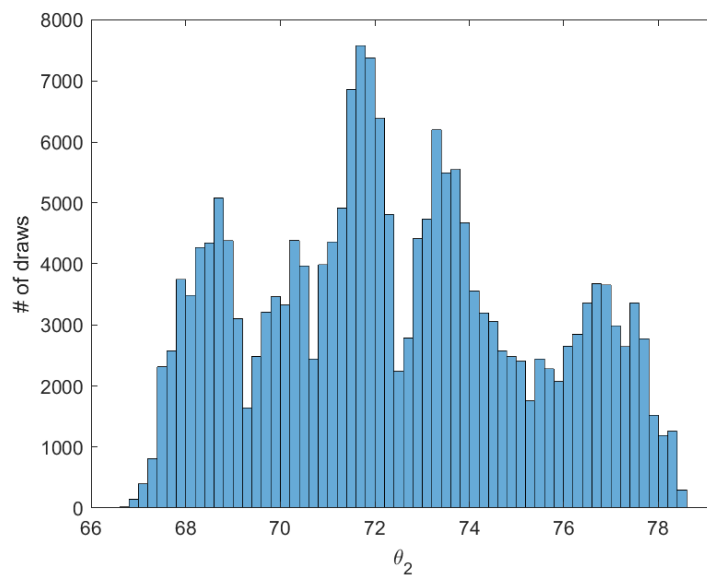
FIGURE 3.19: Density plot of c_1 for model 2.
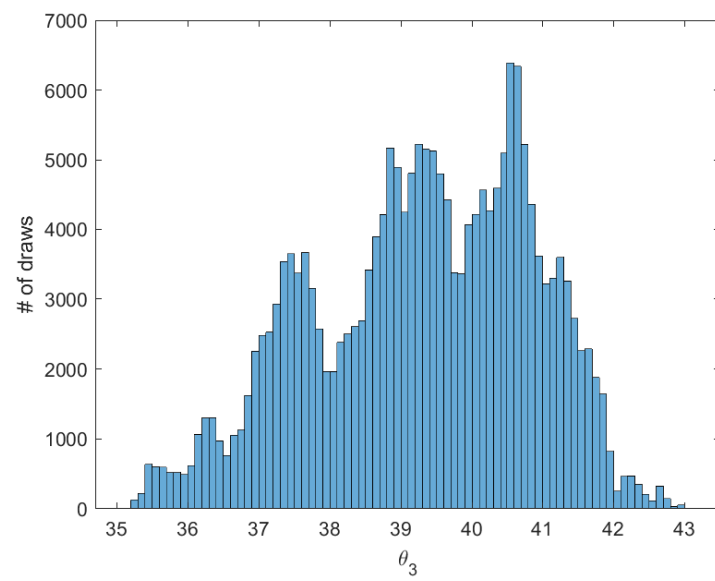
FIGURE 3.20: Density plot of c_2 for model 2.
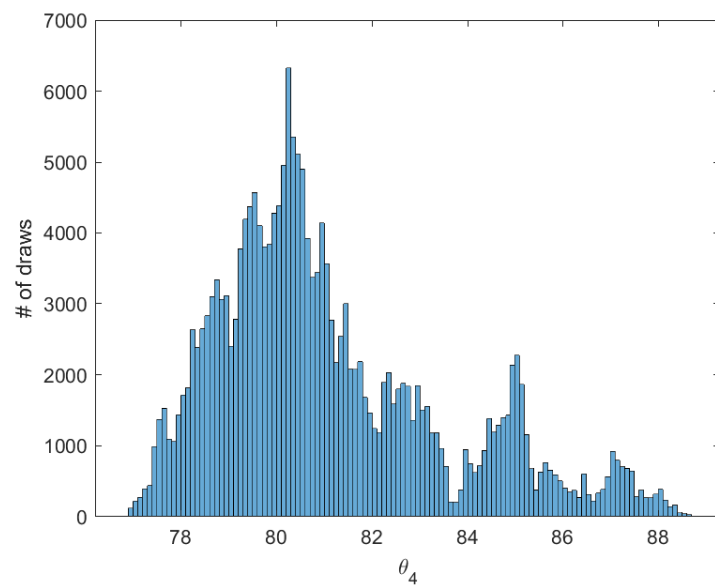
FIGURE 3.21: Density plot of c_3 for model 2.
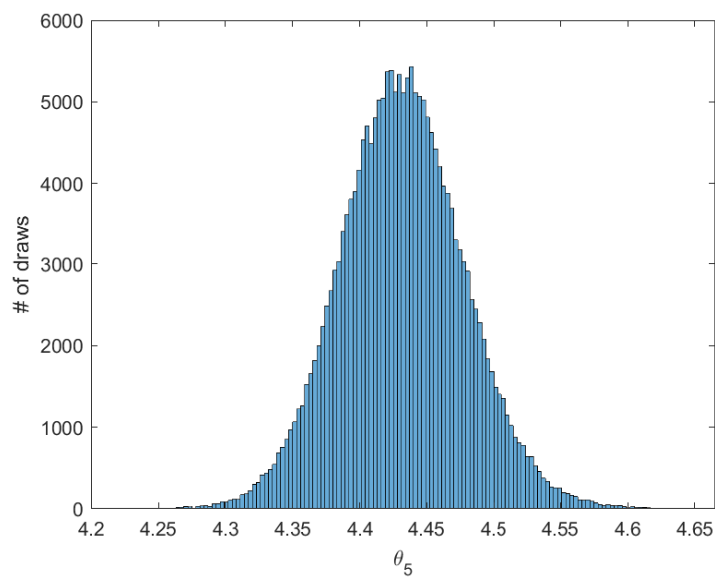
FIGURE 3.22: Density plot of ω_2 for model 2.
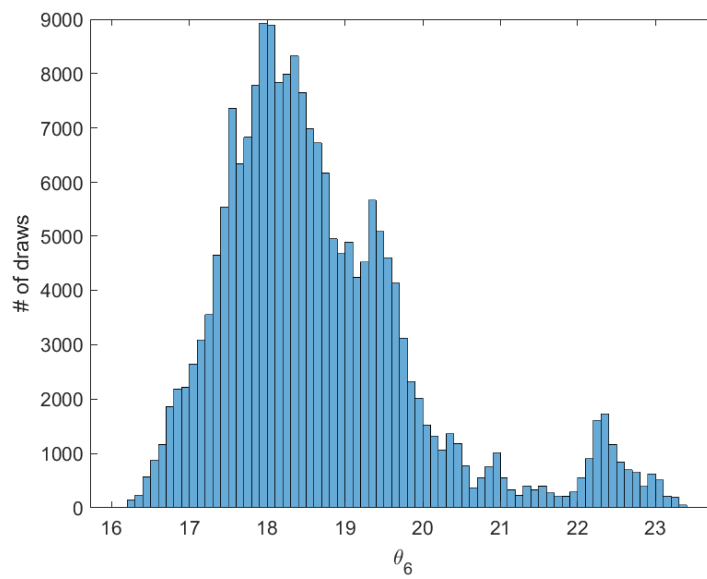
FIGURE 3.23: Density plot of ω_3 for model 2.
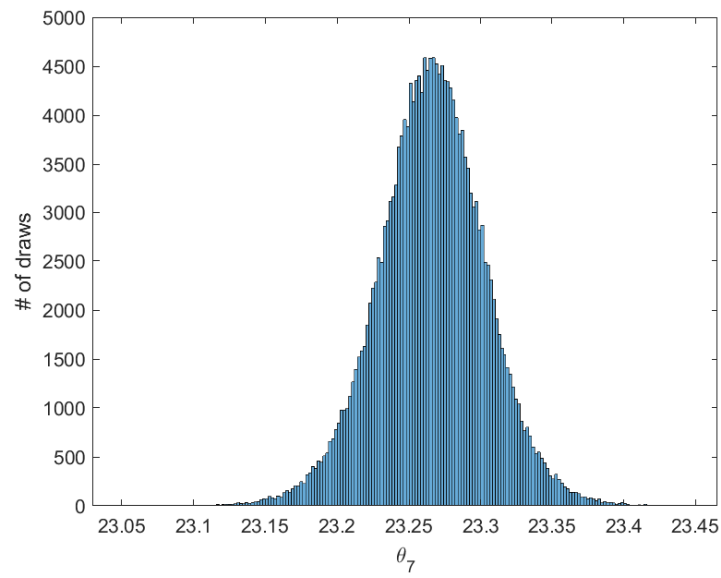
FIGURE 3.24: Density plot of ϕ_1 for model 2.
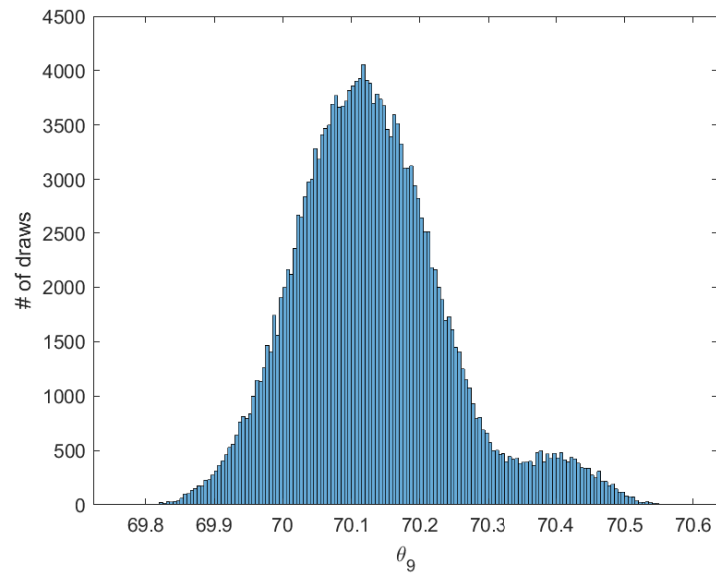
FIGURE 3.25: Density plot of ϕ_2 for model 2.
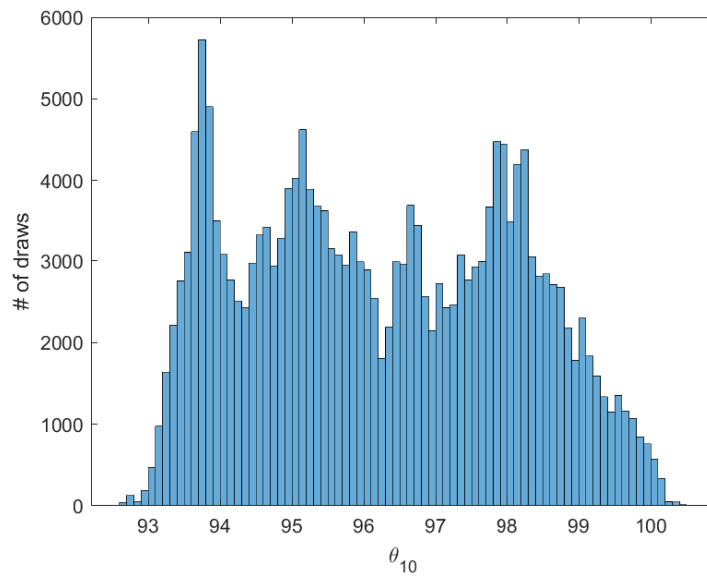
FIGURE 3.26: Density plot of ϕ_3 for model 2.
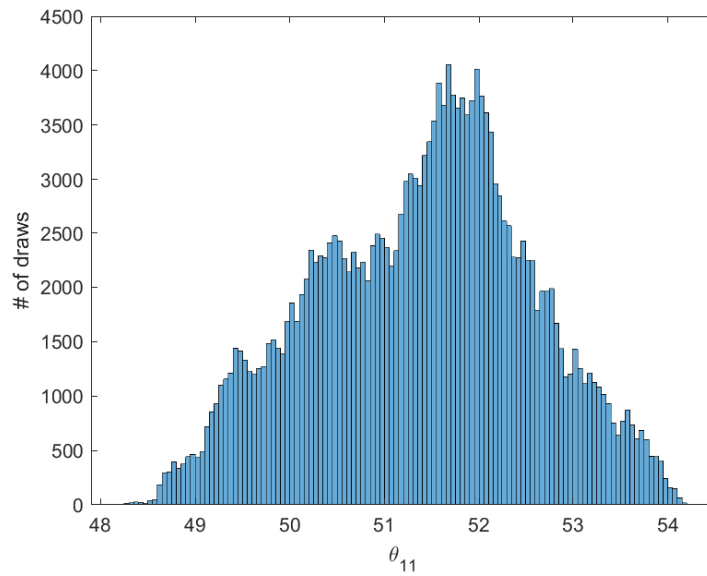
FIGURE 3.27: Density plot of η_1 for model 2.
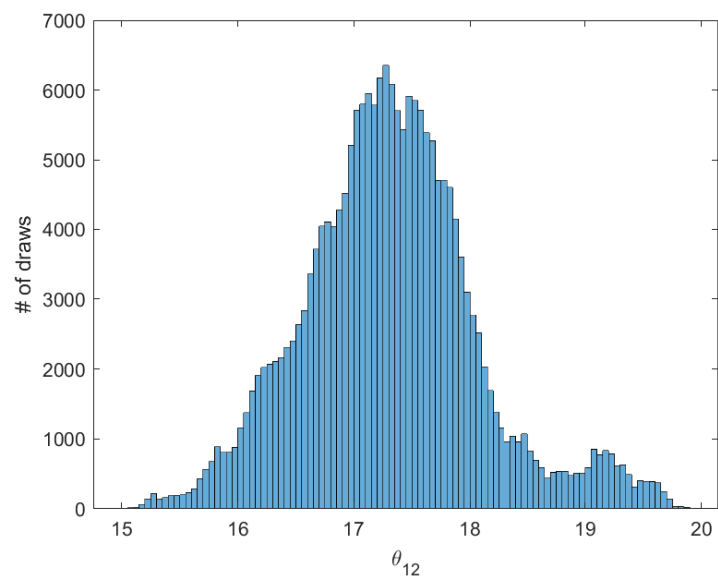
FIGURE 3.28: Density plot of η_2 for model 2.

A.3 Multi-compartment model with district-dependent parameters
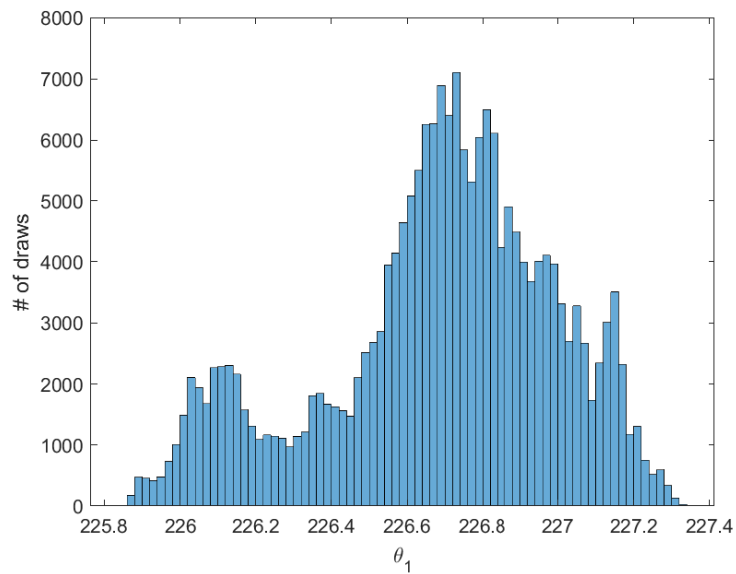
FIGURE 3.29: Density plot of β_0 for model 3, exemplary for West Jakarta.
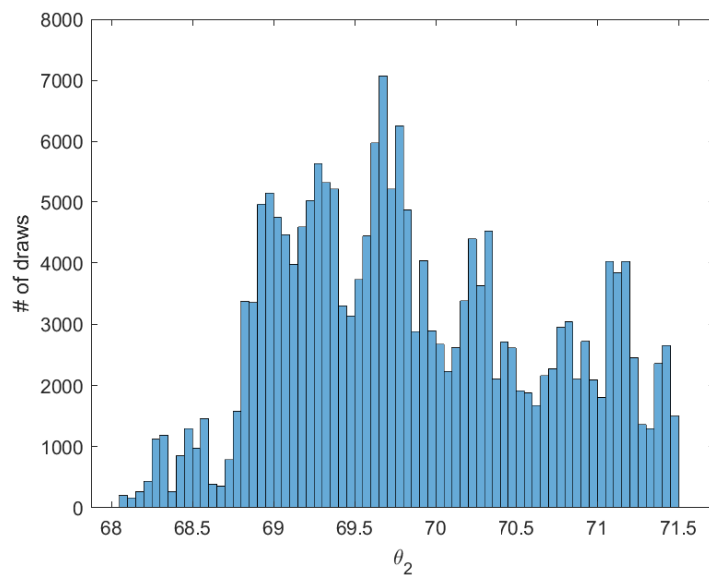
FIGURE 3.30: Density plot of c_1 for model 3, exemplary for West Jakarta.
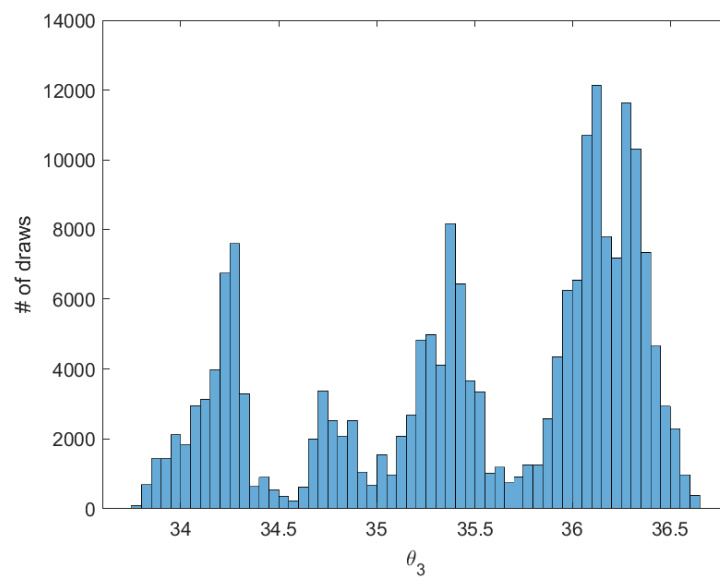
FIGURE 3.31: Density plot of c_2 for model 3, exemplary for West
Jakarta.
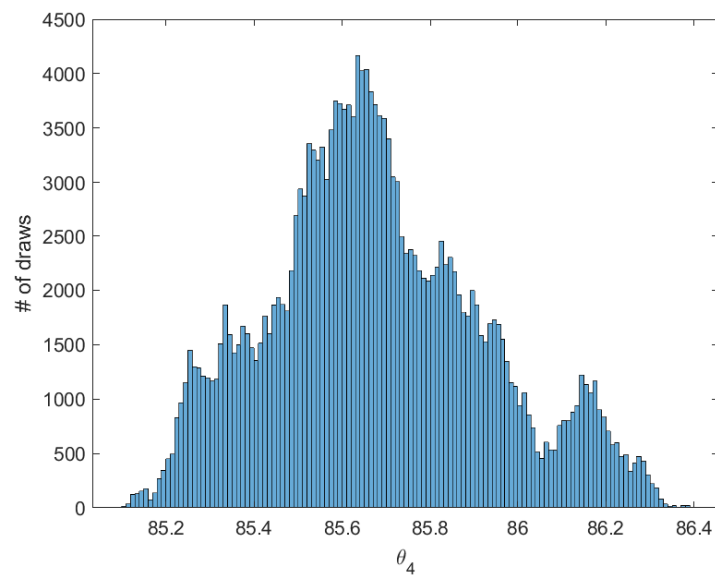
FIGURE 3.32: Density plot of c_3 for model 3, exemplary for West
Jakarta.
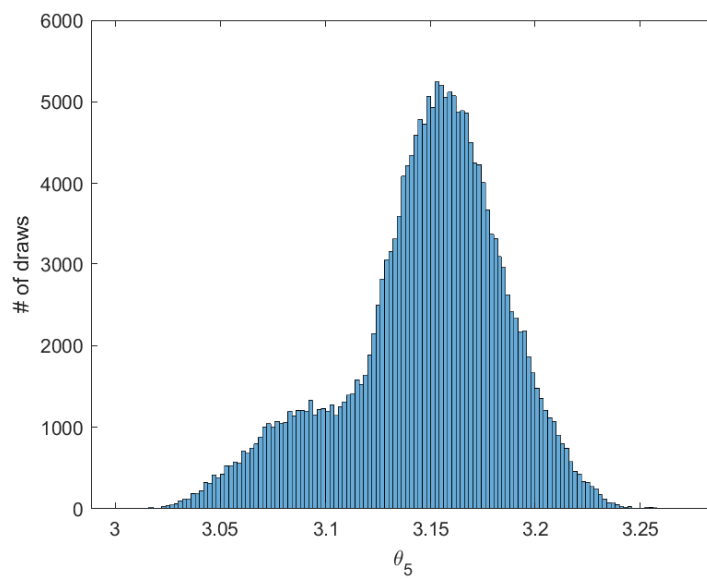
FIGURE 3.33: Density plot of ω_2 for model, exemplary for West Jakarta.
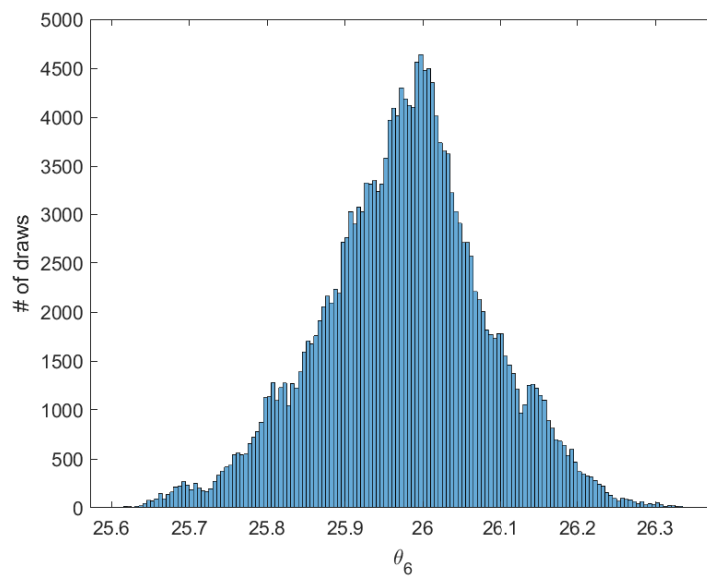
FIGURE 3.34: Density plot of ω_3 for model 3, exemplary for West Jakarta.
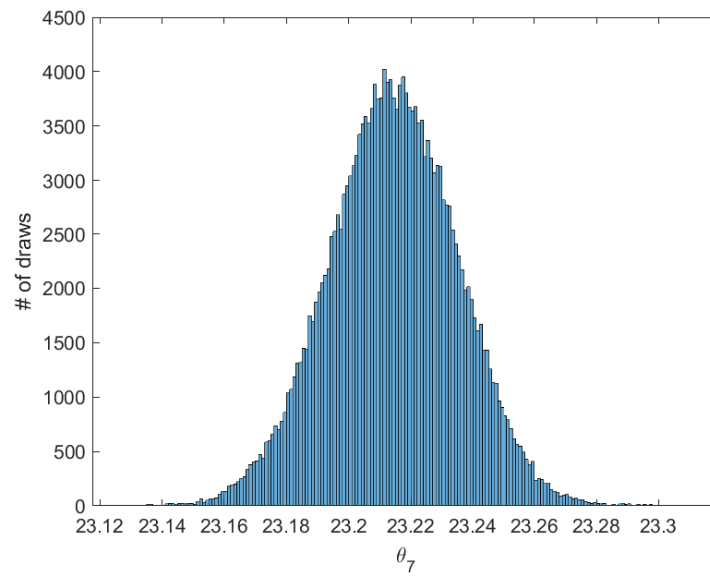
FIGURE 3.35: Density plot of ϕ_1 for model 3, exemplary for West Jakarta.
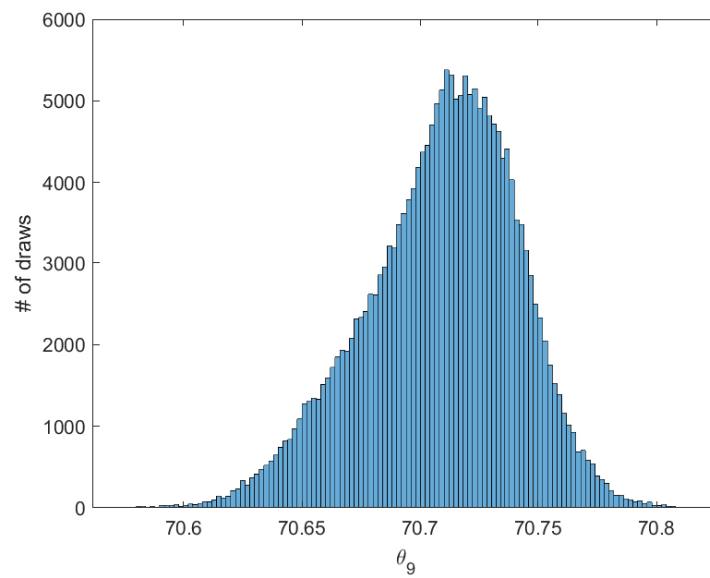
FIGURE 3.36: Density plot of ϕ_2 for model 3, exemplary for West Jakarta.
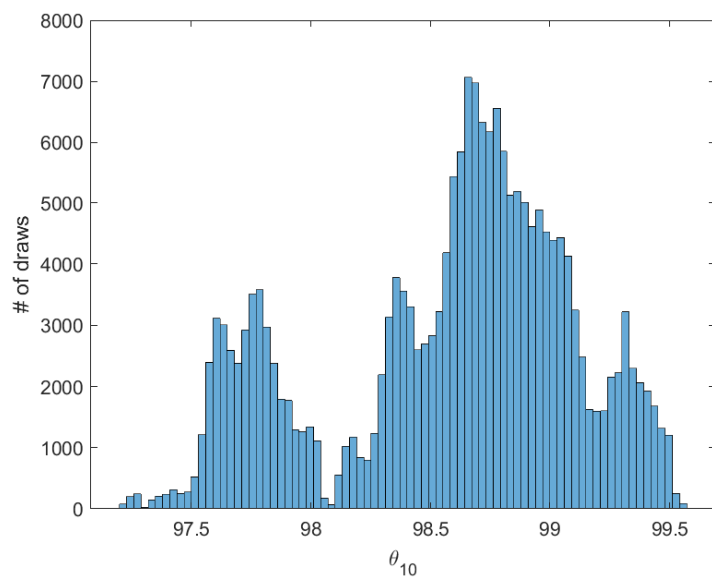
FIGURE 3.37: Density plot of ϕ_3 for model 3, exemplary for West Jakarta.
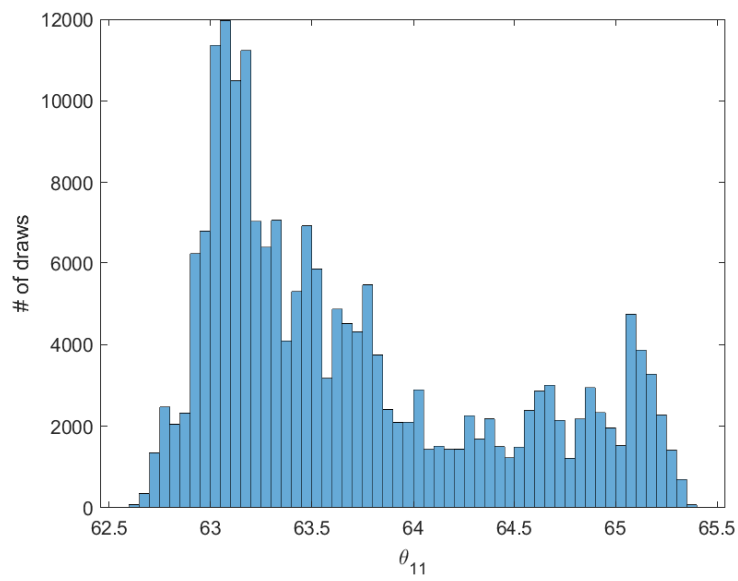
FIGURE 3.38: Density plot of η_1 for model 3, exemplary for West Jakarta.
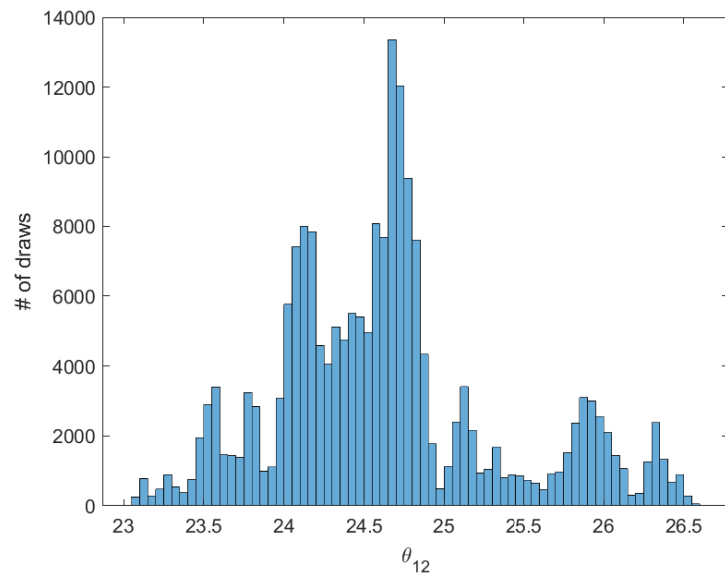
FIGURE 3.39: Density plot of η_2 for model 3, exemplary for West Jakarta.

Bibliography

[1] Schäfer, M. *Mathematical Modelling of Dengue Fever in Jakarta*. Master thesis, University of Koblenz-Landau, 2018.

[2] World Health Organization. *Dengue and severe dengue*. `https://www.who.int/news-room/fact-sheets/detail/dengue-and-severe-dengue`. last visited: 18 December, 2023.

[3] Souza, M. O. "Multiscale analysis for a vector-borne epidemic model". In: *J. Math. Biol.* 68 (2014), pp. 1269–1293.

[4] Olinky, R., Huppert, A., and Stone, L. "Seasonal dynamics and thresholds governing recurrent epidemics". In: *J. Math. Biol.* 56 (2008), pp. 827–839.

[5] Augeraud-Véron, E. and Sari, N. "Seasonal dynamics in an SIR epidemic system". In: *J. Math. Biol.* 68 (2014), pp. 701–725.

[6] Gilks, W.R., Richardson, S., and Spiegelhalter, D.J. *Markov chain Monte Carlo in Practice*. London: Chapman and Hall/CRC, 1996.

[7] Ross, S. *Introduction to Probability Models*. Elsevier India, 2014.

[8] Andrieu, C. et al. "An Introduction to MCMC for Machine Learning". In: *Mach. Learn.* 50 (2003), pp. 5–43.

[9] Perron, O. "Zur Theorie der Matrices". In: *O. Math. Ann.* 64 (1907), pp. 248–263.

[10] Frobenius, G. "Ueber Matrizen aus nicht negativen Elementen". In: *Sitzungsberichte der Koeniglich Preussischen Akademie der Wissenschaften. Jahrgang 1912. Erster Halbband. Januar bis Juni* (1912), pp. 456–477.

[11] Gelman, A. and Rubin, D. B. "Inference from iterative simulation using multiple sequences". In: *Statistical Science* 7 (1992), pp. 457–472. DOI: `10.1214/ss/1177011136`.

[12] Rusatsi, D.N. "Bayesian analysis of SEIR epidemic models". last visited: 18 December, 2023. PhD thesis. Lappeenranta University of Technology, 2015.

[13] Metropolis, N. et al. "Equation of State Calculations by Fast Computing Machines". In: *J.Chem. Phys.* 21 (1953), pp. 1087–1092. DOI: `10.1063/1.1699114`.

[14] *Privat communication with Dipo Aldila, Department of Mathematics, University of Indonesia, Depok.*

[15] Murray, J. D. *Mathematical Biology - I. An Introduction*. Springer, 2002.

[16] Rocha, F. et al. "Time-scale separation and centre manifold analysis describing vector-borne disease dynamics". In: *Int. J. Comput. Math.* 90 (2013), pp. 2105–2125.

[17] Badan Pusat Statistik. *2010 Indonesian Population Census*. last visited: 18 December, 2023.

Chapter 4

The COVID-19 Outbreak in Germany – Models and Parameter Estimation

This article by Peter Heidrich, Moritz Schäfer, Mostafa Nikouei and Thomas Götz has been released in the journal COMMUNICATION IN BIOMATHEMATICAL SCIENCES in 2020, referred to as [1]. The theory, formulation of the optimal control problem and numerical calculations were done by Moritz Schäfer (for the *Metropolis algorithm*) and Peter Heidrich (for the *adjoint method*). Mostafa Nikouei provided some further numerical computations (which did not end up in the present work), while Thomas Götz provided the idea for the article as well as further advice, and wrote the *Introduction*. The format is changed to meet the thesis standard.

Abstract

Since the end of 2019, an outbreak of a new strain of coronavirus, called SARS-CoV-2, is reported from China and later also from other parts of the world. Since 21 January 2020, World Health Organization (WHO) reports daily data on confirmed cases and deaths from both China and other countries [2]. The Johns Hopkins University [3] collects those data from various sources worldwide on a daily basis. For Germany, the Robert-Koch-Institute (RKI) also issues daily reports on the current number of infections and infection related fatal cases and also provides estimates of several disease-related parameters [4]. In this work we present an extended *SEIRD*-model to describe these disease dynamics in Germany. The model takes into account the susceptible, exposed, infected, recovered, and deceased fractions of the population. Epidemiological parameters like the transmission rate, lethality or the detection rate of infected individuals are estimated by fitting the model output to available data. For the parameter estimation itself, we compare two methods: an adjoint based approach and a Monte-Carlo based Metropolis algorithm.

4.1   Introduction

In December 2019, first cases of a pneumonia of unknown cause were reported from Wuhan, China. In the meantime, these cases were identified as infections with a novel strain of coronavirus, called SARS-CoV-2, and the disease it causes was called Coronavirus Disease 2019 (COVID-19). At the beginning of January 2020, the virus spread over mainland China and reached other provinces. From 21 January onwards, WHO's daily situation reports [2] or Johns Hopkins University [3] (JHU) contain the latest figures on confirmed cases and deaths for almost all countries. In this

work, we rely on the data published by the JHU due to their rapid updates and easy accessibility.

The first COVID-19 case in Germany was reported on 27 January 2020 in Bavaria. Later cases were imported by travelers from China, Iran or Italy, as well as tourists returning from ski holidays in Austria and Italy. By 1 March 2020, more than 100 cases were reported in Germany; since then, the number of cases began to rise exponentially. The first deaths were reported on 9 March [4]. By 16 March, the federal government introduced first measures to reduce the spread of the disease: schools, kindergartens and universities were closed. On 22 March, these measures were tightened by implementing a national curfew and contact ban. People are advised to stay at home, leaving only for work related activities, necessary shopping, medical treatment or sports [5]. By mid of April, these mitigation measures showed some success, with the number of new infections declining from its peak of 6,294 on 28 March to less than 1,000 from 2 May onwards. On 6 May, a relaxation of the imposed restrictions to social and economic life was announced. Since then, the federal states are progressing at an individual pace to 'normality'.

Asking the population to remain cautious and not to cause a second wave, local governments of cities or districts are in charge to reinforce restrictions in case the number of new infections surpasses the limit of 50 per 100,000 inhabitants within 7 days as of 6 May [6, 7]. Already four days later five districts exceeded this limit, with no measures reported to alleviate it.

The pandemic continues to spread worldwide (as of June 2020) and the actual possibility of a second wave demands for models to predict epidemic scenarios for the near and mid future. The quality of those models heavily relies on the parameters used. In this study we present *SEIRD*-models which are some sort of quasi standard in epidemiological simulations and estimate their parameters by using the available data from the JHU. The estimation itself is based on a least-squares fit between the model output and the reported data. Both the reported infections and the reported fatalities are taken into account.

4.2 SEIRD-model

Following the classical *SIR*-models introduced by McKendrick [8] and its every-growing number of variants (cf. [9] for an overview), we chose an *SEIRD*-model to describe the COVID-19 outbreak in Germany. The entire population N is subdivided into five subdivisions: susceptibles S, exposed E, infected I, recovered R, and deceased D. The virus is transmitted from infected persons to susceptible persons at a time-dependent rate $\beta(t)$; after an incubation phase of duration κ^{-1}, exposed individuals get infectious. Loss of infectivity is gained after γ^{-1} days and with a probability μ, a patient dies from the disease. This leads us to the following five-dimensional ODE system:

$$S' = -\frac{\beta(t)}{N}SI \qquad S(t_0) = S_0 = N - E_0 - I_0 - R_0 - D_0 > 0, \qquad (4.1a)$$

$$E' = \frac{\beta(t)}{N}SI - \kappa E \qquad\qquad E(t_0) = E_0 \geq 0, \qquad (4.1b)$$

$$I' = \kappa E - \gamma I \qquad\qquad\qquad I(t_0) = I_0 > 0, \qquad (4.1c)$$

$$R' = (1 - \mu)\,\gamma I \qquad\qquad\qquad R(t_0) = R_0 \geq 0, \qquad (4.1d)$$

$$D' = \mu\gamma I \qquad\qquad\qquad\qquad D(t_0) = D_0 \geq 0. \qquad (4.1e)$$

The starting point t_0 is chosen as 1 March, the date the number of reported cases exceeded 100 cases for the first time, see Fig. 4.1.

It is immediate to see that the model (4.1) has non-negative solutions, provided the initial values are all non-negative. Due to the absence of demographic terms, there is just the trivial disease-free equilibrium $S = N$ and $E = I = R = D = 0$. Since the intention of our model is to provide short- and mid-term simulations, we are not interested in its long-term behavior and hence possible endemic equilibria are of no concern.

As a variant of the above basic model, we also consider a delayed differential equation (DDE) version where we introduce a time lag τ between the infected and the deceased state so that the fraction of people who recover or die from the disease is not attained from the amount of infectives on the same day, but from the infectives data τ days earlier. The previous ODE model can thus be seen as a special case of the DDE model with $\tau = 0$.

$$S' = -\frac{\beta(t)}{N}SI \qquad\qquad S(t_0) = S_0 > 0, \qquad (4.2a)$$

$$E' = \frac{\beta(t)}{N}SI - \kappa E \qquad\qquad E(t_0) = E_0 \geq 0, \qquad (4.2b)$$

$$I' = \kappa E - \gamma\big((1-\mu)I + \mu I(t-\tau)\big) \qquad I(t) = \phi(t) > 0, \qquad (4.2c)$$

$$R' = (1-\mu)\gamma I \qquad\qquad R(t_0) = R_0 \geq 0, \qquad (4.2d)$$

$$D' = \mu\gamma I(t-\tau) \qquad\qquad D(t_0) = D_0 \geq 0. \qquad (4.2e)$$

Here, $\phi : [t_0 - \tau, t_0] \to \mathbb{R}_+$ denotes the initial history of the infected required for the well-posedness of the above delay differential equation. Since the initial value I_0 of the infected at the starting date 1 March is later on subject of the estimation procedure, we assume the initial history to show some exponential behavior

$$\phi(t) := I_0 \cdot \exp\left(-\frac{\ln(0.1)}{\tau}(t - t_0)\right) \qquad (4.3)$$

for $t_0 - \tau \leq t \leq t_0$.

The transmission rate $\beta(t)$ can be related to the *basic reproduction number* $\mathcal{R}_0$ via

$$\mathcal{R}_0(t) = \frac{\beta(t)}{\gamma}. \qquad (4.4)$$

At the onset of the epidemic, $\mathcal{R}_0$ in Germany was estimated to be $\mathcal{R}_0 \simeq 2.4\text{--}4.1$ [10]. To take the different levels of restriction imposed on the social and economic life, we assume $\beta(t)$ as a step function in time:

$$\beta(t) := \begin{cases} \beta_0, & t < 16 \text{ March} \\ \beta_1, & 16 \text{ March} \leq t < 22 \text{ March} \\ \beta_2, & 22 \text{ March} \leq t < 20 \text{ April} \\ \beta_3, & 20 \text{ April} \leq t \end{cases} \qquad (4.5)$$

Before the first restrictions were imposed on 16 March, the disease was allowed to spread almost uncontrolled. After kindergarden, school and university closings on 16 March, the measures were tightened on 22 March by introducing a contact ban and closing of a large number of shops and businesses. On 20 April, first relaxations were announced and public life began to re-increase, but along with compulsory wearing

of masks which has been introduced in late April. For each of these stages we assume an specific contact rate between individuals and hence different transmission rates β_i.

The values for the fixed model parameters are given in Table 4.1.

TABLE 4.1: Used parameter values for the DDE-models.

Parameter	Value	Unit	Reference
N	83,019,213	–	[11]
κ	1/3	d^{-1}	[12]
γ	1/10	d^{-1}	[12]
τ	> 7	d	[12]
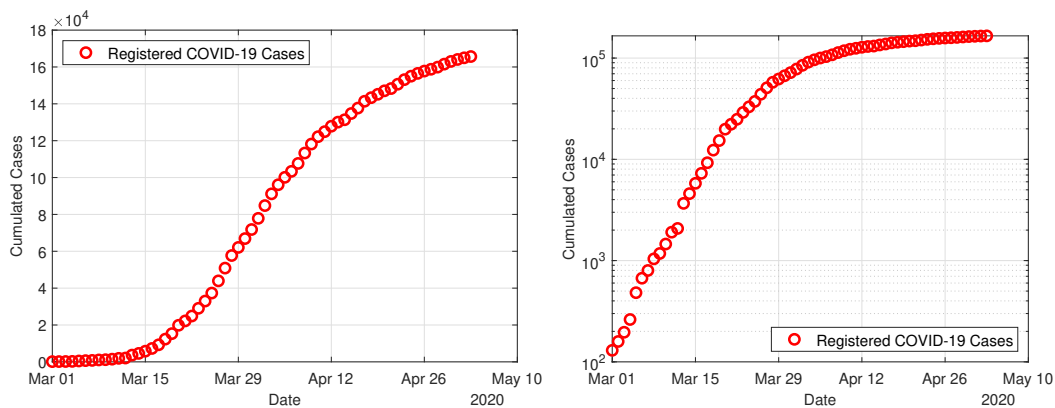
FIGURE 4.1: Cumulative infections in Germany during the first wave, left: normal scaling, right: semi-logarithmic scaling [3].
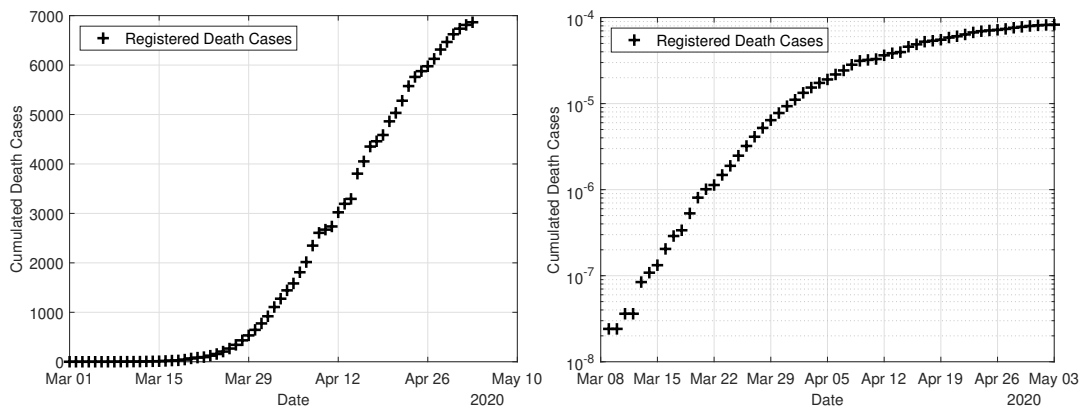
FIGURE 4.2: Cumulative death cases in Germany during the first wave, left: normal scaling, right: semi-logarithmic scaling [3].

4.3 Parameter estimation

The unknown model parameter set u is estimated from a least squares fit of the model output to the given data. Let Y and Z denote the accumulated registered COVID-19 cases or the accumulated COVID-19 deaths in Germany as reported by Johns Hopkins University, see [3]. The reported cases Y consist of the currently infected cases, the recovered and the deceased cases. Since by the very nature of the matter, not all infections are detected, we introduce a detection rate δ. For the currently infected

and the recovered ones, we assume that only this proportion δ is tested and detected and hence appears in the statistics; however, we assume no undetected deceased cases. Hence we compare the data Y to $\delta \cdot (I + R) + D$ from the model output. To put special emphasis on the fatalities, we add a term which just compared the reported and the simulated deaths to the cost functional. As a third contribution we add a regularization term proportional to the norm of the estimated parameters to attain a convex function and prevent unrealistic outliers. With this in mind we arrive at the following cost functional:

$$J(u) := \frac{\|\delta(I + R) + D - Y\|_{L^2}^2}{\|Y\|_{L^2}^2} + \frac{\|D - Z\|_{L^2}^2}{\|Z\|_{L^2}^2} + \omega \|u\|_2^2 \tag{4.6}$$

where $\omega > 0$ denotes some small weight allowing us to adjust the contribution between the normalized least squares terms and the regularization term and $\|f(t)\|_{L^2}^2 = \int_{t_0}^{T} f(t)^2 dt$ denotes the square of the L^2 norm of a function f resp. $\|u\|_2^2 = \sum_i u_i^2$ for the square of the Euclidean norm of a vector u.

The parameters to be estimated in model (4.1) are the transmission rate, the detection rate, lethality and the numbers of exposed on 1 March 2020, i.e.

$$u = (\beta_0, \beta_1, \beta_2, \beta_3, \delta, \mu, E_0) \in \mathbb{R}^7 \tag{4.7}$$

which is the same parameter set as in model (4.2) with added but fixed time lag τ. For the model with free and to-be-optimized time lag τ, we have the parameter set

$$u = (\beta_0, \beta_1, \beta_2, \beta_3, \delta, \mu, \tau, E_0, I_0) \in \mathbb{R}^9. \tag{4.8}$$

Here, we also estimate the initial number of infected on 1 March to allow for more flexibility of the model. The optimal parameters u^* are determined by solving the following minimization problem:

$$\min_u J(u) \quad \text{subject to ODE (4.1) resp. (4.2),} \tag{4.9a}$$

$$u^* = \text{argmin}_u J(u). \tag{4.9b}$$

TABLE 4.2: Simulations with the respective constraints of the fitted parameters.

Sim.	Model	β_i	δ	μ	τ	E_0	I_0	R_0
1	1	> 0.05	$0.05 - 0.5$	≤ 0.05	0	> 0	$114/\delta$	$16/\delta$
2	2	> 0.05	$0.05 - 0.5$	≤ 0.05	11.5	> 0	$114/\delta$	$16/\delta$
3	2	> 0.05	$0.05 - 0.5$	≤ 0.05	> 7	> 0	> 0	$16/\delta$

Tab. 4.2 shows the planned simulations including constraints for the optimized parameters in u. In Sim. 1, no time lag τ is included in the model. The starting values for I_0 and R_0 are only updated in the first two simulations by division with δ in each iteration. In Sim. 2, the time lag $\tau = 11.5$ is fixed, as a mean value within the assumed interval. The parameter τ is also fitted in Sim. 3, just like I_0. All other unknown parameters in this table are adjusted in each simulation.

Previous investigations in [13] already give us orders of magnitude for the initial values of the optimization for β_i and δ. For the lethality rate μ we assume the upper

limit

$$\mu \le \frac{Z(T)}{R(T)/\delta + Z(T)}, \tag{4.10}$$

whereby $Z(T)$ denotes for the death cases, and $R(T)$ denotes the registered recovered individuals at end time T [14]. This upper limit becomes smaller the fewer COVID cases are registered, since δ becomes smaller. For our data set, we find $\mu \approx 0.05$, based on the registered cases, i.e. this upper limit would match, if $\delta = 1$. Building on the assumption that less than 50% of cases are detected, we also assume a starting value for the lethality rate that is less than half of the calculated upper limit of 5%. The order of magnitude of the time interval between the onset of infectiousness and death is derived from the investigations in [12]. From the timelines available, we derive $\tau \in (7, 17)$. In individual cases, this period can be considerably longer, so that τ only represents an average value in the model. The starting values for I_0 and R_0 can be taken from the statistics. Depending on the value of the detection rate, the actual number is calculated by dividing the measured values for the infected and recovered cases by δ. Regarding an estimate of the exposed individuals E_0 at time t_0, we use a derivation using $\mathcal{R}_0$, which indicates how many new infections an infected individual causes on average during its illness in an otherwise susceptible population. In our model, the infected persons I_0 are at different time stages during their infectiousness. As a mean value, we assume the middle of this time interval. Thus, up to this point in time they could infect about $I_0 \mathcal{R}_0 / 2$ persons on average. Depending on the assumed value of $\mathcal{R}_I$, this results in different starting values for E_0. The model adaptations are carried out in the simulations with the values $\mathcal{R}_0 \in \{3, 4, 5\}$, and it is checked if significant effects on the other parameters can be found. The selected start values can be seen in Tab. 4.3.

TABLE 4.3: Orders of magnitude of the initial guesses for adapting the model to the available data.

Parameter	β_0	β_1	β_2, β_3	δ	μ	τ	E_0	I_0	R_0
Initial Guess	0.6	0.4	0.1	0.25	0.02	11.5	$I_0 \mathcal{R}_0 / 2$	$114/\delta$	$16/\delta$

4.3.1 Adjoint based approach

To solve the minimization problem using adjoint functions, we introduce the Lagrangian function

$$\mathcal{L}(u, x, z) = J(u) + \int_{t_0}^{T} z(t) \cdot \left(g(t, x, u) - \frac{dx}{dt} \right) dt, \tag{4.11}$$

whereby $z = (z_S, z_E, z_I, z_R, z_D)$ denotes the adjoint function regarding the state variable $x = (S, E, I, R, D)$, and $g(t, x, u)$ denotes the right side of the ODE resp. DDE system. It should be noted that within the integral, a scalar product of vectors is calculated. A critical point (u^*, x^*, z^*) needs to fulfill the necessary optimality condition

$$\nabla \mathcal{L}(u^*, x^*, z^*) = 0. \tag{4.12}$$

For precise details of the following procedure, please refer to [15]. Thus we find the gradient $\nabla_u \mathcal{L}$ regarding the parameters in u:

$$\frac{\partial \mathcal{L}}{\partial \beta_i} = 2\omega\beta_i + \frac{1}{N} \int_{t_0}^{T} \frac{\partial \beta(t)}{\partial \beta_i} SI \left(z_E - z_S \right) dt, \qquad i = 0, 1, 2, 3 \qquad (4.13\text{a})$$

$$\frac{\partial \mathcal{L}}{\partial \delta} = 2\omega\delta + 2 \int_{t_0}^{T} (I + R) \Big(\delta(I + R) + D - Y \Big) dt, \qquad (4.13\text{b})$$

$$\frac{\partial \mathcal{L}}{\partial \mu} = 2\omega\mu + \gamma \int_{t_0}^{T} I \left(z_D - z_I \right) dt, \qquad (4.13\text{c})$$

$$\frac{\partial \mathcal{L}}{\partial E_0} = 2\omega E_0 + z_E(t_0) - z_S(t_0), \qquad (4.13\text{d})$$

$$\frac{\partial \mathcal{L}}{\partial I_0} = 2\omega I_0 + z_I(t_0) - z_S(t_0), \qquad (4.13\text{e})$$

resp. in model (4.2) we obtain, due to the time delay τ,

$$\frac{\partial \mathcal{L}}{\partial \mu} = 2\omega\mu + \gamma \int_{t_0}^{T} I \left(z_I - z_R \right) + I \left(t - \tau \right) \left(z_D - z_I \right) dt, \qquad (4.13\text{f})$$

$$\frac{\partial \mathcal{L}}{\partial \tau} = 2\omega\tau + \gamma\mu \int_{t_0}^{T} \left(z_I - z_D \right) \frac{dI}{dt}\bigg|_{t=t-\tau} dt. \qquad (4.13\text{g})$$

The adjoint system is given by the equations

$$\frac{dz_S}{dt} = \frac{\beta(t)}{N} I \left(z_S - z_E \right), \qquad (4.14\text{a})$$

$$\frac{dz_E}{dt} = \kappa \left(z_E - z_I \right), \qquad (4.14\text{b})$$

$$\frac{dz_I}{dt} = \frac{\beta(t)}{N} S \left(z_S - z_E \right) + \gamma \left(z_I - z_R + \mu \left(z_R - z_D \right) \right) - \frac{2\delta \left(\delta(I + R) + D - Y \right)}{\|Y\|_{L^2}^2}, \qquad (4.14\text{c})$$

$$\frac{dz_R}{dt} = -\frac{2\delta}{\|Y\|_{L^2}^2} \Big(\delta(I + R) + D - Y \Big), \qquad (4.14\text{d})$$

$$\frac{dz_D}{dt} = -\frac{2}{\|Y\|_{L^2}^2} \Big(\delta(I + R) + D - Y \Big) - \frac{2}{\|Z\|_{L^2}^2} (D - Z), \qquad (4.14\text{e})$$

with the terminal condition $(z_S, z_E, z_I, z_R, z_D)(T) = 0$. By adding the time delay in model (4.2), we receive

$$\frac{dz_I}{dt} = \frac{\beta(t)}{N} S \left(z_S - z_E \right) + (1 - \mu) \gamma \left(z_I - z_R \right) - \frac{2\delta}{\|Y\|_{L^2}^2} \Big(\delta(I + R) + D - Y \Big)$$

$$+ \mu\gamma \Big(z_I(t + \tau) - z_D(t + \tau) \Big) \cdot \chi_{[t_0, T-\tau]}(t). \qquad (4.14\text{f})$$

Here, χ denotes the characteristic function

$$\chi_{[t_0, T-\tau]}(t) = \begin{cases} 1, & t \in [t_0, T - \tau] \\ 0, & \text{else} \end{cases} . \qquad (4.15)$$

Algorithm 3 Pseudocode for the approach including adjoint functions.

1: $u, Y, Z \leftarrow$ load initial values for u and data
2: $x, z \leftarrow$ solve ODE resp. DDE for state variable and adjoint function
3: $J, \nabla J \leftarrow$ compute objective function and gradient regarding u
4: $s \leftarrow$ compute search direction
5: **repeat**
6:    $J_{old} \leftarrow J$
7:    $\theta \leftarrow \mathrm{argmin}_{\theta > 0} \, \psi(\theta)$ with $\psi(\theta) := J(u + \theta s)$
8:    $u \leftarrow u + \theta s$
9:    $x, z, J, \nabla J, s \leftarrow$ update depending on u
10: **until** $\|J - J_{old}\|_2 < \mathrm{TOL}$
11: $u^*, x^*, z^*, J^* \leftarrow u, x, z, J$

Algorithm 3 represents the basic framework of the iterative optimization via adjoint functions. To find a preferably global minimum, n multivariate normally distributed start values for u can be created before step 1. These are then tested one after the other with the presented procedure, and the best result is chosen. The mean values of this distribution are then the values in Tab. 4.3, and the variances can be selected according to the restrictions in Tab. 4.2. In step 2 the ODE or DDE systems are solved using Runge-Kutta methods. Since the state variable is solved forward and the adjoint function backward regarding the time scale, due to the initial and end values, this is also called the forward-backward sweep method [15]. In MATLAB, the ODE45 and DDE23 solvers are suitable for this purpose. The search direction s in steps 4 and 9 is selected as Quasi-Newton method (BFGS). Useful alternative search directions are (conjugated) gradient methods [16]. The line search procedure in step 7 cannot be solved analytically in our case. A common method for an appropriate step size θ^* would be a backtracking procedure considering the Armijo rule [17]. In the present simulation, the procedure in Algorithm 4 is applied. It is based on a Taylor series of $\psi(\theta) := J(u + \theta s)$ developed around θ_0:

$$\psi(\theta_0 + h) = \psi(\theta_0) + \psi'(\theta_0)h + \frac{1}{2}\psi''(\theta_0)h^2 + \dots \,, \tag{4.16}$$

where $\psi', \psi'', \dots$ stand for the respective derivatives of ψ regarding θ. Based on this, we assume that ψ for $\theta_0 = 0$ and sufficiently small values for $h = \theta$ can be approximated by a parabola with

$$\psi(\theta) \simeq a\theta^2 + b\theta + c, \tag{4.17a}$$
$$\psi'(\theta) \simeq 2a\theta + b. \tag{4.17b}$$

Using the information $\psi(0) = J(u)$ and $\psi'(0) = \nabla J(u) \cdot s$ associated with a calculated value $\psi(\theta_1) = J(u + \theta_1 s)$ for small and fixed θ_1 allows for deriving the parameters

$$c = \psi(0), \tag{4.18a}$$
$$b = \psi'(0), \tag{4.18b}$$
$$a = \left(\psi(\theta_1) - \psi'(0)\theta_1 - \psi(0)\right)/\theta_1^2, \tag{4.18c}$$

and, by using the necessary condition $\psi'(\theta^*) = 0$, find the optimum of the parabola in eqn. (4.17a) by

$$\theta^* = -b/(2a) = -0.5\psi'(0)\theta_1^2 / \left(\psi(\theta_1) - \psi'(0)\theta_1 - \psi(0)\right). \tag{4.19}$$
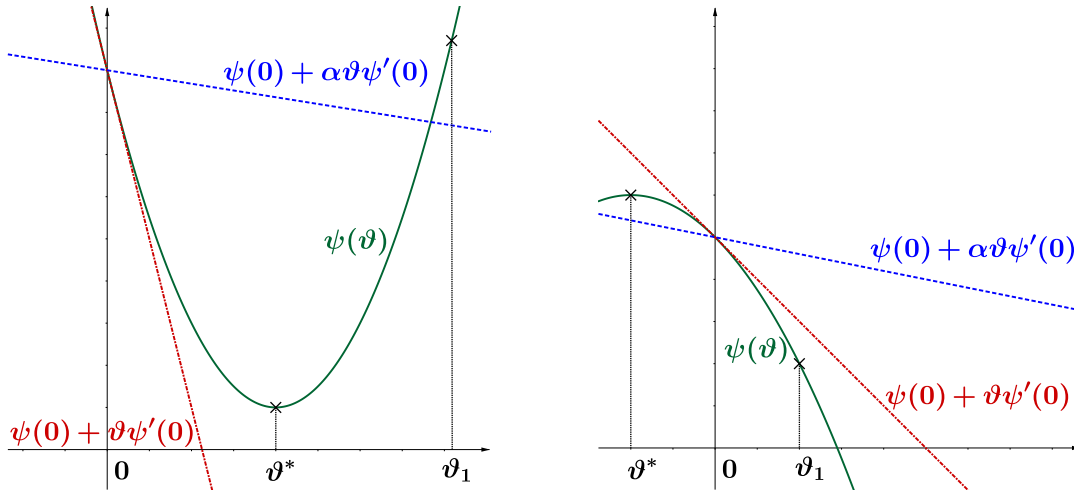
FIGURE 4.3: Example for finding the optimal value θ^* using parabola linesearch.

The left part of Fig. 4.3 shows that the Armijo rule $\psi(\theta) \leq \psi(0) + \alpha\theta\psi'(0)$ is not fulfilled for θ_1 and the new step size is determined using the parabola minimum θ^*. To make sure that the possible minimum of the parabola is below that line, one chooses a small value for $\alpha \in (0, 0.5)$, e.g. $\alpha = 10^{-4}$. In the right figure, the Armijo rule is already fulfilled with the fixed increment θ_1, which can be adopted. There can also be a parabola maximum, so that θ^* takes a negative value. However, this is circumvented because in this case, there is no optimization of the step size.

Algorithm 4 Pseudocode for line search in step 7 of Algorithm 3.

1: $u, J(u), \nabla J(u), s \leftarrow$ input
2: $\theta \leftarrow 1$
3: $\psi(0) \leftarrow J(u)$
4: $x \leftarrow$ compute state variable depending on $u + \theta s$
5: $\psi(\theta) \leftarrow J(u + \theta s)$
6: $\psi'(0) \leftarrow \nabla J(u) \cdot s$
7: $\alpha \leftarrow$ value in $(0, 0.5)$
8: **if** $\psi(\theta) > \psi(0) + \alpha\theta\psi'(0)$ **then**
9:    **repeat**
10:       $\theta \leftarrow -0.5\psi'(0)\theta^2 / \left(\psi(\theta) - \psi'(0)\theta - \psi(0)\right)$
11:       $x \leftarrow$ update depending on $u + \theta s$
12:       $\psi(\theta) \leftarrow J(u + \theta s)$
13:    **until** $\psi(\theta) \leq \psi(0) + \alpha\theta\psi'(0)$ (Armijo rule)
14: **end if**
15: $\theta^* = \theta$

The effect of the weight ω can be seen on the diagonal of the Hessian matrix in model (4.1):

$$\nabla_u^2 \mathcal{L} = 2\, \text{diag}\left(\omega, \omega, \omega, \omega, \omega + \int_{t_0}^{T} (I + R)^2 \, dt, \omega, \omega, \omega\right) \tag{4.20}$$

All other entries in $\nabla_u^2 \mathcal{L}$ are equal to 0. The value of ω directly influences the definiteness of the Hessian matrix and thus the convexity of the objective function. For this reason, different values for ω are tested in the simulations.

4.3.2 Metropolis algorithm

According to the procedure described in [18], a Metropolis algorithm (cf. [19, 20, 21]) for model (4.2) can be set up using the initial history and initial values for the to-be-estimated parameter set u. Using the parameter set u_0 as of Tab. 4.3 as starting conditions, we assign random draws u_{new} from a normally distributed (and thus symmetric) proposal function q, i.e. $u_{new} \sim q(u_{new}|u_{i-1})$, in every iteration i.

Using the previously defined $J(u)$ as the target distribution, we calculate the approximative distribution by

$$\pi(u) = c \cdot \exp\left(-\frac{J(u)^2}{2\sigma^2}\right), \tag{4.21}$$

whereby c is an arbitrary value in $\mathbb{R}$. For the acceptance probability, it follows

$$\alpha(u_{new}|u_{i-1}) = \min\left\{1, \frac{\pi(u_{new}) \cdot q(u_{i-1}|u_i)}{\pi(u_i) \cdot q(u_i|u_{i-1}))}\right\} = \min\left\{1, \frac{\pi(u_{new})}{\pi(u_i)}\right\}. \tag{4.22}$$

In eqn. (4.22), we can see that the value of c is redundant, as it cancels out in the division.

If the sample is accepted with the probability α, we set $u_i = u_{new}$; with the probability $1 - \alpha$, the sample is declined, meaning $u = u_{i-1}$ [22, 18].

Algorithm 5 Pseudocode for the Metropolis algorithm.

1: $u, Y, Z \leftarrow$ load initial values for u and data
2: $x, z \leftarrow$ solve ODE resp. DDE for state variable
3: $J \leftarrow$ compute objective function regarding u
4: $\sigma \leftarrow$ standard distribution of the solution, i.e. $I + R + D$ over time
5: $s \leftarrow$ set step size (standard deviation) for the algorithm, e.g. $s := u/100$
6: **repeat**
7:     $u_{old} \leftarrow$ u from previous draw
8:     $\hat{u}_{new} \leftarrow u \sim \mathcal{N}(u_{old}, s)$
9:     $x, z, J(\hat{u}_{new}) \leftarrow$ update depending on u
10:    $\alpha \leftarrow \min\left\{1, \exp\left(J(u_{old})^2 - J(u_{new})^2/2\sigma^2\right)\right\}$
11:    $u_{new} \leftarrow \hat{u}_{new}$ with probability α and $u_{new} := u$ with probability $1 - \alpha$
12: **until** maximum value of draws is reached
13: $u^*, x^*, J^* \leftarrow$ means of all u, x, J

Algorithm 5 represents the basic framework of the iterative optimization via the Metropolis algorithm. In step 1, the mean values of this distribution as of Tab. 4.3 are loaded as well as the variances according to the restrictions in Tab. 4.2. In step 2 the ODE or DDE are again solved using Runge-Kutta methods via MATLAB's ODE45 and DDE23 solvers. The step size s in step 5 is selected as a fraction of the initial guess for the parameter set u, so that the parameters are allowed to move with an individual "speed" through the entire search space. In steps $6 - 12$, the process is repeated for all draws, the number of draws in our case is set to $2e + 4$. Alternatively, you can think about termination conditions, but we avoided this due to the random nature of the system. Firstly, the update of the parameter set u is done by taking a random value out of the normal distribution with mean u and standard deviation s. After solving the system in step 9, the cost functional $J(u)$ is compared to the previous cost functional with the function α in step 10 and the new parameter set is accepted or rejected according to eqn. (2.117) in step 11. The estimation parameter set can then

be computed out of the mean value of the draws in step 13. Alternatively, in case of non-convergence, it is possible to compute the best fitting u of the set and use this as initial value as of step 1 again, in order to attain better results.

Choosing the weights ω for the target function $J(u)$ was done under two purposes. The first purpose was to create a convex target function so that the algorithm does not converge to local minima (see also the previous subsection for this). The Metropolis algorithm allows steps into parameter sets having a 'worse' target distribution with a certain probability, but it is still possible that it runs into local but not global minima after a *final* amount of steps which justifies the usage of the term $\omega \, ||u||^2$. The other purpose is to not have a too large ω so that the model-related terms still have a major impact on the outcome of $J(u)$. For these two regards, we found that a range for $\omega \in [10^{-9}, 10^{-7}]$ to be decent, but we will also present the results if we neglect the term with ω, i.e. $\omega = 0$. For values $\omega \in (0, 10^{-9})$, no significant changes in the outcomes to $\omega = 0$ were detected, while for $\omega > 10^{-7}$ the model-related terms are negligible and the results are quite unrealistic.

4.4 Numerical results and comparison of the algorithms

Tab. 4.4 shows the respectively best numerical results of the two algorithms. The values for the transmission parameters β_i are of similar magnitudes in almost all simulations and algorithms. In isolated cases, there are more significant deviations, such as $\beta_1 = 0.64$ in Simulation 3 of the Metropolis approach or the value $\beta_3 = 0.099$ in Simulation 1 of the adjoint approach. The values show that the dynamics of the model at the beginning of the measurement period with $\beta_0 \simeq 0.6$ suggest a much higher $\mathcal{R}_0$ than assumed.

TABLE 4.4: Estimated parameters, target function, and number of iterations of adjoint and Metropolis algorithms.

Algorithm	Adjoint			Metropolis		
Simulation	1	2	3	1	2	3
β_0	0.60	0.64	0.62	0.55	0.70	0.64
β_1	0.50	0.48	0.51	0.49	0.40	0.64
β_2	0.101	0.082	0.092	0.113	0.085	0.086
β_3	0.099	0.050	0.058	0.054	0.055	0.055
δ	0.31	0.27	0.18	0.29	0.20	0.19
μ	0.015	0.018	0.011	0.013	0.013	0.011
τ	0	11.5	9.0	0	11.5	7.3
$E_0 + I_0 + R_0$	831	1,105	1,512	1,255	854	1,090
$(J(u) - \omega \, \|u\|_2^2) \cdot 10^3$	23.0	9.1	6.1	18.1	8.2	3.2
No. of iterations	23	22	31	20000	20000	20000

The first measures lead to a small to moderate reduction of the transmission rate to $\beta_1 \simeq 0.5$, whereas the following lockdown causes a significant decrease of the transmission rate to $\beta_2 \simeq 0.1$. This also fits with the estimates of the RKI that the Basic Reproduction Number is said to have dropped to a value of around $\mathcal{R}_0 \simeq 1$ due to the extensive restrictions [4]. In the last phase of the data adaptation, the transfer rate drops to $\beta_3 \simeq 0.06$. Here, due to the loosening of the measurements, one would expect an increase of the transmission rate. However, these were introduced very slowly and under very strict hygiene measures, combined with a mask requirement in public spaces, which apparently has decreased the β value. Regarding the detection

rate δ, we find values of around $20 - 30\%$ in all cases. This means that according to the simulations, the actual number of infected people is 3–5 times higher than the official reports. The computed lethality is between 1–2% and is therefore roughly a third of 5% which was calculated using (4.10) regarding the registered cases at the end time point T. The average time interval τ between the onset of infectivity and death in Simulation 3 is between 7 and 10 days. The influence of τ is also evident with regard to the normalized least squares terms $J(u) - \omega \|u\|_2^2$. By adding a fixed time lag in Simulation 2 and then adjusting it in the third simulation, a significant improvement is shown in all algorithms as $J(u)$ is considerably smaller. Regarding the magnitudes of the least-squares terms, the algorithms show similar values in comparison to each other and lead to useful adjustments with minor deviations of the model from the available data sets. This is also illustrated by the graphical results which are shown in Appendices A and B. The sum of the initial values $E_0 + I_0 + R_0$ lies within a realistic range at $\simeq 1000$. Thus, the unknown initial value for the exposed individuals E_0 is approximately in the order of magnitude of the infected I_0 with an upward tendency, as expected. The variation regarding the initial value for $E_0 = I_0 \mathcal{R}_0 / 2$ in the optimization does not lead to significant differences in the results when $\mathcal{R}_0 \in \{3, 4, 5\}$ is changed. For this reason, the results are presented here only for initial estimations of $\mathcal{R}_0 = 3$.

In the case of the Metropolis algorithm, the number of iterations is much higher than in the adjoint approach. This is due to the fact that the Metropolis approach relies on random draws and thus a large amount of draws is needed to obtain convergence and to diminish the effect of outliers. This seemingly disadvantageous property of the Metropolis algorithm is partly counter-balanced when using n multivariate normally distributed values for u as starting guesses for the adjoint-based optimization. This also increases the iteration number by a factor n. On the other hand, this would have the consequence that the probability of reaching a global minimum for $J(u)$ would increase significantly. This aspect is already been cared for in the Metropolis algorithm, so no additional computations are required unless the chain statistics (as to be seen in the following sections). The value for $J(u)$, especially in Sim. 3, are slightly more accurate using the Metropolis algorithm. The comparison of the runtimes in Sim. 3 on an INTEL CORE I5-6400 with 2.7 GHz and 16 MB-RAM also reflects this. Due to the higher number of iterations, the Metropolis algorithm also has a longer runtime, see Tab. 4.5.

TABLE 4.5: Average required runtime of the algorithms on an INTEL I5-6400 with 2.7 GHz and 16 MB-RAM.

Algorithm	Average runtime [s]
Adjoint approach	10
Metropolis	140

Additionally, the influence of the weight ω on the optimization is tested. Tab. 4.6 shows the results of the least squares term $J(u) - \omega \|u\|_2^2$ for Sim. 3 with the two methods and using different weights.

TABLE 4.6: Values for the normalized least squares terms for the optimization with different weights ω regarding the adjoint algorithm in Sim. 3.

Method	$\omega = 0$	$\omega = 10^{-9}$	$\omega = 10^{-8}$	$\omega = 10^{-7}$
$(J(u) - \omega \|u\|_2^2) \cdot 10^3$ adjoint	8.9	8.8	6.1	12.0
$(J(u) - \omega \|u\|_2^2) \cdot 10^3$ Metropolis	3.8	3.2	3.4	4.1

The results show that an appropriate weight value is $\omega \simeq 10^{-8}$ or $\omega = 10^{-9}$, depending on the chosen algorithm. If the weight is too large, the value of the least squares term also deteriorates. This makes sense, since the disturbance caused by $\omega \|u\|_2^2$ on the objective function becomes too large. On the other hand, a sufficiently small value for ω leads to better optimization performance, since a weight of $\omega = 0$ on the other hand gives a worse result.

4.4.1 Specific results for the adjoint approach

As shown in Tab. 4.4, the approach with adjoint functions leads to similar numerical results as the other tested routine. The graphical results of Sim. 3 are shown in Fig. 4.4.
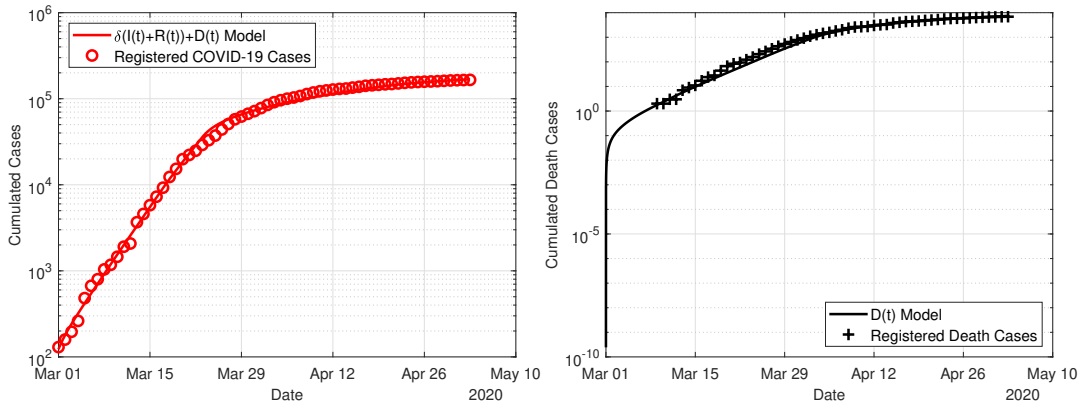
FIGURE 4.4: Results of the adjoint method for $\tau := $ free, $I_0 = $ free, $\mathcal{R}_0 = 3$ and $\omega = 10^{-8}$.

The necessary number of iterations until the convergence of the algorithm shows that the algorithm moves quickly to the corresponding minima, see Fig. 4.5. The process clarifies that the algorithm is very close to the optimal objective function value already after 15 iterations, and needs the remaining calculation steps to reach the given tolerance limit TOL $= 10^{-12}$. However, the prerequisite for rapid convergence is a good starting value for u.
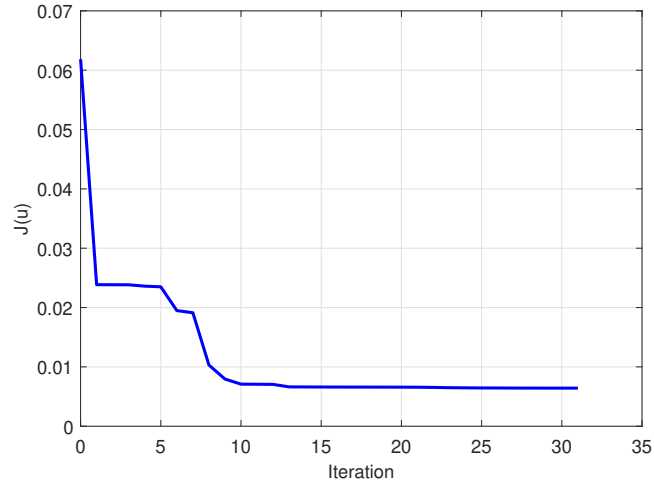
FIGURE 4.5: Development of the target function *J* using the adjoint method.

In addition to the presented simulations with restrictions, the algorithm was performed without limitations for the searched parameters, see Tab. 4.7 and Fig. 4.6.

TABLE 4.7: Numerical results of Sim. 3 without restrictions concerning the estimated parameters.

β_0	β_1	β_2	β_3	δ	μ	τ	$E_0 + I_0 + R_0$	$J(u) - \|u\|_2^2$
0.77	0.46	0.27	0.41	0.002	0.0001	7	65046	$7 \cdot 10^{-4}$

The results show that the normalized least squares term $J(u) - \|u\|_2^2$ can be reduced significantly compared to the restricted variants. It is noticeable that the fitted value for the detection rate δ is very small at about 0.02%. This would mean that only every 500th infected person would be registered. This seems unrealistic, even if the dark figure is unknown. The values for transmission rate, lethality, and actual number of exposed, infected, and recovered at the beginning of the measurement period are changed accordingly. Due to the very low detection rate in this simulation, the spread of the disease would have been much more intense than expected.
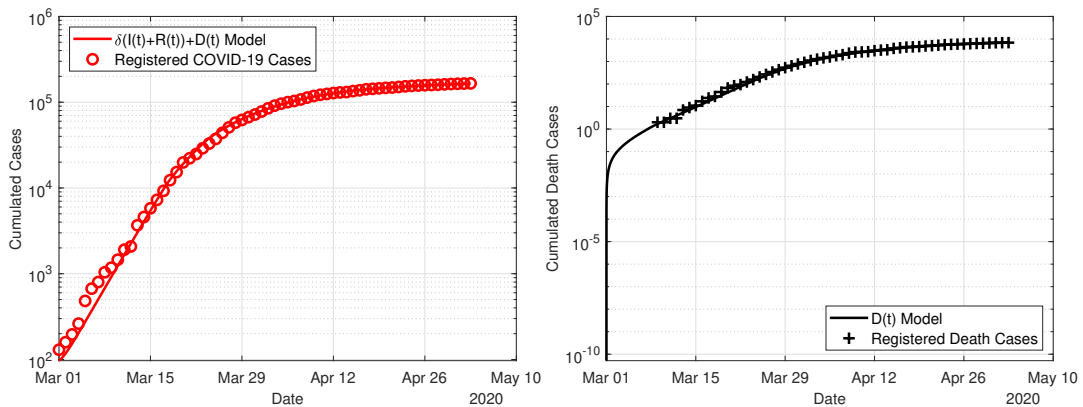
FIGURE 4.6: Results of the adjoint method for Sim. 3 without restrictions on the parameters.

4.4.2 Specific results for the Metropolis algorithm approach

We now consider the value for

$$J(u) - \omega \|u\|_2^2 = \frac{\|\delta(I+R) + D - Y\|_{L^2}^2}{\|Y\|_{L^2}^2} + \frac{\|D - Z\|_{L^2}^2}{\|Z\|_{L^2}^2}, \tag{4.23}$$

i.e., the cost functional $J(u)$ without the last term including the weight ω. This way, we can compare the simulations with different weights ω in terms of $J(u)$, because the last term trivially raises along with ω.

TABLE 4.8: Values for the normalized least squares terms for the optimization with different weights ω regarding the Metropolis algorithm in Sim. 3.

	$\omega = 0$	$\omega = 10^{-9}$	$\omega = 10^{-8}$	$\omega = 10^{-7}$
$(J(u) - \omega \|u\|_2^2) \cdot 10^3$ **Sim. 1**	18.6	18.1	18.6	21.7
$(J(u) - \omega \|u\|_2^2) \cdot 10^3$ **Sim. 2**	8.7	8.2	9.2	9.6
$(J(u) - \omega \|u\|_2^2) \cdot 10^3$ **Sim. 3**	3.8	3.3	3.4	4.1

Tab. 4.8 shows that the weight $\omega = 10^{-9}$ always yields the best, i.e. smallest values for the given cost functional $J(u)$. Moreover, what you can also see in Tables 4.10, 4.12, and 4.14 in Appendix B, the value $J(u)$ for the weight $\omega = 10^{-9}$ is larger than the value $J(u)$ with the weight $\omega = 0$, even when the term $10^{-9} \cdot \|u\|_2^2$ is *not* subtracted, which means that interestingly, the simulation with $\omega = 10^{-9}$ provides a better result for a different cost functional.

The plots for the infected and dead cases in Sim. 3 with $\omega = 10^{-9}$, thus the best simulation, are shown in Fig.4.7.
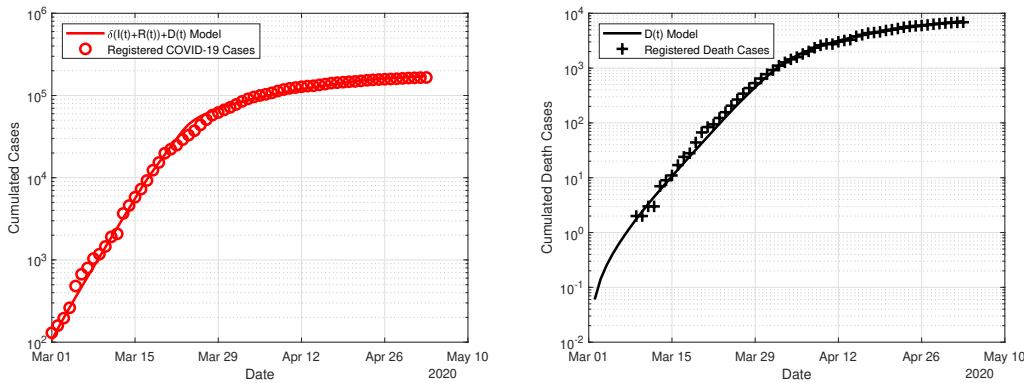
FIGURE 4.7: Results of the Metropolis method for $\tau =$ free, $I_0 =$ free, $\mathcal{R}_0 := 3$, and $\omega = 10^{-9}$.

The chain statistics done with the optimal results in Sim. 2 for $\omega = 10^{-9}$ as of Fig. 4.8 show that for most parameters a normal distribution is visible and thus the Metropolis algorithm appears to have converged. The parameter τ does not appear to be normally distributed, but still remains in the range from 7–8 days. This also affects some smaller side peaks regarding the other parameters. As the infection data has the step size of 1 day, we assume that no further optimization within that range is possible, so an estimation of $\tau \approx 7$–8 days is considered as decent.
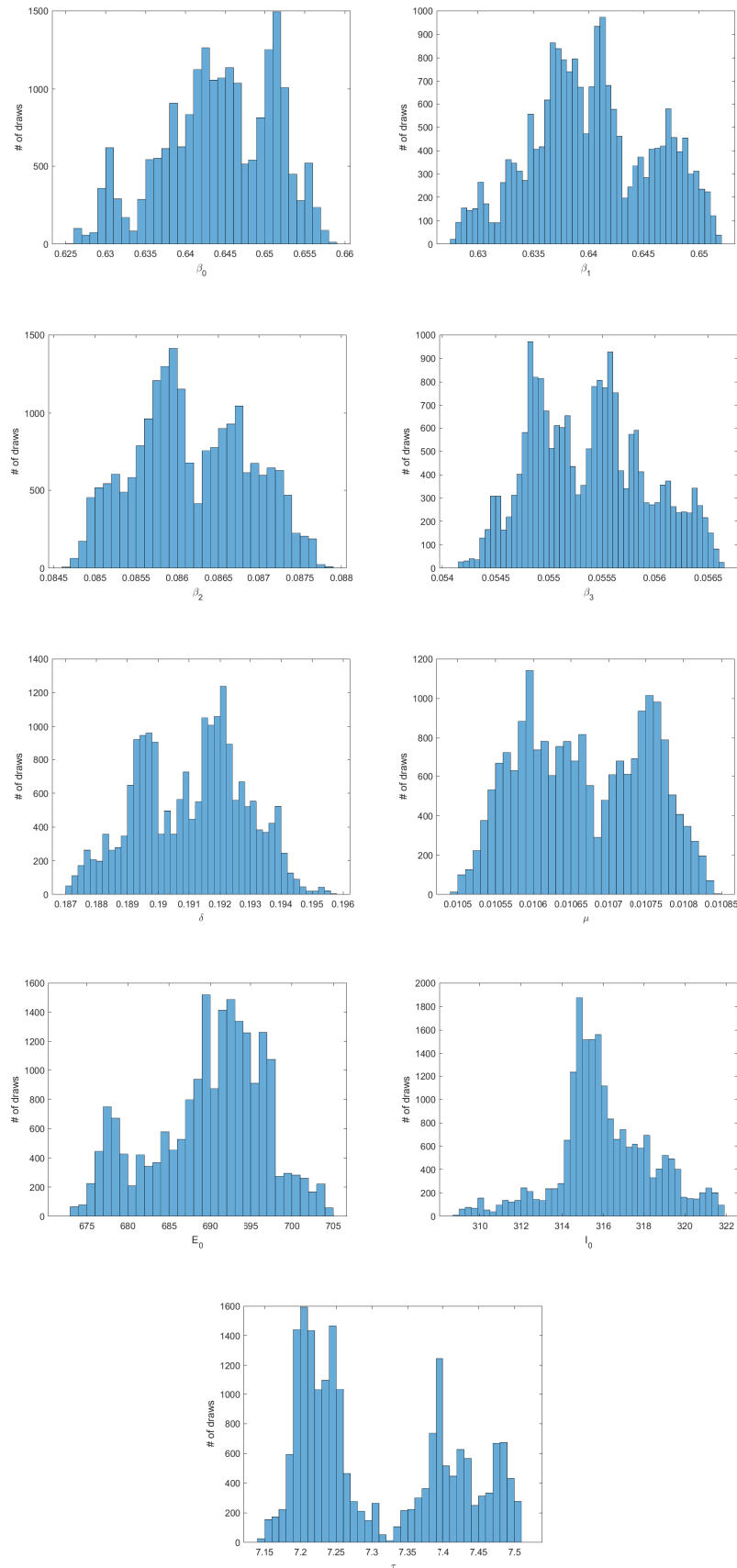
FIGURE 4.8: Metropolis parameter statistics for Sim. 2, $\mathcal{R}_0 = 3$, and $\omega = 10^{-9}$.

A detailed numerical analysis as well as figures for all relevant plots can be found in Appendix B. In the figures it is also visible that with fixed values $\tau = 0$ or $\tau = 11.5$, the estimated death cases run after or run ahead of the data, respectively.

4.5 Conclusion

In the present work, two *SEIRD*-models for modelling the COVID-19 outbreak in Germany were adapted to existing data from 1 March to 3 May. Two different approaches for the estimation of parameters and approximation of the infection data were used and their results and performance were compared. Regarding the graphical and numerical results, all routines have provided similar meaningful results. Each approach has advantages and disadvantages and should be selected depending on the application needs, time, possible analytical and programming effort. The COVID-19 outbreak results show that the restrictions taken by the authorities have had a major impact on the dynamics of spread. The basic reproduction number could be reduced from a presumably much higher value than the assumed $\mathcal{R}_0 \simeq 3$ to the epidemiologically important limit $\mathcal{R}_0 \simeq 1$. Adding a time lag τ between the onset of infectiousness and death significantly increases the accuracy of the tested model. This time delay is estimated by the data adjustment to an average of 8 days, although in reality, there may be very different values, depending on how long life-support measures are maintained in intensive care units. The adjustment regarding the detection rate and lethality showed that, according to the model, the actual number of infected people is approximately 3–5 times higher than registered and at $\mu \approx 1$–2%, the lethality is lower than assumed.

Conceivable extensions of the present work would be the application to other countries, the integration of travelling or commuting after the relaxation of exit restrictions or the integration of control variables to mathematically derive the optimal time intervals for future lockdowns. With respect to the latter, in order to detect a new increase in infections early on – before it returns to exponential growth –, a measure within the model of the possible increase in transmission rate is required.

Declarations

Authors' contributions

All authors contributed a significant part and reviewed the manuscript.

Competing interests

The authors declare that there exist no competing interests.

A   Results and plots for the adjoint approach

FIGURE 4.9: Results of the adjacent method for Sim. 1, $\mathcal{R}_0 = 3$, and $\omega = 10^{-8}$.

FIGURE 4.10: Results of the adjacent method for Sim. 2, $\mathcal{R}_0 = 3$, and $\omega = 10^{-8}$.
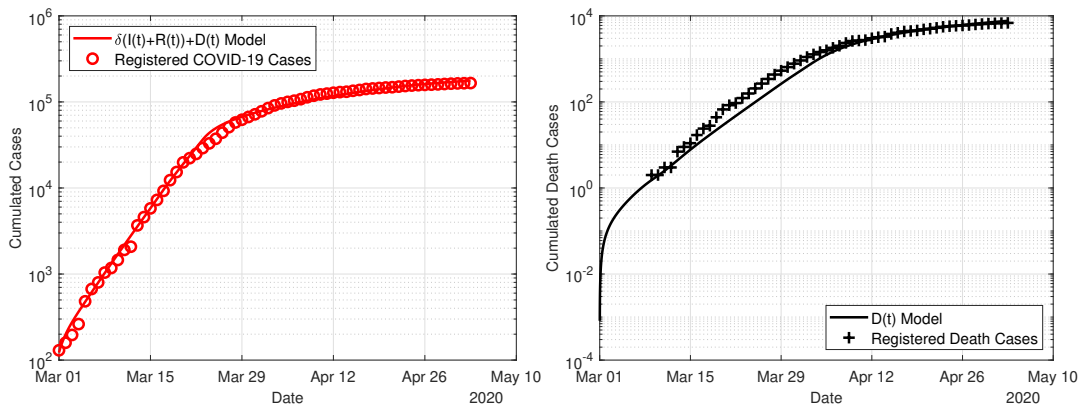
FIGURE 4.11: Results of the adjacent method for Sim. 3, $\mathcal{R}_0 = 3$, and $\omega = 0$.

FIGURE 4.12: Results of the adjacent method for Sim. 3, $\mathcal{R}_0 = 3$, and $\omega = 10^{-9}$.
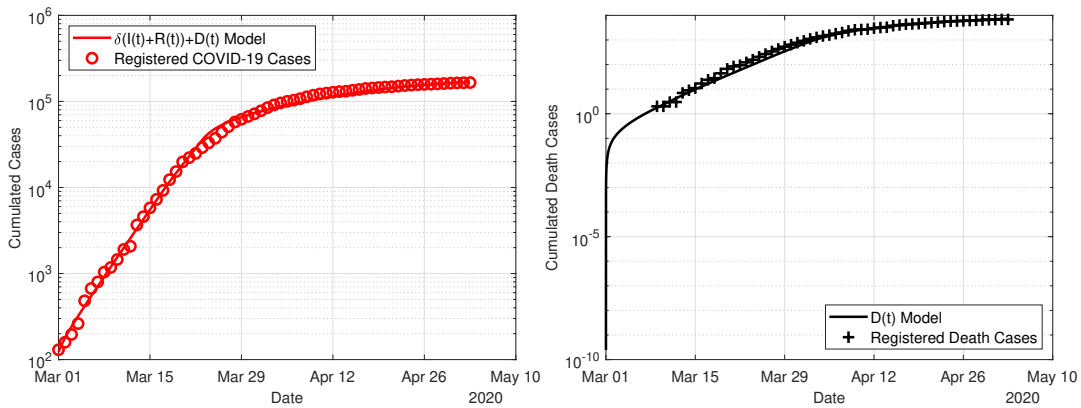
FIGURE 4.13: Results of the adjacent method for Sim. 3, $\mathcal{R}_0 = 3$, and $\omega = 10^{-8}$.
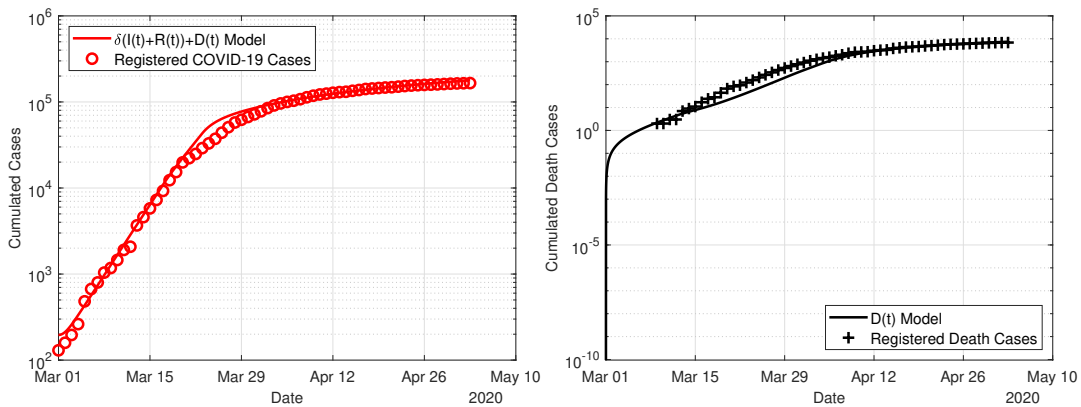
FIGURE 4.14: Results of the adjacent method for Sim. 3, $\mathcal{R}_0 = 3$, and $\omega = 10^{-7}$.

B   Results and plots for the Metropolis algorithm

B.1   Simulation 1 – no delay and fixed initial infectives

TABLE 4.9: Estimates in Sim. 1 for $\tau = 0$, $I_0 = 114/\delta$, $R_0 = 16/\delta$, and $\mathcal{R}_0 = 3$.

Parameter	$\omega = 0$		$\omega = 10^{-9}$		$\omega = 10^{-8}$		$\omega = 10^{-7}$	
	Mean	**Std.**	**Mean**	**Std.**	**Mean**	**Std.**	**Mean**	**Std.**
β_1	.5822	.0353	.5525	.0439	.5935	.0177	.6381	.0227
β_2	.5378	.0169	.4936	.0350	.4828	.0160	.4645	.0348
β_3	.1140	.0111	.1130	.0067	.10940	.0048	.1014	.0130
β_4	.0671	.0032	.0538	.0033	.0502	.0027	.0510	.0056
δ	.2307	.0089	.2933	.0116	.2137	.0104	.3142	.0309
μ	.0105	.0010	.0131	.0016	.0095	.0007	.0137	.0011
E_0	540.7	22.5	811.4	41.5	819.8	52.9	440.8	16.1

TABLE 4.10: Target value of $J(u)$ (in 10^3) for the different weights in Sim. 1. The column represents the weight that is used for $J(u)$ in the Metropolis algorithm, and the row shows the value of $J(u)$ for the respective ω.

wrt ω ╲ **weight** ω	0	10^{-9}	10^{-8}	10^{-7}
0	18.6	18.1	18.6	21.7
10^{-9}	19.2	18.9	19.5	22.1
10^{-8}	24.0	26.2	28.1	25.0
10^{-7}	72.3	99.1	114.2	54.3
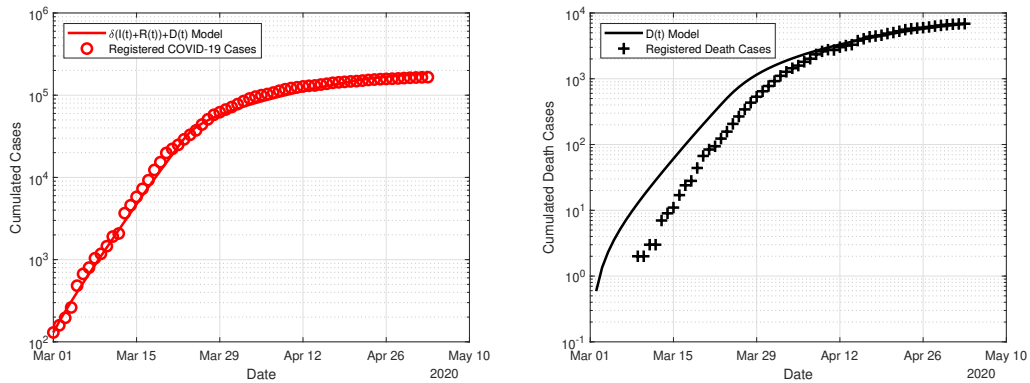
FIGURE 4.15: Results of the Metropolis method for Sim. 1, $\mathcal{R}_0 := 3$, and $\omega = 0$
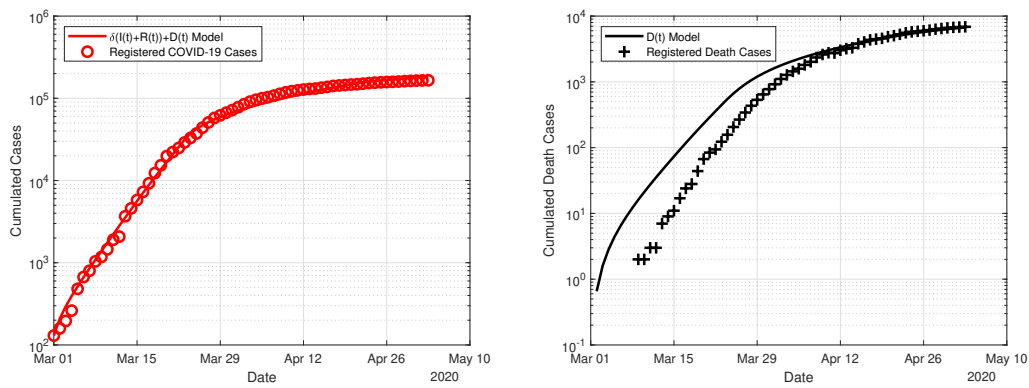
FIGURE 4.16: Results of the Metropolis method for Sim. 1, $\mathcal{R}_0 := 3$, and $\omega = 10^{-9}$.
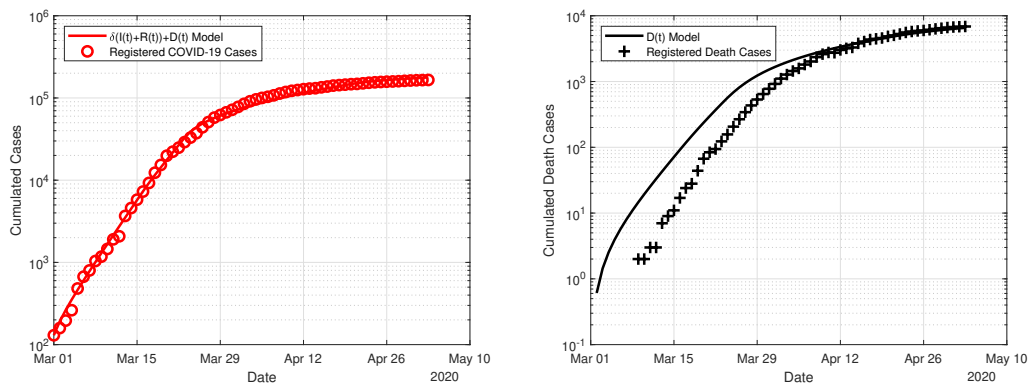
FIGURE 4.17: Results of the Metropolis method for Sim. 1, $\mathcal{R}_0 := 3$, and $\omega = 10^{-8}$.
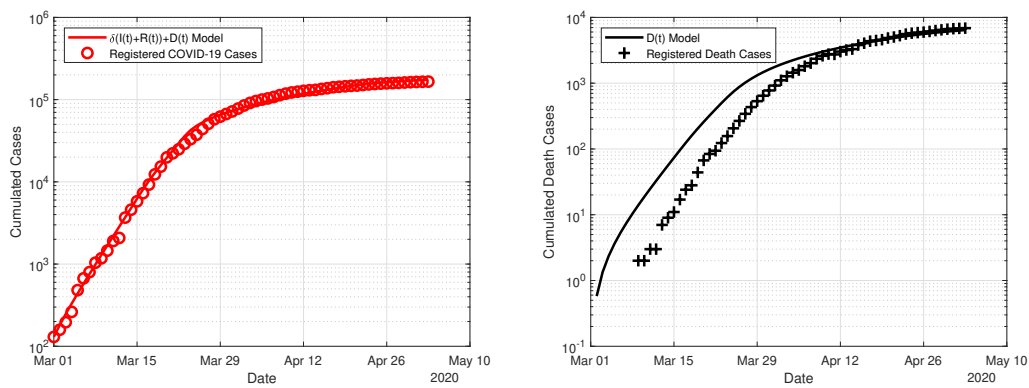
FIGURE 4.18: Results of the Metropolis method for Sim. 1, $\mathcal{R}_0 := 3$, and $\omega = 10^{-7}$.

B.2 Simulation 2 – fixed delay and initial infectives

TABLE 4.11: Estimates in Sim. 2 for $\tau = 11.5$, $I_0 = 114/\delta$, $R_0 = 16/\delta$, and $\mathcal{R}_0 = 3$.

Parameter	$\omega = 0$		$\omega = 10^{-9}$		$\omega = 10^{-8}$		$\omega = 10^{-7}$	
	Mean	**Std.**	**Mean**	**Std.**	**Mean**	**Std.**	**Mean**	**Std.**
β_1	.6735	.0538	.7045	.0600	.6391	.0411	.6678	.0508
β_2	.4414	.0250	.3951	.0336	.4823	.0323	.5011	.0323
β_3	.0810	.0073	.0846	.0075	.0820	.0059	.0790	.0090
β_4	.0672	.0042	.0552	.0073	.0520	.0027	.0605	.0091
δ	.2055	.0228	.2050	.0161	.2761	.0217	.2871	.0214
μ	.0132	.0009	.0131	.0013	.0178	.0011	.0179	.0013
E_0	737.0	62.8	661.2	31.3	620.6	70.5	409.2	18.7

TABLE 4.12: Target value of $J(u)$ (in 10^3) for the different weights in Sim. 2. The column represents the weight that is used for $J(u)$ in the Metropolis algorithm, and the row shows the value of $J(u)$ for the respective ω.

wrt ω \ **weight** ω	0	10^{-9}	10^{-8}	10^{-7}
0	8.7	8.2	9.2	9.6
10^{-9}	9.6	9.0	9.7	9.9
10^{-8}	17.2	15.7	14.7	12.8
10^{-7}	93.8	82.9	64.8	42.1
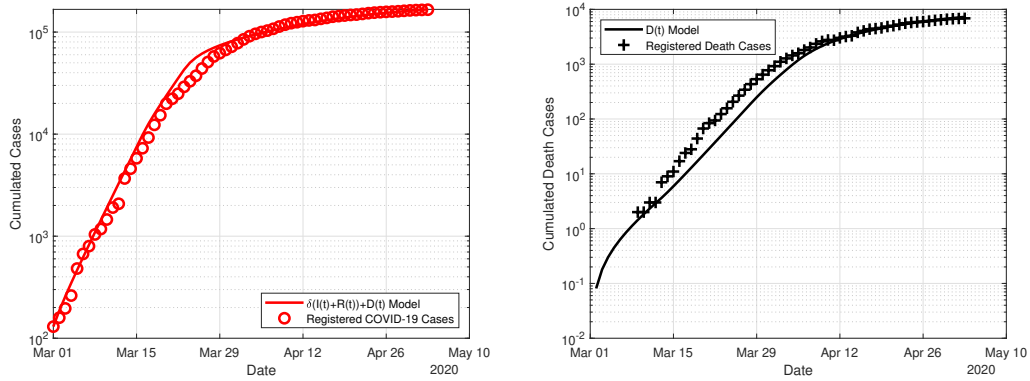
FIGURE 4.19: Results of the Metropolis method for Sim. 2, $\mathcal{R}_0 := 3$, and $\omega = 0$.
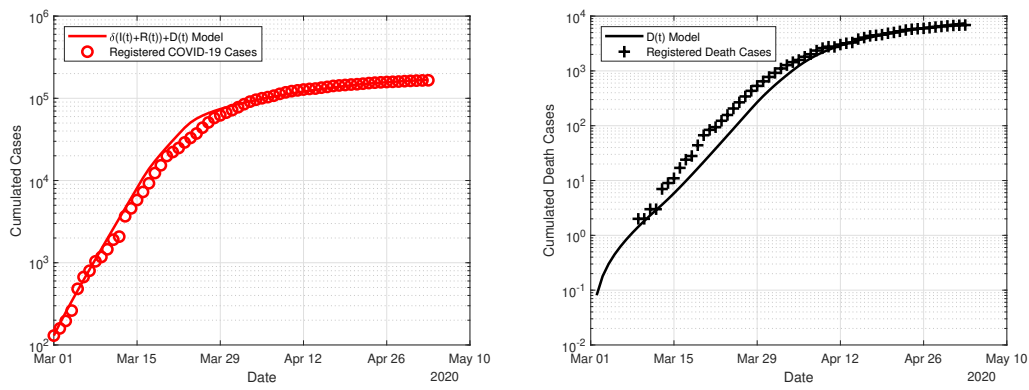
FIGURE 4.20: Results of the Metropolis method for Sim. 2, $\mathcal{R}_0 := 3$, and $\omega = 10^{-9}$.
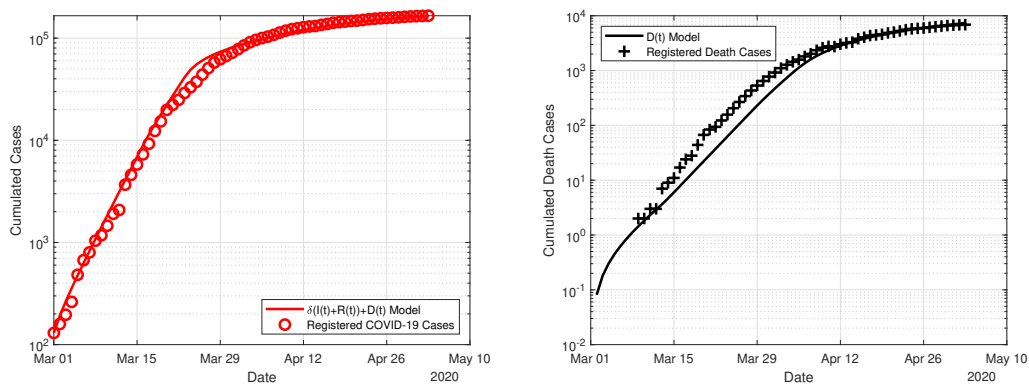
FIGURE 4.21: Results of the Metropolis method for Sim. 2, $\mathcal{R}_0 := 3$, and $\omega = 10^{-8}$.
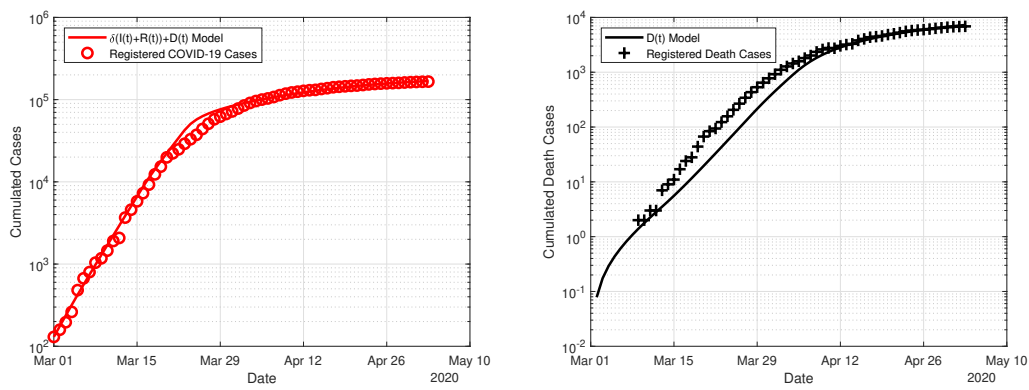
FIGURE 4.22: Results of the Metropolis method for Sim. 2, $\mathcal{R}_0 := 3$, and $\omega = 10^{-7}$.

B.3 Simulation 3 – free delay and initial infectives

TABLE 4.13: Estimates in Sim. 3 for τ = free, I_0 = free, $R_0 = 16/\delta$, and $\mathcal{R}_0 = 3$.

Parameter	$\omega = 0$		$\omega = 10^{-9}$		$\omega = 10^{-8}$		$\omega = 10^{-7}$	
	Mean	Std.	Mean	Std.	Mean	Std.	Mean	Std.
β_1	.5859	.0530	.6442	.0357	.6737	.0300	.7370	.0548
β_2	.4785	.0359	.6403	.0250	.5197	.0396	.4587	.0183
β_3	.0926	.0097	.0862	.0039	.0920	.0037	.0949	.0034
β_4	.0556	.0025	.0554	.0038	.0502	.0019	.0576	.0025
δ	.2768	.0295	.1911	.0115	.2063	.0135	.2237	.0155
μ	.0154	.0008	.0107	.0006	.0117	.0006	.0128	.0005
E_0	790.0	46.7	690.0	52.5	500.8	206.4	351.2	14.9
I_0	493.1	40.1	316.1	30.2	439.0	140.7	350.7	115.7
τ	7.3	.6	7.3	.4	7.4	.3	7.2	.6

TABLE 4.14: Target value of $J(u)$ (in 10^3) for the different weights in Sim. 3. The column represents the weight that is used for $J(u)$ in the Metropolis algorithm, and the row shows the value of $J(u)$ for the respective ω.

wrt ω \ weight ω	0	10^{-9}	10^{-8}	10^{-7}
0	3.8	3.3	3.4	4.1
10^{-9}	4.7	3.8	3.8	4.3
10^{-8}	12.5	9.0	7.8	6.5
10^{-7}	90.5	60.9	47.7	28.7
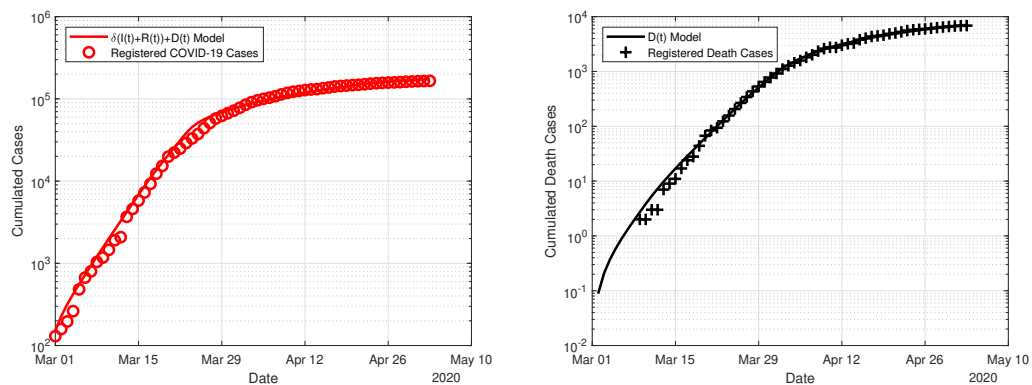
FIGURE 4.23: Results of the Metropolis method for Sim. 3, $\mathcal{R}_0 := 3$, and $\omega = 0$.
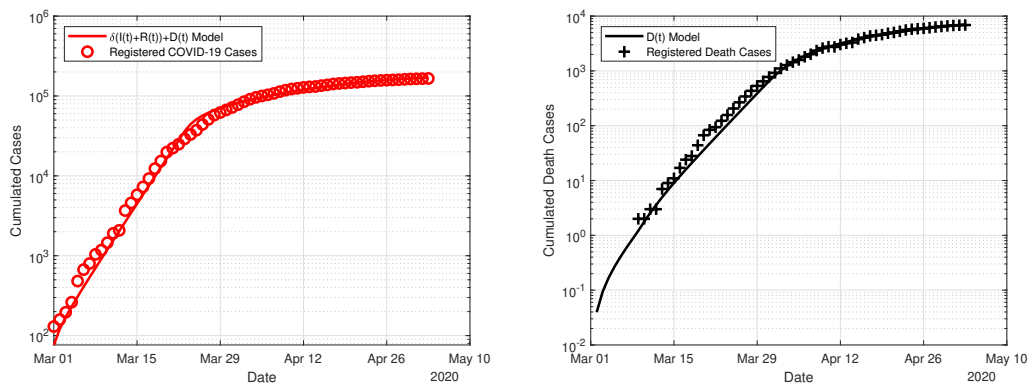
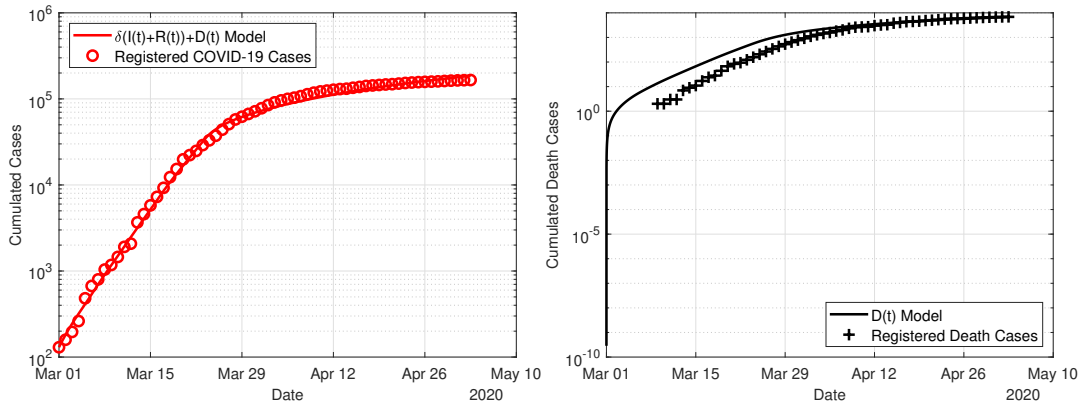FIGURE 4.24: Results of the Metropolis method for Sim. 3, $\mathcal{R}_0 := 3$, and $\omega = 10^{-9}$.
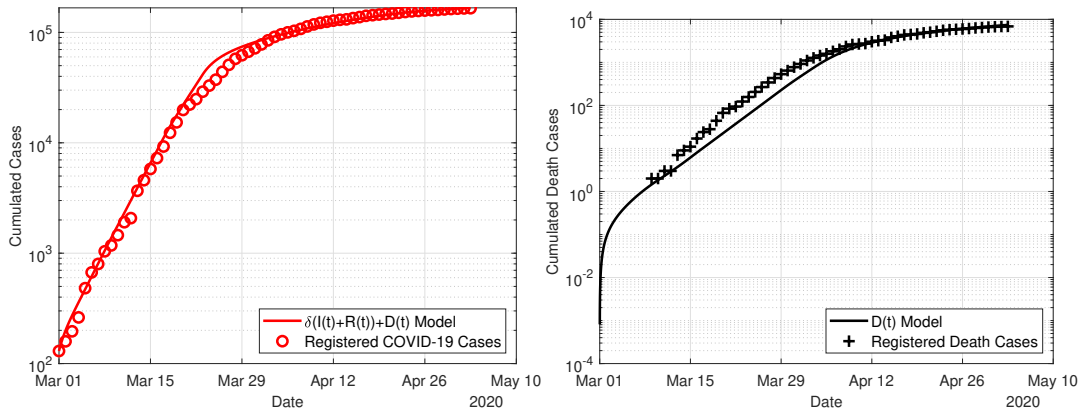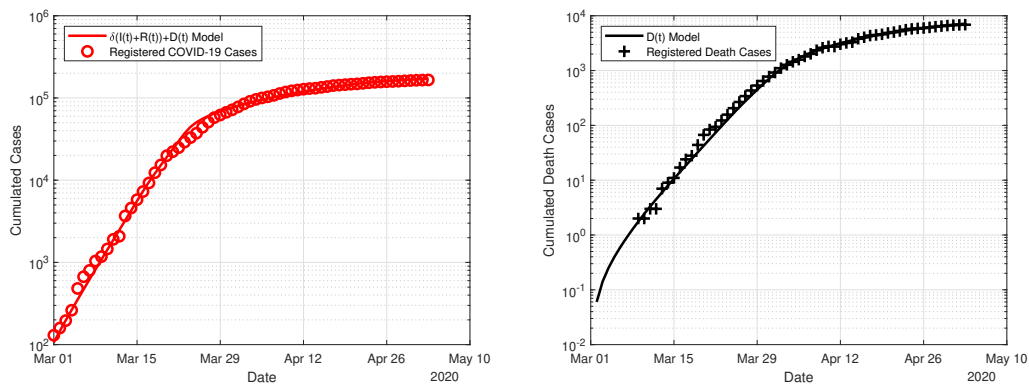

FIGURE 4.25: Results of the Metropolis method for Sim. 3, $\mathcal{R}_0 := 3$, and $\omega = 10^{-8}$.


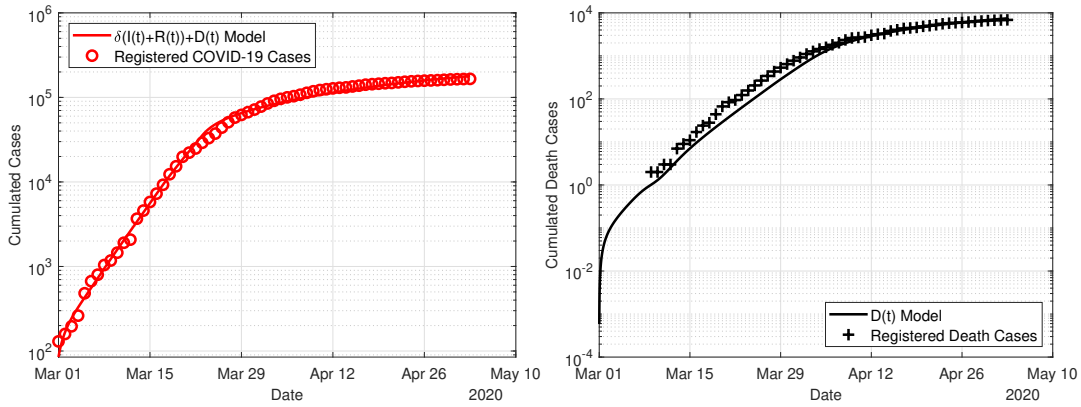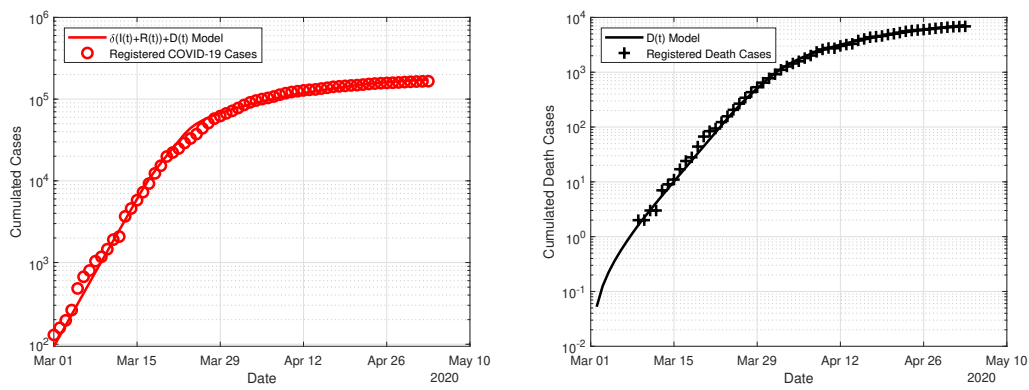FIGURE 4.26: Results of the Metropolis method for Sim. 3, $\mathcal{R}_0 := 3$, and $\omega = 10^{-7}$.

Bibliography

[1]   Heidrich, P. et al. "The COVID-19 outbreak in Germany – Models and Parameter Estimation". In: *Commun. Biomath. Sci.* 3 (2020), pp. 37–59. DOI: `10.5614/cbms.2020.3.1.5`.

[2]   World Health Organization. *Coronavirus disease (COVID-19) Weekly Epidemiological Update and Weekly Operational Update.* `https://www.who.int/emergencies/diseases/novel-coronavirus-2019/situation-reports`. last visited: 18 December, 2023.

[3]   Johns Hopkins University. *Time series of confirmed COVID-19 cases globally.* `github.com/CSSEGISandData/COVID-19/blob/master/csse_COVID_19_data/csse_COVID_19_time_series/time_series_COVID19_confirmed_global.csv`. last visited: 18 December, 2023.

[4]   Robert-Koch-Institute. *Daily situation reports.* `www.rki.de/DE/Content/InfAZ/N/Neuartiges_Coronavirus/Situationsberichte/Gesamt.html`.

[5]   Federal Government of Germany. *Guidelines for reducing social contacts.* `https://www.bundesregierung.de/breg-de/themen/coronavirus/besprechung-der-bundeskanzlerin-mit-den-regierungschefinnen-und-regierungschefs-der-laender-vom-22-03-2020-1733248`. last visited: 18 December, 2023.

[6]   Federal Government of Germany. *Contact Restrictions Extended.* `https://www.bundesregierung.de/breg-en/news/fahrplan-corona-pandemie-1744276`. last visited: 18 December, 2023.

[7]   Chambers, M. and Carrel, P. *Germany eases lockdown, with 'emergency brake' on hand if needed.* `https://www.reuters.com/article/us-health-coronavirus-merkel-idUSKBN22I24E`. last visited: 18 December, 2023.

[8]   Kermack, W.O. and McKendrick, A.G. "Contributions to the mathematical theory of epidemics-I. 1927." In: *Bull. Math. Biol.* 53 (1991), pp. 33–55. DOI: `10.1098/rspa.1927.0118`.

[9]   Martcheva, M. *An introduction to mathematical epidemiology.* Springer, 2015.

[10] Read, J. M. et al. "Novel coronavirus 2019-nCoV: early estimation of epidemiological parameters and epidemic predictions". In: *Philos Trans R Soc Lond B Biol Sci.* 376 (2021), pp. 1–3. DOI: `10.1098/rstb.2020.0265.Epub`.

[11] Statistisches Bundesamt (Germany). *Bevölkerungsstand (31.12.2018).* `https://www.destatis.de/DE/Home/_inhalt.html`. last visited: 18 December, 2023.

[12] Robert-Koch-Institute. *Modellierung von Beispielszenarien der SARS-CoV-2-Epidemie 2020 in Deutschland.* `https://www.rki.de/DE/Content/InfAZ/N/Neuartiges_Coronavirus/Modellierung_Deutschland.pdf?__blob=publicationFile`.

[13] Götz, T. and Heidrich, P. "COVID–19 Disease Dynamics in Germany: First Models and Parameter Identification". In: *Journal of Mathematics in Industry* 10.20 (2020). DOI: `10.1186/s13362-020-00088-y`.

[14] Robert-Koch-Institute. *Corona fact sheet.* `https://www.rki.de/DE/Content/InfAZ/N/Neuartiges_Coronavirus/Steckbrief.html`. last visited: 18 December, 2023.

[15] Lenhart, S. and Workman, J.T. *Optimal control applied to biological models.* CRC Press, 2007.

[16] Nocedal, J. and Wright, S. *Numerical Optimization.* Springer, 2006.

[17] Armijo, L. "Minimization of functions having Lipschitz continuous first partial derivatives". In: *Pacific J. Math.* 16.1 (1966), pp. 1–3.

[18] Schäfer, M. and Götz, T. "Modelling Dengue Fever Epidemics in Jakarta". In: *Int. J. Appl. Comput. Math* 6 (2020). DOI: 10.1007/s40819-020-00834-1.

[19] Metropolis, N. et al. "Equation of State Calculations by Fast Computing Machines". In: *J.Chem. Phys.* 21 (1953), pp. 1087–1092. DOI: 10.1063/1.1699114.

[20] Gelman, A. et al. *Bayesian Data Analysis, 2nd Edition.* London: Chapman and Hall, 1996.

[21] Gilks, W.R., Richardson, S., and Spiegelhalter, D.J. *Markov chain Monte Carlo in Practice*. London: Chapman and Hall/CRC, 1996.

[22] Rusatsi, D.N. "Bayesian analysis of SEIR epidemic models". last visited: 18 December, 2023. PhD thesis. Lappeenranta University of Technology, 2015.

Chapter 5

The Impact of Travelling on the COVID-19 Infection Cases in Germany

This article by Moritz Schäfer, Karunia Putra Wijaya, Robert Rockenfeller and Thomas Götz has been released in the journal BMC INFECTIOUS DISEASES in 2022, referred to as [1]. The theory, formulation and numerical calculations were mainly done by Moritz Schäfer. Karunia Putra Wijaya contributed with the section about confidence intervals and the time-independent sensitivity analysis. Robert Rockenfeller contributed with the section about the time-dependent sensitivity analysis. Thomas Götz provided advice and some linguistic revisions. The format is changed to meet the thesis standard.

Abstract

Background

COVID-19 continues to disrupt social lives and the economy of many countries and challenges their healthcare capacities. Looking back at the situation in Germany in 2020, the number of cases increased exponentially in early March. Social restrictions were imposed by closing e.g. schools, shops, cafés and restaurants, as well as borders for travellers. This reaped success as the infection rate descended significantly in early April. In mid July, however, the numbers started to rise again. Of particular reasons was that from mid June onwards, the travel ban has widely been cancelled or at least loosened. We aim to measure the impact of travellers on the overall infection dynamics for the case of (relatively) few infectives and no vaccinations available. We also want to analyze under which conditions political travelling measures are relevant, in particular in comparison to local measures. By travel restrictions in our model, we mean all possible measures that equally reduce the possibility of infected returnees to further spread the disease in Germany, e.g., travel bans, lockdown, post-arrival tests, and quarantines.

Methods

To analyze the impact of travellers, we present three variants of an susceptible-exposed-infected-recovered-deceased model to describe disease dynamics in Germany. Epidemiological parameters such as transmission rate, lethality, and detection rate of infected individuals are incorporated. We compare a model without inclusion of travellers and two models with a rate measuring the impact of travellers incorporating incidence data from the Johns Hopkins University. Parameter estimation was

performed with the aid of the Monte-Carlo-based Metropolis algorithm. All models are compared in terms of validity and simplicity. Further, we perform sensitivity analyses of the model to observe on which of the model parameters show the largest influence the results. In particular, we compare local and international travelling measures and identify regions in which one of these shows larger relevance than the other.

Results

In the comparison of the three models, both models with the traveller impact rate yield significantly better results than the model without this rate. The model including a piecewise constant travel impact rate yields the best results in the sense of maximal likelihood and minimal Bayesian Information Criterion. We synthesize from model simulations and analyzes that travellers had a strong impact on the overall infection cases in the considered time interval. By a comparison of the reproductive ratios of the models under traveller/no-traveller scenarios, we found that higher traveller numbers likely induce higher transmission rates and infection cases even in the further course, which is one possible explanation to the start of the second wave in Germany as of autumn 2020. The sensitivity analyses show that the travelling parameter, among others, shows a larger impact on the results. We also found that the relevance of travel measures depends on the value of the transmission parameter: In domains with a lower value of the transmission parameter, caused either by the current variant or local measures, it is found that handling the travel parameters is more relevant than the transmission parameter.

Conclusions

We conclude that travellers is an important factor in controlling infection cases during pandemics. Depending on the current situation, travel restrictions can be part of a policy to reduce infection numbers, especially when case numbers and transmission rate are low. The results of the sensitivity analyses also show that travel measures are more effective when the local transmission is already reduced, so a combination of those two appears to be optimal. In any case, supervision of the influence of travellers should always be undertaken, as another pandemic or wave can happen in the upcoming years and vaccinations and basic hygiene rules alone might not be able to prevent further infection waves.

5.1   Introduction

Background.   The COVID-19 disease in Germany started with a first infection case on 26 January 2020 in Bavaria [2]. In March, the number of cases grew rapidly (with a maximum of 6933 cases on 27 March), and various social restrictions were imposed as an active intervention of the disease [3, 4]. On 10 June, only 16 new infection cases were detected [3]. In mid June, travel related restrictions were relaxed within Europe [5]. However, the pandemic continued to spread worldwide and by the end of August, new maxima for the daily cases worldwide set another record for that time [6]. Towards the end of the summer holidays in the first German states in mid to end of August, a second rise of incidence happened with over 1,000 new infection cases per day [3]. Fig. 5.1 shows the temporal evolution of COVID-19 cases in Germany from 26 January until 31 August, as reported by the Johns-Hopkins-University (JHU).

The daily registered COVID-19 are shown on the left side; on the right side, the cumulative registered cases can be seen.
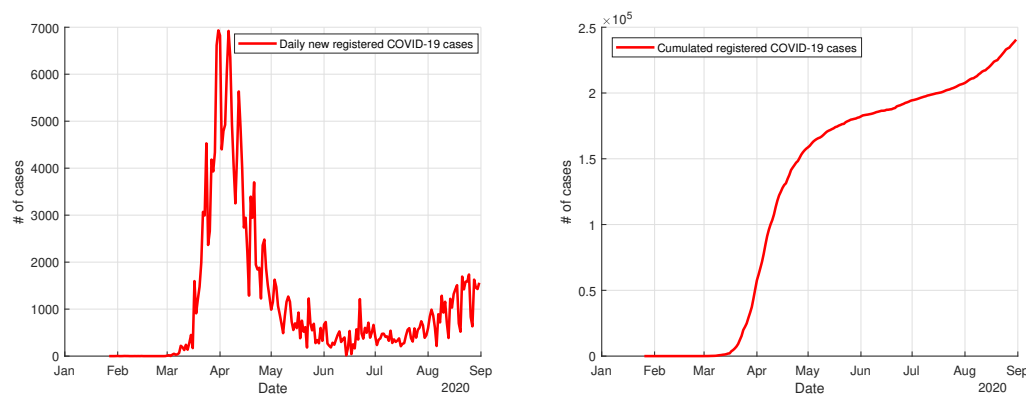
FIGURE 5.1: Daily confimed cases (left) and cumulative confirmed cases (right) with COVID-19 in Germany during the first wave according to JHU [3].

According to the Robert Koch Institute (RKI), a governmental institute for disease control in Germany, many of the cases from June onwards were directly related to German travellers returning home from abroad [7]. Given already long implementation of such travel restrictions (as of 2022), studies that evaluate their effectiveness in Germany are limited. Internationally, however, relevant studies have been preceding and may provide insights for ensuing ones.

Siegenfeld et al. [8] propose and estimate a region-to-region reproduction number, as opposed to the usual person-to-person reproduction number, by assuming that the number of other regions infected by a 'central' region follows a Poisson process. The number appears to be linearly dependent on the probabilities of an infected individual from the central region to travel outside the region, before and after the imposition of travel restrictions. Accordingly, supervision of the number of travellers becomes one of the decisive parameters to contain the spread of COVID-19. They conclude that if high-risk areas impose travel measures coupled with social measures shortly after community transmission, then the reduction of travellers becomes the determining factor if the outbreak can be eliminated. However, without timely social measures that manage to reduce the local reproduction number to a value below 1, travel restrictions only lead to a delay in the spread of epidemics.

Chinazzi et al. [9] emphasize a more broad-minded definition of travel restrictions to include case detection and behavioral changes, as the lone flight traffic limitations around Wuhan in January 2020 (up to 90%) could have only returned a modest containment effect. However they found that, while initially effective – as case importations were reduced by nearly 80% until mid-February by international travel restrictions – after two to three weeks the effect was reduced and numbers grew outside China.

Zou et al. [10] introduce a multi-patch transportation model and also studied the effects of vaccination and quarantine on the disease dynamics of such a multi-patch model. As a result, they propose to control travel or migration in high-risk areas while interventions in low-risk areas are less effective.

Leung et al. [11] also address the combination of traffic flow reduction and testing-quarantine for inbound travellers toward reopening the economy as a good

response in case of weakening public health and social measures (PHSMs) and vaccine limitation.

A systematic review over the impact of travel restrictions on influenza can be found in Mateus et al. [12]. The WHO review considers the effectiveness of internal and external travel restrictions and concludes only very strict restrictions would be expected to have an impact on influenza transmission, but the evidence on these results is proclaimed as low. It is also stated that extensive travel restrictions cause meaningful reduction of the spread of influenza, but only in terms of a delay of several weeks or months, not in terms of containing the disease in areas of high risk.

Also, correspondence by Hollingsworth et al. [13] conveys that for scenarios with few infection cases and a low reproductive value $\mathcal{R}$, travelling can help to contain diseases, while for a higher value of $\mathcal{R}$ only very hard travelling restrictions can prevent spread or postpone the possible wave to a later date, so they conclude that given those latter circumstances, country-based transmission reduction is to be preferred over travel restrictions.

Epstein et al. [14] use stochastic epidemic models to explore the role of international (air) travel restrictions, and also found that strong interventions in travelling can lead to a short-time delay in the spread of epidemics, but they state that this 'saved' time can be effectively used by other disease control measures.

Another systematic review by Grépin et al. [15] regarding the effectiveness of travel restrictions compares the results to the role of travel restrictions on influenza. The authors find that the recommendations of WHO [16] do not necessarily apply to those of COVID-19 as it remains unclear if the findings on influenza can be compared here. Travel measures implemented in Wuhan are found to be effective at the reduction of cases both nationally and internationally, and are more effective when those measures are undertaken early (i.e. in the outbreak).

A diffusion-based and non-international approach can be found in Berestycki et al. [17]. The authors find that fast diffusion effects along major roads are an important factor of the spread of epidemics like COVID-19 in Italy and HIV in the Democratic Republic of Congo.

Structure of the paper.   In the present study our first question is the following:

(Q0) How can we model the spread of infections in Germany with inclusion of travellers to measure the impact they have on the overall numbers?

A susceptible-exposed-infected-recovered-deceased (*SEIRD-*) model introduced in the previous work of Heidrich et al. [18] is used as the foundation for any of the applied systems. In the most simple version, we use a system which does not include travellers as a reference. As a next step, we set up another *SEIRD*-model for Germany which includes travellers to the respective countries and estimate both the 'classical' parameters and also the impact of the infected travellers to the overall epidemics. In one variation of the model, the impact of travellers is assumed to be constant over time, while in a second formulation, we allow a time-dependent value as awareness of the population and political policies might change over time. The travellers are assumed to be part of the infection cycle in the respective destination countries, for which we have also set up another (aiding) *SEIRD*-model.

We estimate the relevant model parameters by using the available data from the Johns-Hopkins University (JHU) [3]. The estimation of several disease-related parameters like, e.g., the transmission rate, death rate or detection rate as of Heidrich et al. [18] is based on a least-squares fit between the model output and the reported data,

where both the reported infections and fatalities are taken into account. Furthermore, the three models are compared in terms of validity and simplicity. Posterior to the fitting and parameter estimation, two questions remain in discussions:

(Q1) Which variable parameters need more careful specifications for which the model solutions, as well as the likelihood function, easily perturb within large orders of magnitude as these parameters slightly change?

(Q2) Which interventions (local interventions like social distancing, masks, lockdown etc. or travelling restrictions) should be more emphasized for possible variations of parameter values in the prediction window?

Our goal will then be to answer these questions with the help of two measures: At first, we consider a time-dependent measure, in which we observe which parameters have a larger impact on the outcome of the five subdivisions. Further, we consider time-independent measures and compare local measures (identified by the overal transmission rate) and travel measures (identified with the newly introduced travel impact rate) and regard under which circumstances one or the other are more relevant for the infection cases. Using the results of questions (Q0), (Q1) and (Q2), we aim to give an answer on the relevance of travel restrictions on the Corona or other infectious diseases in general, and to investigate under which conditions travel restrictions can be a more powerful tool than other non-pharmaceutical measures.

5.2 Methods

All methods were performed in accordance with the relevant guidelines and regulations.

5.2.1 Data

The incidence data used in this study are daily registered COVID-19 cases and deceased cases from Germany (see Fig. 1.2) and other countries from 1 June until 31 August, 2020. Due to the usual independent and identically distributed (iid) assumption on the measurement error (cf. King et al. [19]), only the daily incidence data will be used for optimization parameter estimation of the later introduced models. To accompany the modeling, population data from all countries in consideration are taken from UN data [20].

We only include European countries with available traveller statistics and countries outside of Europe with a total sum of more than 5,000 travellers in the travelling statistics. For the close European countries, the number of travellers is estimated by the travel statistics of 2020 for German travellers [21] (for relative shares) and hospitality statistics in Germany for foreign travellers [22]; these numbers are generally subtracted from the total amount of flight passengers.

The number of travellers from and to farther and non-European countries is gained from analysis of the flight passengers from the respective country [23]. In some larger countries, namely USA, Russia, China, and Japan, the data was problematic. Flight routes from and to these countries are often non-direct, so the plain values of flight passengers would underestimate the real amount of travellers to these countries. As a compromise, we assumed the amount of German travellers to those countries to be the same as the number of foreign visitors from those countries in Germany, which makes this estimation more meaningful.

The populations and amount of travellers per month of this total of 55 countries is presented in Tab. 5.2.

5.2.2 SEIRD-models

Traveller induced model. In the previous work we investigated the dynamics of COVID-19 disease until early May 2020 [18]; this study departs from this approach. Again we use a variation of the *SIR*-model introduced by McKendrick [24]; see also Martcheva [25] for an overview of mathematical models in epidemiology. It builds up on delayed differential equation (DDE-) system to describe the behaviour of the disease in Germany in summer 2020. While the use of stochastic variables can make the model more realistic, but may also lead to further technical questions including noise type, stable ergodicity, and predictability, which go beyond the original scope.

Therefore, we tested a deterministic model for the main aim. The entire population N is subdivided into five subdivisions: susceptible S, exposed E, infected I, recovered R, and deceased D, so that we deal with a so-called *SEIRD*-model. The virus is transmitted from infected persons to susceptible persons at a piecewise constant rate β. After an incubation duration κ^{-1} exposed individuals become infective. Loss of infectivity is gained after an average duration γ^{-1}; the death parameter μ describes the probability for infected persons dying from the disease. A time lag τ between the infected and the deceased state accounts for the fact that the number of people dying from the disease is attained from the infected number τ days earlier. Here, we also introduce an additional : travellers E_t which have been exposed to the disease abroad. Values for the fixed model parameters in Germany are given in Tab. 5.1.

TABLE 5.1: Used parameter values for all travel-based models.

Parameter	Value	Reference
N	83,019,213	[20]
κ	$(3\,\text{d})^{-1}$	[26]
γ	$(10\,\text{d})^{-1}$	[26]

These assumptions lead to the following five-dimensional ODE system.

$$\dot{S} = -\frac{\beta}{N}\,S\,I - E_T(t) \qquad\qquad S(t_0) > 0 \qquad (5.1\text{a})$$

$$\dot{E} = \frac{\beta}{N}\,S\,I + E_T(t) - \kappa\,E \qquad\qquad E(t_0) = E_0 \geq 0 \qquad (5.1\text{b})$$

$$\dot{I} = \kappa\,E - \gamma\,((1-\mu)\,I + \mu\,I(t-\tau)) \qquad I(t_0-\tau \leq t \leq t_0) = \phi(t) > 0 \qquad (5.1\text{c})$$

$$\dot{R} = (1-\mu)\,\gamma\,I \qquad\qquad R(t_0) = R_0 \geq 0 \qquad (5.1\text{d})$$

$$\dot{D} = \mu\,\gamma\,I(t-\tau) \qquad\qquad D(t_0) = D_0 \geq 0 \qquad (5.1\text{e})$$

Here, the initial value of susceptibles is fixed to $S_0 = N - E_0 - I_0 - R_0 - D_0$. Let $X = (X_i)$ and $Z = (Z_i)$ denote the daily new confirmed cases and deaths related to COVID-19 in Germany. The subscript i serves to point out the measurement at time point t_i as reported by the JHU [3]. Not all infections are by nature detected, from which case we introduce detection rates δ for Germany and δ_j for the destination country, respectively. For the persons which are currently infected or have recovered, we assume that only this proportion δ or δ_j is tested and detected and hence appears in the statistics; however, we assume no undetected deceased cases. We assume that the proportion of detected cases versus real infections is constant over the whole time

interval, so that no temporal change of the detection rate is needed in our model. The initial value of the infected cases at the starting date t_0 is later on subject of the estimation procedure. Therefore, we use the infected data as the real data divided by the detection rate, for Germany and destination countries, respectively:

$$\phi(t) := \frac{\text{interp}\{(X_i)\}(t)}{\delta}, \qquad t_0 - \tau \le t \le t_0. \tag{5.2}$$

As travel measures are relaxed as of 15 June, we designed the starting time t_0 of this model as 1 June. This way we allow parameter estimation of the transmission rate β in the first two weeks which is fully independent of the travel impact rate α, so those parameters are not correlated during the optimization process (note that in eqn. (5.3) those parameters are multiplied with each other). The end date is fixed to 31 August because of the end of summer holidays (in most German states) and new restrictions in other countries from September onwards, e.g. a travel warning for Spain [5], which will affect the transmission parameters. The initial values are either gained from the JHU data sets [3] or introduced as free parameters which have to be optimized in the Metropolis algorithm. The function $\phi : [t_0 - \tau, t_0] \to \mathbb{R}_+$ denotes the initial history of the infected required for the well-posedness of the above DDE; the value τ is another free parameter. The number of travellers which have been exposed to the disease is defined as

$$E_T(t) = \alpha(t) \sum_j \frac{\beta^{(j)}(t)}{N^{(j)}} T_{(0)\leftrightarrow(j)}(t) I^{(j)}(t). \tag{5.3}$$

The values $I^{(j)}$ and $N^{(j)}$ are defined by the number of infected people and respectively the resident population in country $(j) \neq (0)$ at time t. The function $T_{(0)\leftrightarrow(j)}(t)$ describes the number of travellers from Germany to country j, whereby the superscript (0) denotes Germany from now on. Travellers are assumed to have a higher risk of getting infected, due to being more active, visiting places and travelling (e.g., in a plane) with more contacts than an average resident. Therefore, we define $\alpha(t)$ to quantify the special risk of getting infected as a traveller. If $\alpha \equiv 1$, then the transmission rate for travellers is equal to the country's specific transmission rate $\beta^{(j)}(t)$. This rate is piecewise constant with switching returned from imposition or relaxation of certain measures. No inclusion of travellers due to bans or closed borders are identical to $\alpha \equiv 0$.

Infection rate induced model. As we aim to estimate $\beta_j(t)$ and $I^{(j)}$ for all relevant countries, we have to set up another ODE system modelling the disease dynamics. Let (j) therefore be the specific country. For all countries $(j), j \in \{1, 2, \dots, M-1, M\}$ with M being the amount of observed countries, we estimate the local transmission rate $\beta_j(t)$ as well as the amount of infected persons $I^{(j)}(t)$ for all relevant time points by using an *SEIRD*-model without a traveller , while the total population $N^{(j)}$ is assumed to be constant over time.

$$\dot{S}^{(j)} = -\frac{\beta_j(t)}{N^{(j)}} S^{(j)} I^{(j)} \qquad\qquad\qquad\qquad S^{(j)}(t_0) > 0 \quad (5.4a)$$

$$\dot{E}^{(j)} = \frac{\beta_j(t)}{N^{(j)}} S^{(j)} I^{(j)} - \kappa E^{(j)} \qquad\qquad \dot{E}^{(j)}(t_0) = E_0^{(j)} \geq 0 \quad (5.4b)$$

$$\dot{I}^{(j)} = \kappa E^{(j)} - \gamma \left((1 - \mu_j) I^{(j)} + \mu_j I^{(j)}(t - \tau_j) \right) \qquad I^{(j)}(t \leq t_0) = \phi^{(j)}(t) > 0 \quad (5.4c)$$

$$\dot{R}^{(j)} = \left(1 - \mu_j \right) \gamma I^{(j)} \qquad\qquad\qquad R^{(j)}(t_0) = R_0^{(j)} \geq 0 \quad (5.4d)$$

$$\dot{D}^{(j)} = \mu_j \gamma I^{(j)}(t - \tau_j) \qquad\qquad\qquad D^{(j)}(t_0) = D_0^{(j)} \geq 0 \quad (5.4e)$$

The starting value of the susceptibles is again defined by $S^{(j)}(t_0) = S_0^{(j)} = N^{(j)} - E_0^{(j)} - I_0^{(j)} - R_0^{(j)} - D_0^{(j)}$ for all compartments j. Let again $X^{(j)} = (X_i^{(j)})$ and $Z^{(j)} = (Z_i^{(j)})$ denote the daily infection and death cases in the respective destination country as reported by the JHU [3]. Then, the history function is denoted analogously to before by

$$\phi_j(t) := \frac{\mathrm{interp}\{(X_i^{(j)})\}(t)}{\delta_j} \qquad t_0 - \tau_j \leq t \leq t_0. \qquad (5.5)$$

The values for κ and γ are assumed to be independent of country (j). In the datasets for the countries, we find a sudden 'step' in the infection rates. This can not be modelled by travellers like in the model for Germany, which has two reasons: (1) Traveller data is not available for each country. (2) The reasons for the raised infection numbers in other countries are not of interest for the traveller model in Germany. Instead of using an additional parameter α and a traveller , we assume the transmission rates to be piecewise constant. By performing various simulations, the best-fitting 'switching date' where the rate is allowed to change value is found to be 20 July:

$$\beta_j(t) := \begin{cases} \beta_0^{(j)}, & t \leq 19 \,\mathrm{July} \\ \beta_1^{(j)}, & 20 \,\mathrm{July} \leq t \end{cases} \qquad (5.6)$$

This system (5.4) is used both for the destination countries of German travellers and also for the model for Germany, which does not include travellers (later on to be called Model A). In the latter case, we can see the system as a special case of system (5.1) with $j = 0$, representing Germany. Travel restrictions are being relaxed as of 15 June [27]. This date is therefore assigned to be the starting time t_0 for the destination countries, while the starting date remains 1 June for the no-travel model for Germany. The end date remains 31 August (in both cases) as we require the values of β_j and $I^{(j)}$ until the end of the observed time interval, and of course nothing changes for the 'German' model. The parameters $N^{(j)}$ reflect the current total populations in all regarded countries which are the destination or origin of travellers from and to Germany; the population values are taken from UN data [20]. Results using the optimized parameters are also shown in Tab. 5.2.

TABLE 5.2:   Country populations, (estimated) number of German travellers travelling to country *j* per month, and country-based transmission parameters.

Country	Population	Travellers			Transmission	
		June	July	August	$\beta_{j,1}$	$\beta_{j,2}$
Decimal Power / Unit	10^6	1	1	1	$10^{-1}d^{-1}$	$10^{-1}d^{-1}$
Albania	2.88	945	3,366	9,505	1.20	1.19
Austria	8.90	312,364	636,414	782,818	1.35	1.36
Belarus	9.45	1,595	1,985	3,102	0.38	0.65
Belgium	11.51	36,210	155,295	92,495	1.17	1.60
Bosnia and Herzegovina	3.30	2,811	2,849	6,702	1.54	1.10
Brazil	211.05	6,715	4,366	3,778	1.22	1.12
Bulgaria	6.95	11,562	42,552	74,363	1.24	1.06
Canada	37.41	4,746	9,778	8,368	0.31	1.33
China	1,433.78	3,711	5,921	7,077	1.55	1.05
Croatia	4.06	66,029	84,952	150,790	0.31	1.10
Cyprus	0.89	360	7,191	14,049	0.42	1.89
Czech Republic	10.69	51,518	130,651	148,353	0.84	1.41
Denmark	5.81	48,986	395,924	571,649	0.77	1.70
Egypt	100.39	2,542	5,134	7,790	0.65	0.36
Estonia	1.33	1,006	3,380	5,967	0.23	2.00
Ethiopia	112.08	1,431	2,089	2,066	1.84	1.45
Finland	5.53	4,624	12,134	19,074	0.31	1.74
France	67.20	105,905	326,298	345,913	0.95	1.96
Greece	10.7	15,930	179,531	372,892	1.41	1.75
Hungary	9.77	30,154	53,080	71,577	0.36	1.71
Iceland	0.34	889	7,892	13,718	1.66	1.56
Ireland	4.97	4,892	8,965	9,065	0.43	2.20
India	1,366.42	5,168	8,676	14,046	1.39	1.25
Israel	88.52	2,455	2,693	797	1.65	1.23
Italy	60.29	126,855	272,324	415,581	0.21	1.75
Japan	126.86	1,457	2,340	3,292	1.78	1.29
Kosovo	1.72	586	7,341	18,626	1.59	1.10
Latvia	1.91	5,936	12,637	20,798	0.31	1.52
Lebanon	6.87	167	1,699	5,298	1.09	1.94
Lithuania	2.79	1,203	1,787	2,415	0.49	1.89
Luxembourg	0.63	4,562	4,466	2,946	2.54	0.51
Malta	0.51	261	9,338	16,974	1.16	1.95
Mexico	127.58	2,079	2,726	2,253	1.70	0.69
Montenegro	0.63	728	2,490	4,118	3.75	0.54
Moldova	4.04	972	1,728	3,815	0.85	1.30
Netherlands	17.40	188,840	721,721	1,592,831	1.04	1.72
Northern Macedonia	2.08	0	3,486	9,875	0.89	1.02
Norway	5.37	8,326	42,589	64,125	0.74	1.70
Poland	27.94	95,372	171,127	268,559	0.52	1.51
Portugal	10.29	17,659	63,369	111,867	0.51	0.81
Qatar	2.83	6,063	8,336	6,747	0.79	1.00
Romania	19.36	5,702	32,822	41,255	1.18	1.35
Russia	145.87	3,550	6,017	7,324	0.61	1.03
Serbia	8.77	5,164	5,577	9,672	1.62	0.61
Slovakia	5.46	19,372	31,161	56,401	1.16	1.54
Slovenia	2.07	3,759	5,361	5,987	1.44	1.14
Spain	47.32	22,209	331,894	436,624	1.19	1.86
Sweden	10.32	9,050	39,584	46,878	0.38	0.55
Switzerland	8.50	102,698	272,121	388,971	1.49	1.35
Tunisia	11.69	644	2,709	11,292	1.09	2.12
Turkey	83.43	36,986	144,350	343,972	0.77	1.14
United Kingdom	66.43	17,026	29,925	32,969	0.92	1.16
Ukraine	43.99	3,020	8,934	14,759	0.77	1.44
United States of America	329.06	24,123	42,409	41,613	0.81	1.62
United Arab Emirates	9.77	3,231	9,394	6,856	0.59	1.10

Travellers and travel impact rate.   We only include European countries with available traveller statistics and countries outside of Europe with a total sum of more than 5,000 travellers in the travelling statistics. For the close European countries, the number of travellers is estimated by the travel statistics of 2019 and 2020 for German travellers [21] (for relative shares) and hospitality statistics in Germany for foreign travellers [22]. The number of travellers from and to farther and non-European countries is gained from analysis of the flight passengers from the respective country [23]. In some larger countries, namely USA, Russia, China, and Japan, the data was problematic. Flight routes from and to these countries are often non-direct, so the plain values of flight passengers would underestimate the real amount of travellers to these countries. As a compromise, we assumed the amount of German travellers to those countries to be the same as the number of foreign visitors from those countries in Germany, which makes this estimation more meaningful. The populations and amount of travellers per month of this total of $M = 55$ countries is presented in Tab. 5.2.

Using Tab. 5.2, we can compute the daily value for $T_{(0)\leftrightarrow(j)}$ by the number of travellers divided by the days in the respective month. E.g., for June, only the 16 days from 15 June to 30 June are considered. Average time of spending time here is 12 days so e.g. for July, we have $T_{(0)\leftrightarrow(j)} = 331{,}894 \cdot \frac{12}{31\mathrm{d}} \approx 128{,}475 \, \mathrm{d}^{-1}$. The uncertainty in the value of 12 days for the average travel length is mitigated by the estimation of α, as these two values are directly multiplied, and thus only the product of those two values is important.

In Model B, $\alpha(t)$ is assumed to be constant over time as soon as the travel ban is loosened:

$$\alpha(t) := \begin{cases} 0 & t \leq 14 \text{ June} \\ \alpha & 15 \text{ June} \leq t \leq 31 \text{ August} \end{cases} \tag{5.7}$$

In Model C, we define a piecewise constant function $\alpha(t)$ as follows:

$$\alpha(t) := \begin{cases} 0 & t \leq 14 \text{ June} \\ \alpha_0 & 15 \text{ June} \leq t \leq 30 \text{ June} \\ \alpha_1 & 1 \text{ July} \leq t \leq 31 \text{ July} \\ \alpha_2 & 1 \text{ August} \leq t \leq 31 \text{ August} \end{cases} \tag{5.8}$$

This way, we are able to identify temporal differences in the travelling subdivision, e.g. caused by a different social behaviour or loosened restrictions. The last three 'switching points' are arbitrarily chosen at the beginning of each month to account for the time-dependency of α.

5.2.3   Optimization models, parameter bounds, and initial values

The parameters to be estimated in eqns. (5.1) and (5.4) are transmission rate, detection rate, lethality, time lag, travel impact rate, and numbers of exposed on 1 June 2020 (Germany) resp. 15 June 2020 (all other countries). The optimal parameters $u^{(j)*}$ and u^* are determined by solving the following maximization problems in the respective models. This results in consideration of the following three models, with an auxiliary model being pre-evaluated before handling models B and C.

Model A: Time-dependent transmission rate, starting 1 June

$$\max_{u^{(0)}} L(u^{(0)}) \qquad\qquad \text{subject to ODE (5.4)}$$

$$\text{where} \quad u^{(0)} = \left(\beta_0^{(0)}, \beta_1^{(0)}, \delta_0, \mu_0, \tau_0, E_0^{(0)}\right) \in \mathbb{R}^6 \qquad (5.9)$$

Auxiliary model for models B and C: For all countries $j = 1, \ldots, 55$, starting 15 June

$$\max_{u^{(j)}} L(u^{(j)}) \qquad\qquad \text{subject to ODE (5.4)}$$

$$\text{where} \quad u^{(j)} = \left(\beta_0^{(j)}, \beta_1^{(j)}, \delta_j, \mu_j, \tau_j, E_0^{(j)}\right) \in \mathbb{R}^6 \qquad (5.10)$$

Model B: Constant travel transmission parameter $\alpha(t)$ from 15 June onwards

$$\max_{u} L(u) \qquad\qquad \text{subject to ODE (5.1)}$$

$$\text{where} \quad u = (\beta, \delta, \mu, \tau, \alpha, E_0) \in \mathbb{R}^6 \qquad (5.11)$$

Model C: Piecewise linear travel transmission function $\alpha(t)$ starting 15 June and jumps on 1 July and 1 August

$$\max_{u} L(u) \qquad\qquad \text{subject to ODE (5.1)}$$

$$\text{where} \quad u = (\beta, \delta, \mu, \tau, \alpha_0, \alpha_1, \alpha_2, E_0) \in \mathbb{R}^8 \qquad (5.12)$$

Tab. 5.4 shows the constraints for all parameters in the three models, which can also be used for u_j (with the starting values R_0 and $Z_0 = D_0$ as of [3]). Previous

TABLE 5.4: Parameter constraints with the respective constraints of the fitted parameters.

$\beta_{0/1}$	δ	μ	τ	α_j	N_0	E_0	δI_0	δR_0	D_0
$> .05$	$.05 - 1$	$\leq .1$	$3 - 40$	> 0	82,846,340	> 0	9,407	165,632	8,555

investigations by [28, 18] already give us orders of magnitude for the initial values of the optimization for β_i and δ. The order of magnitude of the time interval between the onset of infectiousness and death is derived from RKI modelling studies [26]. We allow a larger span in τ and τ_j than in [18] because the onset between infection and death is also dependent of the date on which the death case is registered in the statistics, where significantly different values depending on the country are possible here. A potential reason for this lies in different policies and procedures in reporting infection and death cases. The starting values at time t_0 for the detected cumulated infected X_0, detected recovered $Y_0 = \delta R_0$ and detected dead Z_0 can be taken from the statistics. The initial number of infected is then defined as $I_0 = (X_0 - Y_0 - Z_0)/\delta$. Depending on the detection rate δ, the 'real' numbers I_0 and R_0 can be calculated by dividing those detected values by δ. For the initial guess on the 'real' number of exposed individuals E_0 at time t_0, we use a derivation using the Basic Reproduction Number $\mathcal{R}_0$, which indicates how many new infections an infected individual causes on average during its illness in an otherwise susceptible population. In our model, the share of infected persons I_0 can either be at the start, the middle or the end of the infection, so several possible time stages of the infections are possible. The middle of this time interval is assumed to be the mean of all infected persons at time t_0. Thus,

up to this point in time they could infect about $\mathcal{R}_0/2 \cdot I_0$ persons on average which then become exposed to the virus, i.e. this is identical to E_0. Here, we assume that the initial basic reproductive number is approximately $\mathcal{R}_0 \approx 1$ because of the stagnation of cases on a low level at the beginning of June.

TABLE 5.5: Orders of magnitude of the initial values for adapting the model to the available data.

Parameter	$\beta_{0/1}$	δ	μ	τ	α_j	E_0
Initial Value	.1	.3	.005	20	1	$1/2 \cdot I_0$

5.2.4 Likelihood function

As seen in the previous section, the unknown parameter sets $u^{(j)}$ and u will be estimated by maximization of a likelihood function, which will be developed in this section. Note that the derivation of the function is described in detail only for u, but is equivalent for the likelihood function of $u^{(j)}$.

We denote $\tilde{I}$ and $\tilde{R}$ as the difference between the daily infection cases, i.e. for $i = 1 \ldots N$:

$$\tilde{I}_i = \{\delta[I(t_{i+1}) + R(t_{i+1})] + D(t_{i+1})\} - \{\delta[I(t_i) + R(t_i)] + D(t_i)\} \tag{5.13a}$$
$$\tilde{D}_i = D(t_{i+1}) - D(t_i) \tag{5.13b}$$

Hence we compare the data X to the model output $\tilde{I}$ and $X^{(j)}$ to $\tilde{I}^{(j)}$, as well as Z with $\tilde{D}$ and $Z^{(j)}$ with $\tilde{D}^{(j)}$. At time t_i, our model validation is subject to measurement error, which is assumed to be of degenerate multivariate Gaussian distribution with mean (X_i, Z_i) or (X_i^j, Z_i^j) and covariance matrix Σ or Σ^j, where one covariate corresponds to the measurement error from confirmed cases, and the other to the deceased cases. The time invariance of the covariance matrix was opted only for the sake of simplicity. Further simplification may assert prior assumption that the covariance terms in the measurement error are zero, meaning that each error is an independent process. This leads us to $\Sigma = \text{diag}(\sigma_Y, \sigma_Z)$ or $\Sigma^j = \text{diag}(\sigma_X^j, \sigma_Z^j)$. Our likelihood function for time point t_i reads as

$$L_i(u) := \frac{1}{2\pi \sigma_X \sigma_Z} \exp\left(-\frac{(\tilde{I}_i - X_i)^2}{\sigma_X^2} - \frac{(\tilde{D}_i - Z_i)^2}{\sigma_Z^2}\right). \tag{5.14}$$

Assuming iid processes for all measurements at all time points, Kalbfleisch [29] pointed out a constant $K = (2\pi)^N$ that serves to simplify the joint likelihood function

$$L(u) := K \prod_i L_i(u) = \frac{1}{\sigma_X^N \sigma_Z^N} \exp\left(-\sum_i \frac{(\tilde{I}_i - X_i)^2}{\sigma_X^2} + \frac{(\tilde{D}_i - Z_i)^2}{\sigma_Z^2}\right). \tag{5.15}$$

Our study designates the standard deviations as to approximate the means of confirmed and deceased cases, $\sigma_X := \|X\|/N$ and $\sigma_Z := \|Z\|/N$. Defining $J(u)$ as the sum of squares error of the difference between data and estimation using the parameter set u, i.e.,

$$J(u) = \sum_i \frac{(\tilde{I}_i - X_i)^2}{\|X\|^2} + \frac{(\tilde{D}_i - Z_i)^2}{\|Z\|^2},$$

the likelihood and log-likelihood function then read as

$$L(u) = \frac{N^{2N}}{\|X\|^N \|Z\|^N} \exp\left(-N^2 J(u)\right), \tag{5.16}$$

$$\log L(u) = \log\left(\frac{N^{2N}}{\|X\|^N \|Z\|^N}\right) - N^2 J(u).$$

$$= N(2\log N - \log\|X\| - \log\|Z\| - NJ(u)). \tag{5.17}$$

As the calculation can be done equivalently for the destination countries (j), the log-likelihood $\log L^{(j)}(u)$ is defined as

$$\log L^{(j)}(u) = N^{(j)}(2\log N^{(j)} - \log\|X^{(j)}\| - \log\|Z^{(j)}\| - N^{(j)} J^{(j)}(u)). \tag{5.18}$$

Model specification

The aim in model specification for the fitting of the data is that we have a measure (criterion) based on fit and complexity (information-type criterion). Therefore, regarding models A, B, and C, we opt for a minimal value of the Bayesian Information Criterion (BIC)

$$\text{BIC} = \log N \cdot |u| - 2\log L(u) \tag{5.19}$$

according to Raftery [30], whose first term measures complexity represented by the observation size N and the number of parameters $|u|$, while the second term represents the maximal likelihood function. Note that for the travel destination countries, we do not compare the model output as we only allow the travel-independent system (5.4). The BIC penalizes the number of parameters more than the Akaike Information Criterion (AIC) [31], where the latter would have replaced the factor $\log(N)$ by 2. As far as model specification is concerned, our aim will be to choose between three models by selecting the model with minimal BIC as well as amending the question if the role of travellers is significant.

5.2.5 Metropolis algorithm

In our study, we use a Metropolis algorithm (cf. [32, 33, 34]) for estimation of parameters in the ODE systems (5.1) and (5.4) according to the procedure described in [35, 18]. The parameter set u_0 as of Tab. 5.5 is used for the initial guess. We assign random draws u_{new} from a normally distributed (and thus symmetric) proposal function q, i.e. $u_{new} \sim q(u_{new}|u_{i-1})$, in every iteration i.

Using the previously defined $J(u)$ as the target distribution, we calculate the approximative distribution by

$$\pi(u) = c \cdot \exp\left(-\frac{J(u)^2}{2\sigma^2}\right), \tag{5.20}$$

whereby c is an arbitrary real value. For the acceptance probability, it follows

$$p(u_{new}|u_{i-1}) = \min\left\{1, \frac{\pi(u_{new}) \cdot q(u_{i-1}|u_i)}{\pi(u_i) \cdot q(u_i|u_{i-1})}\right\} = \min\left\{1, \frac{\pi(u_{new})}{\pi(u_i)}\right\}. \tag{5.21}$$

In eqn. (5.21), we can see that the value of c is redundant as it cancels out in the division. If the sample is accepted with the probability p, we set $u_i = u_{new}$; with the probability $1 - p$, the sample is declined, meaning $u = u_{i-1}$ according to [36, 35].

5.2.6 Confidence intervals of the parameters

Considering that the observation size N and the number of parameters $|u|$ hold the relation $N \gg |u|$, we adopt the idea of asymptotic confidence interval proposed in [37, 38]. These works suggest that the asymptotic confidence interval can be a good approximation of the uncertainty in the optimal parameters u^* providing that, besides the aforementioned relation, the measurement error is relatively small as compared to the data. The formula of the confidence interval for each parameter u_k^* is given by $CI_k := \left[u_k^* - \psi, u_k^* + \psi \right]$, with ψ being defined as

$$\psi := \sqrt{2\chi^2(q, df) \cdot (\nabla^{-2}(-\log L(u^*)))_{kk}}. \tag{5.22}$$

The operator ∇^{-2} denotes the inverse of the Hessian while $\chi^2(q, df)$ denotes the q quantile of the χ^2 distribution with the degree of freedom df. The degree of freedom can be chosen between two that further determines the type of confidence interval: $df = 1$ gives the *pointwise asymptotic confidence interval* (PACI) that works on the individual parameter, $df = |u|$ gives the *simultaneous asymptotic confidence interval* (SACI) that works jointly for all the parameters [37].

5.2.7 Current reproductive number

We also calculated the current 7-day reproduction number as of [39]: Defining the reproduction number $\mathcal{R}_{7,t}$ as the 7-day moving average of the infection cases at time t to the infection cases at time $t - 3$ (assuming an incubation period of $\kappa^{-1} = 3$ days), we have

$$\mathcal{R}_{7,t} = \frac{\sum_{k=0}^{6} I_{t-k}}{\sum_{k=0}^{6} I_{t-3-k}}. \tag{5.23}$$

This ratio will be helpful to compare the results to the given infection data and find estimates on how the disease dynamics behave at least shortly after the investigated time interval.

5.2.8 Sensitivity analysis

To answer questions (Q1) and (Q2), the basic idea of sensitivity analysis lies in the definition of a certain measure $\mathcal{M}$ for variable change that is worth of investigation, especially when one would like to describe its sensitivity with respect to a parameter θ. The sensitivity of $\mathcal{M}$ with respect to θ in the sense of first-order change can be measured using Taylor expansion. Suppose that θ is increased to a certain percentage ε from its current value, i.e., $\theta \mapsto \theta + \varepsilon\theta$. This way, the ratio $(\theta + \varepsilon\theta)/\theta = 1 + \varepsilon$ returns the total percentage post perturbation and ε denotes the additional percentage of gain. Note that imposing ε as the percentage is considered more robust than as simply the increase, considering that different parameters may live in disparate scales. In a similar manner as for the parameter, the total percentage in $\mathcal{M}$ post perturbation on

θ is given by

$$\frac{\mathcal{M}(\theta + \varepsilon\theta)}{\mathcal{M}(\theta)} = 1 + \varepsilon\theta\frac{\partial_\theta, \mathcal{M}(\theta)}{\mathcal{M}(\theta)} + \mathcal{O}(\varepsilon^2) \tag{5.24}$$

providing that ε is sufficiently small. Since the percentage of gain is usually considered similar across parameters, the role of ε in the preceding equation is often neglected. The remaining expression thus provides a measurement of the sensitivity. Usually, authors refer $\partial_\theta\mathcal{M}(\theta)$ as the *sensitivity index* and $\theta\partial_\theta\mathcal{M}(\theta)/\mathcal{M}(\theta)$ as the *elasticity*, cf. [40]. Between two parameters θ_1, θ_2, it is logical to say that $\mathcal{M}$ is more sensitive to θ_1 than θ_2 when the absolute normalized sensitivity indices hold the relation

$$\left|\theta_1\frac{\partial_{\theta_1}\mathcal{M}(\theta_1)}{\mathcal{M}(\theta_1)}\right| > \left|\theta_2\frac{\partial_{\theta_2}\mathcal{M}(\theta_2)}{\mathcal{M}(\theta_2)}\right|. \tag{5.25}$$

Time-dependent measures. The question (Q1) conveys the notion of model solution and addresses what our model solutions, including those excluded from the measurement or fitting, could have changed as we perturb the optimal parameter set, i.e. $\Lambda = \{\beta, \alpha, E_T, \kappa, \mu, \gamma, \tau\}$. Our interest is now driven by all the measures $\mathcal{M}$ that represent model state variables $\Psi = \{S, E, I, R, D\}$, which apparently are time-varying. To reveal the elasticity, one first compute the sensitivity index of state $\psi_i \in \Psi$ with respect to parameter $\lambda_j \in \Lambda$; i.e.,

$$S_{ij} := \frac{d}{d\lambda_j}\Psi_i \tag{5.26}$$

from the sensitivity system of equations (cf. [40]):

$$S'_{ij} = \sum_k S_{kj} \cdot \frac{\partial}{\partial\psi_k}f_i + \frac{\partial}{\partial\lambda_j}f_i, \qquad S_{ij}(0) = 0. \tag{5.27}$$

The function f above defines the vector field of the model system, i.e., $\dot{\Psi} = f(t, \Psi, \Lambda)$.

Time-independent measures. The question (Q2) is concerned more with interventions. In this case, we focus more on parameters that can be changed with the help of humans. In our context, such parameters could be β and α. The direct transmission rate β has always been related to the proximity of the susceptible against infected humans and can be reduced with the aid of masks and social/physical distancing. The parameter α is related additional factors that drive the infection more than it could have been in the origin and destination country. For example, travellers are more exposed to physical encounters with other humans during flights, in public transportation, or in touristic areas, whereas locals spend more time at home. More protective apparatuses and educational campaigns will help reduce α. In this regard, two different measures for the sensitivity can be considered. For the first choice, we may take, for example, $\mathcal{M} := \int_0^T I\,dt$, which represents the total number of infected cases over all observations. If $\alpha, \beta > 0$, $\mathcal{M}$ is then more sensitive to β rather than α when it holds

$$\beta \cdot \left|\frac{\int_0^T \partial_\beta I\,dt}{\int_0^T I\,dt}\right| > \alpha \cdot \left|\frac{\int_0^T \partial_\alpha I\,dt}{\int_0^T I\,dt}\right|. \tag{5.28}$$

This inequality, however, includes the terms $\left|\int_0^T \partial_\beta I \, dt\right|, \left|\int_0^T \partial_\alpha I \, dt\right|$ that do not account for entropy or state of disorder. However, it is possible that the integral vanishes due to oscillations of the integrand $\partial_\alpha I$. This will result in a small sensitivity index rather than $\partial_\beta I$ that just forms a 'calm' trajectory above zero, so that the result would not be meaningful. To account for the entropy, we shall therefore consider the second measure

$$\mathcal{M} := \int_0^{\hat{\beta}} \int_0^T |\partial_\beta I(t,s)| \, dt ds, \tag{5.29}$$

which represents the total variation of I with respect to β, evaluated up to the current parameter value $\hat{\beta}$. Now, $\mathcal{M}$ is said to be more sensitive to β than α (or vice versa) if

$$\hat{\beta} \cdot \left| \frac{\int_0^T |\partial_\beta I| \, dt}{\int_0^{\hat{\beta}} \int_0^T |\partial_\beta I(t,s)| \, dt ds} \right| > \hat{\alpha} \cdot \left| \frac{\int_0^T |\partial_\alpha I| \, dt}{\int_0^{\hat{\alpha}} \int_0^T |\partial_\alpha I(t,s)| \, dt ds} \right|. \tag{5.30}$$

From the computational perspective, one can define a certain grid representing domain of interest for the two parameters, for example $[\beta_{\min}, \beta_{\max}] \times [\alpha_{\min}, \alpha_{\max}]$. The next step follows from computing the sensitivity indices for all grid points and applies the ratio of actual total variation and accumulated total variation as in eqn. (5.30). Therefore, the left-hand side should be done via stepping α (vertical mode) and the right-hand side via stepping β (right mode).

5.3   Numerical results

The number of iterations for Germany using the Metropolis algorithm, as well as for the preprocessing in each country should be a high number to prevent the algorithm from local minima. As in our previous work in [18], we set this number to 20,000. While the estimation was done for the daily cases, we plot the cumulated infection and dead because of better visibility. The reported cumulated cases consist of the currently infected cases plus the recovered plus the deceased cases, which are calculated as above by $\delta(I + R) + D$.

5.3.1   Model A

To be able to compare the output of the optimal solutions for the three models, the result of the model with a piecewise constant value for β and no traveller subdivision is shown in Fig. 5.2. The optimization seems to be fairly decent for the death curve (right figure), but the model overestimates the infection cases (left figure) between June and August, which also shows in lower values for $L(u)$ as seen in Tab. 5.9. In Tab. 5.6, the mean and standard deviations for the estimated parameters of the above explained model, starting values and methods are shown. Several parameter estimates are not very reliable, like the detection rate of 18% which is expected to be higher due to comparably few cases yet an increased amount of available tests. For example, [41] suggests a dark figure of slightly less than 50% in total until November. The death rate of 1‰ also appears to be much lower than expected (around 1%; for example, in [42] a fatality rate of 0.83% is calculated for the first wave, while a fatality rate of 2.15% as of November 2020 is found in [43]). These findings suggest that Model A might not be a decent model to describe the disease behaviour in Germany in summer 2020.

TABLE 5.6: Numerical results for Model A without inclusion of α.

Parameter	mean value	σ of Metropolis
β_0	$8.65 \cdot 10^{-2} \mathrm{d}^{-1}$	$0.19 \cdot 10^{-2} \mathrm{d}^{-1}$
β_1	$1.39 \cdot 10^{-1} \mathrm{d}^{-1}$	$0.01 \cdot 10^{-1} \mathrm{d}^{-1}$
δ	$1.84 \cdot 10^{-1}$	$0.03 \cdot 10^{-1}$
μ	$1.56 \cdot 10^{-3}$	$0.06 \cdot 10^{-3}$
τ	$2.60 \cdot 10^{1} \mathrm{d}$	$0.04 \cdot 10^{1} \mathrm{d}$
E_0	$3.60 \cdot 10^{3}$	$0.05 \cdot 10^{3}$
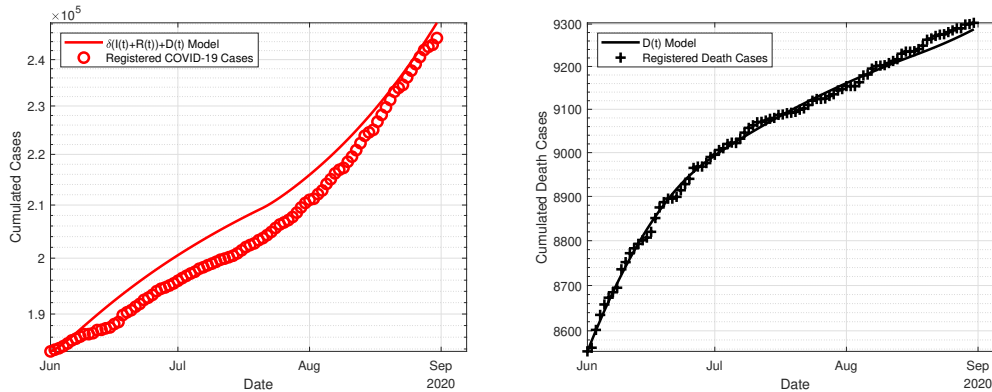
FIGURE 5.2: Infections (left) and death cases (right) in Germany using Model A during summer 2020 – JHU data [3] and estimations. The shaded area represents the SACI interval. The dashed line describes the simulation with $\alpha = 0$, i.e. either no travelling is allowed or the traveller subdivision had been completely free of the disease.

5.3.2 Model B

For Model B with a constant value for α from 15 June onwards, Tab. 5.7 shows the mean and standard deviations for the estimated parameters of the above explained model, starting values and methods. The estimated parameters, as far as known, are in line with what is to be expected. At the beginning of the investigated time interval, a rough estimate for the basic reproduction number without travellers is $\mathcal{R}_0 = \beta/\gamma \approx 0.4$. As β denotes the transmission rate at the beginning of June, without any effect of travellers, this estimate seems to be valid, but less than expected. A detection rate of 50–60% as well as a death rate of 0.6% are also valid estimates at the observed time interval. The time lag between infection and death is obviously dependent on the day of the registration of both infection and death, where 4 weeks is a decent approximation as well. Additionally, the pointwise asymptotic confidence interval and simultaneous asymptotic confidence interval are shown by ψ as of eqn. (5.22), so that the respective interval is defined as $\mathrm{CI}_k := \left[u_k^* - \psi, u_k^* + \psi \right]$.

Fig. 5.3 shows the estimated disease dynamics in comparison to the registered cases using the parameters as of Tab. 5.7. Additionally, the uncertainty range raised by the confidence intervals of the Metropolis algorithm is provided. For this, we add or subtract the standard deviation to or from the mean of the parameter to show the highest or lowest possible values of the registered cumulative infected persons. The range of both PACI and SACI is comparatively lower and almost no differences could be detected in the graphic. It is also observed how large the infected cases and fatalities in this model had been, if $\alpha = 0$, i.e. the travel ban had *not* ended and

travellers had no impact on the disease dynamics whatsoever.

The left graphic in Fig. 5.3 shows that for our estimated parameter set, around 50,000 less infections with COVID-19 had been registered if the travel subdivision had not been active. In the right figure concerning the death cases, we see significant changes only from the end of July, resulting in a difference of roughly 150 death cases. As both the number of infected and the infection rates are higher than in the simulation with no traveller numbers, travellers appear to have created increased infection numbers at least at the beginning of September. However, a reasonable prediction on case numbers appears to be difficult, as interventions by authorities and the public (higher awareness due to higher infection numbers) cannot be predicted in the sense of an pre-calculable change of transmission rates.

TABLE 5.7: Numerical Results for Model B using a constant value of α.

| Parameter	mean value	σ of Metropolis	ψ of PACI	ψ of SACI
β	$3.59 \cdot 10^{-2} \mathrm{d}^{-1}$	$0.03 \cdot 10^{-2} \mathrm{d}^{-1}$	$0.002 \cdot 10^{-2} \mathrm{d}^{-1}$	$0.04 \cdot 10^{-2} \mathrm{d}^{-1}$
δ	$5.78 \cdot 10^{-1}$	$0.18 \cdot 10^{-1}$	$0.002 \cdot 10^{-1}$	$0.03 \cdot 10^{-1}$
μ	$6.18 \cdot 10^{-3}$	$0.19 \cdot 10^{-3}$	$0.004 \cdot 10^{-3}$	$0.09 \cdot 10^{-3}$
τ	$2.59 \cdot 10^{1} \mathrm{d}$	$0.04 \cdot 10^{1} \mathrm{d}$	$0.001 \cdot 10^{1} \mathrm{d}$	$0.03 \cdot 10^{1} \mathrm{d}$
E_0	$2.59 \cdot 10^{3}$	$0.05 \cdot 10^{3}$	$0.001 \cdot 10^{3}$	$0.03 \cdot 10^{3}$
α	2.97	0.06	0.002	0.04
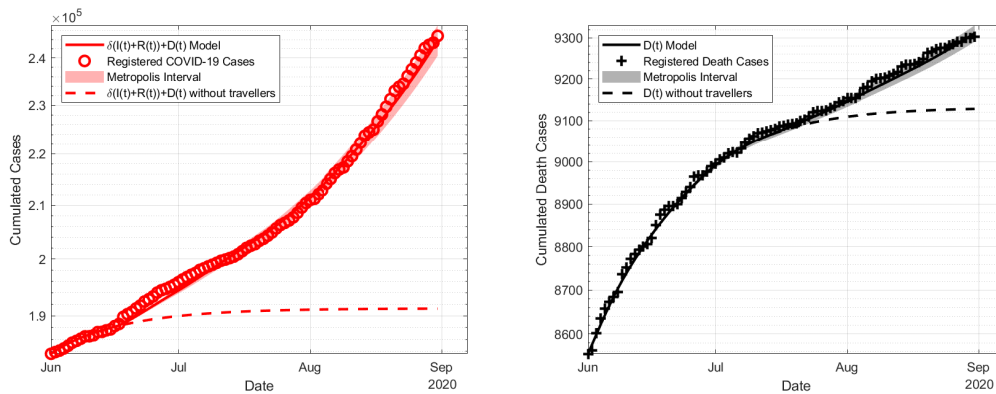
FIGURE 5.3: Infections (left) and death cases (right) in Germany using Model B during summer 2020 – JHU data [3] and estimations. The shaded area represents the SACI interval. The dashed line describes the simulation with $\alpha = 0$, i.e. either no travelling is allowed or the traveller subdivision had been completely free of the disease.

5.3.3 Model C

For Model C, we assume that α is not constant over the whole time from June to August, but rather time-dependent, defining a piecewise constant function of α with three different values. With $\alpha(t)$ being piecewise constant for 15–30 June, July and August, the parameter estimation for system (5.4) yields the following results as to be seen in Tab. 5.8. Parameter estimates are similar to those of Model B by the order of magnitude and thus equally reliable. In Fig. 5.4, similar to above, we show estimates and measured data for the cumulated cases and also the error range with respect to the Metropolis algorithm (which is the largest deviation) and the scenario if no travelling had been allowed.

TABLE 5.8: Numerical Results for Model C using piecewise constant values of α.

Parameter	mean value	σ of Metropolis	ψ of PACI	ψ of SACI
β	$5.09 \cdot 10^{-2} \mathrm{d}^{-1}$	$0.12 \cdot 10^{-2} \mathrm{d}^{-1}$	$0.002 \cdot 10^{-2} \mathrm{d}^{-1}$	$0.06 \cdot 10^{-2} \mathrm{d}^{-1}$
δ	$4.94 \cdot 10^{-1}$	$0.08 \cdot 10^{-1}$	$0.007 \cdot 10^{-1}$	$0.19 \cdot 10^{-1}$
μ	$5.34 \cdot 10^{-3}$	$0.10 \cdot 10^{-3}$	$0.004 \cdot 10^{-3}$	$0.11 \cdot 10^{-3}$
τ	$2.58 \cdot 10^{1} \mathrm{d}$	$0.06 \cdot 10^{1} \mathrm{d}$	$0.01 \cdot 10^{1} \mathrm{d}$	$0.34 \cdot 10^{1} \mathrm{d}$
E_0	$2.45 \cdot 10^{3}$	$0.03 \cdot 10^{3}$	$0.003 \cdot 10^{3}$	$0.07 \cdot 10^{3}$
α_0	2.23	0.05	0.002	0.06
α_1	2.45	0.05	0.008	0.02
α_2	3.14	0.05	0.004	0.11
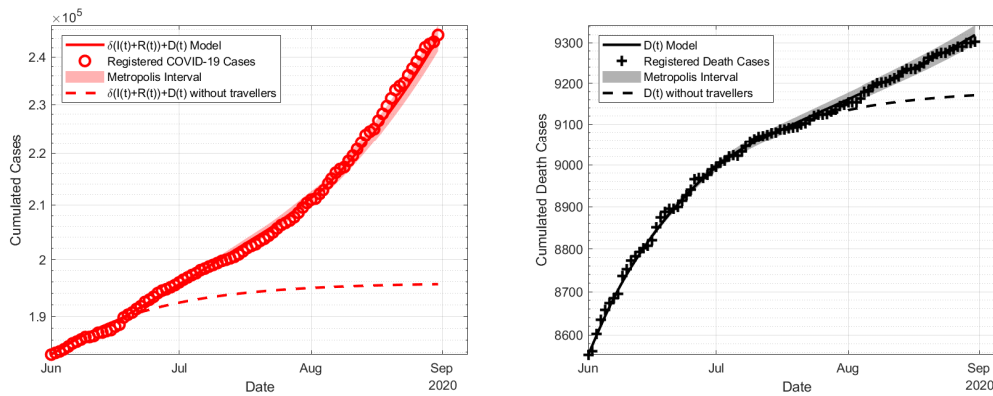
FIGURE 5.4: Infections (left) and death cases (right) in Germany using Model C during summer 2020 – JHU data [3] and estimations. The shaded area represents the SACI interval. The dashed line describes the simulation with $\alpha = 0$, i.e. either no travelling is allowed or the traveller subdivision had been completely free of the disease.

5.3.4 Comparison

For the Bayesian analysis, we can now compare the BIC values of the three models computed by eqns. (5.17) and (5.19). The results for Model A were gained by applying eqns. (5.4), i.e. the model we used to estimate the disease behaviour in all other countries (with no travel impact rate, but two piecewise constant transmission rates $\beta_{1,2}$) to Germany.

TABLE 5.9: Values for the least-square value $J(u)$ and the BIC for the various models.

	$J(u)$	# of Parameters	BIC
Model A	$4.4174 \cdot 10^{-5}$	6	-9,087.0
Model B	$4.1812 \cdot 10^{-1}$	6	-8,538.6
Model C	$4.1919 \cdot 10^{-1}$	8	-8,529.9

Tab. 5.9 shows that in terms of the least-square output, the model with time-dependent, piecewise constant values of α (Model C) shows the best results. Even though the penalization of complexity with two more parameters, the BIC for Model C is the lowest. According to Raftery [30], a BIC difference of 6–10 indicates a "strong"

evidence (posterior probability of 95–99%) that Model C using three piecewise constant values for α is to be preferred over B, while there is "very strong" evidence that Model C, and also B, are to be preferred over Model A with a posterior probability of $> 99\%$ as the difference is larger than 10.

Lastly, we compare the 7-day reproductive number as of eqn. (5.23). Fig. 5.5 shows the values for the two models. Both curves have a similar behaviour and the values of $R_{7,t}$ in Model B and C would remain $\gtrapprox 1$ most of the time, resulting in growing infected values even for at least a short time after the investigated time window, i.e. at the beginning of September.

Additionally, we plotted the dynamics of $R_{7,t}$ for the hypothetic case that no travellers had contributed to the infection cases. In this case the values of $R_{7,t}$ would remain < 1 for the whole time in any of the two models. This means the disease would have been contained if no other effects are assumed.

We can compare future simulations on a short-time scale by extending the time interval of the model. When we assume that travelling had not been allowed during the whole time interval $\alpha(t) \equiv 0$, a simulation until September 15 assumes only 100 new registered infections. However, in the estimation of Model C where travelling is allowed, we computed 21200 new infections if travelling had been disallowed from September 1 onwards and 26300 new infections if the conditions for travelling had not been changed at all between September 1 and 15 when we assume the situation is not changed by any national or international measures, i.e. same travel numbers and impact rates as at 31 August are assumed. Results for Model B show similar values in terms of magnitude; it is important to note that values of those estimates are to be taken with caution.
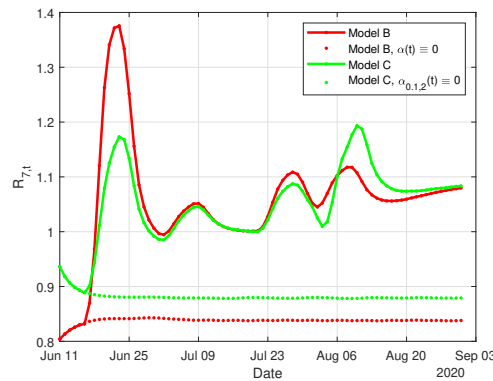
FIGURE 5.5: Reproductive Values $R_{7,t}$ using the estimations of Models B and C. Additionally, the dotted lines show the evolution of the reproductive values in case travellers had no impact on the infections in Germany.

5.3.5 Sensitivity analysis

For the investigation of time-dependent measures, we included the parameters γ and κ from Tab. 5.1 although they were not optimized, yet can be assumed to bear uncertainties, to observe the influence of those parameters to the solutions for all five subdivisions S, E, I, R, and D. For Model B, all the parameters λ_i are almost constant, except E_T and α, and to some extent β and γ (latter of which is however not a mutable parameter in our optimization). Fig. 5.6 shows the elasticities $\lambda_j S_{ij}/\Psi_i$ using (5.27) around the parameter values given in Tabs. 5.7 and 5.8, respectively. Generally, E_T returns the highest sensitivity in all subdivisions, particularly with ongoing

simulation time. Additionally, changes in the parameters α (after a certain time delay, mainly due to differing from zero only after 15 June) and also γ would significantly influence the infected subdivision but not the subdivision of deceased, in which no parameter shows a higher elasticity than 0.15. Note that the parameter E_T is actually proportional to α as of eqn. (5.3). After all, a caveat with these measures remains, as the elasticities are time-varying. Therefore, preference to a certain parameter for the highest elasticity could change over time.

Concerning the time-independent measure, we can now generate a two-region profile for which the inequality in eqn. (5.30) indeed applies or the other direction does. On the basis of Model B for the portraying the upcoming winter outbreaks, Fig. 5.7 shows the comparison of the elasticities in reasonable ranges of β and α, the two parameters where interventions actually can change values. While reducing the overall transmissions in some way is equivalent to a reduction of β, reduction of travellers can be interpreted as a reduction of α: Even if the value α is not related to the amount of travellers, we have seen that α is multiplied with the amount of travellers $T_{\text{Germany}\leftrightarrow j}$. If this value is reduced, then the product is reduced by the same factor, which would yield the same results as a reduction of α by this factor. Alternatively, travel control without reduction of traveller numbers can also reduce α. Using the fitted value $(\alpha, \beta) = (2.97, 0.0309)$ we find that the measure $\mathcal{M}$ as in eqn. (5.29) is more sensitive to β than α.

This finding draws forth further practical relevance. Our model can be calibrated with new incidence data on an initial take-off period in the next winter season, where all parameters except β and α are fixed according to our fitting. At first, the two parameters can be fitted to these new data. May they locate in one of the two regions separated by the zero-curve in Fig. 5.7, we then acquire knowledge on which resources should be drawn in order to attack the most sensitive parameter. One can thus wait and see how the deployment of the resources gives the real-time intervention to the number of infected cases. Re-calibration then follows after some time as short-term feedback from such an intervention is gained, and the values of optimal β and α can once again be evaluated via Fig. 5.7. The area shows the contour of the elasticity in the left-hand side of eqn. (5.30) minus the right-hand side expression. The region below the zero-line thus indicates all possible locations of (β, α) at which the measure $\mathcal{M}$ as in eqn. (5.29) is more sensitive to β than to α, and vice versa. This process of combining sensitivity-based interventions remains continuous until the ultimate disease eradication is achieved without having to waste resources.
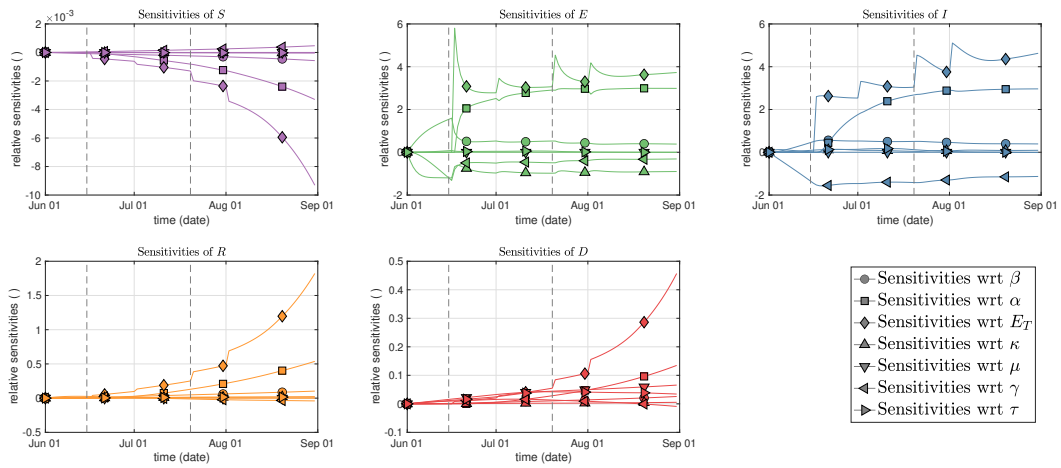
FIGURE 5.6: Sensitivities of the model states in Model B wrt its parameters.
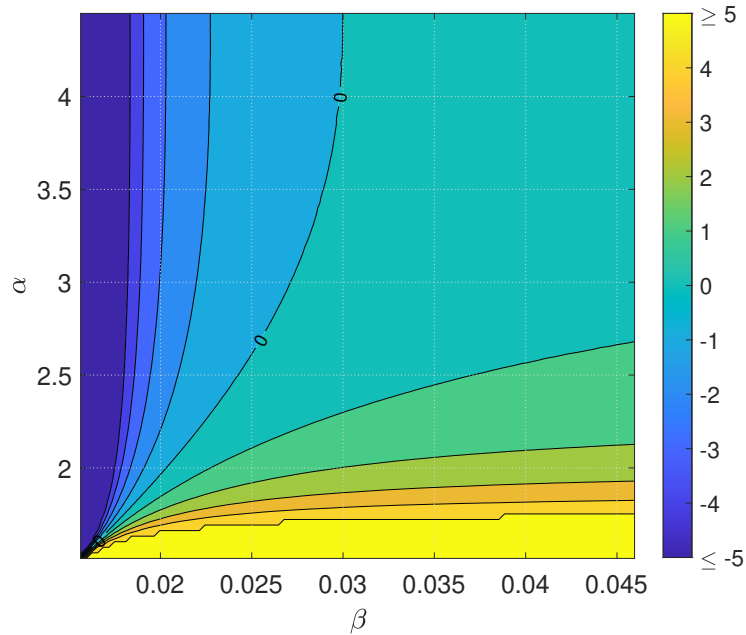
FIGURE 5.7: Comparison of the elasticities in Model B in a domain of interest for β and α.

5.4 Discussion and conclusion

In this present work, we intended to measure the impact of travellers on the overall disease dynamics in Germany during summer 2020 using a modified *SEIRD*-model with a traveller . Travel rates are measured by using international flight and hospitality data. The infection data of all 55 countries with more than 5,000 German travellers in June, July and August together has been used to optimize the single-country infections. Estimates for the transmission rates $\beta_{j,0/1}$ and the infected I_j at all time t in those countries are found using standard *SIRUV*-models and used to estimate the

travel impact rate for Germany. Parameter estimation was done using a Metropolis type algorithm, while other routines like an adjoint based approach are also possible.

The estimated parameter values of the travelling-induced models are generally close to medical estimations, while the model with time-dependent transmission rates delivers less reasonable results in terms of the target function and also the parameter values. In the traveller models, the travel impact rate was estimated to be in the range of $2.2 \leq \alpha \leq 3.2$, meaning a two-to three times higher infection possibility as a traveller than the average inhabitant of the respective country. The model with three time-dependent and piecewise constant values of the travel impact rate $\alpha(t)$ yields better values than a model with only one constant value for $\alpha(t)$ in the $\mathcal{L}_2$-norm and also better BIC values despite two more parameters being used, and can be classified as very strongly preferred.

The raised infection numbers and infection rates by travellers are also assumed to have caused higher infection numbers at least in the following weeks (autumn 2020), based on an analysis of the reproductive number at the end of the investigated time interval. Among other reasons such as seasonality and opening of schools after the summer holidays, these are assumed to have an impact on the second large infection wave in late 2020 [7, 3]. It needs to be clear that due to the lack of precise data, traveller values can be only estimated to a certain degree and some data sets with which the parameter estimates for the various countries are not necessarily reliable. We aimed to reproduce the infection risks for travellers in those countries. Because of the large number of countries, errors are therefore assumed to be evened out as the value of E_T is a sum of the infections from all those countries. Also, using piecewise constant values for α (to some extent also β_j) with switching dates as of the first of each month is slightly arbitrary. While a steady function $\alpha(t)$ or optimization of the switching dates in some way can lead to better results, those are prone to overfitting. The lower BIC of the model with three different values for α indicates this did not happen for Model C.

Further, we performed a sensitivity analysis for Model B, i.e., a constant value of α. In particular, it is found that the sensitivities for the travel impact rate α can be identified after a certain time delay (which is caused by the model definition). The parameters α, E_T – which has the same behaviour as α due to the construction of the model –, β and γ are found to be the most relevant parameters. However, in the further analysis we constricted toward β and α as those are the parameters regarding which political interventions are possible. For those two parameters, we designed a two-region profile for which the detected domains in which a reduction of α is more relevant for disease control in case the transmission rate β, especially when the infection cases are otherwise comparatively low and can be controlled.

Finding those domains is similar to the findings of Hollingsworth et al. [13], as they claimed travel bans are only relevant in case of low values for R, which can be interpreted as a reduction of the transmission rate β. In case of higher infectivity rates like for, e.g., the latest mutants (Delta and, even more so, Omikron), which go along with a larger value of β, those assumptions might thus not hold true in the same way. However, it might be reasonable to consider travelling restrictions for a supposed variant (or other disease) with comparatively low transmission rates yet high mortality. Still, the raised infection rates at the end of summer 2021 are an indicator that higher/'uncontrolled' traveller numbers might have been a reason for another (at that time 'fourth') wave one year after the investigated time interval, which can be part of future investigations.

Not letting aside that installation of travel restrictions has multiple political, legal, social and economical problems (it is not to be forgotten these pose an encroachment

into fundamental rights), we conclude that setting up travel policies can be an epidemiologically reasonable policy component to contain disease numbers at least for short terms, which is in line to the findings of papers [8, 9, 10, 12, 13, 14, 15, 11]. Rather than an exportation of cases as in Siegenfeld et al. [8] or Chinazzi et al. [9] to several countries or internally in China as in Zou et al. [10], we consider importation of cases from many different countries with varying infection rates. Thus, unlike [10], we make general statements of the effectiveness of travel restrictions due to a combination of all countries in the equation for $E_T(t)$.

The analysis of the local reproduction number suggest that the values are fluctuating around 1, and travel measures have the potential to below 1, resulting in an extincting disease. Additionally, short-time simulations for the beginning of September 2020 show a difference of several thousands of infection cases between no (further) travel restrictions and full travel restrictions. These two findings indicate that travel measures should be imposed alongside other social measures for optimal disease control. It is up to further research to regard whether solely a travel ban or tightening of travel restrictions had just postponed the third infection wave to a later date.

Even if this latter assumption holds true, there are possible advantages of delaying the disease: Similar to Epstein et al. [14], the findings show that delaying the epidemics can be achieved inter alia by travel restrictions. This time can then be used to prepare for the income of an infection wave, prevents overload the health care system all at once (which is also found by Leung et al. [11]), or postpones epidemics until vaccines are available so that the amount of severe disease courses is reduced. Travel restrictions to farther countries is comparatively 'cheaper' than to closer ones, where border control is required which induces further political and social problems. While restrictions to a (lower) amount of high-risk areas like several articles propose can be more effective, global measures can be more effective or 'safer' than targeted measures in an epidemiological/stochastic sense, due to the highly connected world we live in and possibly rapid changes in the disease dynamics in single countries.

Awareness of the dynamics of the Corona waves in previous years and its reasons is important in upcoming years of the pandemic and for other fast-spreading diseases as well, and at the start of a pandemic or at least a single wave, a strategy combining local social measures with international measures, in particularly a (heavy) reduction of traveller numbers, should be considered together in terms of optimal control especially when risks cannot be foreseen. It is also to be noted that travel measures are undertaken in a graded way. Details on related regulations have changed from time to time, but certain entry restrictions have been upheld since the earlier rise of the pandemic. For example, all persons entering the country must provide a negative test result or, later, proof of immunity either by recovery or vaccination, then comply with post-arrival quarantines depending on the place of departure. However, it remains a question which of those two to consider primarily, and for that modelling scenarios like the ones presented (Fig. 5.7) can e.g. be updated on the current situation.

Further work in this topic might also include the impact of foreign travellers in Germany and a international multi-patch/network model including travellers from and to all investigated regions or countries. Also, other types of models, e.g., stochastic delayed differential equations (SDDE) or agent-based systems, can be used to model disease dynamics and incorporation of travellers.

Declarations

Competing interests

The authors declare that there exist no competing interests.

Authors' contributions

All authors contributed a significant part and reviewed the manuscript.

Availability of data

We used several of the underlying MATLAB codes for multiple purposes and thus believe the open presentation of the codes would distract readers. However, the codes, datasets used, and/or analyzed during the current study which are not already cited in the article [3, 6, 20, 22, 23, 21], are available from the corresponding author on reasonable request.

A Plots for the epidemic models for the various countries

FIGURE 5.8: Infections and death cases in Albania – JHU data
[3] and estimations.

FIGURE 5.9: Infections and death cases in Austria – JHU data
[3] and estimations.

FIGURE 5.10: Infections and death cases in Belarus – JHU
data [3] and estimations.

FIGURE 5.11: Infections and death cases in Belgium – JHU data [3] and estimations.

FIGURE 5.12: Infections and death cases in Bosnia and Herzegovina – JHU data [3] and estimations.

FIGURE 5.13: Infections and death cases in Brazil – JHU data [3] and estimations.

FIGURE 5.14: Infections and death cases in Bulgaria – JHU
data [3] and estimations.

FIGURE 5.15: Infections and death cases in Canada – JHU
data [3] and estimations.

FIGURE 5.16: Infections and death cases in China – JHU data
[3] and estimations.

FIGURE 5.17: Infections and death cases in Croatia – JHU data [3] and estimations.

FIGURE 5.18: Infections and death cases in Cyprus – JHU data [3] and estimations.

FIGURE 5.19: Infections and death cases in the Czech Republic – JHU data [3] and estimations.

FIGURE 5.20: Infections and death cases in Denmark – JHU
data [3] and estimations.

FIGURE 5.21: Infections and death cases in Egypt – JHU data
[3] and estimations.

FIGURE 5.22: Infections and death cases in Estonia – JHU
data [3] and estimations.

FIGURE 5.23: Infections and death cases in Ethiopia – JHU
data [3] and estimations.

FIGURE 5.24: Infections and death cases in Finland – JHU
data [3] and estimations.

FIGURE 5.25: Infections and death cases in France – JHU
data [3] and estimations.

FIGURE 5.26: Infections and death cases in Greece – JHU
data [3] and estimations.

FIGURE 5.27: Infections and death cases in Hungary – JHU
data [3] and estimations.

FIGURE 5.28: Infections and death cases in Iceland – JHU
data [3] and estimations.

FIGURE 5.29: Infections and death cases in India – JHU data
[3] and estimations.
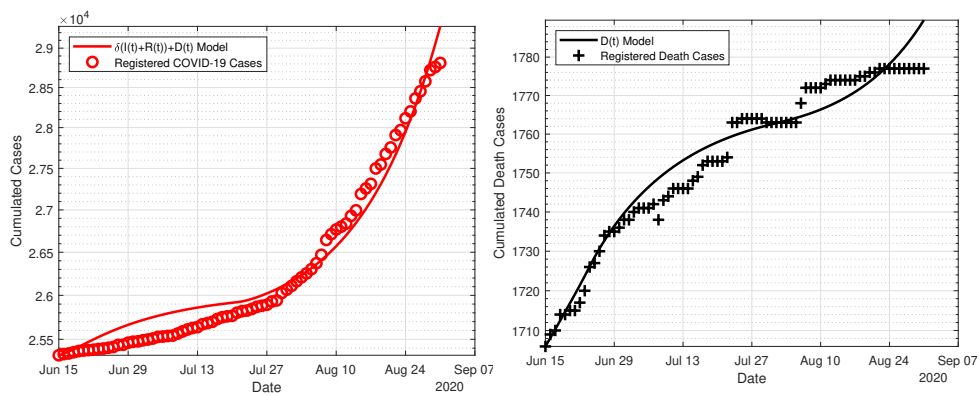
FIGURE 5.30: Infections and death cases in Ireland – JHU
data [3] and estimations.
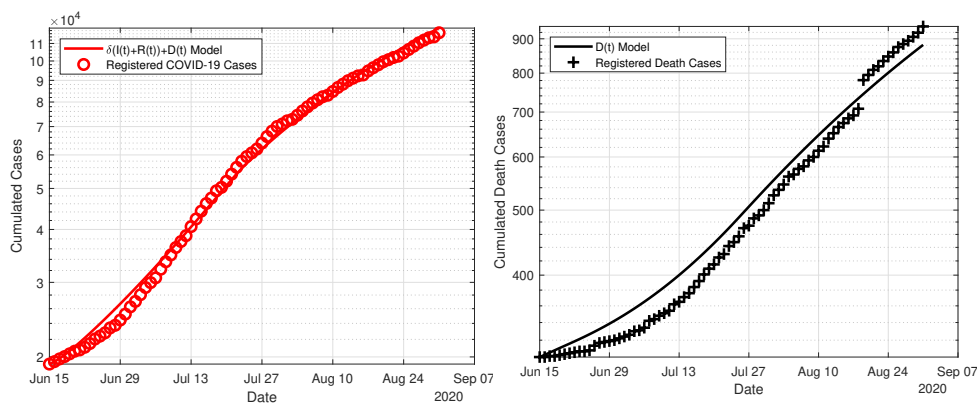
FIGURE 5.31: Infections and death cases in Israel – JHU data
[3] and estimations.
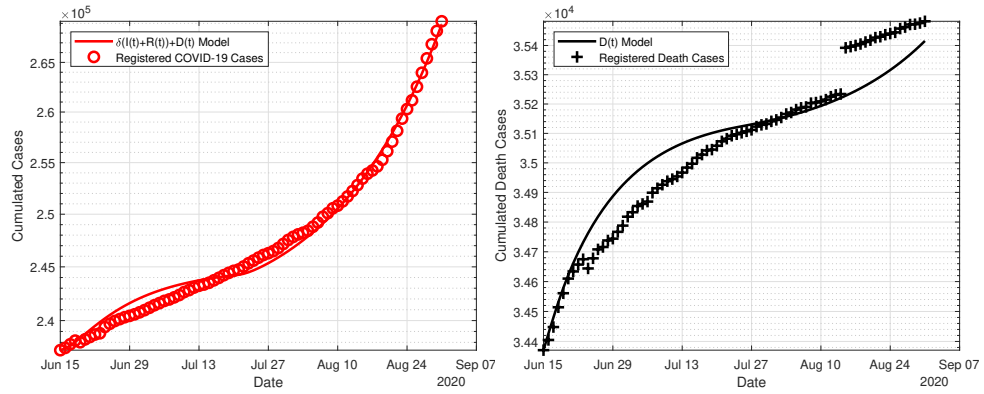
FIGURE 5.32: Infections and death cases in Italy – JHU data
[3] and estimations.
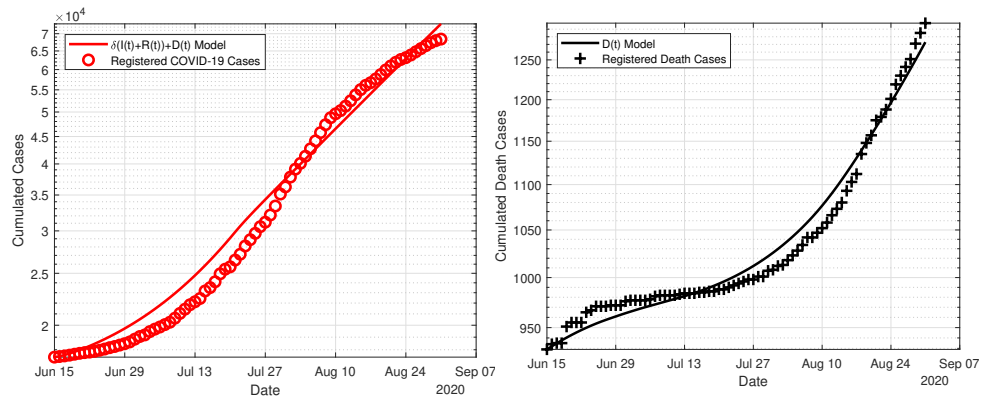
FIGURE 5.33: Infections and death cases in Japan – JHU data
[3] and estimations.
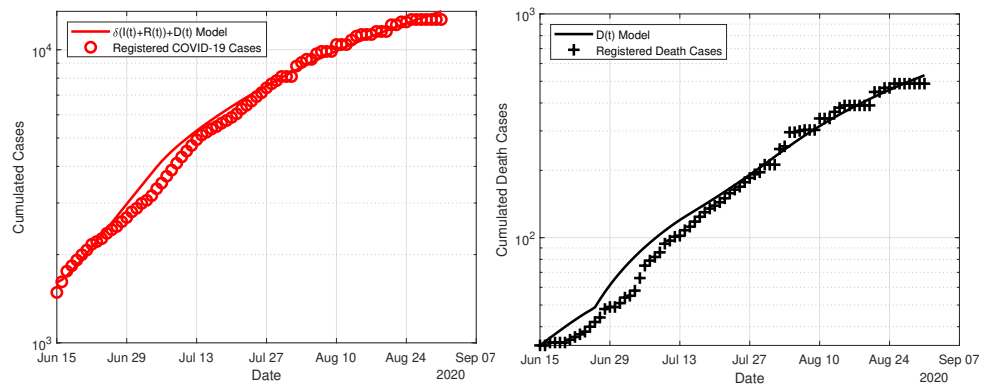
FIGURE 5.34: Infections and death cases in Kosovo – JHU
data [3] and estimations.
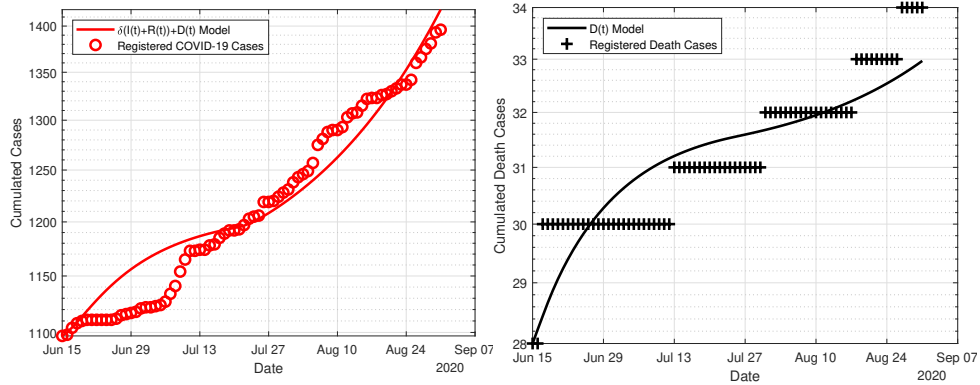
FIGURE 5.35: Infections and death cases in Latvia – JHU data
[3] and estimations.
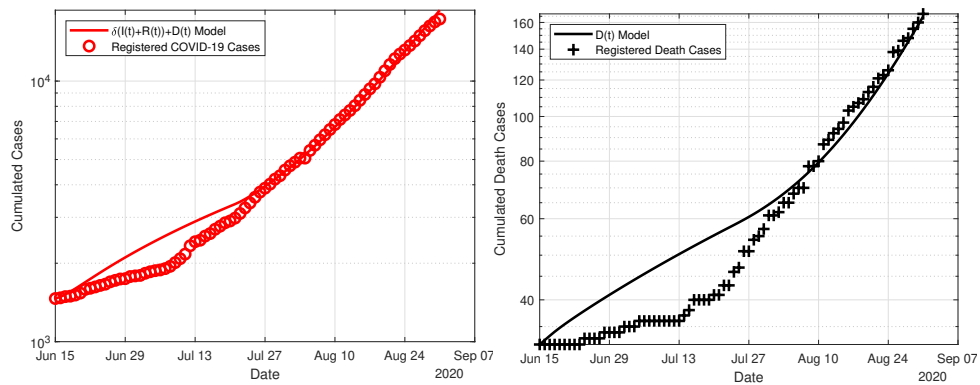
FIGURE 5.36: Infections and death cases in Lebanon – JHU
data [3] and estimations.
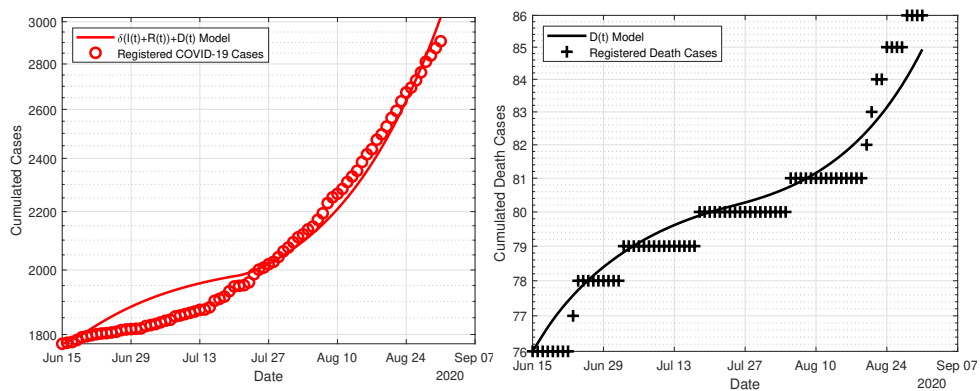
FIGURE 5.37: Infections and death cases in Lithuania – JHU
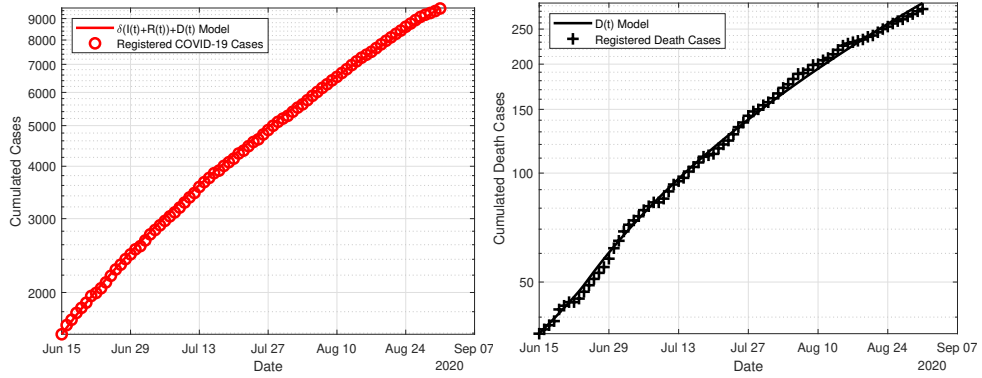data [3] and estimations.
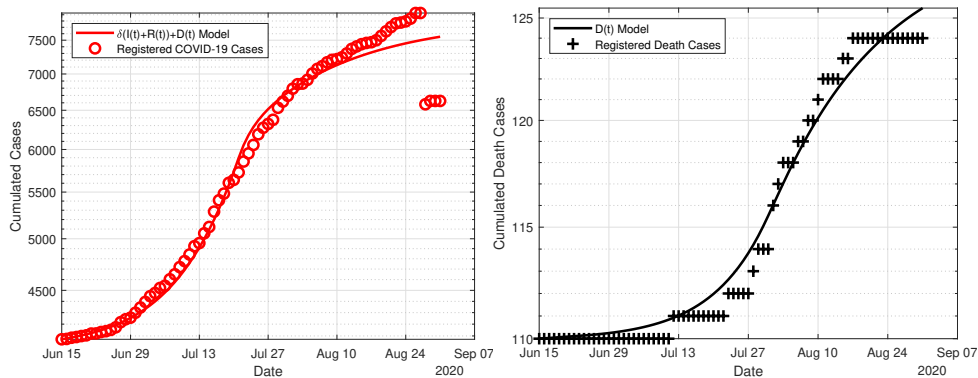
FIGURE 5.38: Infections and death cases in Luxembourg –
JHU data [3] and estimations.
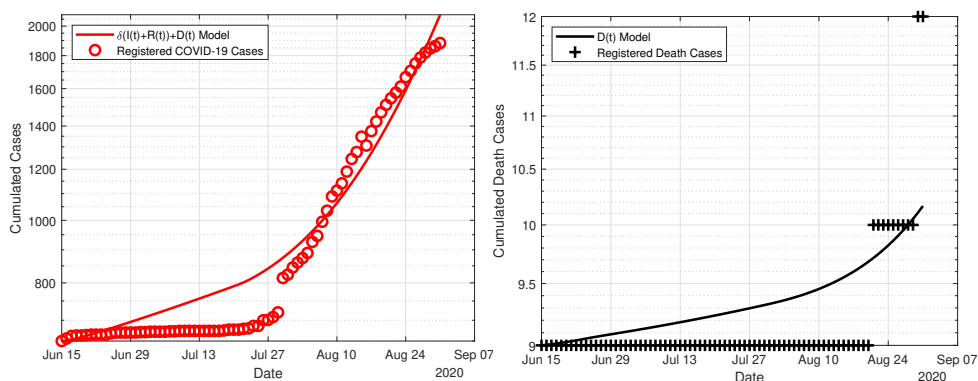
FIGURE 5.39: Infections and death cases in Malta – JHU data
[3] and estimations.
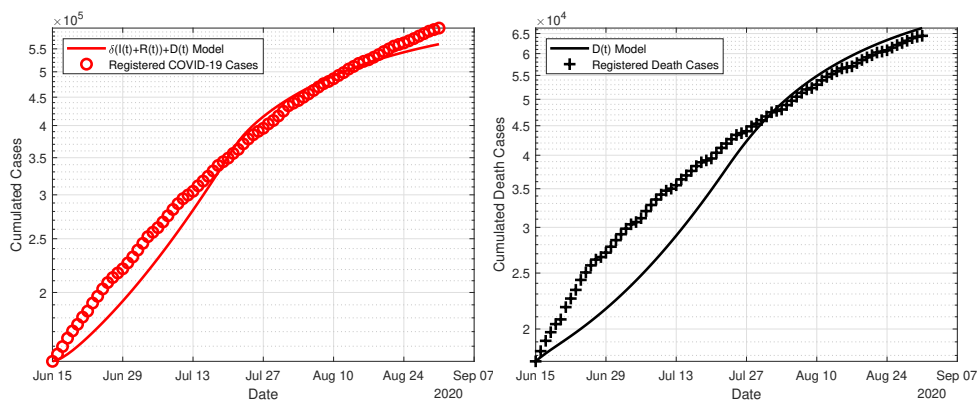
FIGURE 5.40: Infections and death cases in Mexico – JHU
data [3] and estimations.
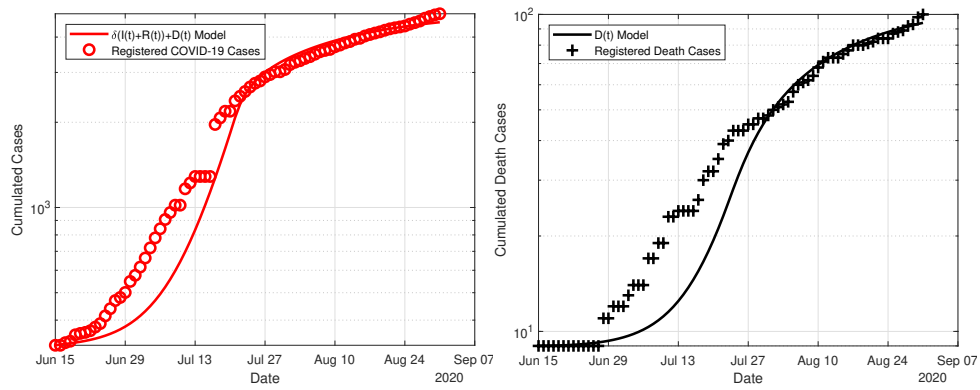
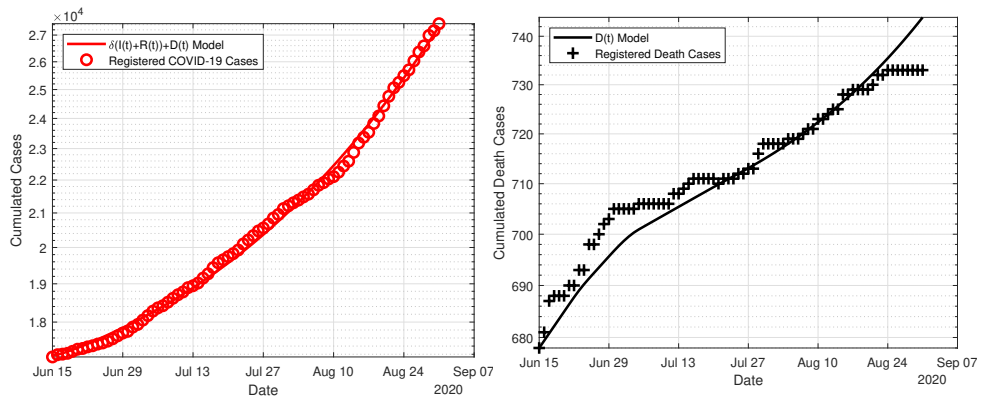FIGURE 5.41: Infections and death cases in Montenegro –
JHU data [3] and estimations.
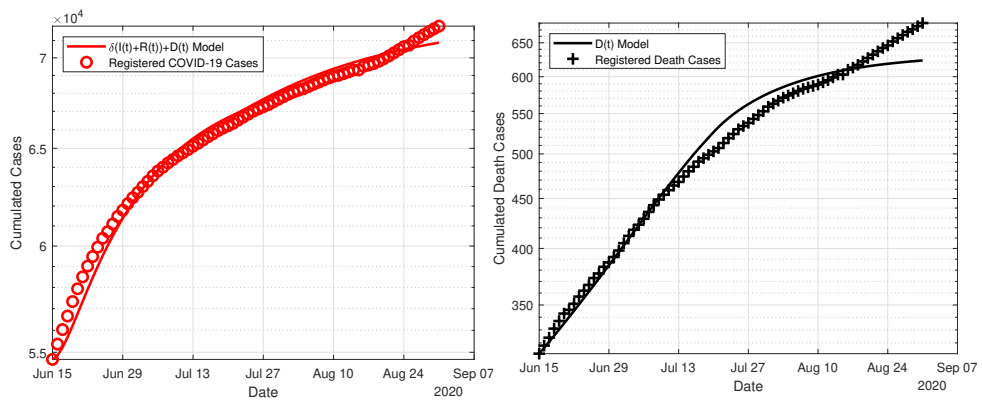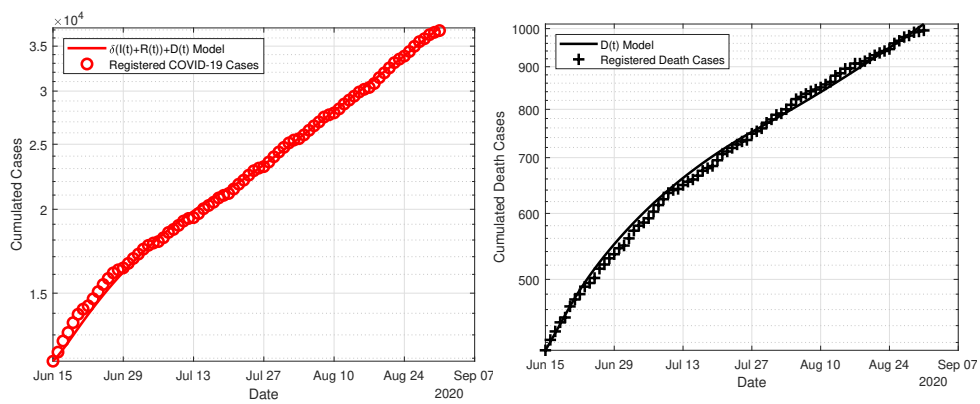

FIGURE 5.42: Infections and death cases in Moldova – JHU
data [3] and estimations.
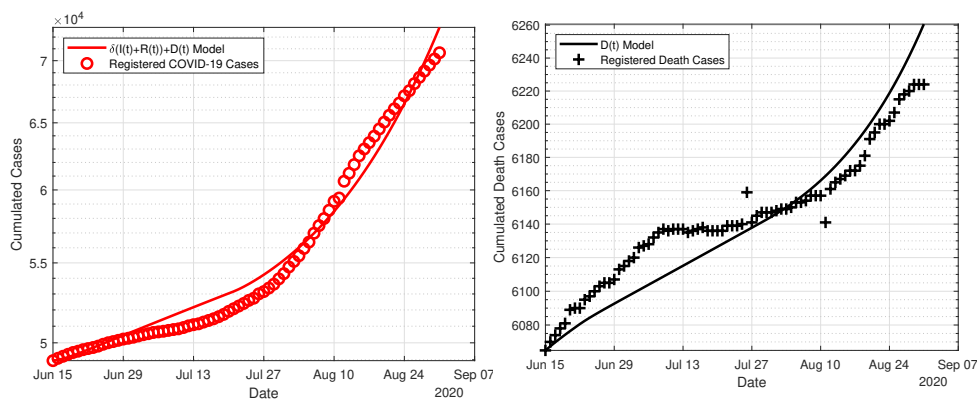
FIGURE 5.43: Infections and death cases in the Netherlands –
JHU data [3] and estimations.
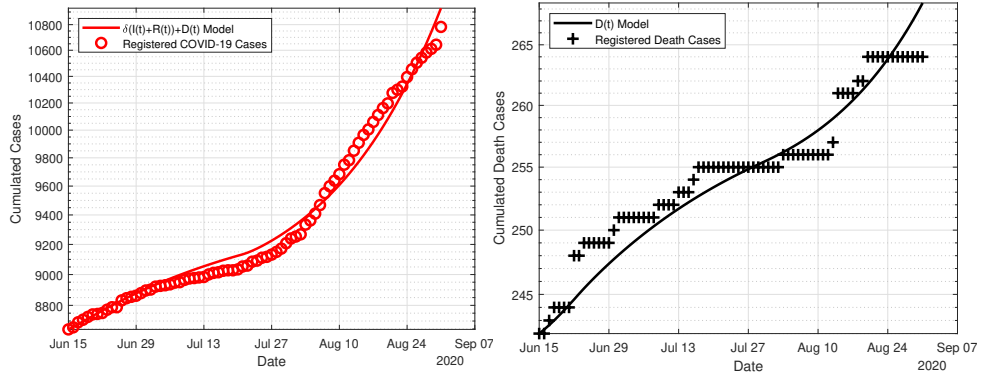
FIGURE 5.44: Infections and death cases in Norway – JHU
data [3] and estimations.
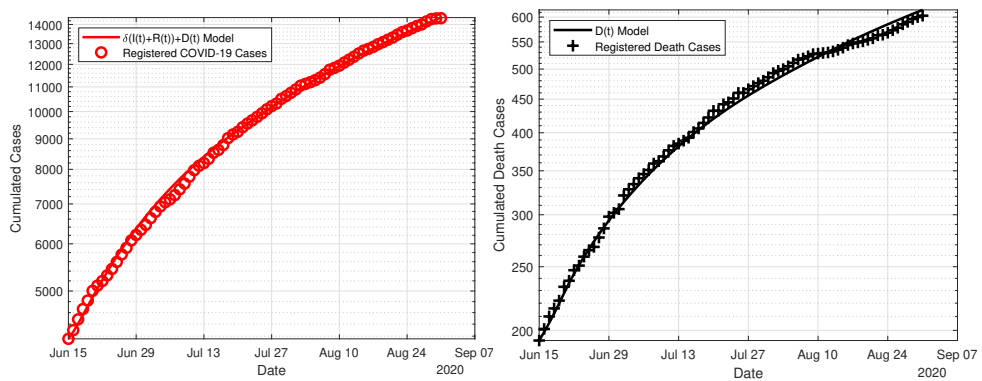
FIGURE 5.45: Infections and death cases in Northern Mace-
donia – JHU data [3] and estimations.
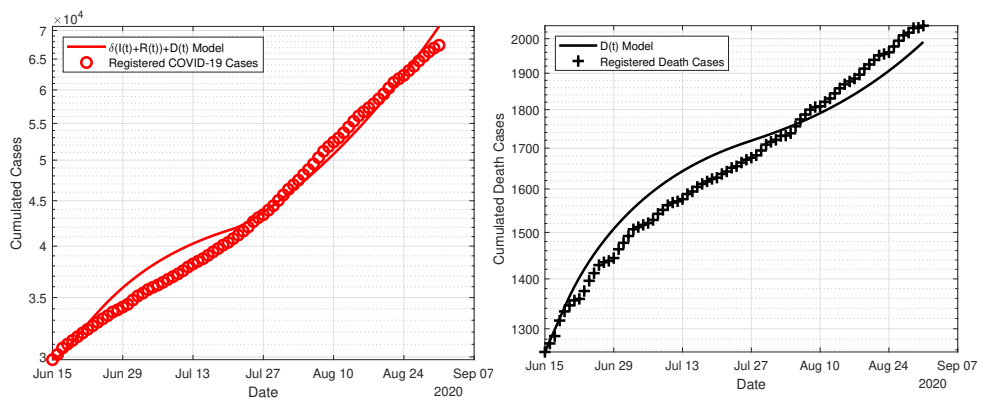
FIGURE 5.46: Infections and death cases in Poland – JHU
data [3] and estimations.
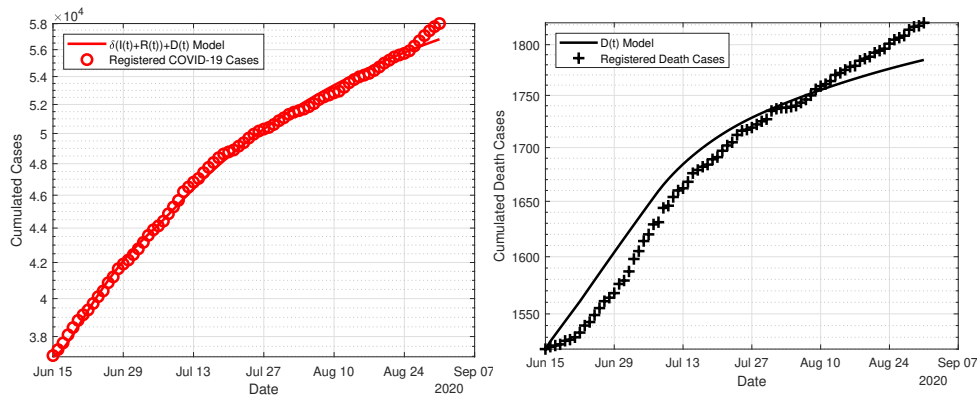
FIGURE 5.47: Infections and death cases in Portugal – JHU
data [3] and estimations.
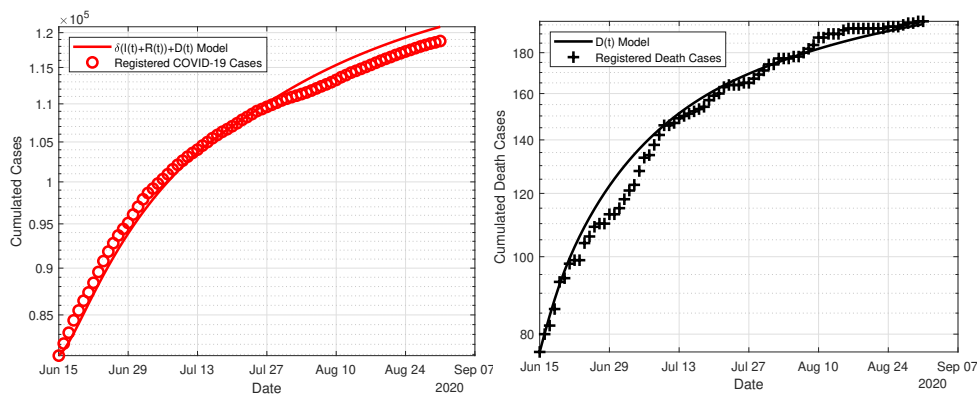
FIGURE 5.48: Infections and death cases in Qatar – JHU data
[3] and estimations.
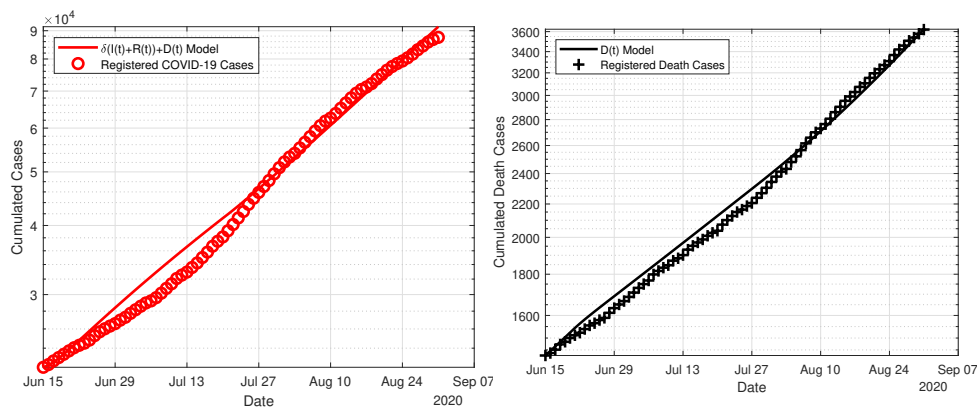
FIGURE 5.49: Infections and death cases in Romania – JHU
data [3] and estimations.
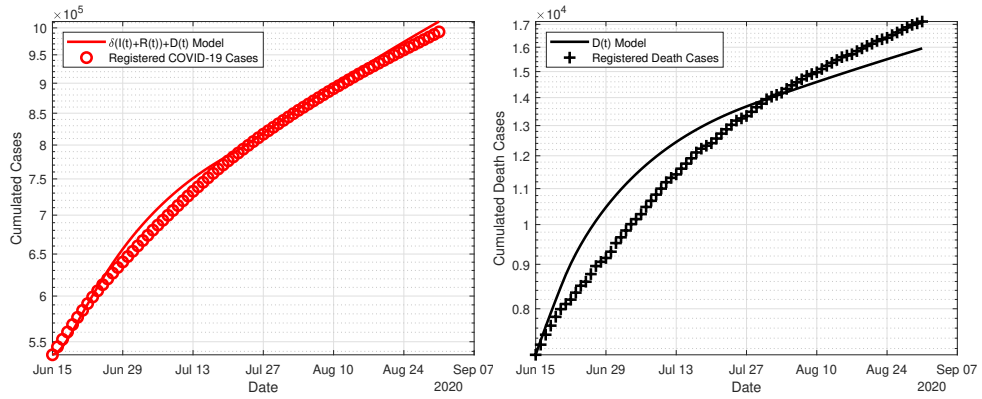
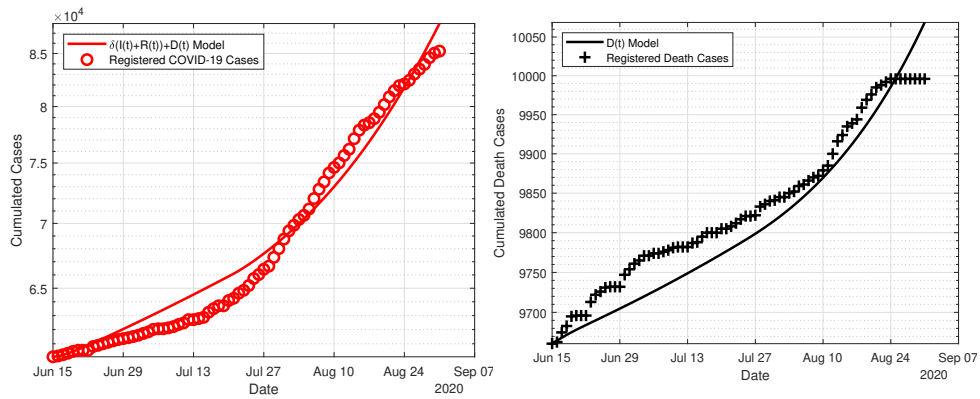FIGURE 5.50: Infections and death cases in Russia – JHU data [3] and estimations.
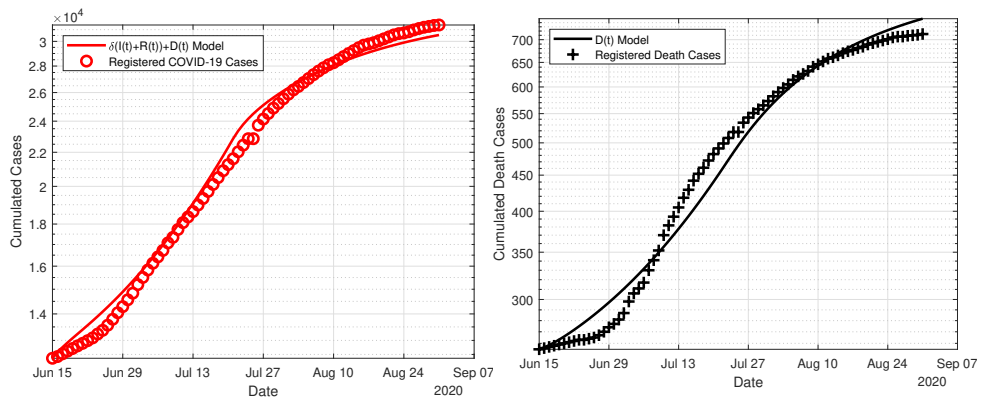
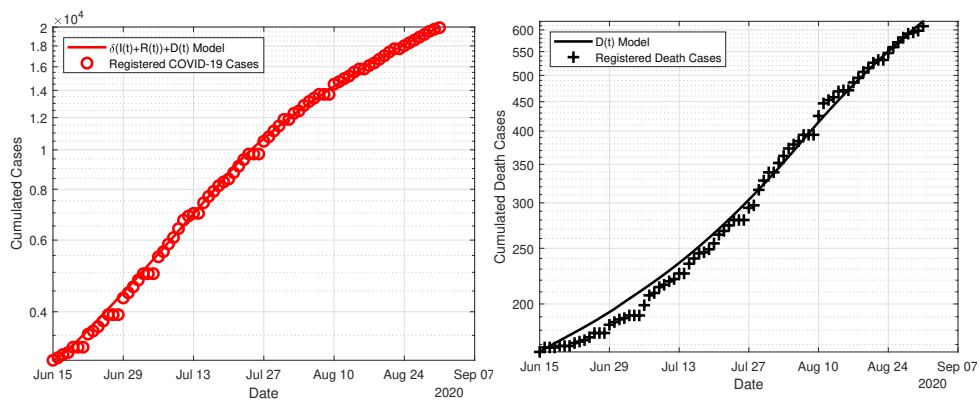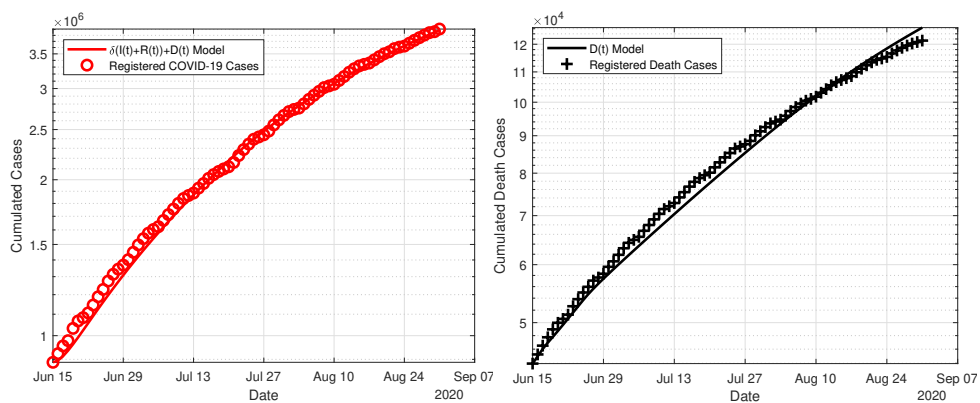FIGURE 5.51: Infections and death cases in Serbia – JHU data [3] and estimations.
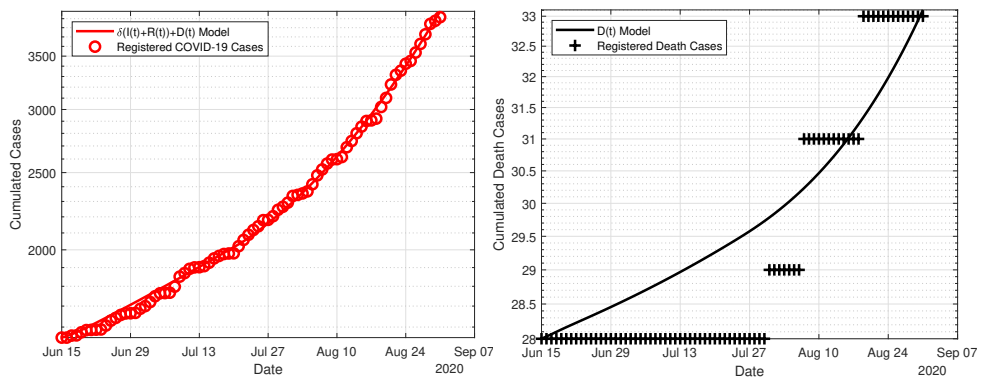
FIGURE 5.52: Infections and death cases in Slovakia – JHU data [3] and estimations.
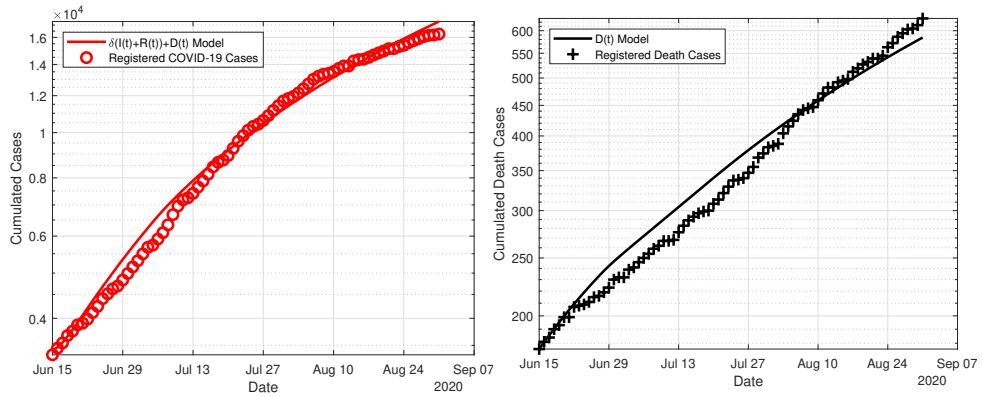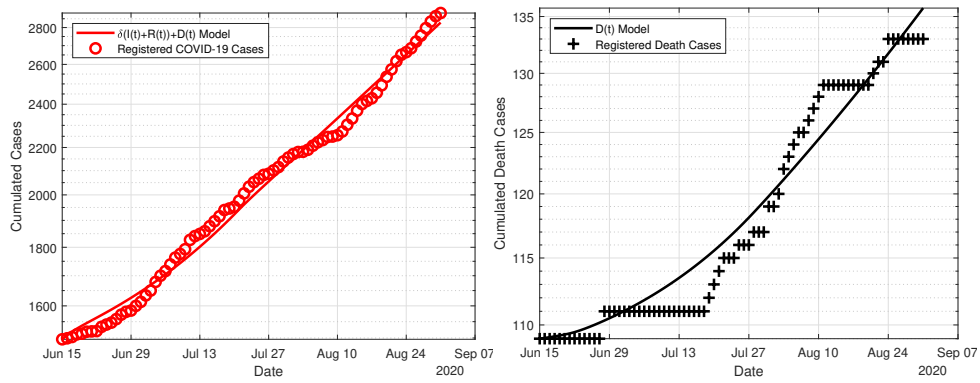
FIGURE 5.53: Infections and death cases in Slovenia – JHU
data [3] and estimations.
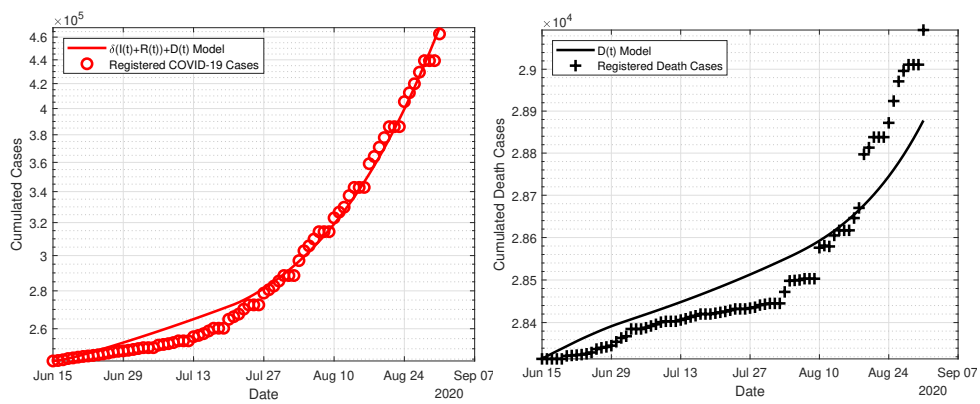
FIGURE 5.54: Infections and death cases in Spain – JHU data
[3] and estimations.
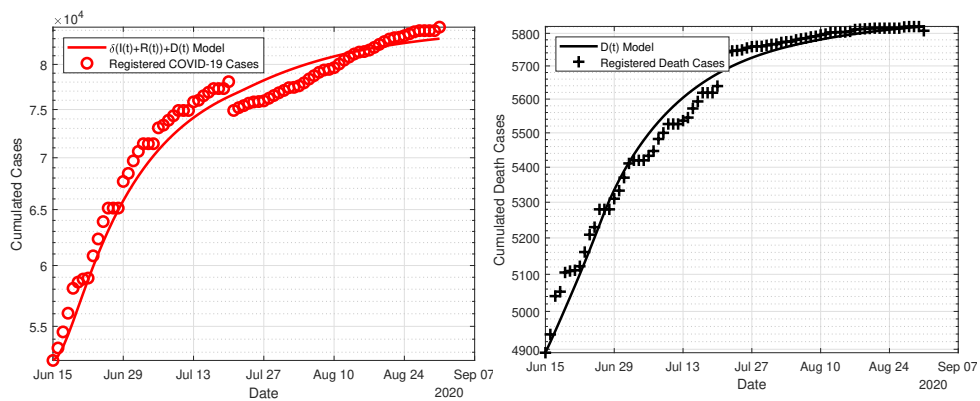
FIGURE 5.55: Infections and death cases in Sweden – JHU
data [3] and estimations.
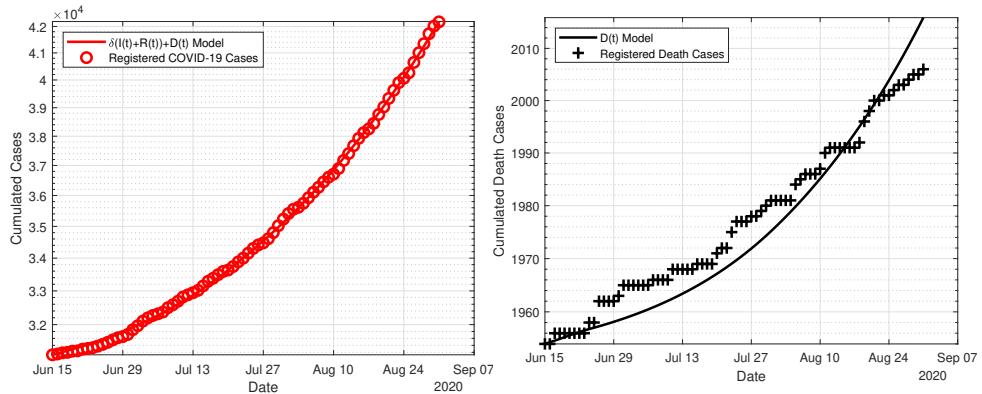
FIGURE 5.56: Infections and death cases in Switzerland –
JHU data [3] and estimations.
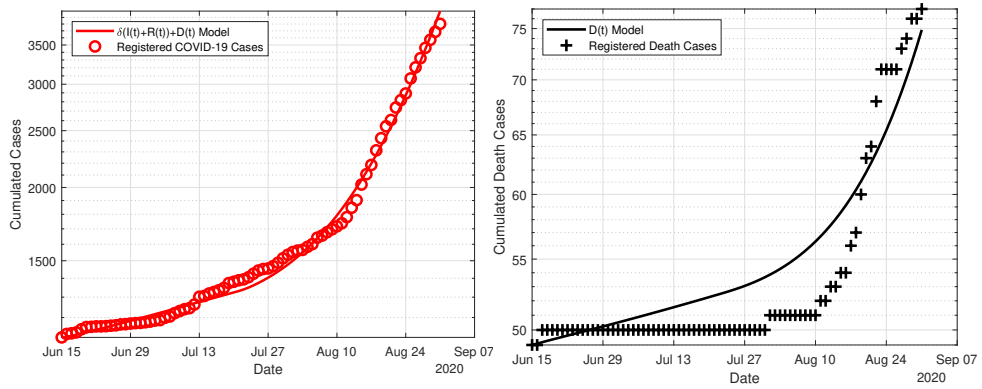
FIGURE 5.57: Infections and death cases in Tunisia – JHU
data [3] and estimations.
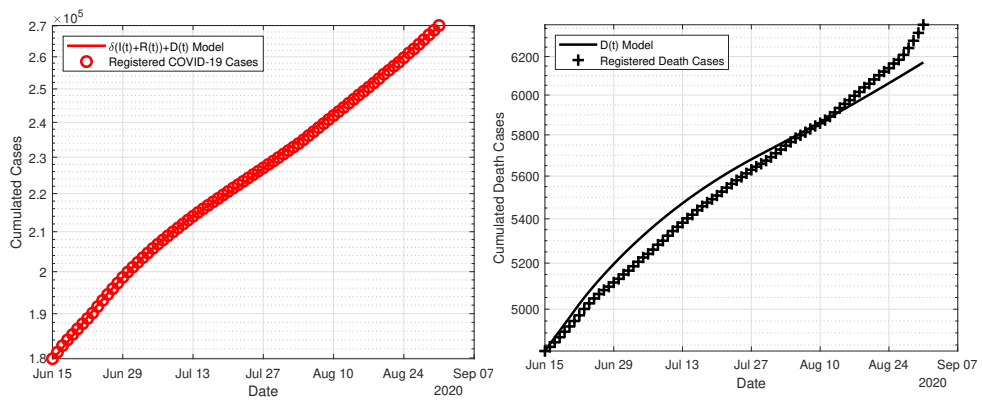
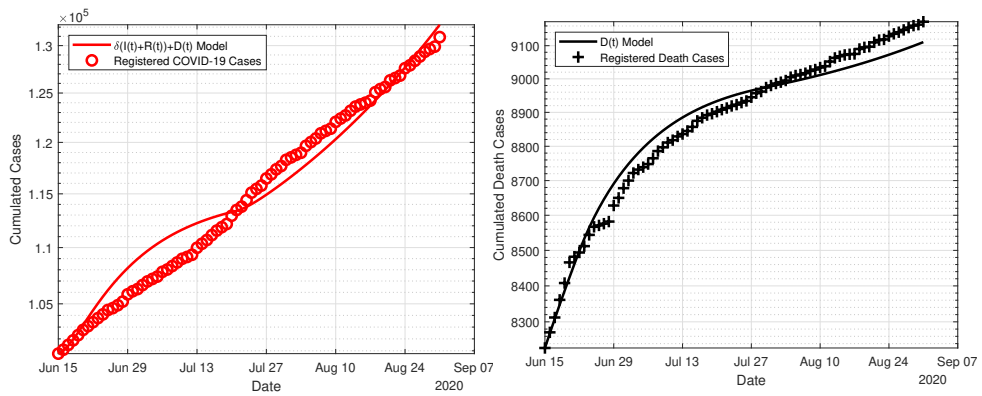FIGURE 5.58: Infections and death cases in Turkey – JHU
data [3] and estimations.
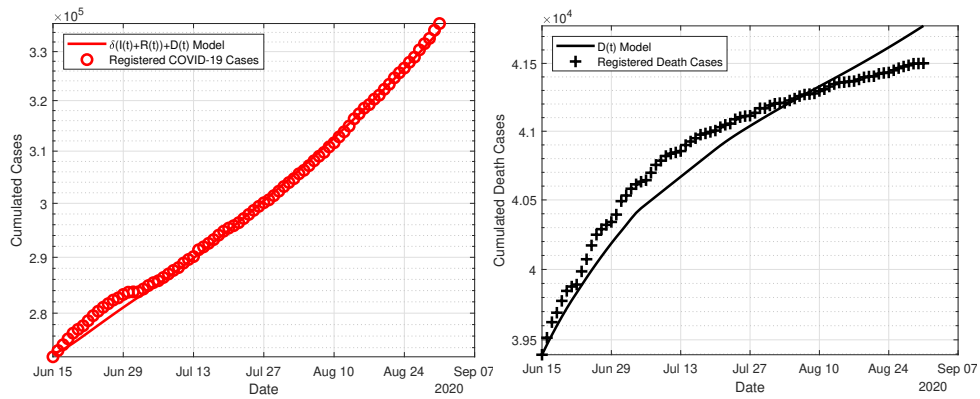
FIGURE 5.59: Infections and death cases in the UK – JHU
data [3] and estimations.
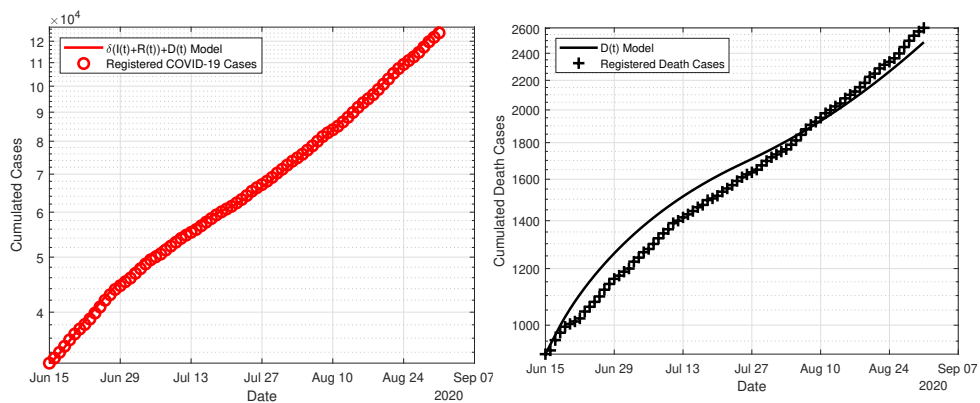
FIGURE 5.60: Infections and death cases in the Ukraine – JHU
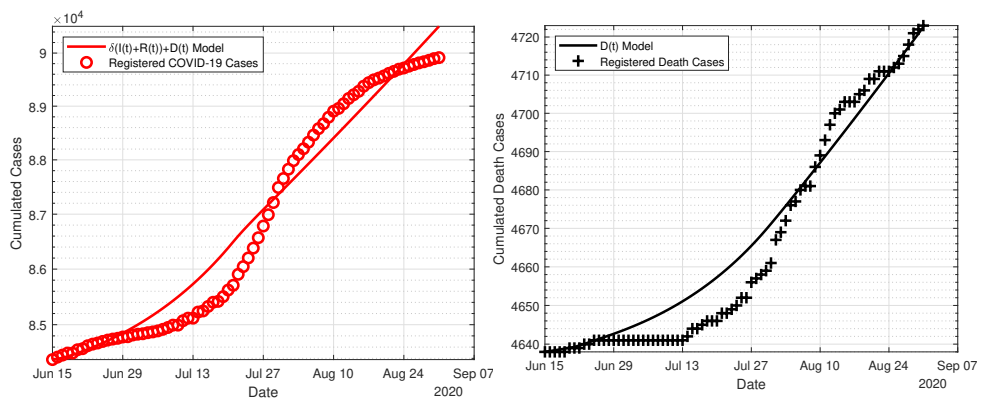data [3] and estimations.
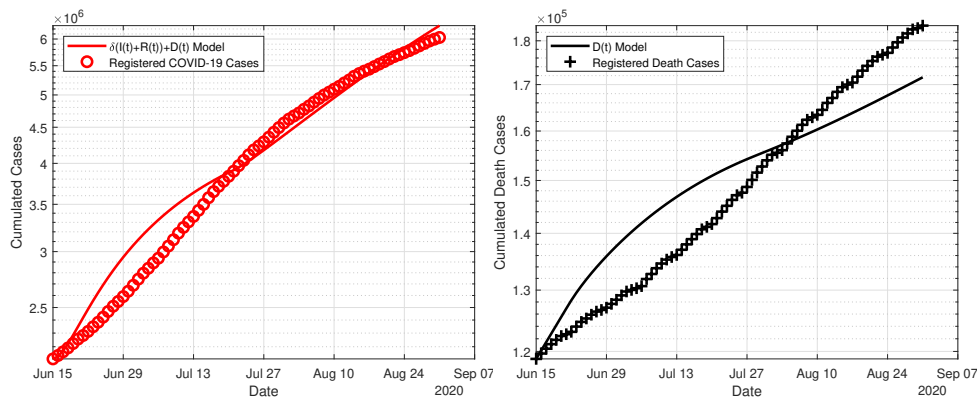
FIGURE 5.61: Infections and death cases in the USA – JHU
data [3] and estimations.
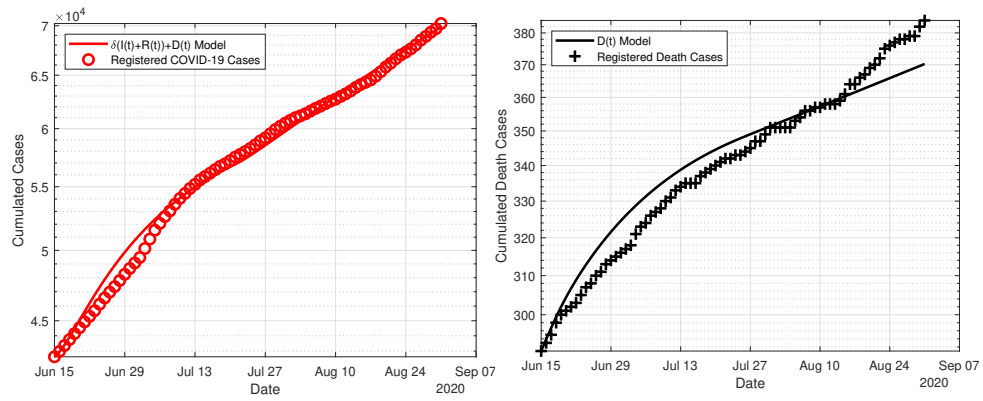
FIGURE 5.62: Infections and death cases in the UAE – JHU
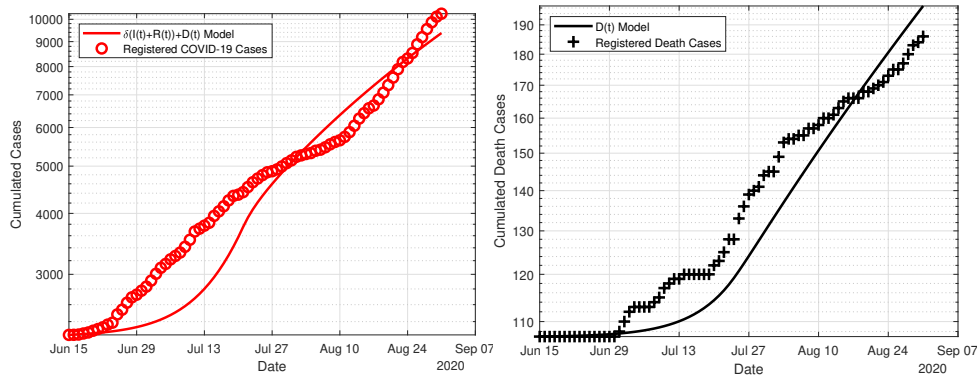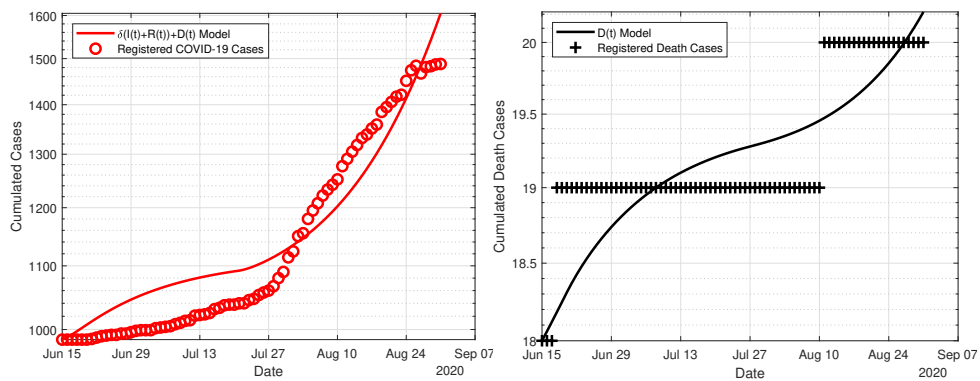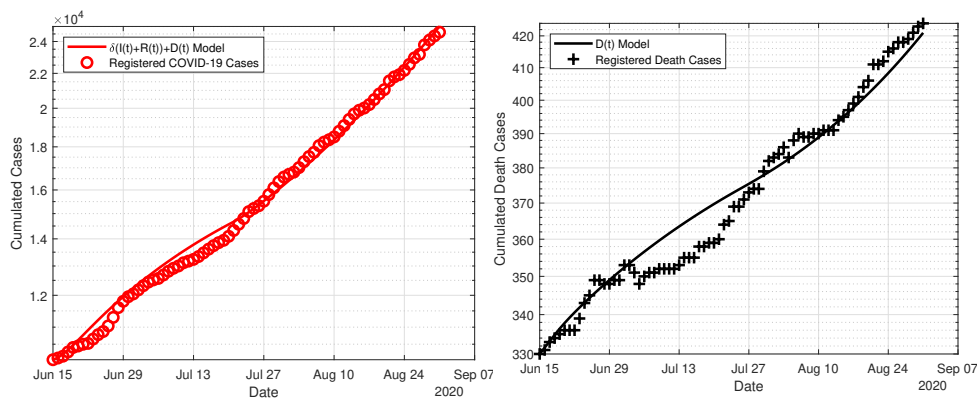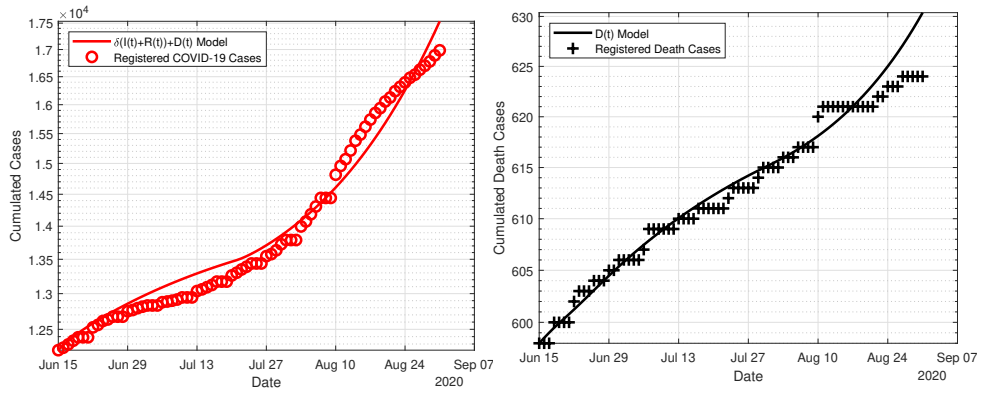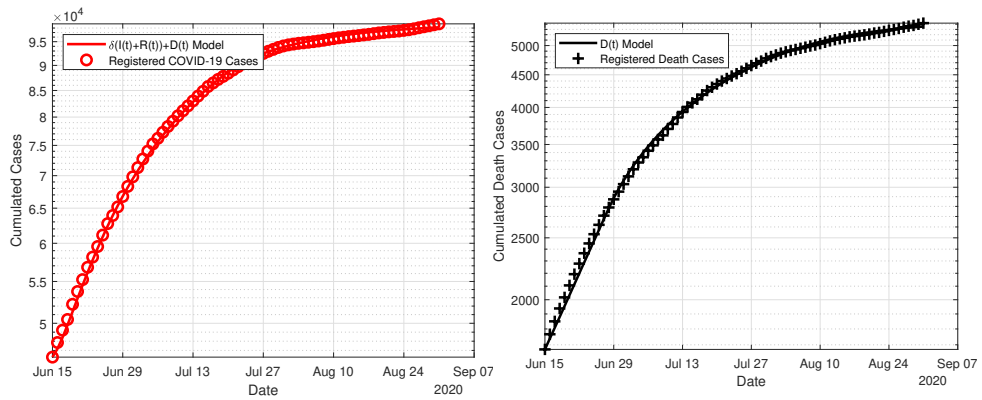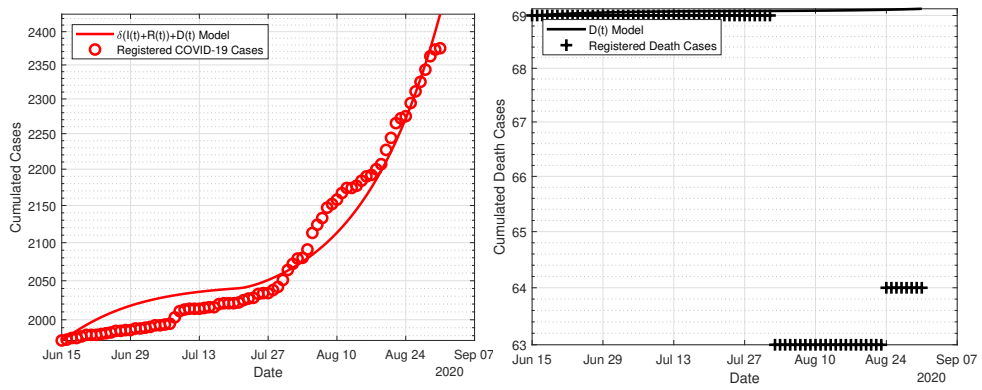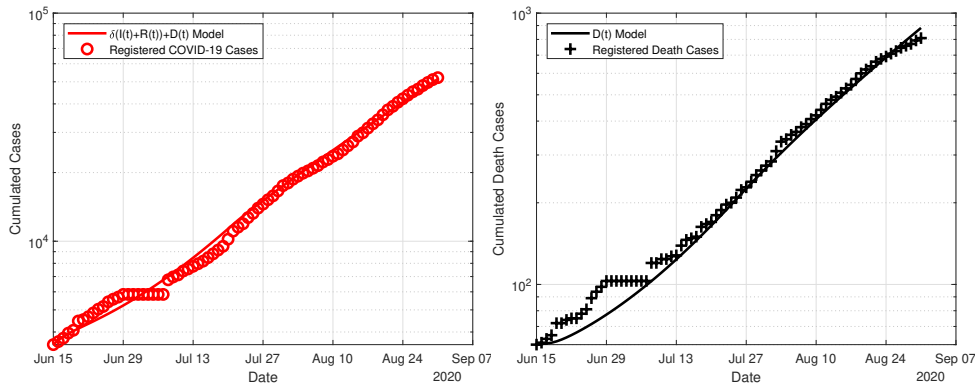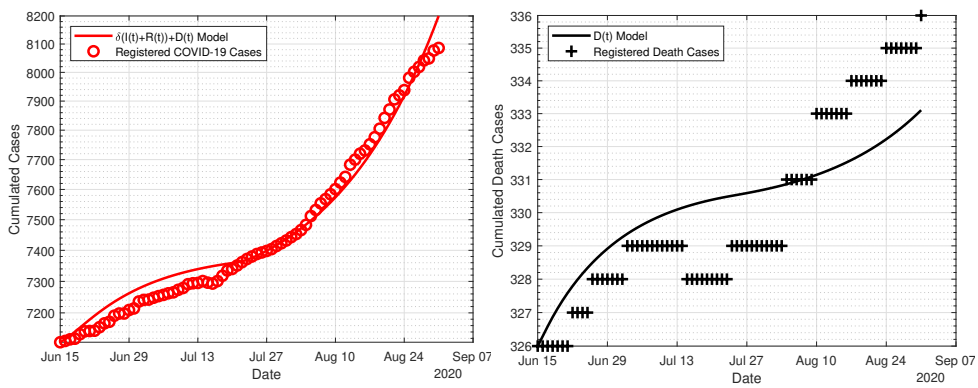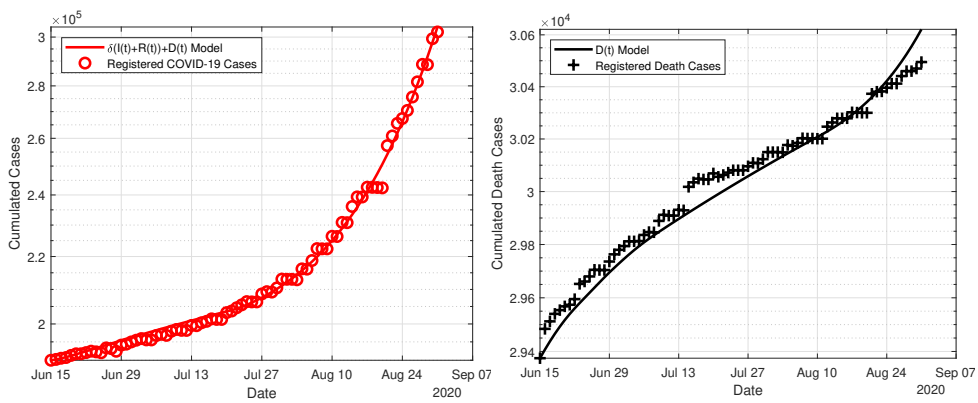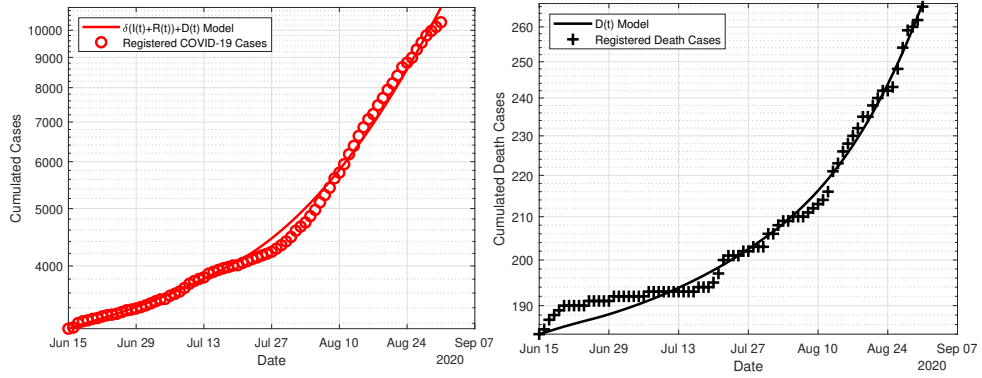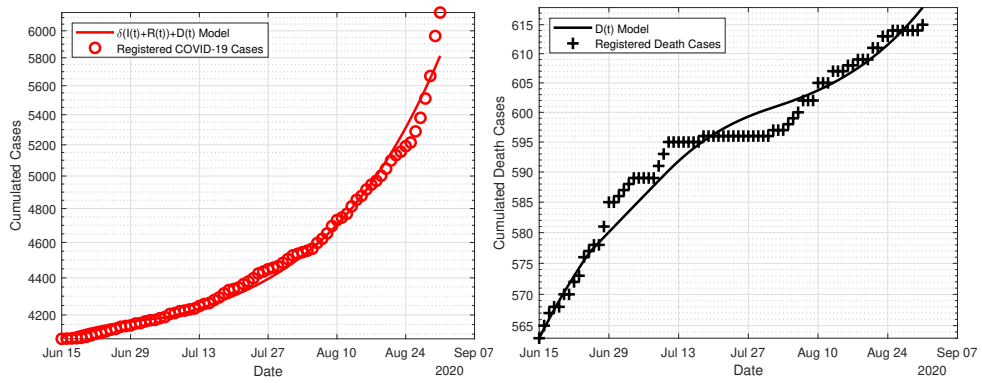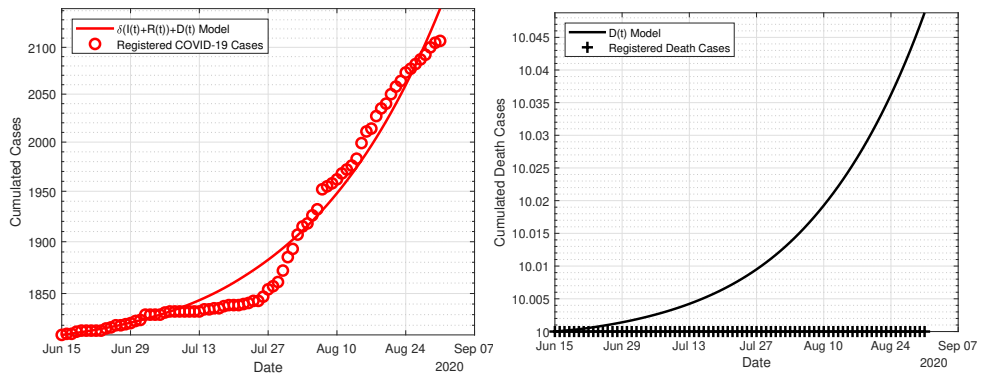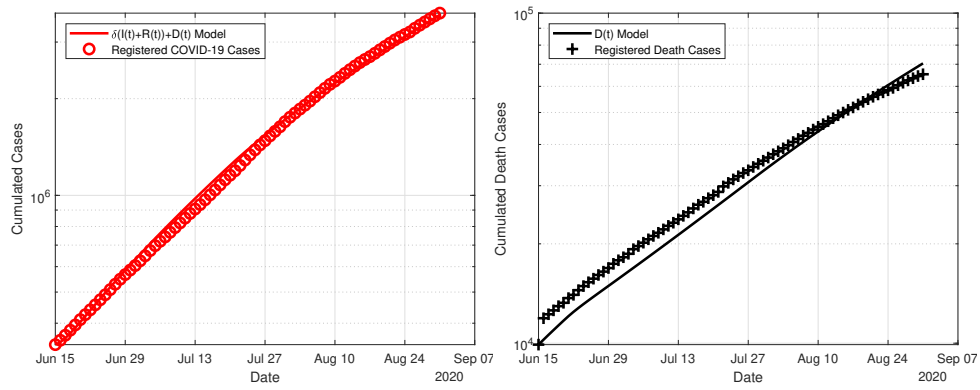data [3] and estimations.

Bibliography

[1] Schäfer, M. et al. "The impact of travelling on the COVID-19 infection cases in Germany". In: *BMC Infectious Diseases* 2.455 (2022). DOI: `10.1186/s12879-022-07396-1`.

[2] Böhmer, M.M. et al. "Investigation of a COVID-19 outbreak in Germany resulting from a single travel-associated primary case: a case series". In: *The Lancet* 20.8 (2020), pp. 920–928. DOI: `10.1016/S1473-3099(20)30314-5`.

[3] Johns Hopkins University. *Time series of confirmed COVID-19 cases globally.* `github.com/CSSEGISandData/COVID-19/blob/master/csse_COVID_19_data/csse_COVID_19_time_series/time_series_COVID19_confirmed_global.csv`. last visited: 18 December, 2023.

[4] Anderson, R.M. et al. "How will country-based mitigation measures influence the course of the COVID-19 epidemic?" In: *Lancet* 395 (2020), pp. 931–934.

[5] Federal Foreign Office of Germany. *Coronavirus / Covid-19: Reisewarnung für Staaten außerhalb der EU/Schengen-Gebiet.* `https://www.auswaertiges-amt.de/de/ReiseUndSicherheit/covid-19/2296762`. last visited: 18 December, 2023.

[6] World Health Organization. *Coronavirus disease (COVID-19) Weekly Epidemiological Update and Weekly Operational Update.* `https://www.who.int/emergencies/diseases/novel-coronavirus-2019/situation-reports`. last visited: 18 December, 2023.

[7] Robert-Koch-Institute. *Daily situation reports.* `www.rki.de/DE/Content/InfAZ/N/Neuartiges_Coronavirus/Situationsberichte/Gesamt.html`.

[8] Siegenfeld, A.F. and Bar-Yam, Y. "The impact of travel and timing in eliminating COVID-19". In: *Commun. Phys.* 3 (2020). DOI: `10.1038/s42005-020-00470-7`.

[9] Chinazzi, M. et al. "The effect of travel restrictions on the spread of the 2019 novel coronavirus (COVID-19) outbreak". In: *Science* 368 (2020), pp. 395–400. DOI: `10.1126/science.aba9757`.

[10] Zou, Y. et al. "Vaccination and Quarantine Effect on COVID-19 Transmission Dynamics Incorporating Chinese-Spring-Festival Travel Rush: Modeling and Simulations". In: *Bull. Math. Biol.* 84.30 (2022). DOI: `10.1007/s11538-021-00958-5`.

[11] Leung, K., Wu, J.T., and Leung, G.M. "Effects of adjusting public health, travel, and social measures during the roll-out of COVID-19 vaccination: a modelling study". In: *Lancet Public Health* 6 (2021), e674–e682. DOI: `10.1016/S2468-2667(21)00167-5`.

[12] Mateus, A.L.P. et al. "Effectiveness of travel restrictions in the rapid containment of human influenza: a systematic review". In: *Bull World Health Organ.* 92.12 (2014), pp. 868–880.

[13] Hollingsworth, T.D., Ferguson, N.M., and Anderson, R.M. "Will travel restrictions control the international spread of pandemic influenza?" In: *Nat. Med.* 12.5 (2006), pp. 497–499. DOI: `10.1038/nm0506-497`.

[14] Epstein, J. et al. "Controlling Pandemic Flu: The Value of International Air Travel Restrictions". In: *PloS one* 5.e401 (2007). DOI: `10.1371/journal.pone.0000401`.

[15] Grépin, K.A. et al. "Evidence of the effectiveness of travel-related measures during the early phase of the COVID-19 pandemic: a rapid systematic review". In: *BMJ Global Health* 6.e004537 (2021), pp. 37–59. DOI: 10.1136/bmjgh-2020-004537.

[16] World Health Organization. *Non-pharmaceutical public health measures for mitigating the risk and impact of epidemic and pandemic influenza.* https://www.who.int/publications/i/item/non-pharmaceutical-public-health-measuresfor-mitigating-the-risk-and-impact-of-epidemic-and-pandemic-influenza. last visited: 18 December, 2023.

[17] Berestycki, H., Roquejoffre, J.-M., and Rossil, L. "Propagation of Epidemics Along Lines with Fast Diffusion". In: *Bull. Math. Biol.* 83.2 (2020). DOI: 10.1007/s11538-020-00826-8.

[18] Heidrich, P. et al. "The COVID-19 outbreak in Germany – Models and Parameter Estimation". In: *Commun. Biomath. Sci.* 3 (2020), pp. 37–59. DOI: 10.5614/cbms.2020.3.1.5.

[19] King, A.A. et al. "Avoidable errors in the modelling of outbreaks of emerging pathogens, with special reference to Ebola". In: *Proc. R. Soc. B* 282.20150347 (1991), pp. 33–55. DOI: 10.1098/rspb.2015.0347.

[20] United Nations, Department of Economic and Social Affairs, Population Dynamics. *World Population Prospects 2019.* https://population.un.org/wpp/DataQuery/. last visited: 18 December, 2023.

[21] Statistisches Bundesamt (Germany). *Statistik über die touristische Nachfrage - Reisen: Deutschland, Jahre, Reiseverhalten, Reiseziel/Reisedauer/Reisegründe/Unterkünfte/Verkehrsmittel.* https://www.destatis.de/DE/Themen/Branchen-Unternehmen/Gastgewerbe-Tourismus/tourismus-reiseverhalten.html. last visited: 18 December, 2023.

[22] Statistische Bibliothek. *Fachserie/6/7/1/Monatlich. Wiesbaden.* https://www.statistischebibliothek.de/mir/receive/DESerie_mods_00000082. last visited: 18 December, 2023.

[23] Statistische Bibliothek. *Fachserie/8/6/Monatlich. Wiesbaden.* https://www.statistischebibliothek.de/mir/receive/DEHeft_mods_00132393. last visited: 18 December, 2023.

[24] Kermack, W.O. and McKendrick, A.G. "Contributions to the mathematical theory of epidemics-I. 1927." In: *Bull. Math. Biol.* 53 (1991), pp. 33–55. DOI: 10.1098/rspa.1927.0118.

[25] Martcheva, M. *An introduction to mathematical epidemiology.* Springer, 2015.

[26] Robert-Koch-Institute. *Modellierung von Beispielszenarien der SARS-CoV-2-Epidemie 2020 in Deutschland.* https://www.rki.de/DE/Content/InfAZ/N/Neuartiges_Coronavirus/Modellierung_Deutschland.pdf?__blob=publicationFile.

[27] Federal Government of Germany. *Vorübergehende Grenzkontrollen an den Binnengrenzen zu Österreich, der Schweiz, Frankreich, Luxemburg und Dänemark.* https://www.bmi.bund.de/SharedDocs/pressemitteilungen/DE/2020/03/grenzschliessung-corona.html. last visited: 18 December, 2023.

[28] Götz, T. and Heidrich, P. "COVID–19 Disease Dynamics in Germany: First Models and Parameter Identification". In: *Journal of Mathematics in Industry* 10.20 (2020). DOI: 10.1186/s13362-020-00088-y.

[29]   Kalbfleisch, J.G. *Probability and Statistical Inference, Volume 1: Probability*. New York, NY: Springer, 1985.

[30]   Raftery, A.E. "Bayesian Model Selection in Social Research". In: *Sociol. Methodol.* 25 (1995), pp. 111–163. DOI: 10.2307/271063.

[31]   Akaike, H. "Information Theory and an Extension of the Maximum Likelihood Principle". In: *Selected Papers of Hirotugu Akaike*. Ed. by Parzen, E., Tanabe, K., and Kitagawa, G. New York, NY: Springer, 1998.

[32]   Metropolis, N. et al. "Equation of State Calculations by Fast Computing Machines". In: *J.Chem. Phys.* 21 (1953), pp. 1087–1092. DOI: 10.1063/1.1699114.

[33]   Gelman, A. et al. *Bayesian Data Analysis, 2nd Edition.* London: Chapman and Hall, 1996.

[34]   Gilks, W.R., Richardson, S., and Spiegelhalter, D.J. *Markov chain Monte Carlo in Practice*. London: Chapman and Hall/CRC, 1996.

[35]   Schäfer, M. and Götz, T. "Modelling Dengue Fever Epidemics in Jakarta". In: *Int. J. Appl. Comput. Math* 6 (2020). DOI: 10.1007/s40819-020-00834-1.

[36]   Rusatsi, D.N. "Bayesian analysis of SEIR epidemic models". last visited: 18 December, 2023. PhD thesis. Lappeenranta University of Technology, 2015.

[37]   Press, W.H. et al. *Numerical Recipes in C++: The Art of Scientific Computing. 3rd edition.* Cambridge University Press, 2007.

[38]   Raue, A. et al. "Structural and practical identifiability analysis of partially observed dynamical models by exploiting the profile likelihood". In: *Bioinformatics* 25 (2009), pp. 1923–1929. DOI: 10.1093/bioinformatics/btp358.

[39]   Götz, T. et al. *Calculation of a local COVID-19 reproduction number for the northern Rhineland-Palatinate (preprint, in German)*. arXiv https://arxiv.org/abs/2011.08632. 2020.

[40]   Rockenfeller, R. et al. "Comparative Sensitivity Analysis of Muscle Activation Dynamics". In: *Comput. Math. Methods Med.* (2015). Article ID 585409. DOI: 10.1155/2015/585409.

[41]   Radon, K. et al. "From first to second wave: follow-up of the prospective COVID-19 cohort (KoCo19) in Munich (Germany)". In: *BMC Infectious Diseases* 21.925 (2021). DOI: 10.1186/s12879-021-06589-4.

[42]   Dimpfl, T. et al. "Estimation of the SARS-CoV-2 infection fatality rate in Germany (preprint)". In: *medRxiv* (2021). DOI: 10.1101/2021.01.26.21250507.

[43]   Morwinsky, S., Nitsche, N., and Acosta, E. "COVID-19 fatality in Germany: Demographic determinants of variation in case-fatality rates across and within German federal states during the first and second waves". In: *Demographic Research* 45.45 (2021), pp. 1355–1372. DOI: 10.4054/DemRes.2021.45.45.

Chapter 6

A Numerical Method for One-Dimensional Space-Fractional Diffusion Models with Mass-Conserving Boundary Conditions

This article by Moritz Schäfer and Thomas Götz has been released in the journal MATHEMATICAL METHODS IN THE APPLIED SCIENCES in 2023, referred to as [1]. The theory, formulation and numerical calculations were mainly done by Moritz Schäfer. Thomas Götz provided several ideas in the theoretical part and for numerical evaluation, as well as some linguistic revisions. The format is changed to meet the thesis standard.

Abstract

The mathematical description of the spread of epidemics is of special interest in the past years, not only due to the omnipresent COVID-19 pandemic but also due to several outbreaks of e.g. Dengue, Ebola or the West Nile Virus. Modelling the spatial spread of this epidemics is particularly of concern. This article considers fractional diffusion as a possibility for handling non-local infection spread. In this more theoretical paper, we consider fractional diffusion by the Grünwald-Letnikov formulation and several possibilities to handle boundary conditions in a mass-conserving way, i.e. no gain or loss of the total population. We will present the basic model formulation as well as *sticky* and *reflecting* boundary conditions and present the stationary points of the model for both. Afterwards, some numerical one-dimensional examples are described. The theoretical and numerical results suggest that reflecting boundary conditions are more reasonable. For sticky boundary conditions, the stationary point has infinite values at the boundaries, while for reflecting boundary conditions, there is only the trivial stationary point for a 'good enough' discretization.

6.1 Introduction

The authors' aim is to find an apt representation about diffusion patterns in the spreading of infections with special kinds of diffusion patterns, and especially to find reasonable boundary conditions for (future) epidemiological investigations. For a short time scale, we can consider countries as isolated, due to, e.g., the geographical or

political situation; in early 2020, for example, border closures prevented the majority of non-economical traffic in many parts of the world. Therefore, epidemics mostly spread only inside those countries. This allows a country-based investigation of the spread neglecting external factors. Spatial spread of epidemics can be modelled locally and non-locally. Local models can be gained by adding mobility matrices in several compartments (see e.g. Goel et al. [2], Schäfer and Götz [3]), traveller matrices (Schäfer et al. [4]), diffusion models or partial differential equation systems (Gai et al. [5] or Kuniya and Wang [6]). This can be described by the equation

$$\frac{\partial}{\partial t} f(x,t) = \kappa \, \Delta f(x,t) + \phi(f(x,t)).$$
(6.1)

A problem lies in the point that local, is that there are a lot of regions with low population density in between and there is little 'exchange' of people between neighboring villages but more to, from, and between larger distances. Thus, *non-local* models which include spread on higher distances can be a helpful tool. While one possibility of attaining non-local spreading effects are integro-differential equations (see e.g. Kergassner et al. [7], Kuniya and Wang [6] or Schäfer et al. 2023 [8]), the focus of this article is the usage of a fractional spatial derivative, i.e., an equation of using a fractional diffusion operator Δ_α, so that eqn. (6.1) transforms into

$$\frac{\partial}{\partial t} f(x,t) = \kappa \, \Delta_\alpha f(x,t) + \phi(f(x,t)).$$
(6.2)

Fractional calculus, i.e., calculus using non-integer powers of integration and derivation, is nowadays used in many applications, e.g., network dynamics (cf. Baleanu and Kumar [9]), viscoelasticity (cf. [9] and Soczkiewicz [10]), field theory and gravity (cf. [9] and Calcagni [11]), advection-dispersion flow equations (cf. Meerschaert and Tadjeran [12]), diffusion processes in epidemiology (cf. [9] and Oldham and Spanier [13]) and price fluctuations in financial markets (cf. Baleanu et al. [14]. Specifically, in modelling of epidemics, both space and time fractional models are used, specifically time-fractional models: Rezapour et al. [15] have set up an *SEIR*-model for transmission of COVID-19). Goufo et al. [16] investigated an time-fractional *SEIR*-model concerning measles. Sidi Ammi et al. [17] provided some useful theoretical results concerning time-fractional *SIR*-models. Kuehn and Mölter [18] also investigate transport effects on epidemics using two coupled models, a static epidemic network and a dynamical transport network, also with non-local, fractional transport dynamics. Hamdan and Kilicman [19] use a system of fractional-order derivative systems to model and analyse control strategies for Dengue Fever epidemics in Malaysia. In this article, we will consider aspects of space-fractional models which have been e.g. considered by Gorenflo and Mainardi [20]. One can show that space-fractional diffusion corresponds to a change from a Markovian random walk to a non-Markovian random walk with Levy flights; cf. [13] and Skwara et al. [21].

Structure of the paper. In the methods section we provide an outline of the definition of fractional derivatives as far as they are relevant for the subsequent model(s). Furthermore, we introduce a finite difference approximation of fractional derivatives that allows numerical simulations. Two different kinds of boundary conditions are introduced and theoretical results for approximations and convergence of the schemes are given. Further on, numerical results for some one-dimensional examples using both types of boundary conditions are provided. Lastly, both theoretical and numerical results are discussed.

6.2 Methods

6.2.1 Fractional derivatives

To generalize the concept of derivatives from integer to non-integer order, there exist several concepts. In our work, we rely on the definitions introduced by Riemann and Liouville and the according discretization given by Grünwald and Letnikov [9, 10, 11, 12]. Let $f : [a, b] \to \mathbb{R}$ denote a sufficiently smooth function on an interval $[a, b]$, where $a = -\infty$ and $b = \infty$ can be included. Let $\Gamma(n) = \int_0^\infty t^{n-1} e^{-t} \, dt = (n-1)!$ denote the gamma function. Then for $n \in \mathbb{N}$ its right-sided n-fold repeated integral is given by (cf. [22, 23])

$$I_{a+}^{(n)} f(x) = \int_a^x d\xi_1 \int_a^{\xi_1} d\xi_2 \cdots \int_a^{\xi_{n-1}} f(\xi_n) \, d\xi_n = \frac{1}{\Gamma(n)} \int_a^x f(\xi)(x - \xi)^{n-1} \, d\xi \, . \quad (6.3)$$

We can straightforwardly extend this to non-integer order $\alpha \in \mathbb{R} \setminus \{-1, -2, \dots\}$ by

$$I_{a+}^{(\alpha)} f(x) = \frac{1}{\Gamma(\alpha)} \int_a^x f(\xi)(x - \xi)^{\alpha-1} \, d\xi \, . \quad (6.4)$$

The above integral is called the *right-sided fractional Riemann-Liouville integral of order α*. Analogously, we may define the *left-sided fractional integral* by

$$I_{b-}^{(\alpha)} f(x) = \frac{1}{\Gamma(\alpha)} \int_x^b f(\xi)(\xi - x)^{\alpha-1} \, d\xi \, . \quad (6.5)$$

It is easy to prove (see e.g. [12]), that for the fractional Riemann-Liouville integral it holds

$$I_{a+}^{(\alpha)} I_{a+}^{(\beta)} f = I_{a+}^{(\alpha+\beta)} f, \quad (6.6a)$$

$$I_{b-}^{(\alpha)} I_{b-}^{(\beta)} f = I_{b-}^{(\alpha+\beta)} f. \quad (6.6b)$$

According to the fundamental theorem of calculus, we identify the derivative of order α as the inverse operators to the integrals of order α, i.e.,

$$D_{a+} f = \frac{d^k}{dx^k} I_{a+}^{(k)} f \, , \quad (6.7a)$$

$$D_{b+} f = \frac{d^k}{dx^k} I_{b-}^{(k)} f \, . \quad (6.7b)$$

To define the fractional derivative of order $\alpha > 0$, let $n = \lceil \alpha \rceil = \min_{k \in \mathbb{N}} \{k > \alpha\}$ denote the smallest integer larger than α. Formally, taking the n-derivative of the fractional Riemann-Liouville integral of order $n - \alpha$, i.e., $\frac{d^n}{dx^n} I^{(n-\alpha)}$, yields the Riemann-Liouville definition of the fractional derivative of order α.

Definition 6.1. Let $f \in \mathcal{C}^n[a, b]$. We call

$$D_{a+}^\alpha f(x) = \frac{\partial^\alpha}{\partial_{a+} x^\alpha} f(x) := \frac{1}{\Gamma(n - \alpha)} \frac{d^n}{dx^n} \int_a^x f(\xi)(x - \xi)^{n-\alpha-1} d\xi \quad (6.8)$$

the *Riemann-Liouville derivative of fractional order* α with left boundary a. Analogously, we define

$$D_{b-}^{\alpha} f(x) = \frac{\partial^{\alpha}}{\partial_{b-} x^{\alpha}} f(x) := \frac{(-1)^n}{\Gamma(n-\alpha)} \frac{d^n}{dx^n} \int_x^b f(\xi)(\xi - x)^{n-\alpha-1} d\xi \qquad (6.9)$$

as the *Riemann-Liouville derivative of fractional order* α with right boundary b [10].

The above fractional derivatives are *linear*, i.e. for all $f, g \in \mathcal{C}^n[a, b]$, all $\lambda, \mu \in \mathbb{R}$ and any $\alpha > 0$ we have

$$D_{a+}^{\alpha} [\lambda f + \mu g] = \lambda D_{a+}^{\alpha} f + \mu D_{a+}^{\alpha} g, \qquad (6.10a)$$
$$D_{b-}^{\alpha} [\lambda f + \mu g] = \lambda D_{b-}^{\alpha} f + \mu D_{b-}^{\alpha} g. \qquad (6.10b)$$

Example 6.2. We consider the monomial x^k and compute its fractional derivative of order α. In alignment with the formal generalization of the integer order derivative

$$\frac{d^m}{dx^m} x^k = k(k-1)\cdots(k-m+1)x^{k-m} = \frac{k!}{(k-m)!} x^{k-m} = \frac{\Gamma(k+1)}{\Gamma(k-m+1)} x^{k-m}$$

we obtain

$$\begin{aligned}
D_{a+}^{(\alpha)} x^k &= \frac{1}{\Gamma(n-\alpha)} \frac{d^n}{dx^n} \int_a^x \xi^k (x-\xi)^{n-\alpha-1} d\xi \\
&= \frac{1}{\Gamma(n-\alpha)} \frac{d^n}{dx^n} \frac{k}{n-\alpha} \int_a^x \xi^{k-1}(x-\xi)^{n-\alpha} d\xi = \dots \\
&= \frac{1}{\Gamma(n-\alpha)} \frac{d^n}{dx^n} \frac{\Gamma(k+1)\Gamma(n-\alpha)}{\Gamma(n+k-\alpha+1)} (x-a)^{n+k-\alpha} \\
&= \frac{\Gamma(k+1)}{\Gamma(k-\alpha+1)} (x-a)^{k-\alpha},
\end{aligned} \qquad (6.11)$$

and analogously

$$D_{b-}^{(\alpha)} x^k = \frac{\Gamma(k+1)}{\Gamma(k-\alpha+1)} (b-x)^{k-\alpha}. \qquad (6.12)$$

For $a = 0$ and $\alpha := n \in \mathbb{N}$, this corresponds to the well-known n-th derivatives of the monomials.

Example 6.3. As a second example, we consider the exponential $f(x) = e^{cx}$ for $c > 0$ and $x \in [0, \infty)$. Using the series representation of the exponential and the above right-sided fractional derivative of the monomials we obtain

$$\begin{aligned}
D_{0+}^{(\alpha)} e^{cx} &= \sum_{k=0}^{\infty} \frac{c^k}{k!} D_{0+}^{(\alpha)} x^k = \sum_{k=0}^{\infty} \frac{c^k}{\Gamma(k+1)} \frac{\Gamma(k+1)}{\Gamma(k-\alpha+1)} x^{k-\alpha} \\
&= x^{-\alpha} \sum_{k=0}^{\infty} \frac{(cx)^k}{\Gamma(k-\alpha+1)}
\end{aligned} \qquad (6.13)$$

After some algebraic manipulations and by introducing the incomplete gamma function $\Gamma(-\alpha, cx) = \int_{cx}^{\infty} t^{-\alpha-1} e^{-t} dt$, we arrive at

$$D_{0+}^{(\alpha)} e^{cx} = e^{cx} c^{\alpha} \cdot \left(1 - \frac{\Gamma(-\alpha, cx)}{\Gamma(-\alpha)}\right). \qquad (6.14)$$

Again, for $\alpha = n \in \mathbb{N}$, this corresponds to the regular n-th derivative of the exponential function.

6.2.2 Sticky boundary conditions

As a next step, we define the fractional diffusion operator Δ_α as a linear combination of the right-sided and the left-sided fractional derivative. For the sake of simplicity, we restrict ourselves on the spatial one-dimensional case on $[a, b]$ with $\phi \equiv 0$. In any non-local fractional diffusion process, *sticky* boundary conditions imply that in a closed domain $[a, b]$, mass that leaves a certain point x and, without the boundaries, would come to rest at a place $y < a$ or $y > b$, is assumed to remain in either boundary a or b (cf. [24]). This kind of boundary condition naturally meets the mass conservation rule for $\phi \equiv 0$ as no mass can leave (or enter) the domain. The fractional diffusion equation for an order α of diffusion with $1 < \alpha \leq 2$ then reads as the sum of both right-sided and left-sided fractional derivatives:

$$\frac{\partial}{\partial t} f(x, t) = \kappa_1 D_{a+}^{(\alpha)} f(x, t) + \kappa_2 D_{b-}^{(\alpha)} f(x, t) \tag{6.15}$$

In order to prevent confusion in the notation, $[a, b] = [-1, 1]$ will be our standard interval from now onwards. Therefore, we can simplify the notation by $D_+^{(\alpha)} := D_{a+}^{(\alpha)}$, and $D_-^{(\alpha)} := D_{b-}^{(\alpha)}$. Also, we will just consider symmetric fractional diffusion, i.e. $\kappa_1 = \kappa_2 =: \kappa > 0$.

Example 6.4. Note that for a symmetrical diffusion operator with $\kappa > 0$, the fractional derivative of the constant c (cf. example 2.35) do *not* vanish; in fact, they are not even constant:

$$\kappa \cdot \left(D_{a+}^{(\alpha)} + D_{b-}^{(\alpha)} \right) c = \kappa c \cdot \frac{\Gamma(k+1)}{\Gamma(k - \alpha + 1)} \left[(x - a)^{-\alpha} + (b - x)^{-\alpha} \right] > 0 \tag{6.16}$$

Also, since mass conservation for $\phi \equiv 0$ is expected from our model, we can only include mass conserving boundary conditions, which excludes standard Dirichlet boundary conditions.

Lemma 6.5. The only stationary solution of the equation is

$$f^*(x) = c_0 \frac{2}{\sqrt{\pi}} \frac{\Gamma(\frac{\beta+2}{2})}{\Gamma(\frac{\beta+1}{2})} \cdot (1 - x^2)^{(\beta-1)/2}. \tag{6.17}$$

Proof. To determine stationary solution of the fractional diffusion, we aim to solve the equation

$$\kappa \left(D_+^{(\alpha)} + D_-^{(\alpha)} \right) f(x) = 0. \tag{6.18}$$

Using the definition of the fractional derivatives, this reads as

$$\begin{aligned}
0 &= \frac{1}{\Gamma(2 - \alpha)} \frac{d^2}{dx^2} \left(\int_{-1}^{x} f(\xi)(x - \xi)^{1-\alpha} \, d\xi + \int_{x}^{1} f(\xi)(\xi - x)^{1-\alpha} \, d\xi \right) \\
&= \frac{1}{\Gamma(2 - \alpha)} \frac{d^2}{dx^2} \int_{-1}^{1} f(\xi) \, |x - \xi|^{1-\alpha} \, d\xi.
\end{aligned} \tag{6.19}$$

This implies that the integral $\int_{-1}^{1} f(\xi)\,|x - \xi|^{1-\alpha}\,d\xi$ is a linear function $c_0 + c_1 x$. Symmetry of the solution requires $c_1 = 0$, hence the integral has to equal the constant c_0.

The work of Shinbrot [25] (pp. 23-24) provides a solution for equations of the type

$$g(x) = \int_{-1}^{1} \frac{f(\xi)}{|x - \xi|^{\beta}}\,d\xi \tag{6.20}$$

for an arbitrary $\beta \in [0, 1]$ is provided (which, for our problem, is guaranteed by the choice $\beta = \alpha - 1$). Defining coefficients

$$\gamma_n := \Gamma\left(n + \tfrac{\beta+1}{2}\right) \cdot \left(\frac{(2n + \beta)\,\Gamma(\beta)\,\cos(\tfrac{\pi\beta}{2})}{\pi \cdot 2^{2n+\beta}} \right)^{1/2} \tag{6.21}$$

and functions

$$\chi_n(x) := \gamma_n \frac{d^n}{dx^n} (1 - x^2)^{n + \frac{\beta-1}{2}}, \tag{6.22}$$

the solution of the above integral equation is given by the series

$$f(x) = \sum_{n=0}^{\infty} \chi_n(x) \int_{-1}^{1} \chi_n(\xi)\psi(\xi)\,d\xi. \tag{6.23}$$

In our case, $g(x) \equiv c_0$. Thus

$$\begin{aligned}
f(x) &= \sum_{n=0}^{\infty} c_0\,\chi_n(x) \int_{-1}^{1} \chi_n(\xi)\,d\xi \\
&= c_0\,\chi_0(x) \int_{-1}^{1} \chi_0(\xi)\,d\xi + \sum_{n=1}^{\infty} c_0 \gamma_n \frac{d^{n-1}}{dx^{n-1}} (1 - x^2)^{n + \frac{\beta-1}{2}} \bigg|_{-1}^{1}.
\end{aligned} \tag{6.24}$$

The series term vanishes, since for $n \geq 1$ all the terms $(1 - x^2)^{n + \frac{\beta+1}{2}}$ or its integer derivatives vanish at the boundaries. Hence

$$\begin{aligned}
f(x) &= c_0\,\gamma_0\,\chi_0(x) \int_{-1}^{1} (1 - \xi^2)^{(\beta-1)/2}\,d\xi \\
&= c_0\,\gamma_0^2\,(1 - x^2)^{(\beta-1)/2} \int_{-1}^{1} (1 - \xi^2)^{(\beta-1)/2}\,d\xi \\
&= c_0\,\frac{2}{\sqrt{\pi}} \frac{\Gamma(\frac{\beta+2}{2})}{\Gamma(\frac{\beta+1}{2})} \cdot (1 - x^2)^{(\beta-1)/2},
\end{aligned} \tag{6.25}$$

where c_0 is a constant defined by the total initial mass. Also notice that for $\alpha = 2$ the constant reduces to c_0 as $\frac{\Gamma(\frac{3}{2})}{\Gamma(1)} = \frac{\pi}{\sqrt{2}}$. For all $1 < \alpha < 2$, i.e. $0 < \beta = \alpha - 1 < 1$, it holds that $\frac{\beta-1}{2} < 0$ and the solution will tend to infinity at the boundary $x = \pm 1$. $\qquad \square$

6.2.3   Reflecting boundary conditions

To prevent the above presented singularities we now assume mass moving 'into' the boundary to get *reflected* and moving back in the opposite direction. To satisfy these mirroring boundary conditions, consider the reflected and periodically continued

version of f, i.e.

$$\phi(x) := \begin{cases} f(x - 4k) & \text{if } -1 + 4k \le x \le 1 + 4k \\ f(4k + 3 - x) & \text{if } 1 + 4k < x < 3 + 4k \end{cases}, \qquad k \in \mathbb{Z}^0. \qquad (6.26)$$

While ϕ is defined on whole $\mathbb{R}$, we only consider fractional diffusion in our closed domain, i.e., for $x \in [-1, 1]$. This is then denoted by the following equation:

$$\frac{\partial}{\partial t} f(x, t) = \frac{1}{\Gamma(2 - \alpha)} \frac{d^2}{dx^2} \left[\int_{-\infty}^x \phi(\xi)(x - \xi)^{1-\alpha} d\xi + \int_x^\infty \phi(\xi)(\xi - x)^{1-\alpha} d\xi \right] \quad (6.27)$$

In fact, the description as 'boundary condition' is rather misleading, as the equations have to be updated for all grid points in this case.

Lemma 6.6. The only stationary solution is the constant, i.e., $f^*(x) \equiv c_0$.

Proof. Stationary equilibria $\phi^*(x)$ are solutions of the equation

$$0 = \frac{1}{\Gamma(2 - \alpha)} \frac{d^2}{dx^2} \left[\int_{-\infty}^x \phi(\xi)(x - \xi)^{1-\alpha} d\xi + \int_x^\infty \phi(\xi)(\xi - x)^{1-\alpha} d\xi \right]. \quad (6.28)$$

In the corollary at [25, p. 24], it is shown that equation has at most one solution given in the form. We show, that $\phi^*(x) = c_0$ (and thus $f(x) \equiv c_0$) solves the problem, hence it is the unique solution:

$$
\begin{aligned}
& \frac{c_0}{(2 - \alpha) \cdot \Gamma(2 - \alpha)} \frac{d^2}{dx^2} \left\{ \lim_{n \to \infty} \left[(x - \xi)^{2-\alpha} \right]_{-n}^x + \lim_{n \to \infty} \left[(\xi - x)^{2-\alpha} \right]_x^n \right\} \\
= & \frac{c_0}{(2 - \alpha) \cdot \Gamma(2 - \alpha)} \left\{ \lim_{n \to \infty} \frac{d^2}{dx^2} \left[(x + n)^{2-\alpha} + (n - x)^{2-\alpha} \right] \right\} \\
= & \frac{c_0}{\Gamma(1 - \alpha)} \left\{ \lim_{n \to \infty} \left[(x + n)^{-\alpha} + (n - x)^{-\alpha} \right] \right\} = 0
\end{aligned}
\qquad (6.29)
$$

To show uniqueness of the (trivial) solution, we assume $\phi^*(x) \not\equiv c_0$ solves eqn. (6.27). Then due to similar thoughts as for the sticky boundary conditions (symmetry of the solution), we know that

$$\hat{c} = \int_{-\infty}^\infty \phi(\xi) \left| x - \xi \right|^{1-\alpha} d\xi. \qquad (6.30)$$

We reconsider [25]: Construct a Fourier transform function $\chi_n(x)$. Then the solution can be explicitly calculated by Fourier transforms using functions $\chi_n(x)$, $n \in \mathbb{N}$:

$$\phi^*(x) = \sum_{n=1}^\infty \chi_n(x) \int_{-\infty}^\infty \hat{c} \, \chi_n(\xi) d\xi. \qquad (6.31)$$

The definition of all $\chi_n(x)$ is unique, so that $\phi(x)^* \equiv c_0$ which contradicts the assumption. Due to mass conservation, $\phi(x) \equiv c_0$ thus is the unique solution for the problem with reflecting boundary conditions. $\qquad \square$

6.3   Numerical methods

In order to derive a finite difference approximation to the fractional derivative, we generalize the standard difference approximation

$$\frac{d^2}{dx^2}f(x) = \lim_{h\to 0} \frac{1}{h^2} \sum_{k=0}^{2} (-1)^k \binom{2}{k} f(x - (k-1)h) \tag{6.32}$$

to fractional orders using $(-1)^k \binom{\alpha}{k} = \dfrac{\Gamma(k-\alpha)}{\Gamma(k+1)\Gamma(-\alpha)}$. This leads us to the following

Definition 6.7. (cf. [26]) Let $f \in C^n[a,b]$ and $\alpha \in [n-1,n)$. The *right-shifted Grünwald-Letnikov difference formulation* to the fractional derivative of order α is given by

$$D_{a+}^{\alpha} f(x) := \lim_{h\to 0} \frac{1}{h^{\alpha}} \sum_{k=0}^{\infty} \frac{\Gamma(k-\alpha)}{\Gamma(k+1)\Gamma(-\alpha)} f(x - (k-1)h) \tag{6.33}$$

The *left-shifted Grünwald-Letnikov difference formulation* to the fractional derivative of order α is given by

$$D_{b-}^{\alpha} f(x) := \lim_{h\to 0} \frac{1}{h^{\alpha}} \sum_{k=0}^{\infty} \frac{\Gamma(k-\alpha)}{\Gamma(k+1)\Gamma(-\alpha)} f(x + (k-1)h) \tag{6.34}$$

In order to simplify notations, we introduce the *Grünwald coefficient*

$$g_k := \frac{\Gamma(k-\alpha)}{\Gamma(k+1)\Gamma(-\alpha)} \tag{6.35}$$

for $k \in \mathbb{N}_0$ and $\alpha > 0$ (cf. [27]).

The sum of all Grünwald coefficients vanishes, i.e., $\sum_{k=0}^{\infty} g_k = 0$, so that the method is conservative (cf. [28]).

In order to approximate eqn. (6.15), assume that we have found a numerical approximation, i.e.,

$$D_{+}^{(\alpha)} f(x,t) + D_{-}^{(\alpha)} f(x,t) \tag{6.36}$$

using a discrete operator $\Delta_{\alpha,h}$ which is yet to be found. Then we can use a standard ODE solver, e.g. the explicit or implicit Euler system or the Runge-Kutta method, to find the numerical solution of this equation for $h > 0$ and $f_h(x,t) = (f(x_0,t), f(x_1,t), \ldots, f(x_m,t))^T$:

$$D_t f = \Delta_{\alpha,h} \cdot f_h(x,t) \tag{6.37}$$

The discrete operator $\Delta_{\alpha,h}$ will now be adapted to the two different boundary conditions.

6.3.1   Sticky boundary conditions

All mass that moves out of the boundary is assumed to find a rest at the boundary, so the mass from x that would be moved to $x - (k-1)h < a$ will be moved to a instead. Analogously, the mass from x that would be moved to $x + (k-1)h > b$ will be moved to b instead. The same thing happens for the transportation of mass from $x = a$ to $a + (k-1)h$ and $k = 0$ for the right-sided fractional derivative, and

the transportation of mass from $x = b$ to $b - (k-1)h$ and $k = 0$ for the left-sided fractional derivative. As $f(x) = 0$ for $x < x_0 := a$ and $x > x_m := b$, the sum in eqns. (6.33) and (6.34) becomes finite. Define $M = \left\lfloor \frac{x-a}{h} + 1 \right\rfloor$ and $K = \left\lfloor \frac{b-x}{h} + 1 \right\rfloor$, respectively. It is assumed that a part of the mass at value $x - (k-1)h$ is moved to x, namely $g_k h^{-\alpha} f(x - (k-1)h)$. This results into the following discrete formulations:

$$D_+^\alpha f(x,t) = \lim_{h \to 0} \frac{1}{h^\alpha} \sum_{k=0}^{M} \tilde{g}_k f(x - (k-1)h) + r_1 \tag{6.38a}$$

$$D_-^\alpha f(x,t) = \lim_{h \to 0} \frac{1}{h^\alpha} \sum_{k=0}^{K} \hat{g}_k f(x + (k-1)h) + r_2 \tag{6.38b}$$

Also, terms $1 - \alpha$ result of the boundary conditions and the formulations for the right-sided fractional derivative at $x = a$ and the left-sided fractional derivative at $x = b$. For the boundary points we have to update the corresponding Grünwald coefficients according to the absorption of mass:

$$\tilde{g}_k = \begin{cases} g_k & \text{if } 0 \leq k < M \\ \sum_{k=M}^{\infty} g_k = -\sum_{k=0}^{M-1} g_k & \text{if } k = M \end{cases} \tag{6.39a}$$

$$\hat{g}_k = \begin{cases} g_k & \text{if } 0 \leq k < K \\ \sum_{k=K}^{\infty} g_k = -\sum_{k=0}^{K-1} g_k & \text{if } k = K \end{cases} \tag{6.39b}$$

For an equidistant grid with $x_0 = a, x_m = b$ and $x_i = x_0 + ih, i = 0, \ldots, n, h = \frac{1}{m+1}$, the discrete operator then reads as

$$\Delta_{\alpha,h} = \kappa(\mathbf{R} + \mathbf{S}). \tag{6.40}$$

with transition matrices for the right-sided fractional diffusion, i.e.,

$$\mathbf{R}_{i,j} = \begin{cases} 1 - \alpha & i = j = 1 \\ g_{j-i+1} & 2 \leq j \leq m, i \leq j+1 \\ \sum_{p=m+1-j}^{\infty} g_p = -\sum_{p=0}^{m-j} g_p & j = m+1 \end{cases} \tag{6.41}$$

as $\sum_{p=0}^{\infty} g_p = 0$. and the left-sided fractional diffusion, i.e.,

$$\mathbf{S}_{i,j} = \begin{cases} 1 - \alpha & i = j = m+1 \\ g_{j-i+1} & 1 \leq j \leq m, j \leq i+1 \\ \sum_{p=m+1-j}^{\infty} g_p = -\sum_{p=0}^{m-j} g_p & i = 1 \end{cases} \tag{6.42}$$

This shifted method using is first-order consistent, so that if

$$\frac{\Delta t}{h^\alpha} \leq \frac{1}{\alpha \kappa}, \tag{6.43}$$

the error terms satisfy $r_1, r_2 = \mathcal{O}(h)$ (cf. Meerschaert and Tadjeran [29]).

6.3.2 Reflecting boundary conditions

For the numerical scheme, consider the discretization on an equidistant grid consisting of $m + 1$ points $x_0 = a, x_m = b$ and $x_i = x_0 + hi, i = 1 \ldots m - 1, h = \frac{1}{m+1}$ as above. When the mass has moved m steps to the left and $k + 1$ steps are actually needed to

be covered, then the mass is transported from the left boundary to the right for the remaining $k + 1 - m$ steps. Same holds true for the right boundary. As the Grünwald coefficient $g_k \to 0$ for $k \to \infty$, but remains nonzero for finite k, we have an infinite process where a decreasing mass is transported infinitely often between the left and right boundaries. Note that there are two possible ways to design the 'mirror': One would be that if mass reaches the boundary and 'has yet one step to cover', then it can either return into the other direction for one step, or remain at the boundary and only moves on into the other direction when there is more than one step yet to cover. The first method is used in this paper to achieve a certain symmetry between all grid points. We know that the Grünwald-Letnikov formulation is consistent of order h for reflecting boundary conditions and the sum from 0 to $\frac{x-a}{h} + 1$ or $\frac{b-x}{h} + 1$, respectively, because the function values vanish for points outside the boundary. For $h > 0$ it holds:

$$D_{a+}^{(\alpha)} f(x, t) = \frac{1}{h^\alpha} \sum_{k=0}^{\infty} g_k f(x - (k-1)h) + \mathcal{O}(h), \tag{6.44a}$$

$$D_{b-}^{(\alpha)} f(x, t) = \frac{1}{h^\alpha} \sum_{k=0}^{\infty} g_k f(x + (k-1)h) + \mathcal{O}(h). \tag{6.44b}$$

For the left-sided fractional derivative and arbitrary k, the mass moving from x_i to x_j is considered. It first moves $i + 2$ steps to the left boundary a, then one step within the left boundary, then j steps to the point x_j, making it $i + j + 3$ steps in total. Because the process is repeated every $2(m + 1)$ steps, all elements $i + j + 3 + 2(m + 1)l$, $l \in \mathbb{N}_0$, have to be summed up as well. After the $i + j + 3$ steps, it also moves $m - j$ points to the right boundary b, another point inside the right boundary and then $m - j$ points back to point x_j, making it $i - j + 2m + 4$ points in total, similar to above it follows that mass is moved from x_i to x_j for every distance $i - j + 2m + 4 + 2(m + 1)l$, $l \in \mathbb{N}_0$.
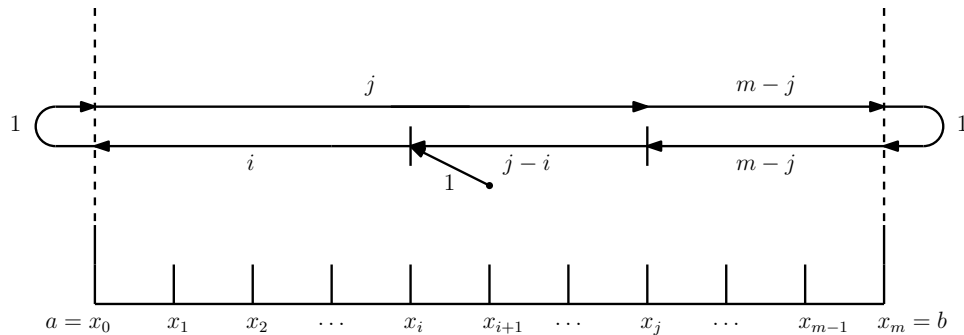
FIGURE 6.1: Left Fractional Derivative.

For the right-sided fractional derivative and an arbitrary (but large enough) k, the mass moving from x_i to x_j is considered. It first moves $m - i + 2$ steps to the right boundary b, then one step within the right boundary, then $m - j$ steps to the point x_j, making it $-i - j + 2m + 2$ steps in total. Thus, as described above, all elements $-i - j + 2m + 2 + 2(m + 1)l$, $l \in \mathbb{N}_0$, are summed up. After the $2m + 2 - i - j$ steps, it also moves j points to the left boundary a, another point inside the left boundary and then j points back to point x_j, making it $j - i + 2m + 3$ points in total, similar to above it follows that mass is moved from i to j for every distance $j - i + 2m + 3 + 2(m + 1)l$, $l \in \mathbb{N}_0$.
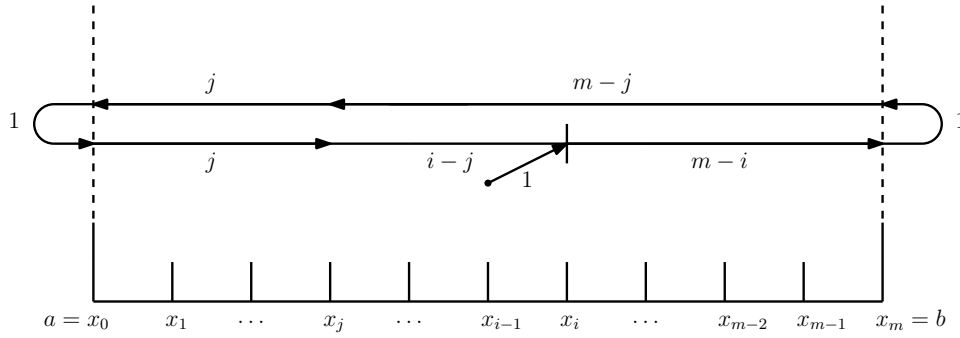
FIGURE 6.2: Right Fractional Derivative.

Until now, the actual position of x_i and x_j has not been regarded. We have to consider the possibilities $x_i < x_j$, $x_i = x_j$, and $x_i > x_j$. These can easily be condensed if we consider a modified modulo formula

$$\text{mod}^*(a, n) := \begin{cases} \text{mod}(a, n) & \text{mod}(a, n) \neq 0 \\ n & \text{mod}(a, n) = 0 \end{cases} \tag{6.45}$$

By using this formula, we can put all distances of the left and right fractional derivatives into one formula for the mass transport from x_i to x_j each. Let therefore $k \in \mathbb{N}_0$. The discrete operator again reads as

$$\Delta_{\alpha,h} = \kappa(\mathbf{R} + \mathbf{S}) \tag{6.46}$$

with

$$\mathbf{R}_{ij} = \sum_{k=0}^{\infty} g_{p_1(k)} f(x - (p_1(k) - 1)h) + g_{q_1(k)} f(x - (q_1(k) - 1)h), \tag{6.47}$$

where

$$\begin{aligned} p_1(k) :&= \text{mod}^*(i + j + 3 + 2(m+1)k, 2(m+1)) + 2(m+1)k \\ &= \text{mod}^*(i + j + 3, 2(m+1)) + 2(m+1)k, \end{aligned} \tag{6.48a}$$

$$\begin{aligned} q_1(k) :&= \text{mod}^*(i - j + 2m + 4 + 2(m+1)k, 2(m+1)) + 2(m+1)k \\ &= \text{mod}^*(i - j + 2, 2(m+1)) + 2(m+1)k, \end{aligned} \tag{6.48b}$$

as well as

$$\mathbf{S}_{ij} = \sum_{k=0}^{\infty} g_{p_2(k)} f(x - (p_2(k) - 1)h) + g_{q_2(k)} f(x - (q_2(k) - 1)h), \tag{6.49}$$

where

$$\begin{aligned} p_2(k) :&= \text{mod}^*(-i - j + 2m + 2 + 2(m+1)k, 2(m+1)) + 2(m+1)k \\ &= \text{mod}^*(-i - j, 2(m+1)) + 2(m+1)k, \end{aligned} \tag{6.50a}$$

$$\begin{aligned} q_2(k) :&= \text{mod}^*(-i + j + 2m + 3 + 2(m+1)k, 2(m+1)) + 2(m+1)k \\ &= \text{mod}^*(-i + j + 1, 2(m+1)) + 2(m+1)k. \end{aligned} \tag{6.50b}$$

A problem lies in the the infinite number of summands in each formula. However, as we know that $g_k \to 0$ for $k \to \infty$, reconsider the formulation of the Grünwald coefficient as of eqn. (6.35). If for an arbitrary, but fixed $N \in \mathbb{N}$, the partial sum

$\sum_{k=N}^{\infty} g_k = \sum_{k=0}^{N-1} g_k$ can be estimated, we can find a decent approximation by the apt choice of N, after which the sum of the Grünwald coefficients is stopped.

Lemma 6.8. It holds

$$\sum_{k=N}^{\infty} g_k \sim \int_N^{\infty} k^{-2} dk = \mathcal{O}(h^p). \tag{6.51}$$

Proof. The term $\Gamma(-\alpha)$ is independent of k and thus can be seen as constant. The term $\Gamma(k+1)$ is equal to $k!$ as k is integer. The term $\Gamma(k-\alpha)$ can be represented by

$$\begin{aligned}
\Gamma(k-\alpha) &= (k-\alpha-1) \cdot \Gamma(k-\alpha-1) \\
&= (k-\alpha-2)(k-\alpha-1) \cdot \Gamma(k-\alpha-2) = \ldots \\
&= (2-\alpha)(3-\alpha)\ldots(k-\alpha-1) \cdot \Gamma(2-\alpha) \\
&\leq 1 \cdot 2 \cdot \ldots \cdot (k-2) \cdot \Gamma(2-\alpha) \\
&= (k-2)! \cdot \Gamma(2-\alpha)
\end{aligned} \tag{6.52}$$

Altogether this implies

$$g_k \leq \frac{\Gamma(2-\alpha)}{\Gamma(-\alpha)} \cdot \frac{(k-2)!}{k!} \propto \frac{1}{(k-2)(k-1)} = \mathcal{O}(k^{-2}). \tag{6.53}$$

For the sum, it then holds

$$\sum_{k=N}^{\infty} g_k \sim \int_N^{\infty} k^{-2} dk = \mathcal{O}(N^{-1}). \tag{6.54}$$

If we now set $N = \mathcal{O}(h^{-p})$, it follows $\sum_{k=N}^{\infty} g_k = \mathcal{O}(h^p)$.   □

We can even improve this estimation by computing the logarithm of the Grünwald coefficient.

Lemma 6.9. It holds
$$\sum_{k=N}^{\infty} g_k = \mathcal{O}(h^{\alpha p}).$$

Proof. For that, we use the Rocktäschel approximation [30]:

$$\log(\Gamma(z)) \approx \left(z - \frac{1}{2}\right) \log(z) - z + \frac{1}{2} \log(2\pi). \tag{6.55}$$

We take the natural logarithm of the non-constant terms of the Grünwald coefficient and apply this approximation:

$$\begin{aligned}
\log\left(\frac{\Gamma(k-\alpha)}{\Gamma(k+1)}\right) &= \log(\Gamma(k-\alpha)) - \log(\Gamma(k+1)) \\
&\approx \left(k - \alpha - \frac{1}{2}\right) \log(k-\alpha) - k + \alpha - \left(k + \frac{1}{2}\right) \log(k+1) + k + 1 \\
&\approx \cdots \approx \left(k + \frac{1}{2}\right) \log\left(1 - \frac{\alpha+1}{\kappa+1}\right) - (\alpha+1) \log(k-\alpha) + (\alpha+1)
\end{aligned} \tag{6.56}$$

Additionally, we can approximate

$$\log(1 - \varepsilon) = -\varepsilon + \mathcal{O}(\varepsilon^2). \tag{6.57}$$

This way we have

$$\log\left(\frac{\Gamma(k-\alpha)}{\Gamma(k+1)}\right) \approx \left(k + \frac{1}{2}\right)\frac{\alpha+1}{k+1} - (\alpha+1)\log(k) - (\alpha+1)\log\left(1 - \frac{\alpha}{k}\right) + \alpha + 1$$

$$\approx \cdots \approx -(\alpha+1)\log(k) + (\alpha+1)\left(\frac{\alpha}{k} + \frac{1}{2k+2}\right). \tag{6.58}$$

In total we have found

$$\log\left(\frac{\Gamma(k-\alpha)}{\Gamma(k+1)}\right) = -(\alpha+1)\log(k) + \mathcal{O}(k^{-1}). \tag{6.59}$$

This implies

$$g_k = \frac{1}{\Gamma(-\alpha)} \cdot \frac{\Gamma(k-\alpha)}{\Gamma(k+1)} \approx C \cdot k^{-(\alpha+1)} \tag{6.60}$$

and thus the better approximation

$$\sum_{k=N}^{\infty} g_k = \mathcal{O}(N^{-\alpha}) \tag{6.61}$$

which by a choice of $N = \mathcal{O}(h^{-p})$ yields $\sum_{k=N}^{\infty} g_k = \mathcal{O}(h^{\alpha p})$. □

Lemma 6.10. The trivial equilibrium of the numerical method is stable if

$$\frac{\tau}{h^\alpha} \leq \frac{1}{2\kappa\alpha}. \tag{6.62}$$

Proof. By eqns. (6.38b), the fractional space derivatives then reduce to $\sum_{k=0}^{\infty} g_k = 0$. This way, no diffusion takes place and the system is stationary. If, however, there is a small varation from the stationary solution, i.e., $\epsilon(t, x)$, then we perform a *von-Neumann-analysis* of the system. Assume a forward difference in time and discrete values $u_n^l = u(x_j, t_n)$. We define the (discrete) error terms as $\epsilon_j^n = \rho_n e^{i\omega jh}$. A relative comparison using the identity $\sum_{k=0}^{\infty} g_k = 0$ gives

$$\left|\frac{\epsilon_j^{n+1}}{\epsilon_j^n}\right| = \left|\frac{\rho_{n+1}}{\rho_n}\right| = \left|1 + \frac{\kappa\tau}{h^\alpha \rho_n e^{i\omega jh}}\left(\sum_{k=0}^\infty g_k \epsilon_{j+1-k}^n + \sum_{k=0}^\infty g_k \epsilon_{j-1+k}^n\right)\right|$$

$$= \left|1 + \frac{\kappa\tau}{h^\alpha}\sum_{k=0}^\infty g_k \left(e^{-i\omega(k-1)h} + e^{i\omega(k-1)h}\right)\right|$$

$$= \left|1 + \frac{2\kappa\tau}{h^\alpha}\sum_{k=0}^\infty g_k \cos(\omega(k-1)h)\right|$$

$$= \left|1 + \frac{2\kappa\tau}{h^\alpha}\sum_{k=0}^\infty g_k \left[1 - 2\sin^2(\omega(k-1)h))\right]\right|$$

$$= \left|1 - \frac{4\kappa\tau}{h^\alpha}\sum_{k=0}^\infty g_k \sin^2\left(\frac{\omega(k-1)}{2}h\right)\right| \overset{!}{\leq} 1. \tag{6.63}$$

It obviously holds that

$$\frac{4\kappa\tau}{h^\alpha}\sum_{k=0}^\infty g_k \sin^2\left(\frac{\omega(k-1)}{2}h\right) \geq 0 \tag{6.64}$$

as the sine function vanishes at $k = 1$ for the only negative Grünwald coefficient $g_1 = -\alpha$. Thus, it remains to show that this term is also ≤ 2, which is guaranteed if

$$\frac{2\kappa\tau}{h^\alpha}\sum_{k=0}^\infty g_k \sin^2\left(\frac{\omega(k-1)}{2}h\right) \leq \frac{2\kappa\tau}{h^\alpha}\sum_{k\neq 1}^\infty g_k = \frac{2\kappa\tau}{h^\alpha}\alpha \leq 1, \tag{6.65}$$

resulting in the desired inequality. This means, that for a 'good enough' discretization, the system will converge to its trivial equlibrium for any disturbance $\epsilon(t,x)$, so that this equilibrium is stable. $\square$

6.4   Numerical results

6.4.1   Sticky boundary conditions

Numerical examples are provided for $\psi(x) \equiv 1$, $\kappa = 10^{-2}$ and various α in in Figs. **??**, **??** and **??**. The border points at $x = \pm 1$ can be evaluated numerically at any time $t < \infty$, but as $t \to \infty$, the value will diverge to ∞ as seen in lemma 6.5. The analytical solution of the stationary solution described there is compared to the numerical results with applied reflecting boundary conditions. The amount of runs of the algorithm is terminated by the $\mathcal{L}_2$-norm. It is visible that the singularity causes a larger discretization error near the boundaries, such that a comparison of the norms is not useful.

This equilibrium is independent of starting values of the function, given the total mass is the same. Also, the singularity at the boundaries is not what we would expect for our problem (infectives in Sri Lanka) so reflecting boundaries are not a good method for fractional diffusion in our case.
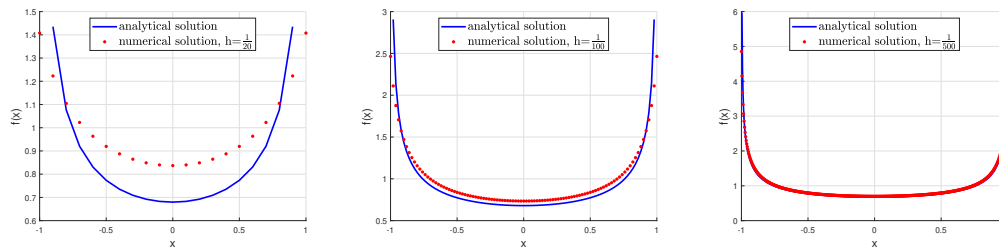
FIGURE 6.3: Sticky boundary conditions for $\alpha = 1.1$ and selected grid sizes.
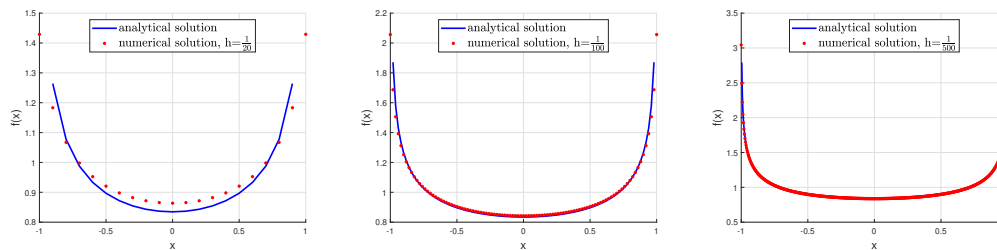
FIGURE 6.4: Sticky boundary conditions for $\alpha = 1.5$ and selected grid sizes.
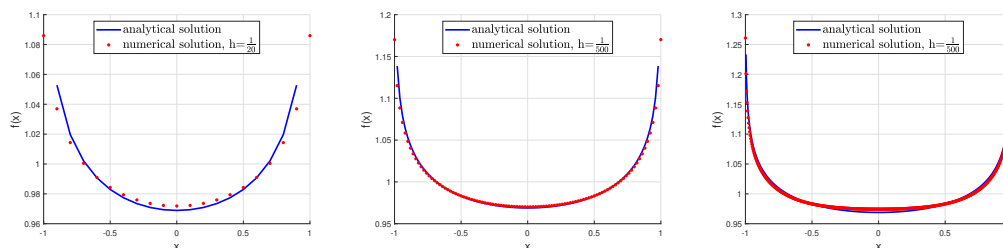
FIGURE 6.5: Sticky boundary conditions for $\alpha = 1.9$ and selected grid sizes.

6.4.2 Reflecting boundary conditions

Numerical examples are provided for the domain $\Omega = [-1, 1] \subset \mathbb{R}$, in Figs. **??** and **??**.These numerical solutions suppport the theoretical findings that the system with mirrored boundary condition runs into the trivial equilibrium $f(x) \equiv c_0$, where c_0 is the mean value of the initial mass. The velocity of diffusion increases with α.

$$f_1(x) = \begin{cases} 2x + 1 & -0.5 \leq x \leq 0 \\ -2x + 1 & 0 \leq x \leq 0.5, \\ 0 & \text{else} \end{cases}$$

$$f_2(x) = -\frac{1}{2}(x + 1),$$

as well as $h = 10^{-2}$, $\tau = 10^{-3}$ and $\alpha \in \{1.1, 1.5, 1.9\}$.

(A) $\alpha = 1.1$ (B) $\alpha = 1.5$ (C) $\alpha = 1.9$
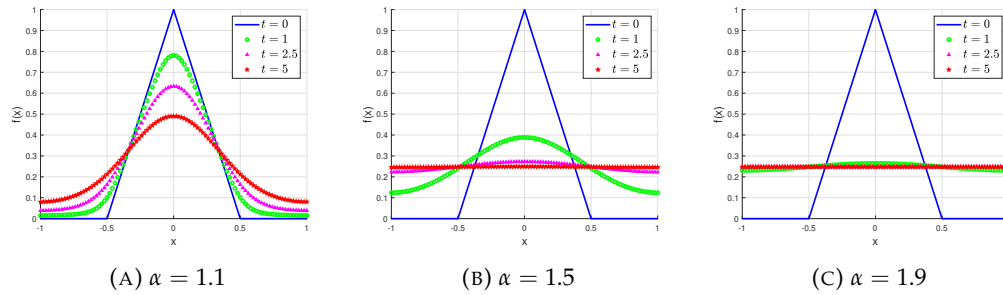
FIGURE 6.6: Reflecting boundary conditions for $f_1(x)$.

(A) $\alpha = 1.1$ (B) $\alpha = 1.5$ (C) $\alpha = 1.9$
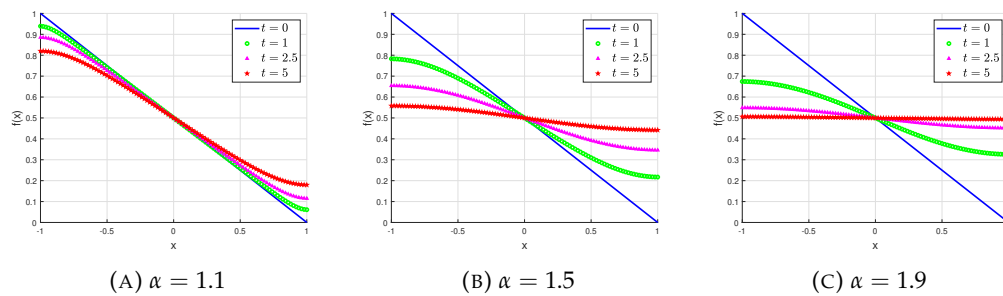
FIGURE 6.7: Reflecting boundary conditions for $f_2(x)$.

6.5   Discussion and conclusion

This article deals with the numerical approximation of space-fractional derivatives, which can be used to solve space-fractional PDE systems which have many applications. We aimed to find a representation with respect to disease spread to be used in future works. Using the finite difference approximation to the Riemann-Liouville definition, the Grünwald-Letnikov formulation provides an easy to discretize the derivative of fractional order. In order to conserve the mass, i.e. the total population in a country, and assuming that there is no exchange of population to other countries or regions, we considered two different boundary conditions; using these we can also handle the non-local nature of the fractional diffusion. For sticky boundary conditions, where all mass moving out of the boundary remains at the boundary, we use the property of the Grünwald coefficients $\sum_k g_k = 0$ and a lemma of Shinbrot to calculated the stationary solution, which tends to infinity at the boundaries even if the integral is finite. This makes the usage of sticky boundary conditions a less realistic choice than reflecting boundary conditions, as by using von-Neumann-stability analysis we can show the only stationary point is the trivial equilibrium. For these kind of 'boundary' conditions that impose an infinite sum on each grid point a finite formulation of order α has been found. Numerical one-dimensional results for both formulations were applied to illustrate the scheme and the structure of the solutions which support the theoretical findings.

In future work, these models can be applied to local epidemics (Dengue fever, COVID-19) with their spatial distribution in an isolated area, e.g., the island of Sri Lanka during the first Corona waves, and it can be 'checked' if certain spreading processes have a 'classical' diffusion character or if the diffusion behaves in a fractional way. A comparison between the results of space- and time-fractional PDE models can also be made.

Declarations

Competing interests

The authors declare that there exist no competing interests.

Acknowledgements

The authors would like to thank Wolfgang Bock (TU Kaiserslautern) for his valuable advice regarding this article.

Authors' contributions

All authors contributed a significant part and reviewed the manuscript.

Bibliography

[1] Schäfer, M. and Götz, T. "A numerical method for space-fractional diffusion models with mass-conserving boundary conditions". In: *Mathematical Methods in the Applied Sciences* (2023). DOI: 10.1002/mma.9310.

[2] Goel, R. et al. "Mobility-based SIR model for complex networks: with case study of COVID-19". In: *Social Network Analysis and Mining* 11.105 (2021). DOI: 10.1007/s13278-021-00814-3.

[3] Schäfer, M. and Götz, T. "Modelling Dengue Fever Epidemics in Jakarta". In: *Int. J. Appl. Comput. Math* 6 (2020). DOI: 10.1007/s40819-020-00834-1.

[4] Schäfer, M. et al. "The impact of travelling on the COVID-19 infection cases in Germany". In: *BMC Infectious Diseases* 2.455 (2022). DOI: 10.1186/s12879-022-07396-1.

[5] Gai, C., Iron, D., and Kolokolnikov, T. "Localized outbreaks in an S-I-R model with diffusion". In: *Journal of Mathematical Biology* 80 (2020), pp. 1389–1411. DOI: 10.1007/s00285-020-01466-1.

[6] Kuniya, T. and Wang, J. "Global dynamics of an SIR epidemic model with nonlocal diffusion". In: *Nonlinear Analysis: Real World Applications* 43 (2018), pp. 262–282. DOI: 10.1016/j.nonrwa.2018.03.001.

[7] Kergaßner, A. et al. "Memory-based meso-scale modeling of Covid-19". In: *Computational Mechanics* (2020). DOI: 10.1007/s00466-020-01883-5.

[8] Schäfer, M. et al. *An integro-differential model for the spread of diseases*. arXiv https://arxiv.org/abs/2307.10087. 2023.

[9] Baleanu, D. and Kumar (eds.), D. *Fractional Calculus and its Applications in Physics*. Frontiers Media, Lausanne, 2019.

[10] Soczkiewicz, E. "Application of Fractional Calculus in the Theory of Viscoelasticity". In: *Mol. Quant. Acoust.* 23 (2002), pp. 397–404.

[11] Calcagni, G. "Towards Multifractional Calculus". In: *Frontiers in Physics* 6.58 (2018).

[12] Meerschaert, M.M. and Tadjeran, C. "Finite difference approximations for fractional advection-dispersion flow equations". In: *Journal of Computational and Applied Mathematics* 172 (2004), pp. 65–77.

[13] Oldham, K. and Spanier, J. *The Fractional Calculus (1st Edition)*. Academic Press, New York, 1974.

[14] Baleanu, D. et al. *Fractional Calculus - Models and Numerical Methods, CNC Series on Complexity, Nonlinearity and Chaos, Vol. 5 (2nd edition)*. World Scientific, New Jersey, 2016.

[15] Rezapour, S., Mohammadi, H., and Samei, M.E. "SEIR epidemic model for COVID-19 transmission by Caputo derivative of fractional order". In: *Advances in Difference Equations* 490 (2020). DOI: 10.1186/s13662-020-02952-y.

[16] Goufo, E.F.D., Noutchie, S.C.O., and Mugisha, S. "A Fractional SEIR Epidemic Model for Spatial and Temporal Spread of Measles in Metapopulations". In: *Abstract and Applied Analysis* 2014.781028 (2014). DOI: 10.1186/s13662-020-02952-y.

[17] Sidi Ammi, M.R. et al. "Global analysis of a time fractional order spatio-temporal SIR model". In: *Scientific Reports* 12.5751 (2022). DOI: 10.1038/s41598-022-08992-6.

[18]   Kuehn, C. and Mölter, J. "The influence of a transport process on the epidemic threshold". In: *Journal of Mathematical Biology* 85.62 (2020), pp. 37–59. DOI: 10.1007/s00285-022-01810-7.

[19]   Hamdan, N.I. and Kilicman, A. "Mathematical Modelling of Dengue Transmission with Intervenction Strategies Using Fractional Derivatives". In: *Bulletin of Mathematical Biology* 84.138 (2022). DOI: 10.1007/s11538-022-01096-2.

[20]   Gorenflo, R. and Mainardi, F. "Random Walk Models for Space-Fractional Diffusion Processes". In: *Fractional Calculus and Applied Analysis* 1.2 (1998), pp. 167–191.

[21]   Skwara, U. et al. "Fractional calculus and superdiffusion in epidemiology: shift of critical thresholds". In: *Conference: 12th International Conference on Computational and Mathematical Methods in Science and Engineering, CMMSE 2012* (2012).

[22]   Tadjeran, C., Meerschaert, M.M., and Scheffler, H.-P. "A second-order accurate numerical approximation for the fractional diffusion equation". In: *Journal of Computational Physics* 213 (2006), pp. 205–213.

[23]   Tadjeran, C. and Meerschaert, M.M. "A second-order accurate numerical method for the two-dimensional fractional diffusion equation". In: *Journal of Computational Physics* 220 (2007), pp. 813–823.

[24]   Borges, G.M. et al. "Superdiffusion in a non-Markovian random walk model with a Gaussian memory profile". In: *Eur. Phys. J. B* 85.310 (2012).

[25]   Shinbrot, M. "The solution of some integral equations of Wiener-Hopf type". In: *Quarterly of Applied Mathematics* 28.1 (1970), pp. 15–36.

[26]   Letnikov, A.V. "Theory of differentiation with an arbitrary index". In: *Mat. Sb.* 3 (1868), pp. 1–66.

[27]   Baeumer, B. et al. "Reprint of: Boundary conditions for fractional diffusion". In: *Journal of Computational and Applied Mathematics* 339 (2018), pp. 414–430.

[28]   Meerschaert, M.M. and Sikorskii, A. *Stochastic Models for Fractional Calculus.* De Gruyter Studies in Mathematics, De Gruyter, Berlin, 2012.

[29]   Meerschaert, M.M. and Tadjeran, C. "Finite difference approximations for two-sided space-fractional partial differential equations". In: *Applied Numerical Mathematics* 56 (2006), pp. 80–90.

[30]   Rocktäschel, O. *Methoden zur Berechnung der Gammafunktion für komplexes Argument*. Dissertation, Dresden. 1922.

Chapter 7

Modelling the Spatial Spread of COVID-19 in a German District using a Diffusion Model

This article by Moritz Schäfer, Peter Heidrich and Thomas Götz has been released in the journal MATHEMATICAL BIOSCIENCES AND ENGINEERING in 2023, referred to as [1]. The theory, formulation and numerical calculations for the Metropolis algorithm, as well as the map creation, were mainly done by Moritz Schäfer. Peter Heidrich contributed to the adjoint theory and the graphical figures for the various models. Thomas Götz provided advice and some linguistic revisions. The format is changed to meet the thesis standard.

Abstract

In this study, we focus on modeling the local spread of COVID-19 infections. As the pandemic continues and new variants or future pandemics can emerge, modelling the early stages of infection spread becomes crucial, especially as limited medical data might be available initially. Therefore, our aim is to gain a better understanding of the diffusion dynamics on smaller scales using partial differential equation (PDE) models.

Previous works have already presented various methods to model the spatial spread of diseases, but, due to a lack of data on regional or even local scale, few actually applied their models on real disease courses in order to describe the behaviour of the disease or estimate parameters. We use medical data from both the Robert-Koch-Institute (RKI) and the Birkenfeld district government for parameter estimation within a single German district, *Birkenfeld* in Rhineland-Palatinate, during the second wave of the pandemic in autumn 2020 and winter 2020-21. This district can be seen as a typical middle-European region, characterized by its (mainly) rural nature and daily commuter movements towards metropolitan areas.

A basic reaction-diffusion model used for spatial COVID spread, which includes subdivisions for susceptibles, exposed, infected, recovered, and the total population, is used to describe the spatio-temporal spread of infections. The transmission rate, recovery rate, initial infected values, detection rate, and diffusivity rate are considered as parameters to be estimated using the reported daily data and least square fit. This work also features an emphasis on numerical methods which will be used to describe the diffusion on arbitrary two-dimensional domains. Two numerical optimization techniques for parameter fitting are used: the Metropolis algorithm and the adjoint method. Two different methods, the Crank-Nicholson method and a finite element method, which are used according to the requirements of the respective optimization

method are used to solve the PDE system. This way, the two methods are compared and validated and provide similar results with good approximation of the infected in both the district and the respective sub-districts.

7.1 Introduction

At the beginning of January 2020, the COVID-19 virus began to spread throughout mainland China, with the consequences that we all have experienced in the last three years. Initially, the number of cases was limited to single clusters in a limited number of locations, but later on expanded throughout the country. In previous studies, we have investigated the macroscopic impact of the epidemic using an *SIR*-model for all cases in Germany. For this, we have used classical differential models such as the *SEIRD-* (susceptible-exposed-infected-recovered-dead) models to describe the spread of infections during the first wave (cf. Heidrich et al. [2]), as well as the impact of travelers on disease dynamics in summer 2020 (cf. Schäfer et al. [3]), both with a strong emphasis on parameter estimation.

In this study, we aim to model the local spread of infections using PDE (partial differential equation) models to gain a better understanding of the diffusion on smaller scales. Viguerie et al. [4] argue that their geographical model simulations could be used to inform authorities to design effective measures and anticipate the allocation of important medical resources. Wang and Yamamoto [5] provide a forecasting model for COVID-19 using Google mobility data and PDE models, as well as find acceptable validity results of their model by comparison with COVID-19 data. Elsonbaty et al. [6] extend the classical models to a fractional *SITRS* model, including treated persons, while Ahmed et al. [7]. Kuehn and Mölter [8] investigate transport effects on epidemics using two coupled models, a static epidemic network and a dynamical transport network, also with non-local, fractional transport dynamics. They find that transport processes induce additional spreading ways and that way lowers the epidemic threshold; generalizing the process to fractional or non-local dynamics, however, raises the epidemic threshold. Logeshwari et al. [9] also provide a fractional PDE model of the spatial spread of COVID-19. Harris and Bodman [10] investigate the spread through a country with different regions of different densities. Another diffusion-based, non-international approach can be found in Berestycki et al.[11]. The authors find that fast diffusion effects along major roads are an important factor of the spread of epidemics like COVID-19 in Italy and HIV in the Democratic Republic of Congo. The work of Abboubakar et al. [12] does not only present a reaction-diffusion model for COVID-19 transmission and also applied them on cumulated data for the entire country of Germany, yet without comparison to local-scale data. Nawaz et al. [13] provide an explicit unconditionally stable scheme for the solution of a PDE model designed for the spread of COVID-19 and applied it on data for the Hubei province.

As we have seen, only few of the previous studies apply the theoretical models to practical examples, and mostly do not make use of regional or even local based medical data. A comparable inclusion of diffusion in compartmental models with a comparison to real data can be found in Grave et al. [14] A general challenge with diffusion-based PDE models is that diffusion of all compartments leads to unwanted diffusion in the total population, which we aim to avoid. We also present two different numerical methods in detail which are able to handle the diffusion on arbitrary two-dimensional domains.
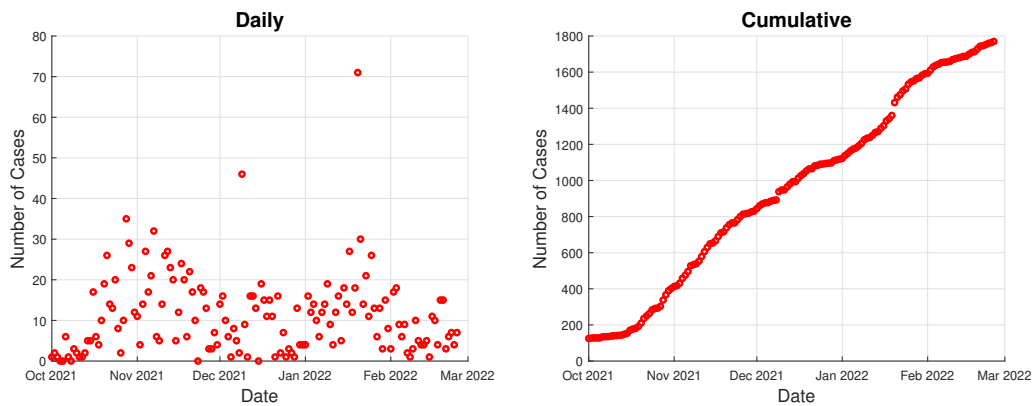
FIGURE 7.1: Confirmed new daily cases (left) and cumulative confirmed cases (right) with COVID-19 in Birkenfeld from October 1, 2020 until February 25, 2021 according to RKI [15].

In this study, we use data down to local level for parameter estimation of the model. We focus our numerical problem on a single district, the district of Birkenfeld in southwestern Germany within the state of Rhineland-Palatinate. Approximately 81,000 people live there in an area of about 780 km^2. The largest city within the district is Idar-Oberstein, with about 28,000 inhabitants in an area of about 92 km^2. The remaining people live in the municipalities of Birkenfeld, Baumholder, and Herrstein-Rhaunen. Within a 1.5 hour drive via federal highways and freeways, the following metropolitan areas can be reached: Mainz, Trier, Koblenz, Kaiserslautern, Saarbrücken, and Frankfurt. In addition, the Frankfurt-Hahn airport is located in the neighboring Rhein-Hunsrück district to the northeast. The region is very rural, with daily commuter movements common in the direction of the aforementioned metropolitan areas. The region is also visited by tourists due to the gemstone industry and trade in Idar-Oberstein, the numerous hiking routes, and the nearby Hunsrück-Hochwald-Nationalpark.

The first COVID-19 case in the district of Birkenfeld was confirmed in March 2020. Until the end of June 2020, there were only 90 registered cases in the entire district. However, the number of cases increased during the second wave in autumn/winter 2020/21, with a cumulative 2,513 cases confirmed until March 2021 [15]. As of October 2022, over 32,000 cases have been counted in the district. We restrict our research to the data from the second wave, since there was only a limited number of previous infections, but comparatively high infection numbers further on; also, no vaccines were available until the beginning of 2021, as well as a very small amount of persons having been exposed to the disease multiple times. Finally, the lockdown restrictions, particularly in November and December 2020, led to a slower mixing of cases between different districts. This inter-district mobility is not taken into account by our models. We consider daily infection data from the district and all of its municipalities in the time frame from October 1, 2020 to February 25, 2021. the cumulative number of infections in the district is depicted in Fig. 7.1. In this figure, the first step visible in the data between end of December and beginning of January is mainly caused by a delay of registration of case numbers due to Christmas holidays. The reasons for a second one in mid January are unknown and could be related to registration delays within the district. Note that there is only one detected initial infection case on October 1, situated in the city of Idar-Oberstein, so there were no detected cases in the rest of the entire district.

The possibility of new variants of the virus or future pandemics highlights the importance of modeling the spread of infections, particularly in their early stages when limited medical data is available. The accuracy of these models depends greatly on the used parameters and the corresponding data. In this study, we present *SEIRD*-models, which are commonly used in simulations, and estimate their parameters using data from the Robert-Koch-Institute (RKI) [15] and private communications with the Birkenfeld district government [16]. We perform estimations using both adjoint and Metropolis methods and base them on a least square fit between the model output and the reported data.

Structure of the paper.   In chapter 2, we provide the relevant epidemiological models as well as two schemes for the numerical solution of PDEs, the Crank-Nicholson method and a Finite Element Method. In chapter 3, we perform the numerical discretization and prepare the optimization of a specific target function. Also, both the Metropolis algorithm and the adjoint method are presented which will be used for the parameter estimation. In chapter 4, we present and compare the numerical solutions for both methods. Finally, in chapter 5, the results of this paper are discussed.

7.2   Materials and methods

7.2.1   PDE models

To model the spatial COVID spread in the presented areas, we use an epidemiological reaction-diffusion model. For this purpose, we consider a corresponding spatial area $(x, y) \in \Omega$ in a time period $t \in \mathcal{T} := [0, t_{end}]$. We are looking for a function $u : V \to \mathbb{R}^m$ with $V = \Omega \times \mathcal{T}$, which is twice continuously differentiable on Ω and once continuously differentiable on $\mathcal{T}$, briefly $u \in \mathcal{C}(V, \mathbb{R}^m)^{2,1}$. The following PDE system has to be fulfilled:

$$\partial_t u = \kappa \Delta_{x,y} u + f(u) \,, \tag{7.1a}$$

$$u = u_0 \,, \qquad\qquad t = 0 \,, \tag{7.1b}$$

$$\partial_\nu u = 0 \,, \qquad\qquad (x, y) \in \partial\Omega \,. \tag{7.1c}$$

Here, $\partial_t u$ stands for the component-wise derivative of u in the direction of time, i.e., $\partial_t u = (\partial_t u_1, ..., \partial_t u_m)^T$ and $\Delta_{x,y} = (\partial_{xx} u_1 + \partial_{yy} u_1, ..., \partial_{xx} u_m + \partial_{yy} u_m)^T$ for the Laplace operator in Ω. The parameter κ describes the diffusivity of the system and the function $f(u)$ contains the epidemiological component(s). As an initial condition, at time $t = 0$ a function $u_0 : \Omega \to \mathbb{R}^m$ is used with $u(x, y, t = 0) = u_0(x, y)$. In addition, Neumann boundary conditions are used, where $\partial_\nu u = (\partial_\nu u_1, ..., \partial_\nu u_m)^T$ stands for the derivative in the direction of the outward pointing unit normal ν and $\partial\Omega$ stands for the boundary of Ω. In terms of context, the latter means that no individual can leave or enter the territory Ω. This seems strange at first, since the district of Birkenfeld in practice can be left or entered by land. On the other hand, we are looking at data sets from a period when profound containment measures had already been taken in the region and social measures, including a significant reduction inter-district mobility, were already implemented.

For epidemiological modelling, we make use of a variant of the *SIR* model introduced by Kermack and McKendrick [17], the *SEIR*-model, and consider subdivisions as functions $S, E, I, R \in \mathcal{C}(V, \mathbb{R})^{2,1}$, which have the following meanings:

- Susceptibles *S*: Depending on the transmission route, these individuals can become infected with the infectious disease when contact occurs.

- Exposed *E*: The corresponding indiviuals have already ingested the pathogen, but are not yet infectious because they are still in the latency period.

- Infected *I*: These individuals are infected with the disease and infectious. Contact with a susceptible individual can therefore lead to transmission of the disease.

- Recovered *R*: After surviving an infection, individuals are considered recovered. These individuals can no longer transmit the disease or get infected.

For instance, $I(x, y, t)$ indicates the number of infected individuals in the spatial coordinate $(x, y) \in \Omega$ at time $t \in \mathcal{T}$. The total population is then defined as $N := S + E + I + R$. Based on these presented groups, different epidemiological models can now be derived. We present PDE systems of three common models in Tab. 7.1.

The derivation and precise functioning of spatial epidemiological models will not be explained in detail here; for this purpose, reference is made to e.g. Martcheva [18]. At the core of every epidemiological model is the so-called incidence term $\frac{\beta(t)}{N} SI$, which indicates how many individuals are newly infected with the disease in coordinate (x, y) at time t. The incidence term depends on a time dependent transmission rate $\beta : [0, t_{end}] \to \mathbb{R}^+$. In simple models, this can also be assumed to be a constant parameter, but we assume that the transmission rate may fluctuate over the observed periods due to the stepwise restrictions on the population. The value of the transmission rate β is generally unknown and must be adjusted using the data sets. Another parameter in the models is the recovery rate γ. This is the reciprocal of the time required on average for an individual to recover from the disease. Thus, if we assume that t is in days and an individual takes 10 days to recover, it holds $\gamma = \frac{1}{10}$. In addition, the *SEIR*-model contains the parameter θ, which is the reciprocal of the latency period, i.e. the time between the uptake of the pathogen into the body and the onset of infectiousness. For example, assuming three days, it holds $\theta = \frac{1}{3}$. It should be noted here that the latency period does not have to be congruent with the incubation period, as the latter indicates the period of time until the onset of the first symptoms. With regard to COVID-19 in particular, it has been shown that infectivity sets in even before the onset of symptoms (cf. He et al. [19]). Due to simplicity, we also chose $\kappa = \kappa_S = \kappa_E = \kappa_I = \kappa_R$. In the following, we will only make use of the *SEIR*-model for later data fitting because it turns out to reflect the epidemics closest.

In the first step, in order to omit a redundant equation, we substitute $R = N - S - E - I$ and thus reduce the system to an *SEI*-model. It should be noted, that also for N a PDE has to be solved:

$$\partial_t N = \kappa \Delta_{x,y} N \,, \tag{7.2a}$$

$$N = S_0 + E_0 + I_0 + R_0 \,, \qquad t = 0 \,, \tag{7.2b}$$

$$\partial_\nu N = 0 \,, \qquad (x, y) \in \partial\Omega \,. \tag{7.2c}$$

For this reason, we normalize the reduced *SEI*-model by dividing all rows by N, assuming that the population density mathematically fulfills $N(x, y, t) > 0$ on V. Defining $u_1 := \frac{S}{N}$, $u_2 := \frac{E}{N}$, $u_3 := \frac{I}{N}$, $u_4 := N$ and $u := (u_1, u_2, u_3, u_4)$, we obtain a system as in (7.1) with a function $f : \mathcal{C}(V, \mathbb{R}^4)^{2,1} \to \mathbb{R}^4$,

$$f(u) = \left(-\beta(t)u_1 u_3, \beta(t)u_1 u_3 - \theta u_2, \theta u_2 - \gamma u_3, 0\right)^T \,. \tag{7.3}$$

TABLE 7.1: Epidemiological subdivision models with flow chart and
PDE system.

Model	Structure	PDE-system
SIS		$\partial_t S = \kappa_S \Delta_{x,y} S - \dfrac{\beta(t)}{N} SI + \gamma I,$ $\quad S(t=0) = S_0;$ $\partial_t I = \kappa_I \Delta_{x,y} I + \dfrac{\beta(t)}{N} SI - \gamma I,$ $\quad I(t=0) = I_0;$ $\partial_\nu S = \partial_\nu I = 0,$ $\quad (x,y) \in \partial\Omega;$ $\quad N = S + I.$
SIR		$\partial_t S = \kappa_S \Delta_{x,y} S - \dfrac{\beta(t)}{N} SI,$ $\quad S(t=0) = S_0;$ $\partial_t I = \kappa_I \Delta_{x,y} I + \dfrac{\beta(t)}{N} SI - \gamma I,$ $\quad I(t=0) = I_0;$ $\partial_t R = \kappa_R \Delta_{x,y} R + \gamma I,$ $\quad R(t=0) = R_0;$ $\partial_\nu S = \partial_\nu I = \partial_\nu R = 0,$ $\quad (x,y) \in \partial\Omega;$ $\quad N = S + I + R.$
SEIR		$\partial_t S = \kappa_S \Delta_{x,y} S - \dfrac{\beta(t)}{N} SI,$ $\quad S(t=0) = S_0;$ $\partial_t E = \kappa_E \Delta_{x,y} E + \dfrac{\beta(t)}{N} SI - \theta E,$ $\quad E(t=0) = E_0;$ $\partial_t I = \kappa_I \Delta_{x,y} I + \theta E - \gamma I,$ $\quad I(t=0) = I_0;$ $\partial_t R = \kappa_R \Delta_{x,y} R + \gamma I,$ $\quad R(t=0) = R_0;$ $\partial_\nu S = \partial_\nu E = \partial_\nu I = \partial_\nu R = 0,$ $\quad (x,y) \in \partial\Omega;$ $\quad N = S + E + I + R.$

Tab. 7.2 summarizes the results for the presented models without the equation for N.

TABLE 7.2: Summary of $f(u)$ for the reduced and normalized models.

$SIS \to I$	$f: \mathcal{C}(V, \mathbb{R})^{2,1} \to \mathbb{R}, \quad f_1(u) = \beta(t)(1-u)u - \gamma u$
$SIR \to SI$	$f: \mathcal{C}(V, \mathbb{R}^3)^{2,1} \to \mathbb{R}^2, \quad f_{1-2}(u) = \begin{pmatrix} -\beta(t)u_1 u_2 \\ \beta(t)u_1 u_2 - \gamma u_2 \end{pmatrix}$
$SEIR \to SEI$	$f: \mathcal{C}(V, \mathbb{R}^4)^{2,1} \to \mathbb{R}^3, \quad f_{1-3}(u) = \begin{pmatrix} -\beta(t)u_1 u_3 \\ \beta(t)u_1 u_3 - \theta u_2 \\ \theta u_2 - \gamma u_3 \end{pmatrix}$

To meaningfully include the biological context, it must hold $\gamma, \theta > 0$ and $\kappa \geq 0$ and, as initial condition, $u_0 \geq 0$ in Ω. In addition, we assume that there are infected individuals in the area Ω, i.e. $\int_\Omega I_0 \, d\omega > 0$. For the reduced and normalized *SEI*-model, it must then hold $\int_\Omega u_{3,0} \, d\omega > 0$, using the notation $u_j(x, y, 0) := u_{j,0}$. The notation $\mathcal{N}_0 := \int_\Omega N(x, y, 0) \, d\omega$ represents the total number of individuals at time $t = 0$ in Ω. It must be valid that $\mathcal{N}_0 > 0$. Moreover, we define the total population in the area Ω at time t as $\mathcal{N} : [0, t_{end}] \to (0, +\infty)$ with $\mathcal{N}(t) := \int_\Omega N(x, y, t) \, d\omega$. Due to Neumann boundary conditions, we receive using the Gauss theorem

$$\partial_t \mathcal{N} = \int_\Omega \partial_t N \, d\omega = \int_\Omega \kappa \, \Delta_{x,y} N \, d\omega = \int_{\partial\Omega} \kappa \, \partial_\nu N \, ds = 0. \tag{7.4}$$

Thus, the total population in the domain Ω is constant with respect to time. Analytically, there exists a unique solution for each of the PDE systems (7.1) with the presented $f(u)$ in Table 7.2 in conjunction with the mentioned preconditions [20].

Due to the formulation using diffusion for the total population, an equilibrium will only set in when the population density in the entire district is equal. Then, the temporal equilibrium will be analogous to the equilibrium of the system without diffusion.

As already mentioned, certain parameters of the model are known, such as γ and θ. The transmission rates β_j and the diffusivity κ are usually unknown. For the transmission rate, we assume that the time-dependancy is piecewise constant. Due to 'light' lockdown restrictions from November 2, 2020, and 'stricter' restrictions from December 17, 2020 to the end of the observed time interval, we assume three different time intervals as follows:

$$\beta(t) = \begin{cases} \beta_0, & 0 \leq t < t_0, \\ \beta_1, & t_0 \leq t < t_1, \\ \beta_2, & t_1 \leq t \leq t_{end}. \end{cases} \tag{7.5}$$

In addition, due to noisy data sets, the initial conditions u_0 must also be adjusted. For that, we present two approaches to solve this in the following sections.

7.2.2 Crank-Nicholson method for the SEIR-model

For this purpose, we discretize the region Ω in x and y directions in equal equidistant step sizes h_x and h_y, respectively. Also, the time interval $\mathcal{T} = [0, t_{end}]$ is divided into equidistant steps of length τ. In the following we use the notation $u_{i,j}^n = u(x_j, y_i, t_n)$.

The Laplacian is expressed by finite differences

$$\Delta u_{i,j}^n = \frac{1}{h_x^2}\left[u_{i,j-1}^n - 2u_{i,j}^n + u_{i,j+1}^n\right] + \frac{1}{h_y^2}\left[u_{i-1,j}^n - 2u_{i,j}^n + u_{i+1,j}^n\right] \tag{7.6}$$

and the Crank-Nicolson scheme reads as

$$\frac{u_{i,j}^{n+1} - u_{i,j}^n}{\tau} = \frac{1}{2}\left[\kappa\Delta u_{i,j}^{n+1} + \kappa\Delta u_{i,j}^n + f(u_{i,j}^{n+1}) + f(u_{i,j}^n)\right] . \tag{7.7}$$

The goal is to transform this approach so that $u_{i,j}^{n+1}$ can be solved with a linear system of equations. The non-linearity of $f(u)$ is solved by evolving f using Taylor expansion for small values τ around the current iteration value $u_{i,j}^n$ with $f(u_{i,j}^{n+1}) = f(u_{i,j}(t^n + \tau))$:

$$f(u_{i,j}(t^n + \tau)) = f(u_{i,j}^n) + \tau\partial_u f(u_{i,j}^n)\partial_t u_{i,j}^n + \mathcal{O}(\tau^2)$$

$$\approx f(u_{i,j}^n) + \tau\partial_u f(u_{i,j}^n)\left[\kappa\Delta u_{i,j}^n + f(u_{i,j}^n)\right] \tag{7.8}$$

If we set $r_x := \kappa\tau/h_x^2$ and $r_y := \kappa\tau/h_y^2$, this leads in eqn. (7.7) using eqn. (7.8) to

$$u_{i,j}^{n+1} - \frac{1}{2}r_x\left[u_{i,j-1}^{n+1} - 2u_{i,j}^{n+1} + u_{i,j+1}^{n+1}\right] - \frac{1}{2}r_y\left[u_{i-1,j}^{n+1} - 2u_{i,j}^{n+1} + u_{i+1,j}^{n+1}\right]$$

$$= u_{i,j}^n + \frac{1}{2}r_x\left[u_{i,j-1}^n - 2u_{i,j}^n + u_{i,j+1}^n\right] + \frac{1}{2}r_y\left[u_{i-1,j}^n - 2u_{i,j}^n + u_{i+1,j}^n\right]$$

$$+ \tau f(u_{i,j}^n) + \frac{1}{2}\tau^2\partial_u f(u_{i,j}^n)\left[\kappa\Delta u_{i,j}^n + f(u_{i,j}^n)\right] . \tag{7.9}$$

Thus, $\frac{1}{2}\tau^2\partial_u f(u_{i,j}^n)\left[\kappa\Delta u_{i,j}^n + f(u_{i,j}^n)\right]$ is negligible for small values of τ, which leads to the system

$$-\frac{1}{2}r_x u_{i,j-1}^{n+1} - \frac{1}{2}r_x u_{i,j+1}^{n+1} + (1 + r_x + r_y)u_{i,j}^{n+1} - \frac{1}{2}r_y u_{i-1,j}^{n+1} - \frac{1}{2}r_y u_{i+1,j}^{n+1}$$

$$= \frac{1}{2}r_x u_{i,j-1}^n + \frac{1}{2}r_x u_{i,j+1}^n + (1 - r_x - r_y)u_{i,j}^n + \frac{1}{2}r_y u_{i-1,j}^n + \frac{1}{2}r_y u_{i+1,j}^n + \tau f(u_{i,j}^n). \tag{7.10}$$

The system (7.10) leads to a linear equation system

$$Aq_{n+1} = Bq_n + \tau f_n \tag{7.11}$$

with, e.g., $q_{n+1} = \left([u_{0,0}^{n+1}, ..., u_{l_y,0}^{n+1}], [u_{0,1}^{n+1}, ..., u_{l_y,1}^{n+1}], ..., [u_{0,l_x}^{n+1}, ..., u_{l_y,l_x}^{n+1}]\right)^T$. The vectors q_n and f_n are defined analogously, where l_x and l_y indicate the number of discretization points in x and y direction with respect to Ω. The square and non singular matrices A and B are defined to contain the Neumann boundary conditions, which are implemented by, e.g. $u_{k+1,j}^{n+1} = u_{k,j}^{n+1}$ if $u_{k,j}^{n+1}$ lies on the boundary of the domain $\partial\Omega$. The previous refers to the solution of the PDE system of the state variable u. The adjoint system must be solved backwards in time, which leads to the approach

$$\frac{z_{i,j}^{n-1} - z_{i,j}^n}{-\tau} = -\frac{1}{2}\left[\kappa\Delta z_{i,j}^{n-1} + \kappa\Delta z_{i,j}^n + p(u_{i,j}^{n-1}) + p(u_{i,j}^n)\right] \tag{7.12}$$

where the $p(u_{i,j}^n)$ contains componentwise the corresponding discretized terms of $\partial_{u_j} g + \sum_{k=1}^{m} z_k \partial_{u_j} f_k$. Proceeding analogously as before yields the system

$$
-\frac{1}{2} r_x z_{i,j-1}^{n-1} - \frac{1}{2} r_x z_{i,j+1}^{n-1} + (1 + r_x + r_y) z_{i,j}^{n-1} - \frac{1}{2} r_y z_{i-1,j}^{n-1} - \frac{1}{2} r_y z_{i+1,j}^{n-1}
$$
$$
= \frac{1}{2} r_x z_{i,j-1}^{n} + \frac{1}{2} r_x z_{i,j+1}^{n} + (1 - r_x - r_y) z_{i,j}^{n} + \frac{1}{2} r_y z_{i-1,j}^{n} + \frac{1}{2} r_y z_{i+1,j}^{n} + \tau p(u_{i,j}^n). \quad (7.13)
$$

Thus, when solving the linear system of equations, the matrices A and B can also be used, due to the same Neumann boundary conditions. Despite the variety of possible solutions to reaction-diffusion problems, we have chosen the Crank-Nicolson method at this point in order to test the method with a standard procedure. With regard to the stability of the procedure, reference is made to Oishi et al. [21]. Analogous investigations with Neumann boundary conditions indicate that the method is numerically stable. In the case of our parameter sizes we therefore have $r_x, r_y < \frac{1}{2}$.

7.2.3 Finite element method for the SEIR-model

An alternative to the Crank-Nicholson method which is used in the adjoint method, we also present a version of the finite element method which produces similar results. By plugging eqn. (7.3) in eqn. (7.1), the PDE system reads as follows:

$$
\begin{aligned}
\partial_t u_1 &= \kappa \, \Delta_{x,y} u_1 - \beta(t) u_1 u_3, & (x,y) &\in \Omega; & (7.14a)\\
\partial_v u_1 &= 0, & (x,y) &\in \partial\Omega;\\
u_1(t = 0) &= u_{1,0};\\
\partial_t u_2 &= \kappa \, \Delta_{x,y} u_2 + \beta(t) u_1 u_3 - \theta u_2, & (x,y) &\in \Omega; & (7.14b)\\
\partial_v u_2 &= 0, & (x,y) &\in \partial\Omega;\\
u_2(t = 0) &= u_{2,0};\\
\partial_t u_3 &= \kappa \, \Delta_{x,y} u_3 + \theta u_2 - \gamma u_3, & (x,y) &\in \Omega; & (7.14c)\\
\partial_v u_3 &= 0, & (x,y) &\in \partial\Omega;\\
u_3(t = 0) &= u_{3,0};\\
\partial_t u_4 &= \kappa \, \Delta_{x,y} u_4 & (x,y) &\in \Omega; & (7.14d)\\
\partial_v u_4 &= 0, & (x,y) &\in \partial\Omega;\\
u_4(t = 0) &= u_{4,0}.
\end{aligned}
$$

As the diffusion and ODE parts in eqns. (7.14) are handled by two different schemes, we can make use of an *operator splitting* (cf. MacNamara [22]) to solve the system. E.g., for one time step Δt, this procedure is as follows:

(1) Solve $\partial_t u_i = \kappa \, \Delta_{x,y} u_i$ for $t = \frac{\Delta t}{2}$ with the corresponding initial and boundary conditions for $i = 1, 2, 3, 4$.

(2) Solve $\partial_t u_i = f_i(u)$ for $t = \Delta t$ with the corresponding initial and boundary conditions for $i = 1, 2, 3, 4$.

(3) Solve $\partial_t u_i = \kappa \, \Delta_{x,y} u_i$ for $t = \frac{\Delta t}{2}$ with the corresponding initial and boundary conditions for $i = 1, 2, 3, 4$.

The equation in (2) is a simple ODE equation which can be solved by any standard solver, e.g. the Euler method or the method of Runge-Kutta. To solve the equation in (1) and (3) on the domain Ω with initial and homogeneous Neumann boundary

conditions on $\partial\Omega$, we consider its weak form gained by multiplication with a test function $v \in H_0^1(\Omega)$; this means, that v vanishes at the boundary, i.e., $v \equiv 0$ at $\partial\Omega$. The weak form reads as follows:Instead of $u \in \mathcal{C}^{2,1}$, we now aim to find a function $u_i \in H^1(\Omega)$ solving

$$
\begin{aligned}
a(u_i, v) &:= \int_\Omega u_i \, v \, d\omega + \int_\Omega \nabla u_i \, \nabla v \, d\omega - \int_{\partial\Omega} u_i \, v \, d\lambda \\
&= \int_\Omega u_i \, v \, d\omega + \int_\Omega \nabla u_i \, \nabla v \, d\omega \\
&= 0.
\end{aligned}
\tag{7.15}
$$

This infinite-dimensional problem has to be solved numerically by discretization. We aim to find a solution $u_{i,h}$ in a finite-dimensional subspace V_h solving

$$
a(u_{i,h}, v_h) = a_1(u_{i,h}, v_h) + a_2(u_{i,h}, v_h) = \int_\Omega u_{i,h} \, v_h \, d\omega + \int_\Omega \nabla u_{i,h} \, \nabla v_h \, d\omega = 0. \tag{7.16}
$$

We define the subspace V_h on the chosen grid and linearly independent basis functions ϕ_j piecewise over subregions $\Omega_k = [x_1, x_2] \times [y_1, y_2] \subset \Omega$:

$$
V_h = \left\{ u_h = \sum_k \sum_{j=1}^4 c_j^{(k)} \, \phi_j^{(k)}(x, y) \right\} \tag{7.17}
$$

where

$$
\phi_1^{(k)}(x, y) = \frac{(x - x_2)(y - y_2)}{(x_1 - x_2)(y_1 - y_2)}, \tag{7.18a}
$$

$$
\phi_2^{(k)}(x, y) = \frac{(x - x_2)(y - y_1)}{(x_1 - x_2)(y_2 - y_1)}, \tag{7.18b}
$$

$$
\phi_3^{(k)}(x, y) = \frac{(x - x_1)(y - y_2)}{(x_2 - x_1)(y_2 - y_2)}, \tag{7.18c}
$$

$$
\phi_4^{(k)}(x, y) = \frac{(x - x_1)(y - y_1)}{(x_2 - x_1)(y_2 - y_1)} \tag{7.18d}
$$

for $(x, y) \in \Omega_k$; otherwise, those functions vanish, i.e., $\phi_j^{(k)}(x, y) \equiv 0$ for $(x, y) \notin \Omega_k$, $j = 1, 2, 3, 4$. Then the weak form $a(u_{i,h}, v_h) = 0$ reads as follows:

$$
a(u_{i,h}, v_h) = a\left(\sum_k \sum_{j=1}^4 c_j^{(k)} \, \phi_j^{(k)}(x, y), \, \phi_{j*}^{(k*)}(x, y) \right) = 0. \tag{7.19}
$$

Due to the linearity of a, we have $\sum_k \sum_{j=1}^4 a\left(\phi_j^{(k)}(x, y), \, \phi_{j*}^{(k*)}(x, y) \right) c_j^{(k)} = 0$. Then, the stiffness matrices A and B are defined by

$$
A_{nm} = a_1\left(\phi_j^{(k)}(x, y), \, \phi_{j*}^{(k*)}(x, y) \right), \tag{7.20a}
$$

$$
B_{nm} = a_2\left(\phi_j^{(k)}(x, y), \, \phi_{j*}^{(k*)}(x, y) \right), \tag{7.20b}
$$

where n represents the row corresponding to (j^*, k^*) and m the column corresponding to (j, k), which depends on the chosen order within the matrices. More information

about this can e.g. be found in Evans et al. [23]. The linear equation system with a mass matrix

$$A\,\partial_t u_i + B\,u_i = 0 \tag{7.21}$$

can be solved by any scheme; e.g., a 4-step Runge-Kutta scheme; cf. e.g. Dormand and Prince [24].

7.3   Optimization and numerical methods

7.3.1   Discretization of the domain

To define the domain Ω for the partial differential equation model, we consider the geographical data for the district (D), the association communities (AC) and the municipalities (M). Using the free online data filtering tool *Overpass Turbo* [25] from *OpenStreetMap*, we extracted the relevant geographical data and created the relevant matrices assuming the map segment as rectangular, which appears reasonable due to the very small size of the investigated window. The relevant data for the starting values of the locations are then equally distributed across all relevant subdomains of Ω. The size of the window is $L_x \times L_y = 39.23$ km $\times$ 56.05 km. Using a step size of $h_x = \frac{L_x}{100}$ and $h_y = \frac{L_y}{100}$, the discretization of the area yields 101×101 matrices as depicted in Figs. 7.2 and 7.3.

7.3.2   Target function

In the following, we present the analysis for the reduced *SEI*-model. The derivation for the other models is analogous. Furthermore, in order to avoid confusion, we rename $(u_s, u_e, u_z, u_N) := (u_1, u_2, u_3, u_4)$. The objective of this section is to present two methods for data fitting of the presented models to the dataset of Birkenfeld County in Germany.

   Therefore, we introduce an objective function $J : \mathbb{R}^d \times \mathcal{C}(\Omega, \mathbb{R}^m)^{2,1}$ (i.e., twice continuously differentiable wrt space and once continously differentiable wrt time), defined by

$$J\,(\chi, u_0) = \frac{w_0}{2} \|\delta\beta(t)u_s u_z - u_z^{data}\|_{L_V^2}^2 + \frac{w_1}{2}\|\chi - \tilde{\chi}\|_2^2 + \frac{w_2}{2}\sum_{j=1}^{m}\|u_{I,j,0} - u_{I,j,0}^{data}\|_{L_\Omega^2}^2. \tag{7.22}$$

This type of objective function has already been proven to be effective in previous studies for adapting reaction-diffusion models to corresponding data sets, see Heidrich et al. [26]. On the one hand we make use of the L^2-norm with respect to V and Ω, defined for example by $\|g\|_{L_X^2} = \left(\int_X g^2 dx\right)^{1/2}$, on the other hand we use the Euclidean norm $\|x\|_2 = \left(\sum_{j=1}^{d} x_j^2\right)^{1/2}$.

   The L_V^2-norm in J involves fitting the model u to the respective data sets, whereby $u_z^{data} : V \to \mathbb{R}^m$ is an interpolation through the data points. Interpolation is performed linearly with respect to the time axis for each grid point. We decided to fit the model to the data point by point in the L_V^2 norm. The reason for this is the necessary analysis in the adjoint method in subsection 7.3.5.

   The Euclidean norm in the objective function corresponds to a regularization term and contains the parameters of the model u, which have to be fitted to the data.

For example, if we assume an unknown constant transmission rate $\beta(t) \equiv \beta$ and a diffusivity κ, we have $\chi = (\beta, \kappa, \delta)$.
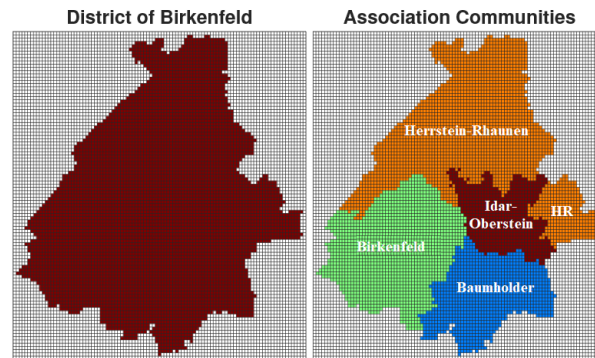
FIGURE 7.2: Discretizations of the district of Birkenfeld (left) and of its association communities (right).
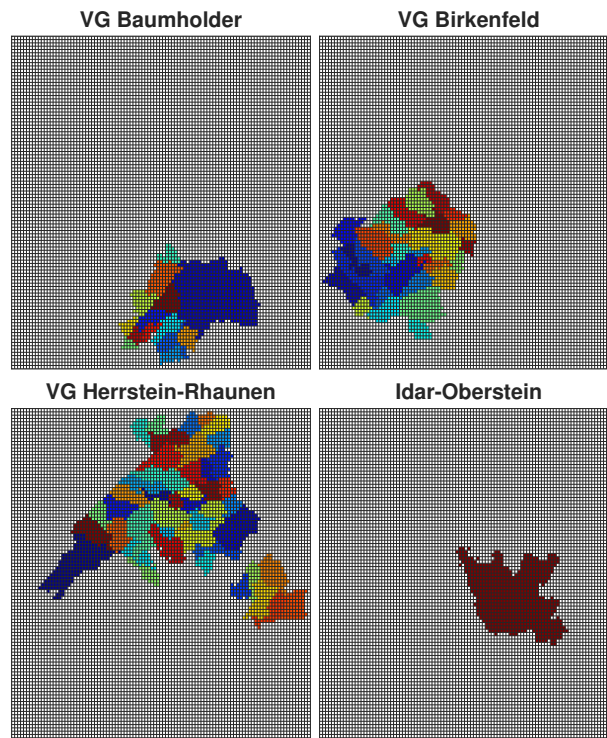
FIGURE 7.3: Discretization of all municipialities in the district of Birkenfeld; upper left: VG Baumholder, upper right: VG Birkenfeld, lower left: VG Herrstein-Rhaunen, lower right: city of Idar-Oberstein, which is classified as one municipiality.

Note, that we only use informations concerning the daily reported new infected individuals. Thus, the data include the percentage of daily new infected individuals which shall be fitted to the incidence term $\beta(t)u_s u_z$ in the reduced and normalized *SEI*-model. In addition, one must assume that only a fraction of those actually infected are reported. Therefore, we introduce a detection rate δ, which is unknown.

The L_Ω^2-norms are to match the initial conditions of u to the corresponding initial guess $u_{j,0}^{data}$, which is in the following simulations assumed to be 0. The same applies to the initial guess of $\tilde{\chi}$.

In addition, the objective function includes weights w_j with $j = 0, 1, 2$, whose choice will be explained later. The goal is now to minimize J while satisfying the model constraints, i.e.,

$$\min_{\chi, u_0} J, \qquad \text{subject to PDE system (7.1).} \tag{7.23}$$

7.3.3 Parameter bounds and initial values

Allowing the following respective constraints of the fitted parameters:

$$[\beta_j, \kappa, u_0, \delta] \in [\mathbb{R}^+, [0,1], \mathbb{R}_+^4, [0,1]], \tag{7.24}$$

the starting values at time t_0 for the detected cumulated infected u_0^3 can be taken from the statistics, while we assume no initial recovered person $u_0^4 = 0$ and, for the initial amount of exposed persons, $u_0^2 = u_0^3/2$ with similar reasoning as in [2]. The initial number of infected is then defined as $I_0 = u_0^1 + u_0^2 + u_0^3 + u_0^4$.

TABLE 7.3: Orders of magnitude of the initial values for adapting the model to the available data, which are chosen from pretesting several parameter choices.

param.	β_j	δ	κ	u_0^1	u_0^2	u_0^3	u_0^4
init. val.	0.1	0.5	0.1	$1/N_1$	$1/N_2$	$1/N_3$	$3/N_4$

7.3.4 Metropolis algorithm

The first presented method makes use of a Metropolis algorithm (cf. Metropolis et al. [27], Gelman et al. [28] or Gilks et al. [29]) for estimation of parameters in the PDE system (7.14) according to the procedure described in Schäfer and Götz [30] and Heidrich, Schäfer et al. [2]. Using the parameter set u_0 as of Tab. 7.3 as starting conditions, we assign random draws u_{new} from a normally distributed (and thus symmetric) proposal function q, i.e. $u_{new} \sim q(u_{new}|u_{i-1})$, in every iteration i.

Using the previously defined $\hat{J}(u)$ as of eqn.(7.22) as the target distribution, we calculate the approximative distribution by

$$\pi(u) = c \cdot \exp\left(-\frac{\hat{J}(\hat{u})^2}{2\sigma^2}\right), \tag{7.25}$$

whereby c is an arbitrary real value and σ the standard deviation of the prior. For the acceptance probability, it follows

$$p(\hat{u}_{new}|u_{i-1}) = \min\left\{1, \frac{\pi(\hat{u}_{new}) \cdot q(u_{i-1}|u_i)}{\pi(\hat{u}_i) \cdot q(\hat{u}_i|\hat{u}_{i-1})}\right\} = \min\left\{1, \frac{\pi(\hat{u}_{new})}{\pi(u_i)}\right\}. \tag{7.26}$$

In eqn. (7.26), we can see that the value of c is redundant, as it cancels out in the division. If the sample is accepted with the probability p, we set $\hat{u}_i = \hat{u}_{new}$; with the probability $1 - p$, the sample is declined, meaning $\hat{u} = \hat{u}_{i-1}$ according to Rusatsi [31] or Schäfer and Götz [30]. For parameter estimation using the Metropolis algorithm, we use Algorithm 6.

Algorithm 6 Pseudocode for the Metropolis algorithm.

1: $\pi, \hat{u}^{\text{data}} \leftarrow$ load initial values for π and data
2: $x, z \leftarrow$ solve PDE for state variable
3: $\hat{J} \leftarrow$ compute objective function regarding π
4: $\sigma \leftarrow$ standard distribution of the solution, i.e. I over time
5: $s \leftarrow$ set step size (standard deviation) for the algorithm, e.g. $s := \pi/100$
6: **repeat**
7:     $\pi_{old} \leftarrow \pi$ from previous draw
8:     $\pi_{new} \leftarrow \pi \sim \mathcal{N}(\pi_{old}, s)$
9:     $x, z, J(\hat{\pi}_{new}) \leftarrow$ update depending on π
10:     $\alpha \leftarrow \min\left\{1, \exp\left(\hat{J}(\pi_{old})^2 - \hat{J}(\pi_{new})^2/2\sigma^2\right)\right\}$
11:     $\pi_{new} \leftarrow \hat{\pi}_{new}$ with probability α and $\pi_{new} := \pi$ with probability $1 - \alpha$
12: **until** maximum value of draws is reached
13: $\pi^*, x^*, \hat{J}^* \leftarrow$ means of all π, x, J

7.3.5   Parameter estimation via adjoint functions

For parameter estimation via adjoint functions $z \in \mathcal{C}(V, \mathbb{R}^m)^{2,1}$ we use them in conjunction with a Lagrange function defined as $\mathcal{L} : \mathbb{R}^d \times \mathcal{C}(\Omega, \mathbb{R}^m)^{2,1} \times \mathcal{C}(V, \mathbb{R}^m)^{2,1} \times \mathcal{C}(V, \mathbb{R}^m)^{2,1} \to \mathbb{R}$, fulfilling

$$\mathcal{L}(\chi, u_0, u, z) = J(\chi, u_0) + \sum_{j=1}^{m} \int_V z_j \left(f_j(u) + \kappa \Delta_{x,y} u_j - \partial_t u_j\right) d\omega dt. \qquad (7.27)$$

At a possible minimum $(\chi_*, u_{0*}, u_*, z_*)$ of problem (7.23) must apply

$$0 = \nabla \mathcal{L} = \left(\partial_{\chi_1}\mathcal{L}, ..., \partial_{\chi_d}\mathcal{L}, \partial_{u_{1,0}}\mathcal{L}, \ldots, \partial_{u_{m,0}}\mathcal{L}, \partial_{u_1}\mathcal{L}, \ldots, \partial_{u_m}\mathcal{L}, \partial_{z_1}\mathcal{L}, \ldots, \partial_{z_m}\mathcal{L}\right). \quad (7.28)$$

The derivatives in directions representing functions are determined with the help of Gâteaux derivatives. The application of the optimal control theory as well as Pontryagin's maximum (minimum) principle provide the optimality conditions listed as follows:

- $0 = \partial_{\chi_k}\mathcal{L}$ for $k = 1, \ldots, d$ (scalar optimality condition),

- $u_{j,0} = u_{j,0}^{data} - \frac{z_j(x,y,0)}{w_2}$ for $j = 1, \ldots, m$ (optimal initial conditions),

- $\partial_t z_j = -\left(\partial_{u_j} g + \sum_{k=1}^{m} z_k \partial_{u_j} f_k + \kappa \Delta_{x,y} z_j\right)$, where $g := \frac{w_0}{2}\left(\delta\beta(t)u_s u_z - u_z^{data}\right)^2$ (adjoint equations),

- $z = 0$ for $t = t_{end}$ (transversality conditions),

- $\partial_\nu z = 0$ for $(x, y) \in \partial\Omega$ (Neumann boundary conditions).

It should be noted that the present conditions are given as g for the reduced *SEI*-model. The adjoint equations PDE system has be solved numerically backward in time. Let us assume a time-dependent transmission rate of the form of eqn. (7.5). This leads to $\chi = (\beta_0, \beta_1, \beta_2, \kappa, \delta)$. Let $\mathcal{I}_0 = [0, t_0]$, $\mathcal{I}_1 = [t_0, t_1]$ and $\mathcal{I}_2 = [t_1, t_{end}]$ for $k = 0, 1, 2$.

The corresponding gradient then reads as follows:

$$\partial_{\beta_k}\mathcal{L} = w_1\left(\beta_k - \tilde{\beta}_k\right) + \int_{\mathcal{I}_k}\int_{\Omega} w_0\delta u_s u_z\left(\delta\beta(t)u_s u_z - u_z^{data}\right) + (z_2 - z_1)\,u_s u_z\,d\omega\,dt\,,$$
$$\tag{7.29a}$$

$$\partial_{\kappa}\mathcal{L} = w_1\left(\kappa - \tilde{\kappa}\right) + \sum_{j=1}^{3}\int_V z_j\Delta_{x,y}u_j\,d\omega\,dt\,,\tag{7.29b}$$

$$\partial_{\delta}\mathcal{L} = w_1\left(\delta - \tilde{\delta}\right) + w_0\int_V \beta(t)u_s u_z\left(\delta\beta(t)u_s u_z - u_z^{data}\right)\,d\omega\,dt\,.\tag{7.29c}$$

The adjoint equations in this case read as

$$\partial_t z_1 = -\left(w_0\delta\beta(t)u_z\left(\delta\beta(t)u_s u_z - u_z^{data}\right) + (z_2 - z_1)\,\beta(t)u_z + \kappa\Delta_{x,y}z_1\right)\,,\tag{7.30a}$$

$$\partial_t z_2 = -\left(\theta\left(z_3 - z_2\right) + \kappa\Delta_{x,y}z_2\right)\,,\tag{7.30b}$$

$$\partial_t z_3 = -\left(w_0\delta\beta(t)u_s\left(\delta\beta(t)u_s u_z - u_z^{data}\right) + (z_2 - z_1)\,\beta(t)u_s - \gamma z_3 + \kappa\Delta_{x,y}z_3\right)\,.\tag{7.30c}$$

For parameter estimation, we use Algorithm 7. Regarding the optimization of χ, a Quasi-Newton Broyden-Fletcher-Goldfarb-Shanno (BFGS) search direction is used. The initial condition u_0 is updated with a convex combination between the old value and current 'optimal' value. The step size is mediated by the Armijo stepsize rule. In each optimization step, the PDE system for the state u and adjoint z variable must be solved. This is done by the Crank-Nicholson method presented above. The fact that the state variable must be solved forward and the adjoint variable backward in time also leads to the term "forward-backward sweep method".

Algorithm 7 Pseudocode for the parameter estimation via adjoint functions.

1: $\beta_k, \kappa, \delta, u_z^{DATA}, u_0^{data} \leftarrow$ load initial values and data
2: $u, z \leftarrow$ solve PDE for state variable and adjoint function
3: $J, \nabla J \leftarrow$ compute objective function and gradient regarding $\chi = (\beta_0, ..., \beta_k, \kappa, \delta)$

4: $s_1 \leftarrow$ compute search direction regarding χ (Quasi-Newton (BFGS))
5: $s_2 \leftarrow (\tilde{u}_0 - u_0)$ compute search direction for u_0 with $\tilde{u}_{j,0} = u_{j,0}^{data} - \frac{z_j(x,y,0)}{w_2}$
6: **repeat**
7:    $J_{old} \leftarrow J$
8:    $\alpha \leftarrow 1$
9:    $\chi \leftarrow \chi + \alpha s_1$
10:   $u_0 \leftarrow u_0 + \alpha s_2$
11:   $u, J \leftarrow$ update
12:   **repeat**
13:     $\alpha \leftarrow 0.5\alpha$
14:     $\chi \leftarrow \chi + \alpha s_1$
15:     $u_0 \leftarrow u_0 + \alpha s_2$
16:     $u, J \leftarrow$ update
17:   **until** $J \leq J_{old} + 0.001\alpha s^T\nabla J_{old}$ (Armijo Rule)
18:   $z, \nabla J, s_1, s_2 \leftarrow$ update
19: **until** $\frac{\|J - J_{old}\|_2}{\|J_{old}\|_2} < \text{TOL}$

7.4   Numerical results

The numerical computations were both done with MATLAB (the Metropolis algorithm) and PYTHON (the adjoint method). All codes are available on request.

7.4.1   Without penalty term (Metropolis)

Using the Metropolis algorithm as of chapter 7.3.4, we first set $w_0 = 1$ and $w_1 = w_2 = 0$ in eqn. (7.22). In Fig. 7.4, the results for the district of Birkenfeld and in Fig. 7.5, the results for the four ACs are presented; the red dots represent the respective data, the blue line the outcome of the model.

FIGURE 7.4: Result of the optimization with the Metropolis algorithm
for the district of Birkenfeld with $w_1 = w_2 = 0$.

FIGURE 7.5: Result of the optimization with the Metropolis algorithm
for the lower level administrative units (Verbandsgemeinden) with
$w_1 = w_2 = 0$.

7.4.2 With penalty term

We now include a penalty term; in eqn. (7.22) we choose $w_0 = 1$ and $w_1 = w_2 = 1 \cdot 10^{-5}$. This guarantees a *convex* problem, cf. Heidrich, Schäfer et al. [2]. Additionally, by pretesting various values, we aimed to find a reasonably large value of $w_1 = w_2$ such that the summands in the target function as of eqn. (7.22), including w_0, w_1, and w_2, respectively, are of the same magnitude. In Fig. 7.6, the results for the district of Birkenfeld and in Fig. 7.7, the results for the four associated communities are presented; the red dots represent the respective data, the blue line the outcome of the model. We also compare the results to those of a standard *SEIR*-model with the usual parameter estimation (using the Metropolis algorithm).
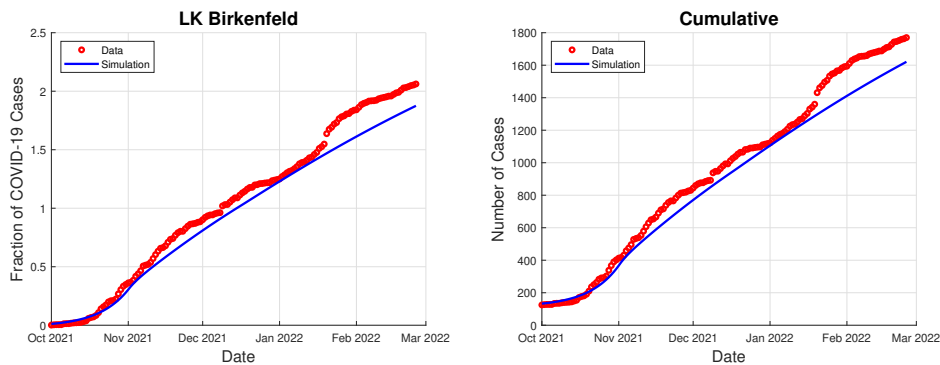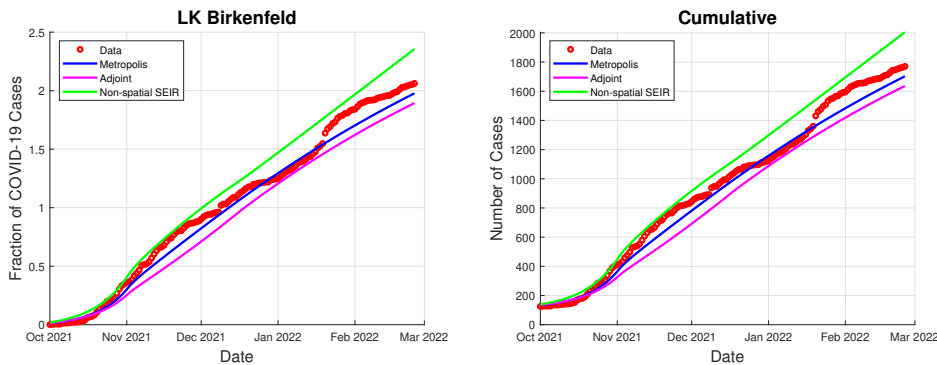

FIGURE 7.6: Result of the optimization with the various methods for the district of Birkenfeld with $w_1 = w_2 = 10^{-5}$.
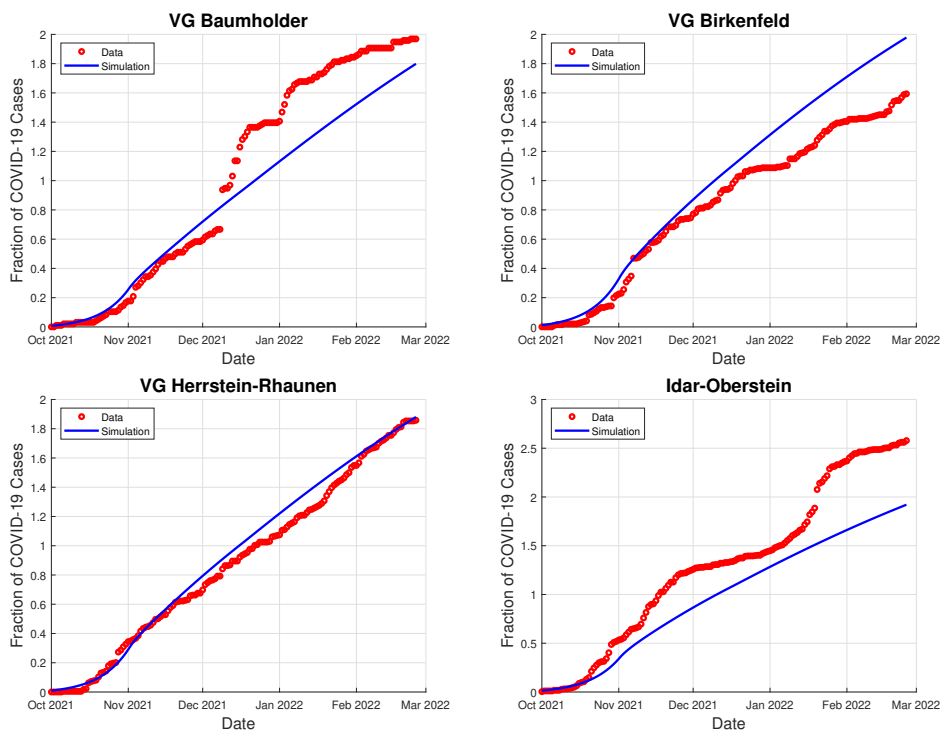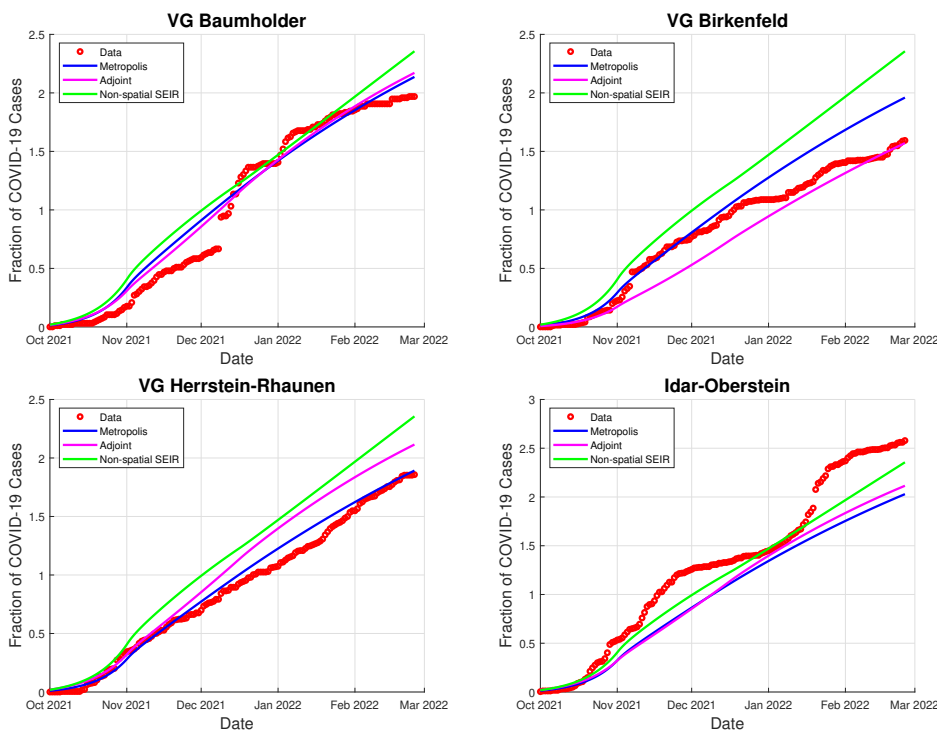

FIGURE 7.7: Result of the optimization with the various methods for the lower level administrative units (Verbandsgemeinden) with $w_1 = w_2 = 10^{-5}$.

7.4.3   Comparison

In the results of the parameter estimation as shown in Tab. 7.4, as well as the target function values for the different methods. The comparison of the absolute values of $J(u)$, e.g. within the Metropolis simulations for $w_1 = w_2 = 0$ and $w_1 = w_2 = 10^{-5}$, is not useful; however, the outcomes of the different models can be compared using the value of J.

TABLE 7.4: Results for the Metropolis algorithm and the adjoint method, compared to an *SEIR*-model without diffusion. For the Metropolis simulations, the standard deviation is given as an addition.

$w_1 = w_2$	Metropolis 0	Metropolis 10^{-5}	Adjoint 10^{-5}	*SEIR* 10^{-5}
β_0	$(0.228 \pm 0.005)\ \mathrm{d}^{-1}$	$(0.218 \pm 0.011)\ \mathrm{d}^{-1}$	$0.202\ \mathrm{d}^{-1}$	0.206
β_1	$(0.097 \pm 0.003)\ \mathrm{d}^{-1}$	$(0.099 \pm 0.003)\ \mathrm{d}^{-1}$	$0.109\ \mathrm{d}^{-1}$	0.092
β_2	$(0.103 \pm 0.029)\ \mathrm{d}^{-1}$	$(0.097 \pm 0.027)\ \mathrm{d}^{-1}$	$0.097\ \mathrm{d}^{-1}$	0.105
κ	0.119 ± 0.004	0.100 ± 0.005	0.102	0.000
I_0^{BA}	3.393 ± 0.077	2.629 ± 0.101	4.007	4.139
I_0^{BI}	11.570 ± 1.183	4.424 ± 0.258	3.275	8.441
I_0^{HR}	10.176 ± 0.276	4.753 ± 0.2615	6.350	9.632
I_0^{IO}	20.681 ± 0.682	8.024 ± 0.291	14.630	12.207
δ	0.202 ± 0.005	0.495 ± 0.010	0.397	0.444
$J(u)$	0.4829	0.4836	0.4850	0.4858

It is notable that across all simulations, we find $\beta_1 \approx \beta_2$, which indicates that the more severe lockdown restrictions from December 17 onwards might be overlaid by the rising number of festivities during Christmas. The adjustment regarding the detection rate shows that, according to the model, the actual number of infected people is approximately three to five times higher than registered, which is in line with previous findings.

The parameter values for the transmission parameters β_i are relatively consistent across the different methods and parameter settings. The values $\beta_0 > \beta_1 \approx \beta_2$ show that the so-called 'light' lockdown in November 2020 had the most significant effect on the case values, while the more 'severe' lockdown before Christmas did not have a significant effect. A reason for this can be Christmas itself during which the amount of contacts has risen by nature, it also has to be noted that the measurement of case numbers during or after Christmas was not consistent, which might lead to delays in the infection data.

The parameter κ is ranging significantly between 0.05 and 0.12, but correlations to the higher initial values of the infected, as well as the detection rate δ, vary across the different methods and parameter settings, depending not only on the weights w_1 and w_2 but also the chosen κ. The results indicate that there is some potential variation in the optimal parameter values and parameter cross-correlation of parameters, e.g. of the initial infection values and the detection rate, as well as to some extent in the diffusivity. This can also be seen in the target function $J(u)$ which, despite the deviations, shows only minor variations among the different methods and parameter settings.

The estimations for some of the districts is generally quite accurate, e.g., for Herrstein-Rhaunen and Baumholder. However, for the city of Idar-Oberstein, the area with most infections, the model underestimates the infection cases, which can be explained by the diffusivity of the model that neglects the urban structures. On

the other side, the model overestimates the infection cases in Birkenfeld. In total, the amount of infected is slightly underestimated towards the end; some (perhaps technical) jumps in the middle of the observed time interval cannot be represented well in the chosen models.

For a convex target function and a weight choice of $c = 10^{-5}$, the Metropolis algorithm provides the most accurate results for the cumulative data. Compared to the *SEIR*-model without diffusion, we see that both Metropolis and adjoint methods provide better target function values than the *SEIR*-model, which generally overestimates the infections in all districts except the largest (Idar-Oberstein).

7.5 Discussion

We present a reaction-diffusion model used to simulate the spatial spread of COVID-19, making use data down to the municipality level for parameter estimation. The *SEIR*-model is based on a set of PDEs that describe the dynamics of susceptible, exposed, infected, and recovered individuals, as well as an incidence term that represents the transmission of the disease. The optimal control is based on a least square fit between the model output and the reported daily data. Two different numerical approaches for the estimation of parameters and approximation of the infection data – the Metropolis algorithm and the adjoint method – were described in detail and implemented on some existent medical data, and their results were plotted and compared.

Regarding the graphical and numerical results, all routines have provided meaningful results. The models depict the infection values quite accurately in several subdistricts, yet slightly over- or underestimate them in others, which can partially be explained by non-homogeneous behaviour of cities compared to rural areas. On a local level, the quality of the estimations decreases – which is as expected, as it cannot be assumed that a global model will apply perfectly to the behavior of single villages, especially as some of them had no or less than a handful of detected infected in the observed time interval. The parameter values, including initial infection values, detection rate, and diffusivity, vary across different methods and parameter settings, while the transmission-related parameters remain relatively consistent, and the target function are very similar. Compared to a non-spatial *SEIR*-model, both Metropolis and adjoint method provide better results with respect to the target function $J(u)$.

The PDE model provides valuable insights and information and manages to describe the diffusion in the epidemiological situation – i.e., very few and locally condensed initial cases in a more or less completely susceptible population. The results in this article suggest that PDE models for the spread of diseases are reasonable tools, which is underpinned by the comparison with the local medical data. The Metropolis and the adjoint methods, coupled by different numerical techniques for the solution of PDEs, lead to similar results and are very similar in terms of the approximation error.

Further refinement of the model or the use of additional data sources may improve its accuracy in the future. Nevertheless, the accuracy of the model on district and sub-district levels make it a valuable tool for understanding the spread of infections. Not only new variants of COVID-19, but also the possibility of future pandemics underscore the need for accurate modeling on local level.

Declarations

Competing interests

The authors declare that there exist no competing interests.

Acknowledgements

We would like to thank Karsten Schultheiß and his staff at Department 1 for Central Tasks and Issues of the Birkenfeld County. The department, among other things, is responsible for press and public relations and provided us with the data used.

Authors' contributions

All authors contributed a significant part and reviewed the manuscript.

Bibliography

[1] Schäfer, M., Heidrich, P., and Götz, T. "Modelling the Spatial Spread of COVID-19 in a German District using a Diffusion Model". In: *Mathematical Biosciences and Engineering* 20.12 (2023). DOI: 10.3934/mbe.2023940.

[2] Heidrich, P. et al. "The COVID-19 outbreak in Germany – Models and Parameter Estimation". In: *Commun. Biomath. Sci.* 3 (2020), pp. 37–59. DOI: 10.5614/cbms.2020.3.1.5.

[3] Schäfer, M. et al. "The impact of travelling on the COVID-19 infection cases in Germany". In: *BMC Infectious Diseases* 2.455 (2022). DOI: 10.1186/s12879-022-07396-1.

[4] Viguerie, A. et al. "Simulating the spread of COVID-19 via a spatially-resolved susceptible–exposed–infected–recovered–deceased (SEIRD) model with heterogeneous diffusion". In: *Appl Math Lett.* 111.106617 (2021). DOI: 10.1016/j.aml.2020.106617.

[5] Wang, H. and Yamamoto, N. "Using a partial differential equation with Google Mobility data to predict COVID-19 in Arizona". In: *Mathematical Biosciences and Engineering* 17.5 (2020), pp. 4891–4904. DOI: 10.3934/mbe.2020266.

[6] Elsonbaty, A. et al. "Dynamical Analysis of a Novel Discrete Fractional SITRS Model for COVID-19". In: *Fractals* 29.08 (2021). DOI: 10.1142/S0218348X21400351.

[7] Ahmed, N. et al. "Numerical simulation and stability analysis of a novel reaction–diffusion COVID-19 model". In: *Nonlinear Dynamics* 106(2) (2021), pp. 1293–1310. DOI: 10.1007/s11071-021-06623-9.

[8] Kuehn, C. and Mölter, J. "The influence of a transport process on the epidemic threshold". In: *Journal of Mathematical Biology* 85.62 (2020), pp. 37–59. DOI: 10.1007/s00285-022-01810-7.

[9] Logeswari, K., Ravichandran, C., and Nisar, K.S. "Mathematical model for spreading of COVID-19 virus with the Mittag–Leffler kernel". In: *Numerical Methods for Partial Differential Equations* (2020), pp. 1–16. DOI: 10.1002/num.22652.

[10] Harris, P.J. and Bodmann, B.E.J. "A mathematical model for simulating the spread of a disease through a country divided into geographical regions with different population densities". In: *Journal of Mathematical Biology* 85.32 (2022). DOI: 10.1007/s00285-022-01803-6.

[11] Berestycki, H., Roquejoffre, J.-M., and Rossil, L. "Propagation of Epidemics Along Lines with Fast Diffusion". In: *Bull. Math. Biol.* 83.2 (2020). DOI: 10.1007/s11538-020-00826-8.

[12] Abboubakar, H., Racke, R., and Schlosser, N. *A Reaction-diffusion Model for the Transmission Dynamics of the Coronavirus Pandemic with Reinfection and Vaccination Process*. Konstanzer Schriften in Mathematik. KOPS Universität Konstanz, 2023.

[13] Nawaz, Y. et al. "An explicit unconditionally stable scheme: application to diffusive COVID-19 epidemic model". In: *Advances in Difference Equations* 363 (2021). DOI: 10.1186/s13662-021-03513-7.

[14] Grave, M. et al. "Assessing the Spatio-temporal Spread of COVID-19 via Compartmental Models with Diffusion in Italy, USA, and Brazil S.I. : Modeling and Simulation of Infectious Diseases". In: *Archives of Computational Methods in Engineering* 28 (2021), pp. 4205–4223. DOI: 10.1007/s11831-021-09627-1.

[15] Robert-Koch-Institute. *Corona fact sheet.* https://www.rki.de/DE/Content/InfAZ/N/Neuartiges_Coronavirus/Steckbrief.html. last visited: 18 December, 2023.

[16] *Privat communication with Dipo Aldila, Department of Mathematics, University of Indonesia, Depok.*

[17] Kermack, W.O. and McKendrick, A.G. "Contributions to the mathematical theory of epidemics-I. 1927." In: *Bull. Math. Biol.* 53 (1991), pp. 33–55. DOI: 10.1098/rspa.1927.0118.

[18] Martcheva, M. *An introduction to mathematical epidemiology.* Springer, 2015.

[19] He, X. and Lau, E.H.Y. and Wu, P. and Deng, X. and Wang, J. and Hao, X. and Lau, Y.C. and Wong, J.Y. and Guan, Y. and Tan, X. and Mo, X. and Chen, Y. and Liao, B. and Chen, W. and Hu, F. and Zhang, Q. and Zhong, M. and Wu, Y. and Zhao, L. and Zhang, F. and Cowling, B.J. and Li, F. and Leung, G.M. "Temporal dynamics in viral shedding and transmissibility of COVID-19". In: *Nat. Med.* 26 (2020), pp. 672–675. DOI: 10.1038/s41591-020-0869-5.

[20] Britton, N. *Reaction-Diffusion Equations and Their Applications to Biology.* London: Academic Press, 1986.

[21] Oishi, C.M. et al. "Stability analysis of Crank-Nicolson and Euler schemes for time-dependent diffusion equations". In: *BIT Numerical Mathematics* 55 (2015), pp. 487–513. DOI: 10.1007/s10543-014-0509-x.

[22] MacNamara, S. and Strang, G. "Operator Splitting". In: *Splitting Methods in Communication, Imaging, Science, and Engineering.* Ed. by Glowinski, R., Osher, S., and Yin, W. Springer, Cham, 2016, pp. 95–114.

[23] Evans, G., Blackledge, J., and Yardley, P. *Numerical Methods for Partial Differential Equations.* London: Springer, 1999.

[24] Dormand, J.R.. and Prince, P.J. "A family of embedded Runge-Kutta formulae". In: *Journal of Computational and Applied Mathematics* 6.1 (1980), pp. 19–26.

[25] Overpass-Turbo. https://overpass-turbo.eu/.

[26] Heidrich, P. and Götz, T. "Parameter Estimation via Adjoint Functions in Epidemiological Reaction-Diffusion Models". In: *Progress in Industrial Mathematics at ECMI 2021.* Vol. 39. Springer, Cham, 2022, pp. 115–122. DOI: 10.1007/978-3-031-11818-0_16.

[27] Metropolis, N. et al. "Equation of State Calculations by Fast Computing Machines". In: *J.Chem. Phys.* 21 (1953), pp. 1087–1092. DOI: 10.1063/1.1699114.

[28] Gelman, A. et al. *Bayesian Data Analysis, 2nd Edition.* London: Chapman and Hall, 1996.

[29] Gilks, W.R., Richardson, S., and Spiegelhalter, D.J. *Markov chain Monte Carlo in Practice.* London: Chapman and Hall/CRC, 1996.

[30] Schäfer, M. and Götz, T. "Modelling Dengue Fever Epidemics in Jakarta". In: *Int. J. Appl. Comput. Math* 6 (2020). DOI: 10.1007/s40819-020-00834-1.

[31] Rusatsi, D.N. "Bayesian analysis of SEIR epidemic models". last visited: 18 December, 2023. PhD thesis. Lappeenranta University of Technology, 2015.

Chapter 8

An Integro-Differential Model for the Spread of Diseases

This article by Moritz Schäfer, Karol Niedzielewski, Thomas Götz and Tyll Krüger has been uploaded as a preprint to *arXiv* in July 2023, referred to as [1]. The theory, formulation and numerical calculations of the integro-differential model were done by Moritz Schäfer. Thomas Götz provided the idea for this work, as well as some concepts and linguistic revisions. Karol Niedzielewski contributed the part with agent-based model. Tyll Krüger provided several ideas and advice as well as the idea of the proof for the uniqueness of the solutions. The format is changed to meet the thesis standard.

Abstract

In this work, we study the optimal control for the mitigation of epidemic diseases on regional levels. Therefore, we make use of a spatial susceptible-infected-recovered (*SIR*-) model which is enhanced by an integral kernel, allowing for non-homogeneous mixing between susceptibles and infectives. We define requirements for the kernel function and derive analytical results for the *SIR*-model, especially the uniqueness of solutions.

An associated control function is aimed to mimic conditions similar to lockdown criteria during the COVID-19 epidemics, including hypothetical economic costs. In order to optimize the balance between disease containment and the social and political costs associated with lockdown measures, we set up requirements for the implementation of control function, and show examples for three different formulations for the control: continuous and time-dependent, continuous and space- and time-dependent, and piecewise constant space- and time-dependent. The latter represent reality more closely, as the control cannot be updated for every time and location and mitigation measures cannot be continuous. We found the optimal control values for all of those setups, which are by nature best for a continuous and space-and time dependent control, yet as well found reasonable results for the discrete (and more realistic) setting.

The numerical results of the integro-differential model are compared to an established agent-based model that incorporates social and other microscopical factors more accurately. This shows that comparatively simple models can be transferred to more realistic, complex models and used in proxy manner for optimization purposes. Inversely, complex models can be used as benchmark for the integro-differential approach; a close match between the results of both models validates the integro-differential model as an efficient macroscopic proxy. Since computing an optimal

control strategy for agent-based models is computationally very expensive, yet comparatively cheap for the integro-differential model, using the proxy model methodology could become a useful tool for policy advices regarding pandemic preparedness.

8.1   Introduction

Since first cases have appeared in December 2019, COVID-19 has shown that there is an increasing value in accurate models for the local and global spread of diseases, also giving advice to policy makers on how to deal with them; cf. e.g. Bracher et al. [2, 3], Sherratt et al. [4] and Priesemann et al. [5]. Country and region based statistics from many countries show that regionally contained cases can spread throughout the country in a short period of time, especially during the initial phase(s) of the disease in spring and summer 2020. Countrywide and regional lockdowns and other social restrictions were imposed in most European countries as a result in order to contain the infection numbers, to relieve the strain on the health system, and to reduce the amount of severely ill or dead, yet were hardly on a scientific basis.

The local or regional spread of infections has been adressed in many previous works. Kuehn and Mölter [6] investigate transport effects on epidemics using two coupled models, a static epidemic network and a dynamical transport network, also including non-local, fractional transport dynamics. They find that transport processes induce additional spreading ways and that way lowers the epidemic threshold; generalising the process to fractional or non-local dynamics, however, raises the epidemic threshold. In several papers, the local spread of infections is modelled by partial differential equations (PDE) models. Viguerie et al. [7] argue that geographical model simulations could be used to inform authorities to design effective measures and anticipate the allocation of important medical resources. Wang and Yamamoto [8] provide a forecasting model for COVID-19 using Google mobility data and PDE models, and find acceptable validity results of their model by comparison with medical data. A fractional PDE modelling of the spatial spread of COVID-19 can be found in Logeshwari et al. [9], where a system is designed in order to predict the outcome of viral spreading in India. Harris and Bodman [10] investigate the spread through a country with different regions of different densities. A diffusion-based and non-international approach can be found in Berestycki et al. [11]. The authors find that fast diffusion effects along major roads are an important factor of the spread of epidemics like COVID-19 in Italy and HIV in the Democratic Republic of Congo. Schäfer and Heidrich [12] analyze the local spread of COVID-19 infections in a German district by another susceptible-exposed-infected-recovered (SEIR) model including PDEs. The inclusion of diffusion in compartmental models can also e.g. be found in Grave et al. [13]. Domoshnitsky et al. [14] study a model of the spread of the COVID-19 pandemic in the form of a system of integro-differential equations. Integro-differential models, as shown for Italy in Salvadore et al. [15] and the united Kingdom in Hritonenko et al. [16], including mitigation measures and a time-dependent transmission rate, and where able to describe the local disease dynamics well.

How well intervention measures actually work is still an open or widely discussed question, and very little is done in optimal control of epidemics and mitigation strategies. By optimal control, we mean the mitigation strategy that fulfills desired constraints (e.g., limits on hospitalization beds) and minimizes political or economical costs, that can be expressed in a quantitative manner. We perceive the topic as very important for assembling of preparedness plans that can be motivated and educated by simulation, as well as for a responsive manner usage, when a wide

spread of pathogen is present and fast, reliable alleviation is required. The EU commission has made a decision regarding European preparedness plans which shall be strongly coordinated with country pandemic plans [17, 18]; also, the WHO planned an international treaty for pandemic preparedness which shall become mandatory for all member states [19]. This work aims to present a toolbox contributing to the optimization of mitigation strategies, which those plans can make use of.

In this article, after setting up a classical susceptible-infected-recovered (*SIR*) model and several theoretical findings, our focus is not on the optimization of the model with respect to medical data or parameter estimation, but toward the optimal control of measures. It is aimed to contain the disease as much as possible, yet on the other side, we also consider the social and political costs of a lockdown, especially when case numbers are (comparatively) low, while attention has to be paid to not overload the health capacities and other problems like Long-COVID or economic burdens given large infection numbers. In order to validate our results, we compare the outcomes to those of an established agent-based model for Poland [20]. The results of this study can act as a framework for disease control in future pandemics.

Structure of the paper. In chapter 2, an *SIR* model is enhanced by an integral kernel. We define several requirements for this kernel function and present a proof for the uniqueness of solutions for the model. Lockdowns and other measures are included in our model(s) by a control function, which can be optimized under various assumptions, making use of three different control functions: a time-dependent, a continuous space- and time-dependent, and a piecewise constant space- and time-dependent control. In the following chapter 3, we define the required target function for the optimization of the "lockdown" control and present the corresponding Forward-Backward method. The agent-based model, in which social factors can be implemented more accurately, is described in chapter 4. The macroscopic outcome of our model is compared to those of the microscopic agent-based model in chapter 5, which we interpret as a kind of 'ground truth'. If the results of both match well enough, we can see our integro-differential model as a macroscopic proxy model for the computationally expensive agent-based model. Finally, in chapter 6, we discuss our results and present an outlook on future work.

8.2 Integro-differential SIR model

8.2.1 Model formulation

The basis of our model is the *SIR*-model introduced by Kermack and McKendrick [21] consisting of the subdivisions S, I, R, which have the following meanings:

- Susceptibles S: Depending on the transmission route, these individuals can become infected with the infectious disease when contact occurs.

- Infected I: These individuals are infected with the disease and infectious. Contact with a susceptible individual can therefore lead to transmission of the disease.

- Recovered R: After surviving an infection, individuals are considered recovered. These individuals can no longer transmit the disease or get infected.

The total number of individuals $N = S + I + R$ is assumed to be constant. We normalize the three subdivisions S, I, and R by dividing all rows by N, resulting

in $s := \frac{S}{N}$, $z := \frac{I}{N}$, $r := \frac{R}{N}$ with $s + z + r = 1$ (in order to avoid confusion, we use a different lower case letter z instead of i). Following the model by Kermack and McKendrick, we assume the pathogen is transmitted from infected persons to susceptible persons at a time-independent rate $\beta > 0$ and a recovery rate of $\gamma > 0$ so that loss of infectivity is gained after γ^{-1} days. Then, replacing $s = 1 - z - r$, the relative *sir*-model for each time point $t \in [0, T] \subset \mathbb{R}$ and point in space $x \in [0, 1]^n \subset \mathbb{R}^n$ as follows:

$$\frac{d}{dt}z(t, x) = \beta(1 - z - r)z - \gamma z \qquad\qquad z(t = 0, x) = z_0(x) \qquad (8.1a)$$

$$\frac{d}{dt}r(t, x) = \gamma z \qquad\qquad\qquad\qquad r(t = 0, x) = r_0(x) \qquad (8.1b)$$

This means that the disease dynamics in a certain point x would entirely depend on the initial relations z_0 and r_0 and the parameters β and γ. To include interaction between the spatial points, we replace the factor z in the term $\beta(1 - z - r)z$ by an integral kernel function $k(t, x - y)$ which depends on the time and the distance between x and y:

$$\frac{d}{dt}z(t, x) = \beta(1 - z - r)\int_0^1 z(t, y)\,k(t, x - y)\,dy - \gamma z \quad z(t = 0, x) = z_0(x) \quad (8.2a)$$

$$\frac{d}{dt}r(t, x) = \gamma z \qquad\qquad\qquad\qquad\qquad\qquad r(t = 0, x) = r_0(x) \quad (8.2b)$$

For the purpose of reasonable modelling of scenarios, the kernel k should consist of three terms as follows:

- an *space-dependent* part $a(x - y)$ which is monotonously decreasing wrt $|x - y|$, e.g., an exponential function decreasing with the distance, i.e., $a(x - y) = c\,e^{-\delta|x-y|}$. This part can be controlled with

- a *control function $u(t) \in \mathcal{U} = C([0, 1])$* which represents the effectiveness of non-pharmaceutical interventions (lockdown, school closings, obligation of wearing masks etc.). Here, $u(t) \equiv 0$ implies no regulations and $u(t) \equiv 1$ implies total lockdown.

- a *non-adjustable* part k^* which represents the fraction of transmission or a kind of 'background noise' you cannot control, e.g. serving as a first proxy for household related infections. We also assume that this fraction does not depend on the spatial distance as interactions between distances can be prevented by political or social measures. For a more detailed view on the importance of households, cf. Dönges et al. [22].

These considerations lead to this formula for the kernel k:

$$k(t, x - y) = (1 - u(t)) \cdot a(x - y) + k^* \qquad (8.3)$$

For the following, assume that the kernel is independent of time t, i.e. $u(t)$ is constant over time. No loss of generality is effected when considering the case, reducing $k(t, x - y)$ to $k(x - y) = a(x - y) + k^*$ for the upcoming. The following assumptions regarding the interaction kernel k should be met:

1. k is continuous.

2. k is non-negative.

3. $k(0) = k^* > 0$.

4. k is monotonically decreasing wrt $|x - y|$.

5. $k_1 := \|k\|_1 = \int_0^1 k(r)\,dr > 0$

6. $k_1 < K = \max_{x \in [0,1]} \int_0^1 k(|x - y|)\,dy$

Note, that in case of a strict monotonically decreasing kernel, we get $K = 2\int_0^{1/2} k(r)\,dr$.

8.2.2 Uniqueness of solutions

The existence and quality of equilibria of the integro-differential model is the main question in this subsection. Even for the comparatively 'simple' *SIS*-model in the previous section, it is not possible to proof the uniqueness of equilibria using classical fixpoint theory (cf. App. A). However, we can find satisfying results for uniqueness even for the *SIR*-model using the prevalence. Again, wlog, we will consider the time-independent kernel function, i.e., $k(x - y)$.

Lemma 8.1. For the *SIR*-model (8.2), there exists exactly one equilibrium.

Proof. To proof those numerical findings for the integro-differential SIR-model (8.1), we will compute its prevalence for $s_0 = s(0, x) \approx 1$ and $r_0 = r(0, x) \equiv 0$. Reconsider the equation for the susceptibles, i.e.,

$$\frac{ds}{dt} = -s\int_0^1 k(t, x - y)z(t, y)dy. \tag{8.4}$$

By substituting of the equation $\frac{dr}{dt} = \gamma z$, we obtain

$$\frac{ds}{dt} = -\frac{s}{\gamma}\int_0^1 k(t, x - y)\frac{dr}{dt}\,dy = -\frac{s}{\gamma}\frac{d}{dt}\int_0^1 k(t, x - y)\,r(y)\,dy. \tag{8.5}$$

Integrating this over t, it follows

$$\ln s_\infty = -\frac{1}{\gamma}\int_0^1 k_\infty(x - y)r_\infty(y)\,dy. \tag{8.6}$$

Now let T_k be the integral operator on a (generalized) ground space (S, μ), whereas $S = [0, 1]$ and $\mu(y) = y$, be defined by

$$(T_k f)(x) = \int_0^1 k_\infty(x - y)\,f(y)\,dy. \tag{8.7}$$

Together with the necessary condition $1 = s_\infty(x) + r_\infty(x)$ for all $x \in [0, 1]$, we find

$$r_\infty(x) = 1 - \exp\left(-\frac{1}{\gamma}\int_y k_\infty(x - y)\,r_\infty(y)\right)\,dy = 1 - \exp(-T_k r_\infty(x)). \tag{8.8}$$

This system of nonlinear equations can e.g. be solved numerically. Uniqueness can be shown using the paper of Bollobás-Janson-Riordan [23]: Following their Theorem 6.1, if

$$\|T_k\| := \sup\{\|T_k f\|_2 : f \geq 0, \|f\|_2 \leq 1\} < 1, \tag{8.9}$$

the equation only has the zero solution; if $1 \leq \|T_k\| < \infty$, and k_∞ is irreducible, then the equation has a unique non-zero solution for the prevalence.

This uniqueness result for the prevalence can be transferred to the uniquess of the solution: Assume there exist two solutions (s_1, z_1, r_1) and (s_2, z_2, r_2) with the same initial conditions, which have the same prevalence r_∞. Consider the difference function $\tilde{z}(t) := (z_1 - z_2)(t)$ which must satisfy $\tilde{z}(0) = 0$. Then the solution is $z(t, x) \equiv r(t, x) \equiv 0$, and the two solutions are equal. $\qquad\square$

As an addition, this provides a nice definition for basic reproductive number $\mathcal{R}_0$: By plugging this ansatz using the next-generation method [24], we find $\mathcal{R}_0 = \frac{\beta}{\gamma} \|k\|_2$, so that it also depends on the kernel function $k : [0,1] \to \mathbb{R}$.

8.3 Optimization

8.3.1 Time-dependent control

In this article, we restrict our research on the case $n = 1$; higher-dimensional models will be introduced in future research. In a first formulation of the optimal control problem, we aim to minimize the total amount of infectives, along keeping the costs, i.e. the control $u(t)$, as low as possible. In order to maintain convexity of the problem and avoid bang-bang controls due to linearity in u, the cost function term is squared. Also, case numbers should be kept under a certain threshold $z_{\max}$, otherwise the capacities of the medical infrastructure can be exceeded. This could be either modelled locally, i.e., $z(t, x) \leq z_{\max,1}$ or globally, i.e., $\int_0^1 z(t, x)\, dx \leq z_{\max,2}$. If $z_{\max,1} \leq z_{\max,2}$ for all x, the two terms fall together, which is also assumed here for the sake of simplicity. Defining $\mathcal{U}$ as the set of continuous functions $u \in \mathcal{U} = \mathcal{C}([0, T])$, we find the following minimization problem:

$$
\min_{u(t)\in\mathcal{U}} J(u,z) = \min_{u(t)\in\mathcal{U}} \int_0^T \int_0^1 z(t,x)\, dx\, dt + \frac{\eta}{2} \int_0^T u^2(t)\, dt
$$
$$
\text{subject to} \qquad 0 \leq u(t) \leq 1, \tag{8.10}
$$
$$
z(t,x) \leq z_{\max}.
$$

For implementation of the constraint $z < z_{\max}$, we add a sigmoidal term $\psi : [0,1] \to \mathbb{R}^+$ in the cost functional, which holds $\psi(z > 0) \approx 0$ and $\psi(z < 0) \gg 1$. Using the function $\psi(z - z_{\max})$, case numbers $z > z_{\max}$ are 'punished' severely. Also, if case numbers are low, we aim to 'punish' larger values for $u(t)$ because social restrictions are less accepted by the population and the political costs to implement harder restrictions increase. We therefore also define a threshold $z_{\min}$ under which political costs are assumed to be high, i.e., $\psi(z > z_{\min})$, such that case numbers $z < z_{\min}$ are also punished severely. This results in the following maximization problem:

$$
\min_{u(t)\in\mathcal{U}} J(u,z) = \int_0^T \int_0^1 z(t,x)\, dx\, dt + \frac{\eta}{2} \int_0^T u^2(t) \int_0^1 \left[1 + \frac{c_1}{2} \psi(z_{\min} - z(t,x)) \right] dx\, dt
$$
$$
+ \frac{\omega}{2} \int_0^T \int_0^1 c_2 \psi(z(t,x) - z_{\max})\, dx\, dt \tag{8.11}
$$
$$
\text{subject to} \qquad 0 \leq u(t) \leq 1.
$$

Alternatively, the control u can also depend on space, i.e., let $\tilde{\mathcal{U}}$ be the set of continuous functions $u \in \mathcal{U} = \mathcal{C}([0, T] \times [0, 1] \to [0, 1])$. Then the minimization problem reads

as follows:

$$\min_{u(t) \in \mathcal{U}} J(u, z) = \int_0^T \int_0^1 z(t, x) \, dx \, dt + \frac{\eta}{2} \int_0^T \int_0^1 u^2(t, x) \left[1 + \frac{c_1}{2} \psi \left(z_{min} - z(t, x) \right) \right] dx \, dt$$

$$+ \frac{\omega}{2} \int_0^T \int_0^1 c_2 \psi \left(z(t, x) - z_{max} \right) dx \, dt \tag{8.12}$$

subject to $\quad 0 \leq u(t, x) \leq 1$.

On a discrete level, solving the above minimization problems might be complicated. On a continuous level, we can introduce the Lagrangian function (see also Lenhart and Workman [25] for further information):

$$\mathcal{L}(z, u, r) = \int_0^T \int_0^1 \lambda_1(t, x) \left[z'(t, x) - (1 - z(t, x) - r(t, x)) \int_0^1 z(t, y) \, k(t, x - y) \, dy + \gamma z(t, x) \right] dx \, dt$$

$$+ \int_0^T \int_0^1 \lambda_2(t, x) \left[r'(t, x) - \gamma z(t, x) \right] dx \, dt \tag{8.13}$$

$$- J(z, u)$$

We now want to find the stationary points of the partial derivatives of $\mathcal{L}$ with respect to u, z, and r:

$$\frac{\partial \mathcal{L}}{\partial u} = \int_0^T \left\{ \int_0^1 \lambda_1(t, x) \left(1 - z(t, x) - r(t, x) \right) \int_0^1 z(t, y) \, a(x - y) \, dy \right.$$

$$\left. - \eta \, u(t) \int_0^1 \left[1 + \frac{c_1}{2} \psi \left(z_{min} - z(t, x) \right) \right] dx \right\} dt \qquad \overset{!}{=} 0$$

$$\tag{8.14a}$$

$$\frac{\partial \mathcal{L}}{\partial z} = \int_0^T \int_0^1 \left\{ -\lambda_1'(t, x) + \lambda_1(t, x) \int_0^1 z(t, y) \, k(t, x - y) \, dy \right.$$

$$- \lambda_1(t, x) \left(1 - z(t, x) - r(t, x) \right) \int_0^1 k(t, x - y) \, dy + \gamma \lambda_1(t, x)$$

$$- \gamma \lambda_2(t, x)$$

$$\left. - 1 + \frac{c_1 \, \eta}{4} u^2(t) \cdot \psi' \left(z_{min} - z(t, x) \right) - \frac{c_2 \, \omega}{2} \psi' \left(z(t, x) - z_{max} \right) \right\} dx \, dt \quad \overset{!}{=} 0$$

$$\tag{8.14b}$$

$$\frac{\partial \mathcal{L}}{\partial r} = \int_0^T \int_0^1 \left\{ \lambda_1(t, x) \int_0^1 z(t, y) \, k(t, x - y) \, dy \right.$$

$$\left. - \lambda_2'(t, x) \right\} dx \, dt \qquad \overset{!}{=} 0$$

$$\tag{8.14c}$$

For the second and third equation we swapped the integrals and performed partial integration with respect to time t. This leads us to the following system:

$$z'(t,x) = (1 - z(t,x) - r(t,x)) \int_0^1 z(t,y) \, k(t, x-y) \, dy - \gamma \, z(t,x),$$

$$z(t=0,x) = z_0(x); \tag{8.15a}$$

$$r'(t,x) = \gamma \, z(t,x),$$

$$r(t=0,x) = r_0(x); \tag{8.15b}$$

$$\lambda_1'(t,x) = \lambda_1(t,x) \left[\int_0^1 z(t,y) \, k(t, x-y) \, dy - (1 - z(t,x) - r(t,x)) \int_0^1 k(t, x-y) \, dy + \gamma \right]$$

$$- \gamma \, \lambda_2(t,x)$$

$$- 1 + \frac{c_1 \, \eta}{4} u^2(t) \cdot \psi'(z_{\min} - z(t,x)) - \frac{c_2 \, \omega}{2} \psi'(z(t,x) - z_{\max}) \Big\},$$

$$\lambda_1(T,x) = 0; \tag{8.15c}$$

$$\lambda_2'(t,x) = \lambda_1(t,x) \int_0^1 z(t,y) \, k(t, x-y) \, dy,$$

$$\lambda_2(T,x) = 0; \tag{8.15d}$$

$$u(t) = \frac{\int_0^1 \lambda_1(t,x) \, (1 - z(t,x) - r(t,x)) \left(\int_0^1 z(t,y) \, a(x-y) \, dy \right) dx}{\eta \int_0^1 \left[1 + \frac{c_1}{2} \psi(z_{\min} - z(t,x)) \right] dx}. \tag{8.15e}$$

This is the so-called Forward-Backward sweep method according to the method described in Lenhart and Workman [25]. For convergence and stability results, also see Hackbusch [26]. Starting with an initial guess of the control u over the entire interval, e.g., $u(t) \equiv 0.5$ or $u(t,x) \equiv 0.5$, the forward problem is solved according to the differential equations for first solution of z and r. The transversality conditions $\lambda_1(T) = \lambda_2(T) = 0$ and the values for u, z and r are used to solve the backward problem for λ_1 and λ_2. Using the results for λ_1, λ_2, z, and r, we calculate an update $\hat{u}$ on the time-dependent control function. The update of $u(t)$ is done by moving only a fraction σ of the previous u_{old} towards $\hat{u}(t)$:

$$u(t) = (1 - \sigma) \, u_{\text{old}}(t) + \sigma \, \hat{u}(t) \qquad \text{for all } t \in [0, T] \tag{8.16}$$

This procedure will be repeated until the norm of two subsequent controls is 'close enough', i.e. $\|u - u_{\text{old}}\| < \text{TOL}$. By numerical experiments a choice of $\sigma = 0.1$ provided decent results which were convergent and the target function is monotonously decreasing with respect to the iteration.

8.3.2   Space- and time-dependent control

We now assume that the control u also depends on space, i.e., the kernel function reads as

$$k(t, x-y, x) = (1 - u(t,x)) \cdot a(x-y) + k^*. \tag{8.17}$$

For this space-dependent formulation, we replace $u(t)$ by $u(t,x)$ in the previous equations. Regarding $\frac{\partial \mathcal{L}}{\partial u}$, this leads to the following formulation:

$$\frac{\partial \mathcal{L}}{\partial u} = \int_0^T \int_0^1 \left\{ \lambda_1(t,x)\,(1 - z(t,x) - r(t,x)) \int_0^1 z(t,y)\,a(x-y)\,dy \right.$$

$$\left. - \eta\,u(t,x)\left[1 + \frac{c_1}{2}\psi\left(z_{\min} - z(t,x)\right)\right] \right\} dx\,dt \qquad \overset{!}{=} 0 \quad (8.18)$$

and while the formulas for z and r remain the same, we find

$$\lambda_1'(t,x) = \lambda_1(t,x)\left[\int_0^1 z(t,y)\,k(t,x-y)\,dy - (1 - z(t,x) - r(t,x))\int_0^1 k(t,x-y)\,dy + \gamma \right]$$

$$- \gamma\,\lambda_2(t,x)$$

$$- 1 + \frac{c_1\,\eta}{4}u^2(t,x)\cdot\psi'\left(-z_{\min} - z(t,x)\right) - \frac{c_2\,\omega}{2}\psi'\left(z(t,x) - z_{\max}\right)\Big\},$$

$$\lambda_1(T,x) = 0; \qquad\qquad\qquad (8.19a)$$

$$\lambda_2'(t,x) = \lambda_1(t,x) \int_0^1 z(t,y)\,k(t,x-y)\,dy,$$

$$\lambda_2(T,x) = 0; \qquad\qquad\qquad (8.19b)$$

$$u(t,x) = \frac{\lambda_1(t,x)\,(1 - z(t,x) - r(t,x))\int_0^1 z(t,y)\,a(x-y)\,dy}{\eta\left[1 + \frac{c_1}{2}\psi\left(z_{\min} - z(t,x)\right)\right]}. \qquad (8.19c)$$

8.3.3 Space- and time-dependent, discretized control

While the concept of a space- and time-dependent control is certainly reasonable, it is not realistic to design the control in a continuous way. We therefore consider a control function $u(t,x)$ that is designed as a piecewise constant function in both time and space. The control function $u(t,x)$ takes different constant values over different rectangular regions. Let's denote the control value within each rectangle as u_{ij}, where i represents the time interval number and j represents the spatial interval number.

Mathematically, we can express the piecewise constant control function as follows: Let $t_0 < t_1 < \ldots < t_{n-1} < t_n$ be the time instants that define the intervals, and $x_0 < x_1 < \ldots < x_{m-1} < x_m$ be the spatial locations that define the intervals. Then

$$u(t,x) = u_{ij} \qquad \text{if } t \in [t_{i-1}, t_i) \text{ and } x \in [x_{j-1}, x_j) \qquad (8.20)$$

represents the control value within the corresponding rectangular region for $i = 1\ldots n$ and $j = 1\ldots m$. For the piecewise constant functions, we use the *starting value* for the time interval $[t_{i-1}, t_i)$, i.e., t_{i-1}, and the *average* of the space interval $[x_{j-1}, x_j)$. This is then plugged into the spatial model as described in section 8.3.2.

8.4 Agent-based model

In order to validate the model, we compare the above described integro-differential model to a stochastic, microscopic agent-based model developed at the Interdisciplinary Centre for Mathematical and Computational Modelling at the University of Warsaw. Complete details of this model are given in Niedzielewski et al. [20, 27]. In this model, agents have certain states (susceptible, infected, recovered, hospitalized, deceased, etc.) and infection events occur in certain contexts, i.e., on the streets, workplaces, and several more. A similar comparison can be found in Dönges et al. [22], but

to ignore in-household transmission we use only single household contexts. Location space is one dimensional with 100 location points that are available. The single households are distributed uniformly in space. The agents are assigned individually to households and corresponding street context (only these two types of contexts are in use). When probability of infection is computed every street context infectivity is taken into account. To allow for control of diffusion of infected throughout the whole space, we also use the transmission kernel function $k(t, x - y)$. As a result, the infectivity decreases with distance between location of agent and street context. Since the ODE-model (8.1) is a variant of an SIR-model, the agent-based model also just uses the SIR-states and ignores all other states. The agent-based model uses a recovery time for each infected individual that is sampled from an exponential distribution with mean 10 days.

8.5 Numerical Simulations

In this section, the Lagrangian optimization of the integro-differential model as of eqns. (8.11) and (8.12) is presented and the numeric results are shown. We denote the initial condition function as follows:

$$z_0^1(x) \equiv 2 \cdot 10^{-5},$$

$$z_0^2(x) = \begin{cases} 1 \cdot 10^{-5} & x < 0.9 \\ 1 \cdot 10^{-4} & x \geq 0.9 \end{cases}.$$

For reasons of comparability, at a choice of 100 spatial grid points almost the same mass is used for the initial infected in both variants (as the average of z_0^2 is equal to $\bar{z}_0^2 = 1.9 \cdot 10^{-5}$). We listed all six model simulations in Tab. 8.1, including parameter values for the optimal control as of system (8.11). Also, we choose parameter values of $c = \delta = 50$ (resulting in a kernel-based reproductive number of $\mathcal{R}_0 \approx 2$), $\beta = \gamma = 0.1$, $c_1 = c_2 = 1000$, $z_{\min} = 1 \cdot 10^{-5}$, and $z_{\max} = 5 \cdot 10^{-3}$. For both η and ω, we choose two different values which are described in Tab. 8.1. Lastly, wrt the penalization, we use the function

$$\psi(z) = 1 + \tanh\left(1000\,z\right),$$

with its derivative

$$\psi'(z) = 1000 \operatorname{sech}^2(z).$$

In Sims. A, no space-dependent control is included in the model and the initial values are constant. In Sims. B, again the control is only time-dependent, but we induce an 'infection wave' at one of the boundaries. In Sims. C, we also induce this infection wave at the boundary, but additionally allow a control depending on both space and time. Two different choices for the parameter values η and ω as well as a different maximal duration T are imposed on all of these simulations. In Sims. D, we use a space-time-dependent control, but use 10-days resp. 10-cells average to account for a more realistic representation of the control. The results are compared to 10 ABM runs for each scenario and also their mean.

TABLE 8.1: Listing of all simulations and different parameter values
used for optimization of the integro-differential model.

Variant	space-dependent u?	piecewise constant u?	T	z_0	η	ω
A1	no	no	400	$z_0^1(x)$	0.02	1
A2	no	no	800	$z_0^1(x)$	0.005	0.2
B1	no	no	400	$z_0^2(x)$	0.02	1
B2	no	no	800	$z_0^2(x)$	0.005	0.2
C1	yes	no	400	$z_0^2(x)$	0.02	1
C2	yes	no	800	$z_0^2(x)$	0.005	0.2
D1	yes	yes	400	$z_0^2(x)$	0.02	1
D2	yes	yes	800	$z_0^2(x)$	0.005	0.2

Choosing an arbitrary starting value for $u(x)$ or $u(t,x)$, we use the Forward-Backward sweep method as of eqns. (8.15) and (8.19) and evaluate the target function in each step. As an example, the convergence of the target function value is presented in Fig. 8.1.
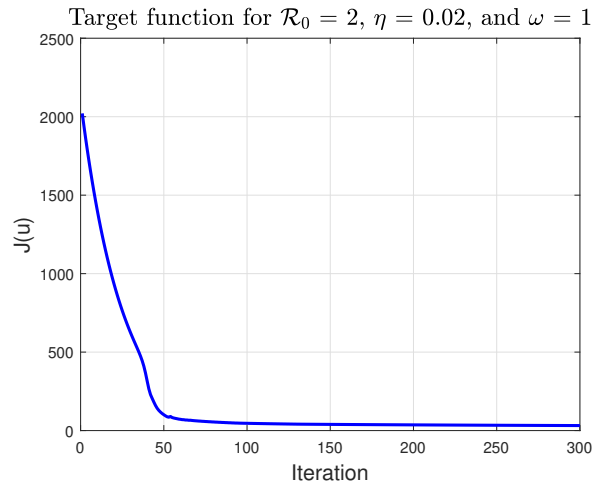

FIGURE 8.1: Exemplary behavior of the target function for model A1
and $u(t) \equiv 1$.

8.5.1 Simulation Results

In this section, the results for the optimal control, the infected (both using the *SIR*-model and the ABM model) as well as the time mean of infected and the difference between the models are presented and compared.

Simulation A1

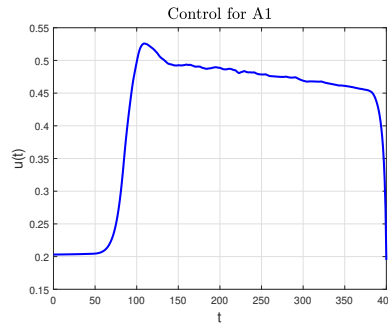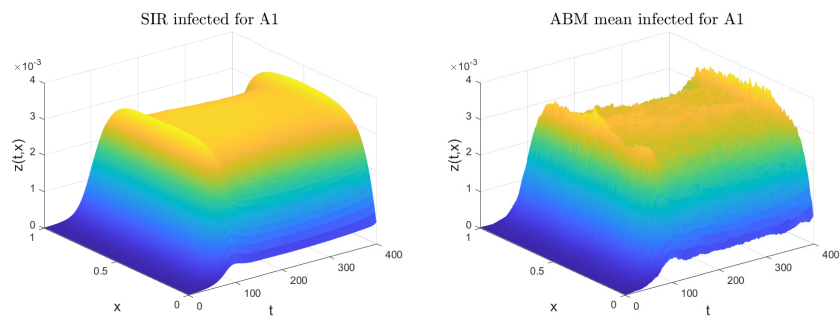FIGURE 8.2: Evolution of the control in Sim. A1.

FIGURE 8.3: Spatio-temporal evolution of the infected in Sim. A1 for the integro-differential *SIR*-model (left) and the ABM model (right).

FIGURE 8.4: Difference between the *SIR*-model to the ABM model mean (left) and temporal evolution of the spatial mean in the *SIR*-model and all single runs of the ABM model, as well as their mean (right) in Sim. A1.

Simulation A2

FIGURE 8.5: Evolution of the control in Sim. A2.

FIGURE 8.6: Spatio-temporal evolution of the infected in Sim. A2, on the left for the integro-differential *SIR*-model, on the right for the ABM model.

FIGURE 8.7: Difference between the *SIR*-model to the ABM model mean (left) and temporal evolution of the spatial mean in the *SIR*-model and all single runs of the ABM model, as well as their mean (right) in Sim. A2.

Simulation B1

FIGURE 8.8: Evolution of the control in Sim. B1.

FIGURE 8.9: Spatio-temporal evolution of the infected in Sim. B1, on the left for the integro-differential *SIR*-model, on the right for the ABM model.
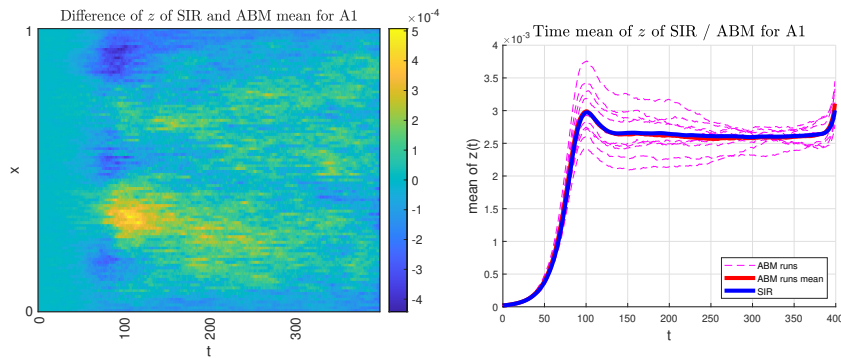

FIGURE 8.10: Difference between the *SIR*-model to the ABM model mean (left) and temporal evolution of the spatial mean in the *SIR*-model and all single runs of the ABM model, as well as their mean (right) in Sim. B1.
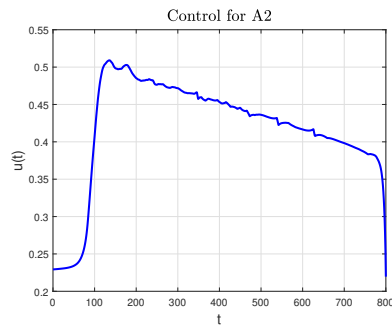
Simulation B2

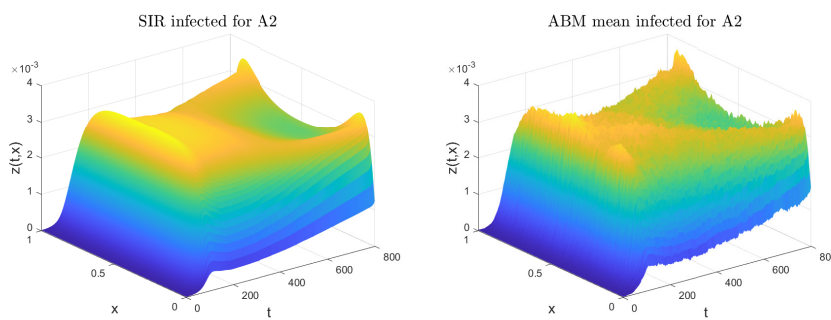FIGURE 8.11: Evolution of the control in Sim. B2.

FIGURE 8.12: Spatio-temporal evolution of the infected in Sim. B2, on the left for the integro-differential *SIR*-model, on the right for the ABM model.

FIGURE 8.13: Difference between the *SIR*-model to the ABM model mean (left) and temporal evolution of the spatial mean in the *SIR*-model and all single runs of the ABM model, as well as their mean (right) in Sim. B2.

Simulation C1

FIGURE 8.14: Evolution of the control in Sim. C1.

FIGURE 8.15: Spatio-temporal evolution of the infected in Sim. C1, on the left for the integro-differential *SIR*-model, on the right for the ABM model.
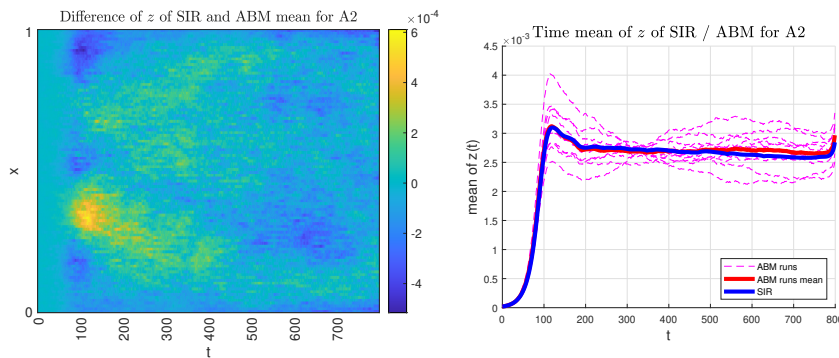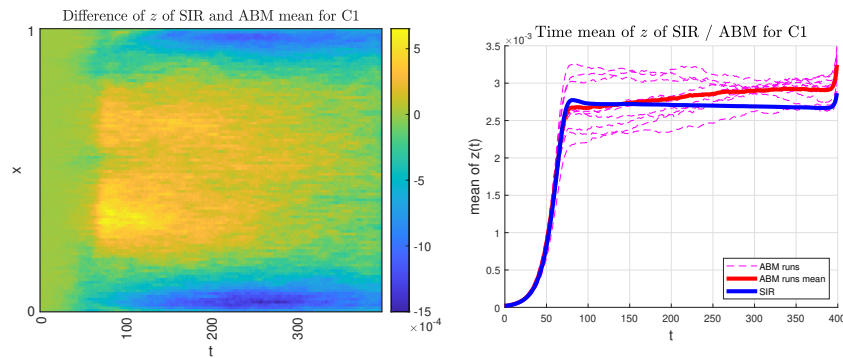

FIGURE 8.16: Difference between the *SIR*-model to the ABM model mean (left) and temporal evolution of the spatial mean in the *SIR*-model and all single runs of the ABM model, as well as their mean (right) in Sim. C1.
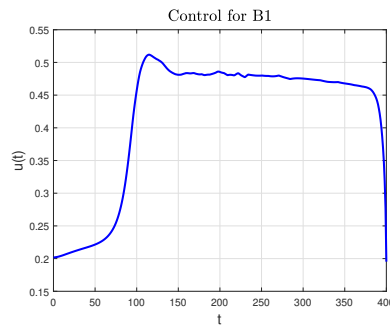
Simulation C2

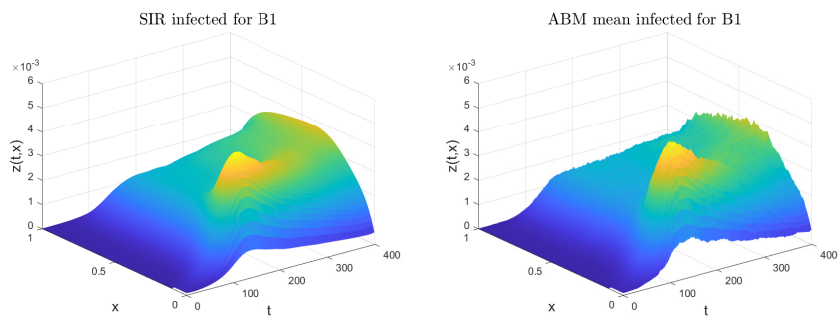FIGURE 8.17: Evolution of the control in Sim. C2.

FIGURE 8.18: Spatio-temporal evolution of the infected in Sim. C2, on the left for the integro-differential *SIR*-model, on the right for the ABM model.
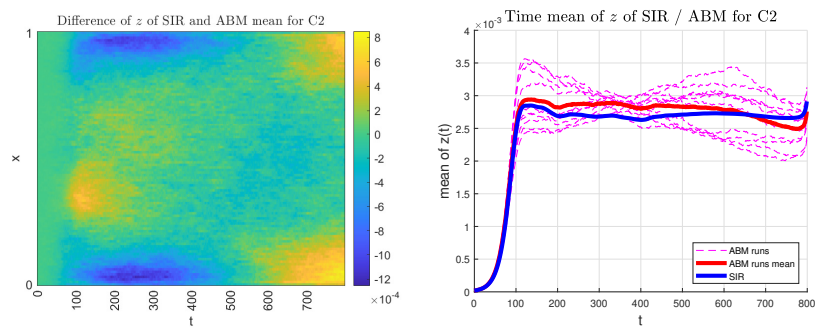
FIGURE 8.19: Difference between the *SIR*-model to the ABM model mean (left) and temporal evolution of the spatial mean in the *SIR*-model and all single runs of the ABM model, as well as their mean (right) in Sim. C2.

Simulation D1

FIGURE 8.20: Evolution of the control in Sim. D1.

FIGURE 8.21: Spatio-temporal evolution of the infected in Sim. D1, on the left for the integro-differential *SIR*-model, on the right for the ABM model.
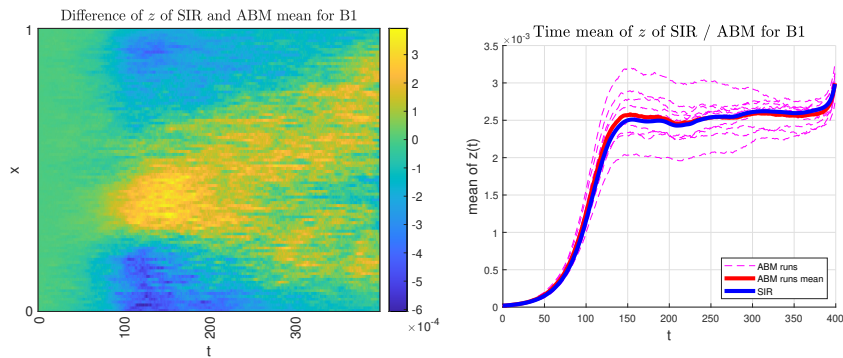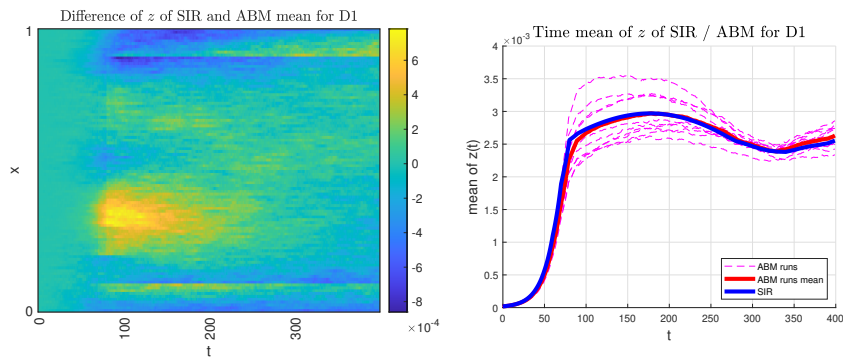

FIGURE 8.22: Difference between the *SIR*-model to the ABM model mean (left) and temporal evolution of the spatial mean in the *SIR*-model and all single runs of the ABM model, as well as their mean (right) in Sim. D1.
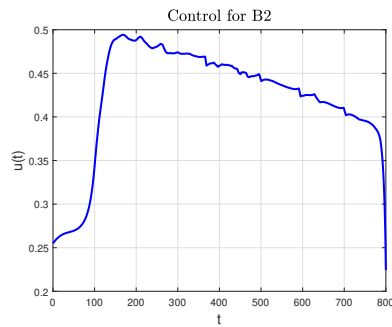
Simulation D2

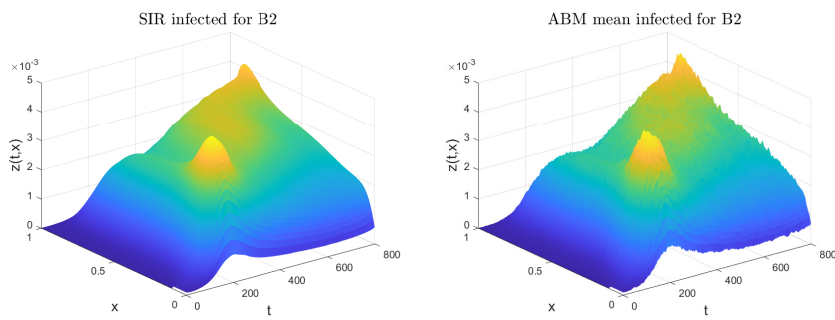FIGURE 8.23: Evolution of the control in Sim. D2.

FIGURE 8.24: Spatio-temporal evolution of the infected in Sim. D2, on the left for the integro-differential *SIR*-model, on the right for the ABM model.
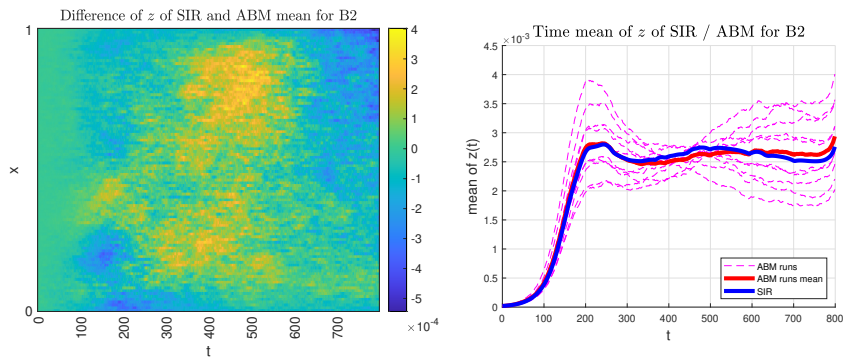

FIGURE 8.25: Difference between the *SIR*-model to the ABM model mean (left) and temporal evolution of the spatial mean in the *SIR*-model and all single runs of the ABM model, as well as their mean (right) in Sim. D2.

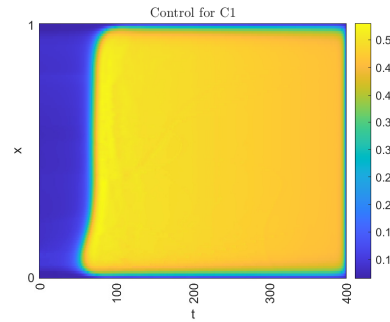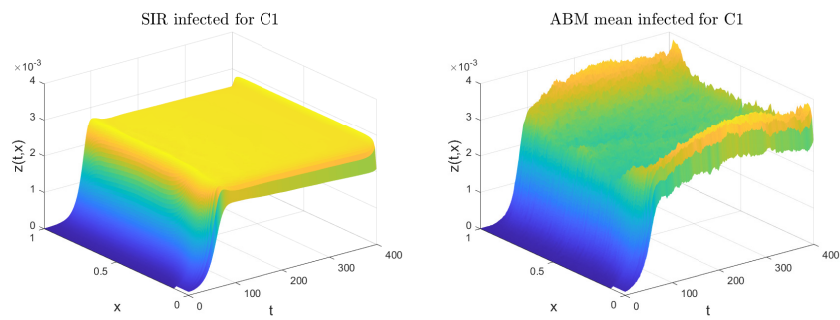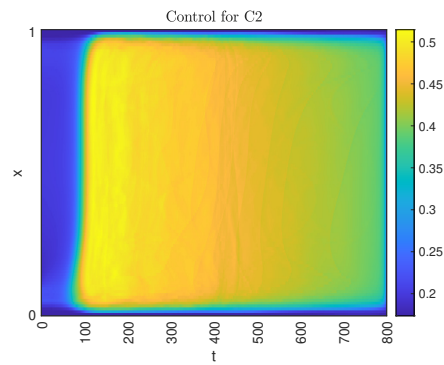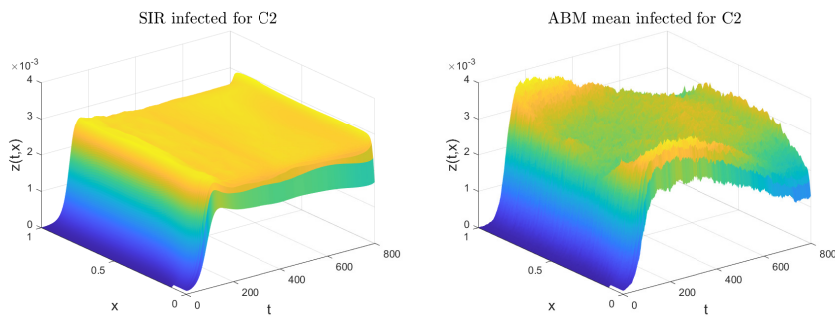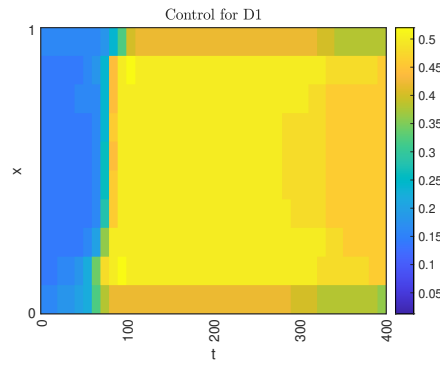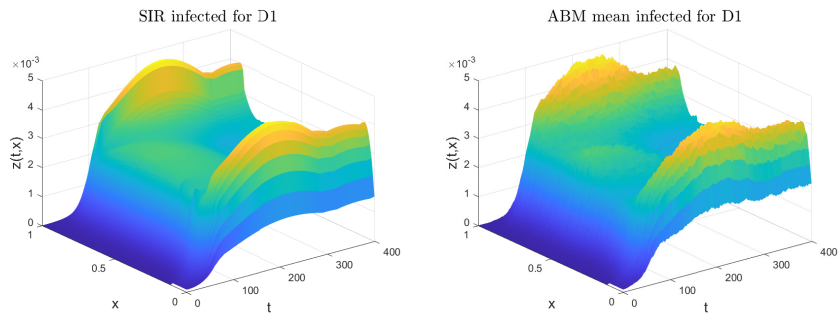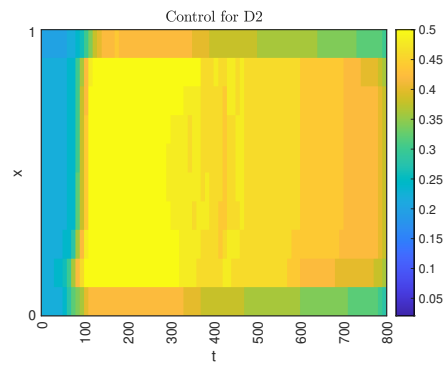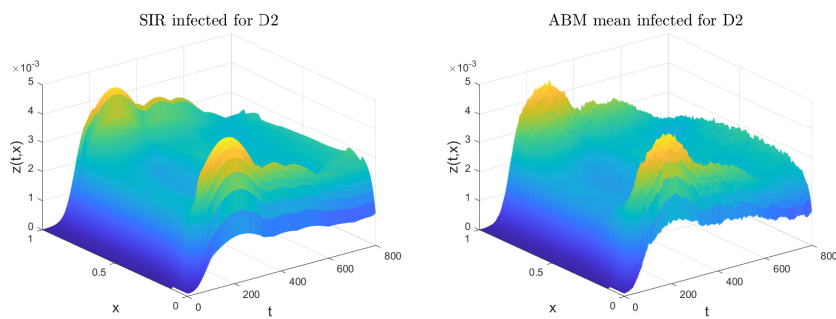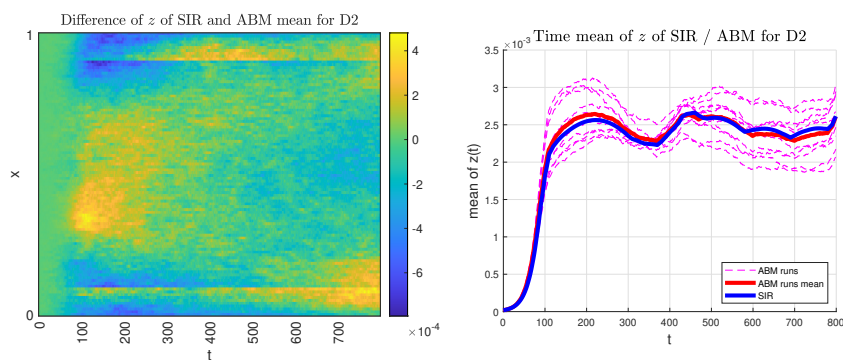### 8.5.2   Observations for the integro-differential model

In simulation A1 (cf. Figs. 8.2,8.3,8.4), using an only time-dependent control function and homogeneous initial conditions, we see that after light restrictions causing raising numbers of infectives, a sudden increase in lockdown restrictions causes falling numbers. The control only rises as late as possible in order not to surpass or get close to z_{max}, and thereon remains relatively constant. Raising to levels at or slightly above 0.5, it manages to contain the disease spread due to $\mathcal{R}_0 = 2$. Later on, the effective reproduction rate lowers as there is a higher amount of recovered which are assumed to not get infected again in this simplified model. At the end, roughly 10 % of the total population is infected or recovered, homogeneously spread on the whole spatial domain. The drop of the control function towards the end can be explained as the system regulates the epidemics such that the maximally allowed rates are just slightly missed at the end. This observation is in fact independent of the chosen duration or simulation. The convergence of the target function $J(u)$ is exemplary shown for Sim. A1 (Fig. 8.1) and looks similar for all other simulations. The results of Sim. A2 (cf. Figs. 8.5,8.6,8.7) are comparable to Sim. A1, yet due to different values of η and ω, the control reduces more quickly in a quite linear fashion after rising above 0.5. As a result, the total amount of recovered and infectives is roughly equal to 20 % at the end.

In simulations B1 (cf. Figs. 8.8,8.9,8.10) and B2 (cf. Figs. 8.11,8.12,8.13), an only time-dependent control function and an inhomogeneous initial condition are used. We observe similar optimal control functions in Sims. B1 and B2 as in A1 and A2, respectively, resulting in a spatially delimited peak of infections slightly propagating in time. Due to generally higher infection cases in Sim. B2, there is another peak at the end of the observed time interval. The share of recovered again reaches values around 10 % for B1, with a peak close to the boundary from which the disease was important, and 20 % for B2, with homogeneously distributed values across the spatial domain.

Simulations C1 (cf. Figs. 8.14,8.15,8.16) and C2 (cf. Figs. 8.17,8.18,8.19) feature a space-time-dependent control function and an inhomogeneous initial condition. While the spatially averaged behaviour of the control function in C1 and C2 is similar as in B1 and B2, respectively, a more or less slight spatial 'propagation' of the control is visible. This adaptive behaviour allows for the control term to never surpass 0.5, resulting in less effort and thus a lower target function. The share of recovered again reaches values around 10 % for C1, and 20 % for C2, both with homogeneously distributed values across the spatial domain.

Finally, simulations D1 (cf. Figs. 8.20,8.21,8.22) and D2 (cf. Figs. 8.23,8.24,8.25) feature a piecewise constant space-time-dependent control function and an inhomogeneous initial condition. In those simulations, as to be expected, the control is similar to the one in the continuous simulations C1 and C2. However, using the starting value as the control for the next (10) days, causes higher infection rates in the initial phase of the disease, such that it can be said that globally the control has to be slightly larger as in the continuous simulations. The share of recovered again reaches values around 10 % for D1, and 20 % for D2, yet features significant peaks at both boundaries.

8.5.3   Comparison with the agent-based model

Tab. 8.2 lists the values of the target function of all simulations according to eqns. (8.11) and (8.12). Additionally, the target function of a model without any control

measures, i.e. $u(t) \equiv 0$ or $u(t, x) \equiv 0$, is listed, showing significant improvement in the target function for simulations C1 and C2, while D1 and D2 were still reasonably good in reducing the cost function values despite their restrictions.

TABLE 8.2: Target function values for the various simulations, according to eqns. (8.11) and (8.12).

Simulation	$J(u \equiv 0)$	$J(u^*)_{\mathrm{sir}}$	$J(u^*)_{\mathrm{abm}}$
A1	132.4	31.9	29.5
A2	32.9	13.4	12.6
B1	132.5	40.6	39.0
B2	32.9	19.9	19.3
C1	132.5	10.1	12.6
C2	32.9	8.5	9.0
D1	132.5	19.8	21.5
D2	32.9	12.2	12.5

If we compare the results of the target function, it shows that by using the optimal control, it was possible to reduce the target function compared to $u \equiv 0$ by a factor depending on the chosen simulation and parameter values of η and ω. As to be expected, the best results for $J(u)$ were found in the space-dependent, yet continuous control. Comparing the results for the target function for the *SIR*-model and the ABM model, we see that there are only minor differences in the outcome, mainly in C1 and C2 and there especially close to the boundaries. Those can be explained by the stochastic nature of the ABM model of which also not all features can be adapted to the integro-differential model.

8.6 Discussion and Outlook

In this work, we have presented a spatial integro-differential *SIR*-model, have proved several theoretical properties (including uniqueness of the solution) and provided setups in order to apply optimal control on the transmission of the disease. We aimed to design the cost function in a reasonable way, including both the avoidance of the overload of health capacities and the political and economical costs of measures and lockdowns. The results were compared to the ABM model and are overall very much accordant. This has an interesting consequence; the *SIR*-model is 'cheap' to compute, compared to the computationally 'expensive' ABM model, for which an optimal control is hardly possible. Thus, by optimization of the *SIR*-model, we are now able to find a good proxy for the ABM model. While it will not be possible to reproduce the results perfectly, the averages of both models are very similar and match very well in most simulations except the space-and time-dependent continuous control. The results always remain within the designed range $[z_{\min}, z_{\max}]$, such that the healthcare capacities are not overloaded, even in the model with piecewise constant values for u that is less flexible to quickly raising infection numbers. The system still remains in the range of stochastic fluctuations of the ABM model.

The model can be implemented with a set of real world mitigation measures that are equipped with their expected effect on the transmission. Our approach and methodology are of practical use since the lockdown cost function can be designed freely depending on setting related to different countries or other circumstances, in order to make it more realistic and accountable.

In future work, multidimensional problems can be put under scrutiny as the presented approach is not constrained on a specific dimensionality of the space, i.e., a spatially 2D-problem with a commuting structure between inhabited spaces, which actually represents a more realistic approach for entire countries (like Poland in the ABM model in Niedzielewski et al. [20, 27]), can also be implemented. Another interesting application lies in models of age-structure, where the parameter x is interpreted as the age, and a discrete contact matrix for age cohorts can be transformed into a kernel function. We can extend the presented models with more complex representation of generation time like an *SEIR*-model in a straightforward manner, which can effect the speed and peak of the wave.

Another interesting topic for further investigation would be the implementation of vaccination as it is a subject of high interest for public health professionals; it is not easy to anticipate the effect on the optimal control results. It seems it should be more beneficial to have strong mitigation before and during vaccination to avoid health costs, but on the other hand, when vaccine introduction takes too long or the efficacy is too low, restrictions should be loosened. Furthermore, optimization of vaccination administration with limited resources could be possible as well. In scenarios where a new pathogen is introduced in an almost completely susceptible population, those effects are rather negligible and the presented model assumptions are sufficient. Another potential subject of research is the inclusion of households, e.g., using the strategy described in Dönges [22]. Using the parameters and knowledge gained from this work, we can implement the ABM model including households, and perform parameter estimation to find reasonable values for k^* in the integro-differential *SIR*-model. The optimization of system complexity should be tailored to the specific application, facilitating a comprehensive grasp of the system's inherent mechanisms. This entails a balance between the topical requirements and the mathematics at hand, so that it is possible to aim for an feasible and effective implementation of even highly sophisticated systems.

Declarations

Competing interests

Funding

Acknowledgements

Authors' contributions

Availability of data

We used several of the underlying MATLAB codes for multiple purposes and thus believe the open presentation of the codes would distract readers. However, the codes, datasets used, and/or analyzed during the current study are available from the corresponding author on reasonable request.

A   Existence and uniqueness of solutions of the SIS-model

The proof of uniqueness of solutions of the *SIR*-model made some theory redundant that was previously performed for the *SIS*-model. However, we decided to publish the most relevant parts of it in this appendix.

Consider an *SIS*-version of eqns. (8.1), wlog setting $\beta = \gamma = 1$. Then, this equation reads in fix point form as

$$z(x) = (1 - z(x)) \cdot \int_0^1 z(y) \cdot k(x - y)\, dy. \tag{8.21}$$

The trivial disease free equilibrium of the model (8.21) is given by $z \equiv 0$. Before dealing with the question, whether there might exist other, non-trivial equilibria, we will first prove

Lemma 8.2. Let $z : [0,1] \to [0,1]$ be a continuous solution of the fix point equation (8.21). Then z is symmetric, i.e. $z(x) = z(1 - x)$ for all $x \in [0,1]$.

Proof. It holds that

$$z(1 - x) = (1 - z(1 - x)) \int_0^1 z(y)\, k(1 - x - y)\, dy. \tag{8.22}$$

After substituting $s = 1 - y$ in the integral we arrive at

$$z(1 - x) = (1 - z(1 - x)) \int_0^1 z(1 - s)\, k(s - x)\, ds. \tag{8.23}$$

Hence, $\tilde{z}(x) := z(1 - x)$ solves

$$\tilde{z}(x) = (1 - \tilde{z}(y)) \int_0^1 \tilde{z}(y)\, k(x - y)\, dy\,. \tag{8.24}$$

This implies that $\tilde{z}$ solves the same equation as z. Also, consider the following □

Lemma 8.3. Let $z : [0,1] \to [0,1]$ be a continuous solution of the fix point equation (8.21). Then either $z(x) = 0$ for all $x \in [0,1]$ or $z(x) > 0$ for all $x \in [0,1]$.

Proof. Assume that $z(x) \not\equiv 0$. Then there exists $x_0 \in [0,1]$ such that $z(x_0) = 0$ and wlog $z(x_0 + \delta) > 0$ for all $0 < \delta < \delta_0$. Due to continuity of k and $k_0 > 0$, there exists a $\delta_1 > 0$, such that $k(r) > 0$ for all $0 \le r < \delta_1$. Thus, it follows

$$z(x_0) = (1 - z(x_0)) \int_0^1 z(y)\, k(|x_0 - y|)\, dy \tag{8.25}$$

$$\ge (1 - z(x_0)) \int_0^{\min(\delta_0, \delta_1)} z(x_0 + r)\, k(r)\, dr > 0. \tag{8.26}$$

□

Next, we define $\chi[z](x) := \int_0^1 z(y)\, k(|x - y|)\, dy$. Then the fix point equation (8.21) reads as

$$z = \Phi[z] := \frac{\chi[z]}{1 + \chi[z]}\,. \tag{8.27}$$

We show, that any non–trivial solution of (8.21) has to satisfy a–priori bounds

Lemma 8.4. Let $z : [0,1] \to [0,1]$ be a non–trivial solution of $z = (1-z)\chi[z]$. Then for all $x \in [0,1]$ we find

$$\frac{k_1 - 1}{k_1} \leq z(x) \leq \frac{K-1}{K}. \tag{8.28}$$

Proof. To show the upper bound: By $z(x) > 0$, we know $\chi[z](x) > 0$ and therefore $z = \chi[z]/(1+\chi[z]) < 1$. If $z(x) < 1$, then $\chi[z](x) < K$ and due to $\chi[z] < K$ we get $z(x) < K/(1+K)$. Iterating this, for all $n \in \mathbb{N}$ it holds

$$z(x) < \frac{K^n}{1 + K + \cdots + K^n} = \frac{(K-1)K^n}{K^{n+1} - 1} = \frac{K-1}{K - K^{-n}} \tag{8.29}$$

Passing to the limit $n \to \infty$ yields $z(x) \leq (K-1)/K$. On the other hand, if z is non–trivial, then due to Lemma 8.3, there exists an $\varepsilon > 0$ such that $z(x) > \varepsilon$ for all x. Hence $\chi[z](x) > \varepsilon k_1$ and using $z = \chi[z]/(1+\chi[z])$ as well as the monotonicity of the function $x \mapsto x/(1+x)$ we get $z(x) > \varepsilon k_1/(1+\varepsilon k_1)$. Iterating again between estimates for $\chi[z]$ and z finally yields

$$z(x) > \frac{\varepsilon k_1^n}{1 + \varepsilon k_1 + \cdots + \varepsilon k_1^n} = \frac{\varepsilon k_1^n}{1 + \frac{\varepsilon k_1 (k_1^n - 1)}{k_1 - 1}} = \varepsilon \left[k_1^{-n} + \frac{\varepsilon k_1}{k_1 - 1}(1 - k_1^{-n}) \right] \tag{8.30}$$

for all $n \in \mathbb{N}$ and after passing to the limit $n \to \infty$ we get $z(x) \geq (k_1 - 1)/k_1$. $\qquad\square$

As an immediate consequence of Lems. 8.3 and 8.4 we obtain the following: Let $z : [0,1] \to [0,1]$ be a non–trivial solution of $z = (1-z)\chi[z]$. Then for all $x \in [0,1]$, we have $\chi[z](x) \in M_\chi := [k_1 - 1, K - 1]$. Also, we conclude that if $K = \max_x \int_0^1 k(|x-y|)\,dy \leq 1$, then no non–trivial solution of eqn. (8.21) can exist.

To prove the existence of non–trivial solutions we will apply a fix point argument. As we know from previous results, possible non–trivial solutions have to satisfy the bounds of Lem. 8.4. Therefore we define

$$M_z := \left\{ z \in C^0([0,1]; \mathbb{R}) : \frac{k_1 - 1}{k_1} \leq z(x) \leq \frac{K-1}{K} \right\} \tag{8.31}$$

as the subset of continuous functions satisfying the needed bounds. It is immediate to see that for $K > 1$, the set M_z is non–empty. We equip M with the usual sup-norm

$$\|z\|_\infty := \max_{x \in [0,1]} |z(x)| . \tag{8.32}$$

Lemma 8.5. The operator $\Phi[z] := \chi[z]/(1+\chi[z])$ is a self–mapping on M_z, i.e. $\Phi : M_z \to M_z$.

Proof. Let $z \in M$. Then $k_1 - 1 \leq \chi[z] \leq K - 1$ and, due to the monotonicity of $x \mapsto x/(1+x)$, we get

$$\frac{k_1 - 1}{k_1} \leq \Phi[z] = \frac{\chi[z]}{1 + \chi[z]} \leq \frac{K-1}{K} , \tag{8.33}$$

hence $\Phi[z] \in M_z$. $\qquad\square$

Lemma 8.6. If $K/k_1^2 < 1$, then the operator $\Phi : (M, \|\cdot\|_\infty) \to (M, \|\cdot\|_\infty)$ is a contraction on M with respect to the sup–norm.

Proof. Let $u, v \in M$, $x \in [0,1]$ and $K/k_1^2 < 1$. Then

$$\Phi[u](x) - \Phi[v](x) = \frac{\chi[u](x)}{1 + \chi[u](x)} - \frac{\chi[v](x)}{1 + \chi[v](x)} \tag{8.34}$$

$$= \frac{\chi[u-v](x)}{1 + \chi[u](x) + \chi[v](x) + \chi[u](x) \cdot \chi[v](x)} \tag{8.35}$$

and

$$\|\Phi[u] - \Phi[v]\|_\infty \leq \frac{\int_0^1 [u-v](y) \cdot k(|x-y|)\, dy}{1 + 2(k_1 - 1) + (k_1 - 1)^2} \leq \frac{K}{k_1^2} \cdot \|u - v\|_\infty < \|u - v\|_\infty . \tag{8.36}$$

$\square$

Theorem 8.7. For $K/k_1^2 < 1$, there exists a unique non–trivial solution $z^* \in M_z$ of the fix point problem (8.21).

Proof. The assertion follows from Banach's fix point theorem applied to the operator Φ on the set $M_z \subset (\mathcal{C}^0, \|\cdot\|_\infty)$. $\square$

If $k_1 < 1$, a solution can be the trivial equilibrium due to $0 \in M_z = \mathcal{C}^0[k_1 - 1, K - 1]$. While no uniqueness properties can yet be made for the case $K/k_1^2 \geq 1$, existence can be guaranteed by

Lemma 8.8. If $K > 1$ and $k_1 > 1$, the iteration Φ has at least one nontrivial solution $z^*(x) \in M_z$.

Proof. M is a convex closed subset of the Banach space $\mathcal{C}^0(\mathbb{R}, \|\cdot\|)$. It is also non-empty provided $K > 1$. The lemma of Arzelà-Ascoli says that for a compact and metric space (S, d) and $M \subset \mathcal{C}[S]$ equipped with the supremum norm, it holds that M is compact if it is limited, closed, and equicontinuous. This holds for any $\mathcal{C}[a, b]$ (for a proof refer to standard literature) and thus for $M_z = \mathcal{C}[k_1 - 1, K - 1]$. Since Φ is a continuous mapping of M_z (which is a compact and convex subset of a metric space) into itself, it has at least one fix point in M according to the fix point theorem of Schauder [28]. $\square$

However, this result alone would not be satisfying, as the requirement on the kernel k being 'flat enough' to satisfy $K < k_1^2$ is quite strict: Consider a standard SIS model without any spatial terms. This would be equivalent to the above model with a Dirac delta kernel at $|x - y| = 0$, which obviously does *not* satisfy the above equation.

Bibliography

[1] Schäfer, M. et al. *An integro-differential model for the spread of diseases*. arXiv `https://arxiv.org/abs/2307.10087`. 2023.

[2] Bracher, J. et al. "A pre-registered short-term forecasting study of COVID-19 in Germany and Poland during the second wave". In: *Nature Communications* 12 (2021). DOI: `10.1038/s41467-021-25207-0`.

[3] Bracher, J. et al. "National and subnational short-term forecasting of COVID-19 in Germany and Poland during early 2021". In: *medRxiv* (2021). DOI: `10.1101/2021.11.05.21265810`.

[4] Sherratt, K. et al. "Predictive performance of multi-model ensemble forecasts of COVID-19 across European nations". In: *eLife* 12 (2023). DOI: `10.7554/eLife.81916`.

[5] Priesemann, V., Meyer-Hermann, M., and Pigeot, I. "Der Beitrag von epidemiologischen Modellen zur Beschreibung des Ausbruchsgeschehens der COVID-19-Pandemie". In: *Bundesgesundheitsblatt - Gesundheitsforschung - Gesundheitsschutz* 64 (2021), pp. 1058–1066. DOI: `10.1007/s00103-021-03390-1`.

[6] Kuehn, C. and Mölter, J. "The influence of a transport process on the epidemic threshold". In: *Journal of Mathematical Biology* 85.62 (2020), pp. 37–59. DOI: `10.1007/s00285-022-01810-7`.

[7] Viguerie, A. et al. "Simulating the spread of COVID-19 via a spatially-resolved susceptible–exposed–infected–recovered–deceased (SEIRD) model with heterogeneous diffusion". In: *Appl Math Lett.* 111.106617 (2021). DOI: `10.1016/j.aml.2020.106617`.

[8] Wang, H. and Yamamoto, N. "Using a partial differential equation with Google Mobility data to predict COVID-19 in Arizona". In: *Mathematical Biosciences and Engineering* 17.5 (2020), pp. 4891–4904. DOI: `10.3934/mbe.2020266`.

[9] Logeswari, K., Ravichandran, C., and Nisar, K.S. "Mathematical model for spreading of COVID-19 virus with the Mittag–Leffler kernel". In: *Numerical Methods for Partial Differential Equations* (2020), pp. 1–16. DOI: `10.1002/num.22652`.

[10] Harris, P.J. and Bodmann, B.E.J. "A mathematical model for simulating the spread of a disease through a country divided into geographical regions with different population densities". In: *Journal of Mathematical Biology* 85.32 (2022). DOI: `10.1007/s00285-022-01803-6`.

[11] Berestycki, H., Roquejoffre, J.-M., and Rossil, L. "Propagation of Epidemics Along Lines with Fast Diffusion". In: *Bull. Math. Biol.* 83.2 (2020). DOI: `10.1007/s11538-020-00826-8`.

[12] Schäfer, M., Heidrich, P., and Götz, T. "Modelling the Spatial Spread of COVID-19 in a German District using a Diffusion Model". In: *Mathematical Biosciences and Engineering* 20.12 (2023). DOI: `10.3934/mbe.2023940`.

[13] Grave, M. et al. "Assessing the Spatio-temporal Spread of COVID-19 via Compartmental Models with Diffusion in Italy, USA, and Brazil S.I. : Modeling and Simulation of Infectious Diseases". In: *Archives of Computational Methods in Engineering* 28 (2021), pp. 4205–4223. DOI: `10.1007/s11831-021-09627-1`.

[14] Domoshnitsky, A., Sitkin, A., and Eisenstein, L. "Mathematical Modeling of COVID-19 Transmission in the Form of System of Integro-Differential Equations". In: *Mathematics* 10.23 (2022). DOI: 10.3390/math10234500.

[15] Salvadore, F., Fiscon, G., and Paci, P. "Integro-differential approach for modeling the COVID-19 dynamics - Impact of confinement measures in Italy". In: *Computers in Biology and Medicine* 139 (2021). DOI: 10.1016/j.compbiomed.2021.105013.

[16] Hritonenkoa, N., Satskyb, C., and Yatsenkoc, Y. "Integral Model of COVID-19 Spread and Mitigation in UK: Identification of Transmission Rate". In: *Mathematical Modelling and Analysis* 27.4 (2022). DOI: 10.3846/mma.2022.15708.

[17] EUR-Lex. *Regulation (EU) 2022/2371 of the European Parliament and of the Council of 23 November 2022 on serious cross-border threats to health and repealing Decision No 1082/2013/EU (Text with EEA relevance).* https://eur-lex.europa.eu/legal-content/EN/TXT/?uri=CELEX:32022R2371. 2023.

[18] European Commission. *Preparedness and response planning.* https://health.ec.europa.eu/health-security-and-infectious-diseases/preparedness-and-response-planning_en. 2023.

[19] Council of the European Union. *Infographic – The global agreement on pandemics in a nutshell.* https://www.consilium.europa.eu/en/infographics/towards-an-international-treaty-on-pandemics/. 2023.

[20] Niedzielewski, K. et al. "The Overview, Design Concepts and Details Protocol of ICM Epidemiological Model (PDYN 1.5)". In: *SSRN Electronic Journal* (2022). DOI: 10.2139/ssrn.4039054.

[21] Kermack, W.O. and McKendrick, A.G. "Contributions to the mathematical theory of epidemics-I. 1927." In: *Bull. Math. Biol.* 53 (1991), pp. 33–55. DOI: 10.1098/rspa.1927.0118.

[22] Dönges, P. and Götz, T. and Krüger, T. and Niedzielewski, K. and Priesemann, V. and Schäfer, M. *SIR-Model for Households (preprint).* arXiv https://arxiv.org/pdf/10.48550/arXiv.2301.04355. 2023.

[23] Bollobás, B., Janson, S., and Riordan, O. "The phase transition in inhomogeneous random graphs". In: *Random Structures and Algorithms* 31 (2007), pp. 3–122. DOI: 10.1002/rsa.20168.

[24] Driessche, P. van den and Watmough, J. "Reproduction numbers and subthreshold endemic equilibria for compartmental models of disease transmission". In: *Math. Biosci.* 180 (2002), pp. 29–48. DOI: 10.1016/s0025-5564(02)00108-6.

[25] Lenhart, S. and Workman, J.T. *Optimal control applied to biological models.* CRC Press, 2007.

[26] Hackbusch, W. "A numerical method for solving parabolic equations with opposite orientations". In: *Computing* 20.3 (1978), pp. 229–240. DOI: 10.1007/bf02251947.

[27] Niedzielewski, K. et al. *A Deep Dive into the Delta Wave: Forecasting SARS-CoV-2 Epidemic Dynamic in Poland with the pDyn Agent-Based Model (preprint).* 2023. DOI: 10.21203/rs.3.rs-2966996/v1.

[28] Schauder, J. "Der Fixpunktsatz in Funktionalräumen". In: *Stud. Math.* 2 (1930), pp. 171–180.

Part III

Summary

Chapter 9

Summary

In this thesis, after an introduction to epidemics and pandemics in general and Dengue fever adn COVID-19 in particular, the mathematical background for ODEs, fractional diffusion models, PDEs, and integro-differential models, as well their application in epidemiology were presented. We focussed on the dynamics of Dengue fever and COVID-19, yet the models can be used for other infectious diseases as well if they are adapted to specific properties of the respective problem. Afterwards, the basics for optimization of target functions using Bayesian analysis (Metropolis algorithm) and classical Lagrange multipliers were presented.

In the research concerning Dengue fever, a steady-state approximation enabled us to reduce the *SIRUV*- to an *SIR*-model, with which we were able to deal with an exemplary data set from Jakarta. This enabled a useful parameter estimation using the adjoint approach and allowed studying the direct impact of seasonal meteorological conditions on the disease, which we modelled using a time-dependent transmission rate, represented by a finite Fourier sum. We introduced a mobility matrix for commuters in order to show the spatial spread of infectious across the districts of Jakarta. The Metropolis algorithm is used for parameter estimation and gave a generally good approximation for the districts. We also performed convergence checks for the parameters of the Metropolis algorithm, which showed that most parameters are normal distributed, but some show a slightly different behaviour, which indicates minor cross-correlation between some of the parameters. To account for the specific properties of Dengue fever (four serotypes and long immunity against one, but only temporary immunity against the others) a refinement toward a multistrain model should be considered, along with a more differentiated modeling that accounts for external influences such as meteorological factors. Also, spatially dependent models using some of the methods described below can be applied here.

In the context of the COVID-19, we firstly considered a *SEIRD*-model with and without time delay. The model was applied to the spread of diseases during the first wave in Germany, i.e., the initial phase of the disease dynamics, and the results demonstrated that the model with time delay and the presented parameter estimation provided realistic values, especially concerning the detection rate and lethality rate, which were not accurately known at the time. Additionally, we compared the outcome of the Metropolis algorithm with an adjoint based approach, which both provided similar results for the optimal parameter set, yet showed different performances with respect to computation time. While the Metropolis algorithm featured a slightly better target function, it was more computationally expensive than the adjoint method. Ongoing research with respect to the dynamics of COVID-19 is useful, despite it that it is considered a pandemic anymore; there is still a risk of new variants with unknown properties, as well as a general risk of new pandemics, so the models are aimed to be adaptable towards future events, with a focus on practical applicability.

These two approaches have also been compared in the PDE approach, where the disease dynamics of a German district during the second wave has been analysed. There were comparatively few cases in the first wave in this district, so this can be interpreted as a kind of initial phase of the disease in this region. We set up a *SEIR*-model with diffusion and performed parameter estimation using the two approaches, which both showed similar outcomes and similar values for the transmission-based parameters, yet different diffusion-based parameters, detection rates and initial values. We also aim for models that also includes a more international-based approach of the spatial spread of COVID-19 and its significance.

Three more possibilites to model spatial transmission of infections were presented. In the traveller-based research paper, we analysed the influence of travellers on the 'regular' disease dynamics in an *SEIRD*-model, incorporating a traveller compartment which take part on other countries' disease dynamics and play a substantial role in international propagation of diseases. A sensitivity analysis however indicates that given a necessity to reduce infection cases, the role of travellers is not as important as the control of transmission on a local scale.

Fractional diffusion is also a potential way to describe propagation of diseases. In a more theoretical approach we introduced the necessary mathematical background and provided reasonable numerical methods in order to set up models using fractional, non-local diffusion. In numerical experiments without data basis, an *SI*-model with fractional diffusion was used to demonstrate the scheme and to reveal the dependence on the behavior of the system with respect to the value of the fractional derivative α. In the case of a regional epidemic, the fractional model predicts that with a rise in α, the disease will spread rapidly to previously unaffected regions, yet also suggests a decline in the number of cases in the original epicenter of the pandemic. In order to meaningfully include fractional diffusion, is also aimed to use parameter estimation to find reasonable values for the fractional diffusion parameter and the diffusivity parameter. In the future, several of the presented models cab be applied to describe specific epidemics (not restricted to Dengue or COVID-19 outbreaks), the results of space-fractional or even time-fractional partial differential equation models to epidemiological data and better understand the behavior of disease spread in a specific area.

In general, the spatial spread of diseases is still a largely unexploited field. The influence of roads in epidemics can also be analyzed, which can, e.g., include a combination of 1D- and 2D-diffusion, which can be used to describe the fast diffusion along major roads.

In a system making use of an integro-differential *SIR*-model, we set up the equations of the model and showed uniqueness of the solution. Also, we performed various numerical simulations and optimal control calculations regarding reducing the amount of infected, yet also aimed to minimize the control used to contain the transmission parameter (and thus the infection cases), as it is connected to potentially high political costs, especially when the current case numbers are fairly low. This interplay provided interesting results on the spatially and time dependent optimal control. A comparison to an existing and established agent-based model, which is assumed to represent reality more closely, verified the approach. Since the computationally expensive agent-based model can hardly be optimized, due to extremely high computing efforts have to be spent in it, the optimization of the 'cheaper' *SIR*-model can have practical applications when coupled with the agent-based model. As the numerical computations have been done with spatially one-dimensional models only, further research should involve the inclusion of two-dimensional spread. While several more 'features' like vaccinations, partial immunity, households (etc.) can

be included in the integro-differential models, it is specifically important to keep this model as simple as possible as its important feature is that it is simple enough to be optimized in significantly smaller times than agent-based models. Further research should also include a closer investigation of realistic controls; a first ansatz is presented in the piecewise constant space- and time-dependent controls.

Both the design of the models and the theoretical and numerical concepts this work presents, require and deserve further research to explore the 'world' of infectious diseases and I hope that this work can act at least as a small brick in a large building.

Bibliography

[1] Abboubakar, H., Racke, R., and Schlosser, N. *A Reaction-diffusion Model for the Transmission Dynamics of the Coronavirus Pandemic with Reinfection and Vaccination Process*. Konstanzer Schriften in Mathematik. KOPS Universität Konstanz, 2023.

[2] Ahmed, N. et al. "Numerical simulation and stability analysis of a novel reaction–diffusion COVID-19 model". In: *Nonlinear Dynamics* 106(2) (2021), pp. 1293–1310. DOI: 10.1007/s11071-021-06623-9.

[3] Akaike, H. "Information Theory and an Extension of the Maximum Likelihood Principle". In: *Selected Papers of Hirotugu Akaike*. Ed. by Parzen, E., Tanabe, K., and Kitagawa, G. New York, NY: Springer, 1998.

[4] Anderson, R.M. et al. "How will country-based mitigation measures influence the course of the COVID-19 epidemic?" In: *Lancet* 395 (2020), pp. 931–934.

[5] Andrieu, C. et al. "An Introduction to MCMC for Machine Learning". In: *Mach. Learn.* 50 (2003), pp. 5–43.

[6] Armijo, L. "Minimization of functions having Lipschitz continuous first partial derivatives". In: *Pacific J. Math.* 16.1 (1966), pp. 1–3.

[7] Arnold, V. I. *Ordinary Differential Equations*. Cambridge, MA: M.I.T. Press, 1973.

[8] Augeraud-Véron, E. and Sari, N. "Seasonal dynamics in an SIR epidemic system". In: *J. Math. Biol.* 68 (2014), pp. 701–725.

[9] Aulbach, B. *Gewöhnliche Differentialgleichungen*. Spektrum, 2004.

[10] Bacaër, N. and Binder, C. *Eine kurze Geschichte der mathematischen Populationsdynamik*. Cassini, 2008.

[11] Badan Pusat Statistik. *2010 Indonesian Population Census*. last visited: 18 December, 2023.

[12] Baeumer, B. et al. "Reprint of: Boundary conditions for fractional diffusion". In: *Journal of Computational and Applied Mathematics* 339 (2018), pp. 414–430.

[13] Baleanu, D. and Kumar (eds.), D. *Fractional Calculus and its Applications in Physics*. Frontiers Media, Lausanne, 2019.

[14] Baleanu, D. et al. *Fractional Calculus - Models and Numerical Methods, CNC Series on Complexity, Nonlinearity and Chaos, Vol. 5 (2nd edition)*. World Scientific, New Jersey, 2016.

[15] Berestycki, H., Roquejoffre, J.-M., and Rossil, L. "Propagation of Epidemics Along Lines with Fast Diffusion". In: *Bull. Math. Biol.* 83.2 (2020). DOI: 10.1007/s11538-020-00826-8.

[16] Böhmer, M.M. et al. "Investigation of a COVID-19 outbreak in Germany resulting from a single travel-associated primary case: a case series". In: *The Lancet* 20.8 (2020), pp. 920–928. DOI: 10.1016/S1473-3099(20)30314-5.

[17]   Bollobás, B., Janson, S., and Riordan, O. "The phase transition in inhomogeneous random graphs". In: *Random Structures and Algorithms* 31 (2007), pp. 3–122. DOI: 10.1002/rsa.20168.

[18]   Borges, G.M. et al. "Superdiffusion in a non-Markovian random walk model with a Gaussian memory profile". In: *Eur. Phys. J. B* 85.310 (2012).

[19]   Bracher, J. et al. "National and subnational short-term forecasting of COVID-19 in Germany and Poland during early 2021". In: *medRxiv* (2021). DOI: 10.1101/2021.11.05.21265810.

[20]   Bracher, J. et al. "A pre-registered short-term forecasting study of COVID-19 in Germany and Poland during the second wave". In: *Nature Communications* 12 (2021). DOI: 10.1038/s41467-021-25207-0.

[21]   Britton, N. *Reaction-Diffusion Equations and Their Applications to Biology*. London: Academic Press, 1986.

[22]   Calcagni, G. "Towards Multifractional Calculus". In: *Frontiers in Physics* 6.58 (2018).

[23]   Centers for Disease Control and Prevention. *Dengue and Dengue Hemorrhagic Fever.* https://www.cdc.gov/dengue/resources/denguedhf-information-for-health-care-practitioners_2009.pdf, last visited: 18 December, 2023.

[24]   Centers for Disease Control and Prevention. *Dengue vaccine.* https://www.cdc.gov/dengue/vaccine/index.html, last visited: 18 December, 2023.

[25]   Centers for Disease Control and Prevention. *Principles of Epidemiology.* https://www.cdc.gov/csels/dsepd/ss1978/SS1978.pdf. last visited: 18 December, 2023.

[26]   Chambers, M. and Carrel, P. *Germany eases lockdown, with 'emergency brake' on hand if needed.* https://www.reuters.com/article/us-health-coronavirus-merkel-idUSKBN22I24E. last visited: 18 December, 2023.

[27]   Chinazzi, M. et al. "The effect of travel restrictions on the spread of the 2019 novel coronavirus (COVID-19) outbreak". In: *Science* 368 (2020), pp. 395–400. DOI: 10.1126/science.aba9757.

[28]   Cochet, A. et al. "Autochthonous dengue in mainland France, 2022: geographical extension and incidence increase". In: *Euro. Surveill.* 27.44 (2022). DOI: 10.2807/1560-7917.ES.2022.27.44.2200818.

[29]   Columbia Mainland School of Public Health. *Epidemic, Endemic, Pandemic: What are the Differences?* https://www.publichealth.columbia.edu/news/epidemic-endemic-pandemic-what-are-differences. last visited: 18 December, 2023.

[30]   Council of the European Union. *Infographic – The global agreement on pandemics in a nutshell.* https://www.consilium.europa.eu/en/infographics/towards-an-international-treaty-on-pandemics/. 2023.

[31]   Deuflhard, P. and Bornemann, F. *Scientific Computing with Ordinary Differential Equations*. Springer, 2002.

[32]   Deutscher Wetterdienst. *Klimadiagramm von Jakarta (Stadt, Obs.), West-Java / Indonesien*. last visited: 18 December, 2023.

[33]   Diekmann, O., Heesterbeek, J. A. P., and Metz, J. A. J. "On the definition and the computation of the basic reproduction ratio R0 in models for infectious diseases in heterogeneous populations". In: *J. Math. Biol.* 28 (1990), pp. 365–382.

[34] Dimpfl, T. et al. "Estimation of the SARS-CoV-2 infection fatality rate in Germany (preprint)". In: *medRxiv* (2021). DOI: 10.1101/2021.01.26.21250507.

[35] Domoshnitsky, A., Sitkin, A., and Eisenstein, L. "Mathematical Modeling of COVID-19 Transmission in the Form of System of Integro-Differential Equations". In: *Mathematics* 10.23 (2022). DOI: 10.3390/math10234500.

[36] Dönges, P. and Götz, T. and Krüger, T. and Niedzielewski, K. and Priesemann, V. and Schäfer, M. *SIR-Model for Households (preprint)*. arXiv https://arxiv.org/pdf/10.48550/arXiv.2301.04355. 2023.

[37] Dormand, J.R.. and Prince, P.J. "A family of embedded Runge-Kutta formulae". In: *Journal of Computational and Applied Mathematics* 6.1 (1980), pp. 19–26.

[38] Elsonbaty, A. et al. "Dynamical Analysis of a Novel Discrete Fractional SITRS Model for COVID-19". In: *Fractals* 29.08 (2021). DOI: 10.1142/S0218348X21400351.

[39] Epstein, J. et al. "Controlling Pandemic Flu: The Value of International Air Travel Restrictions". In: *PloS one* 5.e401 (2007). DOI: 10.1371/journal.pone.0000401.

[40] EUR-Lex. *Regulation (EU) 2022/2371 of the European Parliament and of the Council of 23 November 2022 on serious cross-border threats to health and repealing Decision No 1082/2013/EU (Text with EEA relevance)*. https://eur-lex.europa.eu/legal-content/EN/TXT/?uri=CELEX:32022R2371. 2023.

[41] European Commission. *Preparedness and response planning*. https://health.ec.europa.eu/health-security-and-infectious-diseases/preparedness-and-response-planning_en. 2023.

[42] Evans, G., Blackledge, J., and Yardley, P. *Numerical Methods for Partial Differential Equations*. London: Springer, 1999.

[43] Federal Foreign Office of Germany. *Coronavirus / Covid-19: Reisewarnung für Staaten außerhalb der EU/Schengen-Gebiet*. https://www.auswaertiges-amt.de/de/ReiseUndSicherheit/covid-19/2296762. last visited: 18 December, 2023.

[44] Federal Government of Germany. *Contact Restrictions Extended*. https://www.bundesregierung.de/breg-en/news/fahrplan-corona-pandemie-1744276. last visited: 18 December, 2023.

[45] Federal Government of Germany. *Guidelines for reducing social contacts*. https://www.bundesregierung.de/breg-de/themen/coronavirus/besprechung-der-bundeskanzlerin-mit-den-regierungschefinnen-und-regierungschefs-der-laender-vom-22-03-2020-1733248. last visited: 18 December, 2023.

[46] Federal Government of Germany. *Vorübergehende Grenzkontrollen an den Binnengrenzen zu Österreich, der Schweiz, Frankreich, Luxemburg und Dänemark*. https://www.bmi.bund.de/SharedDocs/pressemitteilungen/DE/2020/03/grenzschliessung-corona.html. last visited: 18 December, 2023.

[47] Frobenius, G. "Ueber Matrizen aus nicht negativen Elementen". In: *Sitzungsberichte der Koeniglich Preussischen Akademie der Wissenschaften. Jahrgang 1912. Erster Halbband. Januar bis Juni* (1912), pp. 456–477.

[48] Gai, C., Iron, D., and Kolokolnikov, T. "Localized outbreaks in an S-I-R model with diffusion". In: *Journal of Mathematical Biology* 80 (2020), pp. 1389–1411. DOI: 10.1007/s00285-020-01466-1.

[49] Ganegoda, N., Götz, T., and Wijaya, K.P. "An age-dependent model for dengue transmission: Analysis and comparison to field data". In: *Applied Mathematics and Computation* 388 (2020).

[50] Gelman, A. et al. *Bayesian Data Analysis, 2nd Edition.* London: Chapman and Hall, 1996.

[51] Gelman, A. and Rubin, D. B. "Inference from iterative simulation using multiple sequences". In: *Statistical Science* 7 (1992), pp. 457–472. DOI: 10.1214/ss/1177011136.

[52] Gilks, W.R., Richardson, S., and Spiegelhalter, D.J. *Markov chain Monte Carlo in Practice*. London: Chapman and Hall/CRC, 1996.

[53] Goel, R. et al. "Mobility-based SIR model for complex networks: with case study of COVID-19". In: *Social Network Analysis and Mining* 11.105 (2021). DOI: 10.1007/s13278-021-00814-3.

[54] Gorenflo, R. and Mainardi, F. "Random Walk Models for Space-Fractional Diffusion Processes". In: *Fractional Calculus and Applied Analysis* 1.2 (1998), pp. 167–191.

[55] Götz, T. and Heidrich, P. "COVID–19 Disease Dynamics in Germany: First Models and Parameter Identification". In: *Journal of Mathematics in Industry* 10.20 (2020). DOI: 10.1186/s13362-020-00088-y.

[56] Götz, T. et al. *Calculation of a local COVID-19 reproduction number for the northern Rhineland-Palatinate (preprint, in German)*. arXiv https://arxiv.org/abs/2011.08632. 2020.

[57] Goufo, E.F.D., Noutchie, S.C.O., and Mugisha, S. "A Fractional SEIR Epidemic Model for Spatial and Temporal Spread of Measles in Metapopulations". In: *Abstract and Applied Analysis* 2014.781028 (2014). DOI: 10.1186/s13662-020-02952-y.

[58] Grave, M. et al. "Assessing the Spatio-temporal Spread of COVID-19 via Compartmental Models with Diffusion in Italy, USA, and Brazil S.I. : Modeling and Simulation of Infectious Diseases". In: *Archives of Computational Methods in Engineering* 28 (2021), pp. 4205–4223. DOI: 10.1007/s11831-021-09627-1.

[59] Grépin, K.A. et al. "Evidence of the effectiveness of travel-related measures during the early phase of the COVID-19 pandemic: a rapid systematic review". In: *BMJ Global Health* 6.e004537 (2021), pp. 37–59. DOI: 10.1136/bmjgh-2020-004537.

[60] Gubler, D.J. "Dengue and Dengue Hemorrhagic Fever". In: *Clinical Microbiology Reviews* 11.3 (1998), pp. 480–496. DOI: 10.1128/cmr.11.3.480.

[61] Gubler, D.J. "Dengue/dengue haemorrhagic fever: history and current status". In: *Novartis Found Symp.* 277 (2006), pp. 3–16. DOI: 10.1002/0470058005.ch2.

[62] Hackbusch, W. "A numerical method for solving parabolic equations with opposite orientations". In: *Computing* 20.3 (1978), pp. 229–240. DOI: 10.1007/bf02251947.

[63] Hamdan, N.I. and Kilicman, A. "Mathematical Modelling of Dengue Transmission with Intervenction Strategies Using Fractional Derivatives". In: *Bulletin of Mathematical Biology* 84.138 (2022). DOI: 10.1007/s11538-022-01096-2.

[64] Harris, P.J. and Bodmann, B.E.J. "A mathematical model for simulating the spread of a disease through a country divided into geographical regions with different population densities". In: *Journal of Mathematical Biology* 85.32 (2022). DOI: 10.1007/s00285-022-01803-6.

[65] He, X. and Lau, E.H.Y. and Wu, P. and Deng, X. and Wang, J. and Hao, X. and Lau, Y.C. and Wong, J.Y. and Guan, Y. and Tan, X. and Mo, X. and Chen, Y. and Liao, B. and Chen, W. and Hu, F. and Zhang, Q. and Zhong, M. and Wu, Y. and Zhao, L. and Zhang, F. and Cowling, B.J. and Li, F. and Leung, G.M. "Temporal dynamics in viral shedding and transmissibility of COVID-19". In: *Nat. Med.* 26 (2020), pp. 672–675. DOI: 10.1038/s41591-020-0869-5.

[66] Heidrich, P. and Götz, T. "Parameter Estimation via Adjoint Functions in Epidemiological Reaction-Diffusion Models". In: *Progress in Industrial Mathematics at ECMI 2021*. Vol. 39. Springer, Cham, 2022, pp. 115–122. DOI: 10.1007/978-3-031-11818-0_16.

[67] Heidrich, P. et al. "The COVID-19 outbreak in Germany – Models and Parameter Estimation". In: *Commun. Biomath. Sci.* 3 (2020), pp. 37–59. DOI: 10.5614/cbms.2020.3.1.5.

[68] Hempel, S. *The Medical Detective: John Snow and the Mystery of Cholera*. London: Granta, 2006.

[69] Hollingsworth, T.D., Ferguson, N.M., and Anderson, R.M. "Will travel restrictions control the international spread of pandemic influenza?" In: *Nat. Med.* 12.5 (2006), pp. 497–499. DOI: 10.1038/nm0506-497.

[70] Hritonenkoa, N., Satskyb, C., and Yatsenkoc, Y. "Integral Model of COVID-19 Spread and Mitigation in UK: Identification of Transmission Rate". In: *Mathematical Modelling and Analysis* 27.4 (2022). DOI: 10.3846/mma.2022.15708.

[71] Huremović, D. *Psychiatry of Pandemics*. Springer Nature Switzerland, 2019, Chapter 2: Brief History of Pandemics (Pandemics Throughout History).

[72] Johns Hopkins University. *Time series of confirmed COVID-19 cases globally.* github.com/CSSEGISandData/COVID-19/blob/master/csse_COVID_19_data/csse_COVID_19_time_series/time_series_COVID19_confirmed_global.csv. last visited: 18 December, 2023.

[73] Kalbfleisch, J.G. *Probability and Statistical Inference, Volume 1: Probability*. New York, NY: Springer, 1985.

[74] Kalra, S. et al. "Endemic or epidemic? Measuring the endemicity index of diabetes". In: *Indian J Endocrinol Metab.* 19.1 (2015), pp. 5–7. DOI: 10.4103/2230-8210.144633.

[75] Kergaßner, A. et al. "Memory-based meso-scale modeling of Covid-19". In: *Computational Mechanics* (2020). DOI: 10.1007/s00466-020-01883-5.

[76] Kermack, W.O. and McKendrick, A.G. "Contributions to the mathematical theory of epidemics-I. 1927." In: *Bull. Math. Biol.* 53 (1991), pp. 33–55. DOI: 10.1098/rspa.1927.0118.

[77] King, A.A. et al. "Avoidable errors in the modelling of outbreaks of emerging pathogens, with special reference to Ebola". In: *Proc. R. Soc. B* 282.20150347 (1991), pp. 33–55. DOI: 10.1098/rspb.2015.0347.

[78]   Kuehn, C. and Mölter, J. "The influence of a transport process on the epidemic threshold". In: *Journal of Mathematical Biology* 85.62 (2020), pp. 37–59. DOI: 10.1007/s00285-022-01810-7.

[79]   Kuniya, T. and Wang, J. "Global dynamics of an SIR epidemic model with nonlocal diffusion". In: *Nonlinear Analysis: Real World Applications* 43 (2018), pp. 262–282. DOI: 10.1016/j.nonrwa.2018.03.001.

[80]   Landesamt für Vermessung und Geobasisinformation Rheinland-Pfalz. *Landkreis Birkenfeld. Verwaltungsgrenzen und zentrale Orte.*

[81]   Lenhart, S. and Workman, J.T. *Optimal control applied to biological models*. CRC Press, 2007.

[82]   Letnikov, A.V. "Theory of differentiation with an arbitrary index". In: *Mat. Sb. 3* (1868), pp. 1–66.

[83]   Leung, K., Wu, J.T., and Leung, G.M. "Effects of adjusting public health, travel, and social measures during the roll-out of COVID-19 vaccination: a modelling study". In: *Lancet Public Health* 6 (2021), e674–e682. DOI: 10.1016/S2468-2667(21)00167-5.

[84]   Logeswari, K., Ravichandran, C., and Nisar, K.S. "Mathematical model for spreading of COVID-19 virus with the Mittag–Leffler kernel". In: *Numerical Methods for Partial Differential Equations* (2020), pp. 1–16. DOI: 10.1002/num.22652.

[85]   MacNamara, S. and Strang, G. "Operator Splitting". In: *Splitting Methods in Communication, Imaging, Science, and Engineering*. Ed. by Glowinski, R., Osher, S., and Yin, W. Springer, Cham, 2016, pp. 95–114.

[86]   Mahmood, S.S. et al. "The Framingham Heart Study and the Epidemiology of Cardiovascular Diseases: A Historical Perspective". In: *Lancet* 383.9921 (2014), pp. 999–1008. DOI: 10.1016/S0140-6736(13)61752-3.

[87]   Martcheva, M. *An introduction to mathematical epidemiology*. Springer, 2015.

[88]   Mateus, A.L.P. et al. "Effectiveness of travel restrictions in the rapid containment of human influenza: a systematic review". In: *Bull World Health Organ.* 92.12 (2014), pp. 868–880.

[89]   Meerschaert, M.M. and Sikorskii, A. *Stochastic Models for Fractional Calculus*. De Gruyter Studies in Mathematics, De Gruyter, Berlin, 2012.

[90]   Meerschaert, M.M. and Tadjeran, C. "Finite difference approximations for fractional advection-dispersion flow equations". In: *Journal of Computational and Applied Mathematics* 172 (2004), pp. 65–77.

[91]   Meerschaert, M.M. and Tadjeran, C. "Finite difference approximations for two-sided space-fractional partial differential equations". In: *Applied Numerical Mathematics* 56 (2006), pp. 80–90.

[92]   Metropolis, N. et al. "Equation of State Calculations by Fast Computing Machines". In: *J.Chem. Phys.* 21 (1953), pp. 1087–1092. DOI: 10.1063/1.1699114.

[93]   Ministry of Health Republic of Indonesia. https://www.kemkes.go.id/. last visited: 18 December, 2023.

[94]   Morwinsky, S., Nitsche, N., and Acosta, E. "COVID-19 fatality in Germany: Demographic determinants of variation in case-fatality rates across and within German federal states during the first and second waves". In: *Demographic Research* 45.45 (2021), pp. 1355–1372. DOI: 10.4054/DemRes.2021.45.45.

[95]   Murray, J. D. *Mathematical Biology - I. An Introduction*. Springer, 2002.

[96]   Nawaz, Y. et al. "An explicit unconditionally stable scheme: application to diffusive COVID-19 epidemic model". In: *Advances in Difference Equations* 363 (2021). DOI: 10.1186/s13662-021-03513-7.

[97]   Niedzielewski, K. et al. "The Overview, Design Concepts and Details Protocol of ICM Epidemiological Model (PDYN 1.5)". In: *SSRN Electronic Journal* (2022). DOI: 10.2139/ssrn.4039054.

[98]   Niedzielewski, K. et al. *A Deep Dive into the Delta Wave: Forecasting SARS-CoV-2 Epidemic Dynamic in Poland with the pDyn Agent-Based Model (preprint)*. 2023. DOI: 10.21203/rs.3.rs-2966996/v1.

[99]   Nocedal, J. and Wright, S. *Numerical Optimization*. Springer, 2006.

[100] Oishi, C.M. et al. "Stability analysis of Crank-Nicolson and Euler schemes for time-dependent diffusion equations". In: *BIT Numerical Mathematics* 55 (2015), pp. 487–513. DOI: 10.1007/s10543-014-0509-x.

[101] Oldham, K. and Spanier, J. *The Fractional Calculus (1st Edition)*. Academic Press, New York, 1974.

[102] Olinky, R., Huppert, A., and Stone, L. "Seasonal dynamics and thresholds governing recurrent epidemics". In: *J. Math. Biol.* 56 (2008), pp. 827–839.

[103] Overpass-Turbo. https://overpass-turbo.eu/.

[104] Perron, O. "Zur Theorie der Matrices". In: *O. Math. Ann.* 64 (1907), pp. 248–263.

[105] Press, W.H. et al. *Numerical Recipes in C++: The Art of Scientific Computing. 3rd edition.* Cambridge University Press, 2007.

[106] Priesemann, V., Meyer-Hermann, M., and Pigeot, I. "Der Beitrag von epidemiologischen Modellen zur Beschreibung des Ausbruchsgeschehens der COVID-19-Pandemie". In: *Bundesgesundheitsblatt - Gesundheitsforschung - Gesundheitsschutz* 64 (2021), pp. 1058–1066. DOI: 10.1007/s00103-021-03390-1.

[107] *Privat communication with Dipo Aldila, Department of Mathematics, University of Indonesia, Depok.*

[108] Radon, K. et al. "From first to second wave: follow-up of the prospective COVID-19 cohort (KoCo19) in Munich (Germany)". In: *BMC Infectious Diseases* 21.925 (2021). DOI: 10.1186/s12879-021-06589-4.

[109] Raftery, A.E. "Bayesian Model Selection in Social Research". In: *Sociol. Methodol.* 25 (1995), pp. 111–163. DOI: 10.2307/271063.

[110] Raue, A. et al. "Structural and practical identifiability analysis of partially observed dynamical models by exploiting the profile likelihood". In: *Bioinformatics* 25 (2009), pp. 1923–1929. DOI: 10.1093/bioinformatics/btp358.

[111] Read, J. M. et al. "Novel coronavirus 2019-nCoV: early estimation of epidemiological parameters and epidemic predictions". In: *Philos Trans R Soc Lond B Biol Sci.* 376 (2021), pp. 1–3. DOI: 10.1098/rstb.2020.0265.Epub.

[112] Rezapour, S., Mohammadi, H., and Samei, M.E. "SEIR epidemic model for COVID-19 transmission by Caputo derivative of fractional order". In: *Advances in Difference Equations* 490 (2020). DOI: 10.1186/s13662-020-02952-y.

[113] Robert-Koch-Institute. *Corona fact sheet.* https://www.rki.de/DE/Content/InfAZ/N/Neuartiges_Coronavirus/Steckbrief.html. last visited: 18 December, 2023.

[114]   Robert-Koch-Institute. *Daily situation reports.* `www.rki.de/DE/Content/InfAZ/N/Neuartiges_Coronavirus/Situationsberichte/Gesamt.html`.

[115]   Robert-Koch-Institute. *Nowcasting und R-Schätzung: Schätzung der aktuellen Entwicklung der SARS-CoV-2-Epidemie in Deutschland.* `www.rki.de/DE/Content/InfAZ/N/Neuartiges_Coronavirus/Situationsberichte/Gesamt.html`. last visited: 18 December, 2023.

[116]   Robert-Koch-Institute. *Modellierung von Beispielszenarien der SARS-CoV-2-Epidemie 2020 in Deutschland.* `https://www.rki.de/DE/Content/InfAZ/N/Neuartiges_Coronavirus/Modellierung_Deutschland.pdf?__blob=publicationFile`.

[117]   Rocha, F. et al. "Time-scale separation and centre manifold analysis describing vector-borne disease dynamics". In: *Int. J. Comput. Math.* 90 (2013), pp. 2105–2125.

[118]   Rockenfeller, R. et al. "Comparative Sensitivity Analysis of Muscle Activation Dynamics". In: *Comput. Math. Methods Med.* (2015). Article ID 585409. DOI: `10.1155/2015/585409`.

[119]   Rocktäschel, O. *Methoden zur Berechnung der Gammafunktion für komplexes Argument.* Dissertation, Dresden. 1922.

[120]   Ross, R. *The Prevention of Malaria.* John Murray, London, 1911.

[121]   Ross, S. *Introduction to Probability Models.* Elsevier India, 2014.

[122]   Roy, V. "Comparative Sensitivity Analysis of Muscle Activation Dynamics". In: *Annual Review of Statistics and Its Application* 7 (2020), pp. 387–412. DOI: `10.1146/annurev-statistics-031219-041300`.

[123]   Rusatsi, D.N. "Bayesian analysis of SEIR epidemic models". last visited: 18 December, 2023. PhD thesis. Lappeenranta University of Technology, 2015.

[124]   Salvadore, F., Fiscon, G., and Paci, P. "Integro-differential approach for modeling the COVID-19 dynamics - Impact of confinement measures in Italy". In: *Computers in Biology and Medicine* 139 (2021). DOI: `10.1016/j.compbiomed.2021.105013`.

[125]   Schäfer, M. *Mathematical Modelling of Dengue Fever in Jakarta.* Master thesis, University of Koblenz-Landau, 2018.

[126]   Schäfer, M. and Götz, T. "A numerical method for space-fractional diffusion models with mass-conserving boundary conditions". In: *Mathematical Methods in the Applied Sciences* (2023). DOI: `10.1002/mma.9310`.

[127]   Schäfer, M. and Götz, T. "Modelling Dengue Fever Epidemics in Jakarta". In: *Int. J. Appl. Comput. Math* 6 (2020). DOI: `10.1007/s40819-020-00834-1`.

[128]   Schäfer, M., Heidrich, P., and Götz, T. "Modelling the Spatial Spread of COVID-19 in a German District using a Diffusion Model". In: *Mathematical Biosciences and Engineering* 20.12 (2023). DOI: `10.3934/mbe.2023940`.

[129]   Schäfer, M. et al. *An integro-differential model for the spread of diseases.* arXiv `https://arxiv.org/abs/2307.10087`. 2023.

[130]   Schäfer, M. et al. "The impact of travelling on the COVID-19 infection cases in Germany". In: *BMC Infectious Diseases* 2.455 (2022). DOI: `10.1186/s12879-022-07396-1`.

[131]   Schauder, J. "Der Fixpunktsatz in Funktionalräumen". In: *Stud. Math.* 2 (1930), pp. 171–180.

[132] Sherratt, K. et al. "Predictive performance of multi-model ensemble forecasts of COVID-19 across European nations". In: *eLife* 12 (2023). DOI: 10.7554/eLife.81916.

[133] Shinbrot, M. "The solution of some integral equations of Wiener-Hopf type". In: *Quarterly of Applied Mathematics* 28.1 (1970), pp. 15–36.

[134] Sidi Ammi, M.R. et al. "Global analysis of a time fractional order spatio-temporal SIR model". In: *Scientific Reports* 12.5751 (2022). DOI: 10.1038/s41598-022-08992-6.

[135] Siegenfeld, A.F. and Bar-Yam, Y. "The impact of travel and timing in eliminating COVID-19". In: *Commun. Phys.* 3 (2020). DOI: 10.1038/s42005-020-00470-7.

[136] Skwara, U. et al. "Fractional calculus and superdiffusion in epidemiology: shift of critical thresholds". In: *Conference: 12th International Conference on Computational and Mathematical Methods in Science and Engineering, CMMSE 2012* (2012).

[137] Soczkiewicz, E. "Application of Fractional Calculus in the Theory of Viscoelasticity". In: *Mol. Quant. Acoust.* 23 (2002), pp. 397–404.

[138] Souza, M. O. "Multiscale analysis for a vector-borne epidemic model". In: *J. Math. Biol.* 68 (2014), pp. 1269–1293.

[139] Statistisches Bundesamt (Germany). *Bevölkerungsstand (31.12.2018)*. https://www.destatis.de/DE/Home/_inhalt.html. last visited: 18 December, 2023.

[140] Statistische Bibliothek. *Fachserie/6/7/1/Monatlich. Wiesbaden*. https://www.statistischebibliothek.de/mir/receive/DESerie_mods_00000082. last visited: 18 December, 2023.

[141] Statistische Bibliothek. *Fachserie/8/6/Monatlich. Wiesbaden*. https://www.statistischebibliothek.de/mir/receive/DEHeft_mods_00132393. last visited: 18 December, 2023.

[142] Statistisches Bundesamt (Germany). *Statistik über die touristische Nachfrage - Reisen: Deutschland, Jahre, Reiseverhalten, Reiseziel/Reisedauer/Reisegründe/Unterkünfte/Verkehrsmittel*. https://www.destatis.de/DE/Themen/Branchen-Unternehmen/Gastgewerbe-Tourismus/tourismus-reiseverhalten.html. last visited: 18 December, 2023.

[143] Tadjeran, C. and Meerschaert, M.M. "A second-order accurate numerical method for the two-dimensional fractional diffusion equation". In: *Journal of Computational Physics* 220 (2007), pp. 813–823.

[144] Tadjeran, C., Meerschaert, M.M., and Scheffler, H.-P. "A second-order accurate numerical approximation for the fractional diffusion equation". In: *Journal of Computational Physics* 213 (2006), pp. 205–213.

[145] Tindale, L. et al. "Evidence for transmission of COVID-19 prior to symptom onset". In: *eLife* 9.3 (2020). DOI: 10.7554/eLife.57149.

[146] United Nations News. *WHO chief declares end to COVID-19 as a global health emergency*. https://news.un.org/en/story/2023/05/1136367. last visited: 18 December, 2023.

[147] United Nations, Department of Economic and Social Affairs, Population Dynamics. *World Population Prospects 2019*. https://population.un.org/wpp/DataQuery/. last visited: 18 December, 2023.

[148] Driessche, P. van den and Watmough, J. "Reproduction numbers and sub-threshold endemic equilibria for compartmental models of disease transmission". In: *Math. Biosci.* 180 (2002), pp. 29–48. DOI: 10.1016/s0025-5564(02)00108-6.

[149] Viguerie, A. et al. "Simulating the spread of COVID-19 via a spatially-resolved susceptible–exposed–infected–recovered–deceased (SEIRD) model with heterogeneous diffusion". In: *Appl Math Lett.* 111.106617 (2021). DOI: 10.1016/j.aml.2020.106617.

[150] Vukobratović, R. T. M. *General Sensitivity Theory*. New York, NY, USA: Elsevier, 1962.

[151] Walter, W. *Ordinary Differential Equations*. Springer, 1998.

[152] Wang, H. and Yamamoto, N. "Using a partial differential equation with Google Mobility data to predict COVID-19 in Arizona". In: *Mathematical Biosciences and Engineering* 17.5 (2020), pp. 4891–4904. DOI: 10.3934/mbe.2020266.

[153] Werner, D. *Funktionalanalysis*. Springer, 1995.

[154] World Health Organization. *Coronavirus disease (COVID-19) Weekly Epidemiological Update and Weekly Operational Update*. https://www.who.int/emergencies/diseases/novel-coronavirus-2019/situation-reports. last visited: 18 December, 2023.

[155] World Health Organization. *Dengue and severe dengue*. https://www.who.int/news-room/fact-sheets/detail/dengue-and-severe-dengue. last visited: 18 December, 2023.

[156] World Health Organization. *Dengue Control*. last visited: 18 December, 2023.

[157] World Health Organization. *Non-pharmaceutical public health measures for mitigating the risk and impact of epidemic and pandemic influenza*. https://www.who.int/publications/i/item/non-pharmaceutical-public-health-measuresfor-mitigating-the-risk-and-impact-of-epidemic-and-pandemic-influenza. last visited: 18 December, 2023.

[158] Zou, Y. et al. "Vaccination and Quarantine Effect on COVID-19 Transmission Dynamics Incorporating Chinese-Spring-Festival Travel Rush: Modeling and Simulations". In: *Bull. Math. Biol.* 84.30 (2022). DOI: 10.1007/s11538-021-00958-5.